

Air Force Institute of Technology

AFIT Scholar

Theses and Dissertations

Student Graduate Works

3-2003

Quantum Mechanical Calculations of Monoxides of Silicon Carbide Molecules

John W. Roberts Jr.

Follow this and additional works at: <https://scholar.afit.edu/etd>



Part of the [Electronic Devices and Semiconductor Manufacturing Commons](#), and the [Quantum Physics Commons](#)

Recommended Citation

Roberts, John W. Jr., "Quantum Mechanical Calculations of Monoxides of Silicon Carbide Molecules" (2003). *Theses and Dissertations*. 4294.
<https://scholar.afit.edu/etd/4294>

This Thesis is brought to you for free and open access by the Student Graduate Works at AFIT Scholar. It has been accepted for inclusion in Theses and Dissertations by an authorized administrator of AFIT Scholar. For more information, please contact AFIT.ENWL.Repository@us.af.mil.



**QUANTUM MECHANICAL CALCULATIONS
OF MONOXIDES OF SILICON CARBIDE
MOLECULES**

THESIS

John W. Roberts Jr., First Lieutenant, USAF

AFIT/GNE/ENP/03-09

**DEPARTMENT OF THE AIR FORCE
AIR UNIVERSITY**

AIR FORCE INSTITUTE OF TECHNOLOGY

Wright-Patterson Air Force Base, Ohio

APPROVED FOR PUBLIC RELEASE; DISTRIBUTION UNLIMITED.

The views expressed in this thesis are those of the author and do not reflect the official policy or position of the United States Air Force, Department of Defense, or the United States Government.

AFIT/GNE/ENP/03-09

QUANTUM MECHANICAL CALCULATIONS OF MONOXIDES OF SILICON
CARBIDE MOLECULES

THESIS

Presented to the Faculty

Department of Engineering Physics

Graduate School of Engineering and Management

Air Force Institute of Technology

Air University

Air Education and Training Command

In Partial Fulfillment of the Requirements for the

Degree of Master of Science (Nuclear Science)

John W. Roberts Jr., BS

First Lieutenant, USAF

March 2003

APPROVED FOR PUBLIC RELEASE; DISTRIBUTION UNLIMITED.

AFIT/GNE/ENP/03-09

QUANTUM MECHANICAL CALCULATIONS OF MONOXIDES OF SILICON
CARBIDE MOLECULES

John W. Roberts Jr., BS
First Lieutenant, USAF

Approved:




Dr. Larry W. Burggraf (Chairman)

10 Mar 2003
date



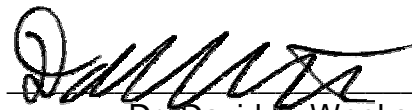
Dr. Xiaofeng F. Duan (Member)

10 Mar. 2003
date



LTC James C. Petrofsky, USA (Member)

10 MAR 03
date



Dr. David E. Weeks (Member)

10 Mar 03
date

Acknowledgments

It is impossible to accomplish any worthwhile work of this nature alone, and I am indebted to many for their contributions and support. This list is certainly not all inclusive, but there are some people without which I could not have completed this.

First and foremost I thank God, without Whom I could do nothing (“I can do all things through Christ who strengthens me”—Php 4:13). I am thankful for all the blessings, abilities, and grace that He has given me. My life would be nothing without faith in my Lord and Savior Jesus Christ, and the strength that He gives me.

Proverbs 22:6 says “Train up a child in the way he should go, And when he is old he will not depart from it.” Without the training, discipline, inspiration, and support that I have received from my parents throughout my life, I would not be where I am. The values and love of learning that you taught me have helped me immeasurably both in this endeavor and in life in general.

I am particularly grateful for the support of my thesis advisor, Dr Larry Burggraf. Thank you for asking me to do this research, saving me, at least temporarily, from the nuclear world. None of this would have been possible without your constant guidance, discussion, and support.

To Dr Frank Duan: Thanks for answering my unending questions on both computer and theory problems. Many of these calculations never would have happened without your support.

To Dr Alan Yeates, Dr Jean Bleadaeu, and Dr Mark Gordon: Thanks for lending your theoretical and GAMESS troubleshooting skills. Your experience was invaluable in solving many troublesome calculations.

To Lt Col Bob Canfield: Thanks for your help in repeatedly getting us more computer hours. Without your help, this research would have stalled.

To my fellow quantum chemist student Captain Eric Beck: Thanks for your discussion, opinions, and suggestions on many a topic.

And finally, and most certainly not least, to my best friend and sister in Christ, Carey: Thank you for all your support, friendship, encouragement, prayers, and everything you do for me. You've always been there when I needed someone to pick me up; with your words and example, you have been indispensable in showing me the Way and the Truth (as well as maintaining my sanity). You're a true friend and sister.

John W. Roberts Jr.

Table of Contents

	Page
Acknowledgments.....	iv
List of Figures	vii
List of Tables	viii
Abstract.....	ix
I. Introduction.....	1
1.1. Problem Statement	1
1.2. Background.....	2
1.3. Scope.....	6
1.4. Research Approach	7
1.5. Thesis Outline.....	8
II. Theory.....	10
2.1. Introduction	10
2.2. Single Particle Quantum Mechanics	10
2.3. Single Electron Atoms.....	15
2.3.1. Angular Solution	18
2.3.2. Radial Solution.....	21
2.3.3. Total Hydrogen-Like Atomic Wave Functions	22
2.4. Many Electron Wave Functions	24
2.4.1. Atomic Units.....	24
2.4.2. Many Electron Hamiltonian	25
2.4.3. Born-Oppenheimer Approximation	26
2.4.4. Potential Energy Surfaces	27
2.4.5. Molecular Vibration and Rotation.....	29
2.4.6. Variational Principle	31
2.4.7. Pauli Exclusion Principle, <i>Aufbau</i> Principle, and Multiplicity.....	32
2.4.8. Perturbation Theory	34
2.4.9. Self Consistent Field (SCF)	36
2.4.10. Basis Sets.....	37
2.4.11. Spin Orbitals	40
2.5. Hartree-Fock (HF) Approximation	42
2.6. Post-Hartree-Fock Methods.....	47
2.6.1. Møller-Plesset Second Order Perturbation Theory (MP2) ..	49
2.6.2. Configuration Interaction (CI).....	50
2.6.3. Multi-Configuration Self-Consistent Field (MCSCF).....	51
2.6.4. Coupled Cluster (CC) Theory	51
2.7. Density Functional Theory (DFT).....	53

2.7.1. Early DFT Theory	53
2.7.2. Hohenberg-Kohn Theorems	55
2.7.3. Kohn-Sham Approach	56
2.7.4. Exchange-Correlation Functional.....	59
III. Methodology	62
3.1. Introduction	62
3.2. GAMESS Input	63
3.3. GAMESS Output.....	69
3.4. Step 1: Identify Isomers	70
3.5. Steps 2-10: Hartree-Fock Optimization.....	71
3.6. Steps 11-19: Density Functional Theory Optimization	73
3.7. Steps 20-22: Vibrational Analysis	78
3.8. Steps 23-25: Post-Hartree-Fock Analysis	79
3.9. Steps 26-27: Determine Electron Affinities	82
IV. Results and Analysis	84
4.1. Introduction	84
4.2. O, CO, and SiO.....	85
4.3. CSiO	87
4.4. C ₂ O	89
4.5. Si ₂ O	90
4.6. C ₂ SiO.....	90
4.7. CSi ₂ O.....	93
4.8. C ₂ Si ₂ O	95
4.9. C ₃ O	96
4.10. Si ₃ O	97
4.11. C ₃ SiO.....	99
4.12. CSi ₃ O.....	101
4.13. C ₃ Si ₂ O	102
4.14. C ₂ Si ₃ O	105
4.15. C ₃ Si ₃ O	107
4.16. C ₄ O	108
4.17. Si ₄ O	109
4.18. C ₄ SiO.....	112
4.19. CSi ₄ O.....	114
4.20. C ₄ Si ₂ O	114
4.21. C ₂ Si ₄ O	117
4.22. Functional Group Analysis	120
4.23. Vibrational Analysis Accuracy.....	125
4.24. Thermodynamics	126
V. Conclusions and Recommendations	135
5.1. Conclusions	135
5.2. Recommendations for Future Work.....	138

Appendix A. Glossary	140
Appendix B. Initial Isomers for HF/VDZ Calculations	142
Appendix C. Detailed Calculation Data	160
Appendix D. Tools Developed for Data Analysis.....	195
Appendix E. Calculation Troubleshooting Guide.....	197
Appendix F. Detailed Thermodynamics Data.....	199
Bibliography	201
Vita.....	210

List of Figures

Figure	Page
1. Map of the Ground State Geometries of Si_mC_n Clusters	4
2. Photoelectron Spectroscopy Experimental Setup.....	5
3. 364 nm photoelectron spectrum of C_3Si^-	5
4. Potential Energy Curve for H_2^+	28
5. Sample GAMESS input.....	64
6. Initial 23 isomers for Si_2CO calculation	70
7. Stable isomers for Si_2CO calculation using HF/VDZ.....	72
8. Stable isomers for Si_2CO calculation using HF/cc-pVDZ	74
9. Stable isomers for Si_2CO calculation using HF/aug-cc-pVDZ	75
10. Stable isomers for Si_2CO calculation using DFT/B3LYP/VDZ.....	76
11. Stable isomers for Si_2CO calculation using DFT/B3LYP/cc-pVDZ.....	77
12. Stable isomers for Si_2CO calculation using DFT/B3LYP/aug-cc-pVDZ.....	77
13. Vibrational modes of Si_2CO using DFT/B3LYP/aug-cc-pVDZ.....	78
14. Sample Gaussian 98 input for Coupled Cluster calculation	82
15. Geometry Comparison for Si_2CO at several levels of theory	83
16. Calculated geometry and vibrational modes for ground state CO neutral and anion	86
17. Calculated geometry and vibrational modes for ground state SiO neutral and anion	87

18. Calculated geometry and vibrational modes for ground state SiCO neutral and anion	88
19. Calculated geometry and vibrational modes for ground state C ₂ O neutral and anion	89
20. Calculated geometry and vibrational modes for ground state Si ₂ O neutral and anion	91
21. Calculated geometry and vibrational modes for ground state C ₂ SiO neutral and anion	92
22. Calculated geometry and vibrational modes for ground state CSi ₂ O neutral and anion	93
23. Calculated geometry and vibrational modes for ground state C ₂ Si ₂ O neutral and anion	95
24. Calculated geometry for ground state C ₃ O neutral and anion.....	96
25. Calculated geometry for ground state Si ₃ O neutral and anion	98
26. Calculated geometry for ground state C ₃ SiO neutral and anion.....	100
27. Calculated geometry for ground state CSi ₃ O neutral and anion.....	101
28. Calculated geometry for ground state C ₃ Si ₂ O neutral and anion	103
29. Calculated geometry for ground state C ₂ Si ₃ O neutral and anion	106
30. Calculated geometry for ground state C ₃ Si ₃ O neutral and anion	107
31. Calculated geometry for ground state C ₄ O neutral and anion.....	109
32. Calculated geometry for ground state Si ₄ O neutral and anion	111
33. Calculated geometry for ground state C ₄ SiO neutral and anion.....	113
34. Calculated geometry for ground state CSi ₄ O neutral and anion.....	115
35. Calculated geometry for ground state C ₄ Si ₂ O neutral and anion	116
36. Calculated geometry for ground state C ₂ Si ₄ O neutral and anion	118

37. Neutral ground state isomers for C_mSi_nO , $m, n \leq 4$ with DFT/B3LYP/aug-cc-pVDZ.....	121
38. Anion ground state isomers for C_mSi_nO , $m, n \leq 4$ with DFT/B3LYP/aug-cc-pVDZ.....	122
39. Neutral ground state isomers for C_mSi_n , $m, n \leq 4$ with DFT/B3LYP/aug-cc-pVDZ.....	124
40. Initial isomers for C_2Si_2O calculations with HF/VDZ.....	142
41. Initial isomers for C_3O and Si_3O calculations with HF/VDZ	143
42. Initial isomers for C_3SiO and CSi_3O calculations with HF/VDZ	144
43. Initial isomers for C_3Si_2O and C_2Si_3O calculations with HF/VDZ.....	145
44. Initial isomers for C_3Si_3O calculations with HF/VDZ.....	147
45. Initial isomers for C_4O and Si_4O calculations with HF/VDZ	150
46. Initial isomers for C_4SiO and CSi_4O calculations with HF/VDZ	151
47. Initial isomers for C_4Si_2O calculations with HF/VDZ.....	152
48. Initial isomers for C_2Si_4O calculations with HF/VDZ.....	153
49. Initial isomers for C_4Si_3O calculations with HF/VDZ.....	156
50. Initial isomers for C_3Si_4O calculations with HF/VDZ.....	157
51. Initial isomers for C_4Si_4O calculations with HF/VDZ.....	158
52. Batch file for extracting data from output files	195

List of Tables

Table	Page
1. SCF Iterations for $x = x - e^x + 1$	37
2. Steps used in my method for determining ground state geometries of C_mSi_nO , $m, n \leq 4$, molecules	63
3. Vibrational analysis for C_3O	97
4. Vibrational analysis for Si_3O	99
5. Vibrational analysis for C_3SiO	100
6. Vibrational analysis for CSi_3O	102
7. Vibrational analysis for C_3Si_2O	104
8. Vibrational analysis for C_2Si_3O	106
9. Vibrational analysis for C_3Si_3O	108
10. Vibrational analysis for C_4O	110
11. Vibrational analysis for Si_4O	112
12. Vibrational analysis for C_4SiO	113
13. Vibrational analysis for CSi_4O	116
14. Vibrational analysis for C_4Si_2O	117
15. Vibrational analysis for C_2Si_4O	119
16. Adiabatic electron affinities for C_mSi_nO , $m, n \leq 4$ calculated with DFT/B3LYP/aug-cc-pVDZ.....	126
17. Vertical electron affinities for C_mSi_nO , $m, n \leq 4$ calculated with DFT/B3LYP/aug-cc-pVDZ.....	127

18. Comparison of calculated vibrational frequencies with experimental values	128
19. Ideal gas phase enthalpies of formation for C_mSi_nO neutral ground states at 298.15K calculated with DFT/B3LYP/aug-cc-pVDZ	129
20. Ideal gas phase enthalpies of formation for C_mSi_n neutral ground states at 298.15K calculated with DFT/B3LYP/aug-cc-pVDZ	129
21. . Ideal gas phase reaction enthalpies for atomic oxidation of C_mSi_n neutral ground states at 298.15K calculated with DFT/B3LYP/aug-cc-pVDZ	130
22. Ideal gas phase reaction enthalpies for molecular oxidation of C_mSi_n neutral ground states at 298.15K calculated with DFT/B3LYP/aug-cc-pVDZ	131
23. Ideal gas reaction enthalpies for one-atom dissociation of C_mSi_n neutral ground states at 298.15K calculated with DFT/B3LYP/aug-cc-pVDZ	132
24. Ideal gas reaction enthalpies for dissociation of C_mSi_nO neutral ground states at 298.15K calculated with DFT/B3LYP/aug-cc-pVDZ	133
25. Detailed Calculation Data for O.....	160
26. Detailed Calculation Data for CO	161
27. Detailed Calculation Data for SiO	162
28. Detailed Calculation Data for CSiO.....	163
29. Detailed Calculation Data for C_2O	165
30. Detailed Calculation Data for Si_2O	166
31. Detailed Calculation Data for C_2SiO	168
32. Detailed Calculation Data for CSi_2O	170
33. Detailed Calculation Data for C_2Si_2O	173
34. Detailed Calculation Data for C_3O	175
35. Detailed Calculation Data for Si_3O	177
36. Detailed Calculation Data for C_3SiO	180

37. Detailed Calculation Data for CSi_3O	181
38. Detailed Calculation Data for $\text{C}_3\text{Si}_2\text{O}$	182
39. Detailed Calculation Data for $\text{C}_2\text{Si}_3\text{O}$	184
40. Detailed Calculation Data for $\text{C}_3\text{Si}_3\text{O}$	185
41. Detailed Calculation Data for C_4O	186
42. Detailed Calculation Data for Si_4O	187
43. Detailed Calculation Data for C_4SiO	189
44. Detailed Calculation Data for CSi_4O	190
45. Detailed Calculation Data for $\text{C}_4\text{Si}_2\text{O}$	191
46. Detailed Calculation Data for $\text{C}_2\text{Si}_4\text{O}$	193
47. Detailed Thermodynamics Data for C_nSi_m	199
48. Detailed Thermodynamics Data for $\text{C}_n\text{Si}_m\text{O}$	200

Abstract

Modern semiconductor devices are principally made using the element silicon. In recent years, silicon carbide (SiC), with its wide band-gap, high thermal conductivity, and radiation resistance, has shown prospects as a semiconductor material for use in high temperature and radiation environments such as jet engines and satellites. A limiting factor in the performance of many SiC semiconductor components is the presence of lattice defects formed at oxide dielectric junctions during processing. Recent theoretical work has used small quantum mechanical systems embedded in larger molecular mechanics structures to attempt to better understand SiC surfaces and bulk materials and their oxidation.

This research uses quantum mechanical models to calculate geometries and electronic properties of small $\text{Si}_m\text{C}_n\text{O}$ molecular clusters of silicon carbide oxides with $0 \leq m, n \leq 4$. Calculations are primarily done using Hartree-Fock and Density Functional Theory (DFT) with the B3LYP exchange and correlation functionals. Møller-Plesset Second Order Perturbation (MP2), Configuration Interaction (CI), Multi-Configurational Self-Consistent Field (MCSCF), and Coupled Cluster (CC) are used on the CSi_2O molecule to confirm the accuracy of selected levels of DFT. Molecular properties examined include ground state multiplicity, vibrational modes and frequencies, and geometry for both the neutral and anion, adiabatic and vertical electron affinities, and thermodynamic heats of

formation. Qualitative predictions are made regarding the photoelectron spectrum experimentalists may see. Finally, preferred geometries, functional groups, and bonding locations are qualitatively determined. Later research will be able to use these results to study the oxidation of larger SiC structures and surfaces and their defects.

QUANTUM MECHANICAL CALCULATIONS OF MONOXIDES OF SILICON CARBIDE MOLECULES

I. Introduction

1.1. Problem Statement

Modern semiconductor devices are made principally using the element silicon. In recent years, there has been interest in investigating the prospects of silicon carbide (SiC) as a semiconductor material. With its wide band-gap, high thermal conductivity, and radiation resistance, SiC has particular promise for use in high temperature and radiation environments. Such applications include devices in jet engines and satellites. An important type of semiconductor device in which SiC may be used is the MOSFET (metal-oxide semiconductor field effect transistor) which has an oxide layer on the semiconductor surface.

A limiting factor in the performance of MOSFETs and other semiconductor components is the presence of lattice defects. Recent experimental research has used photoluminescence and cathodoluminescence spectroscopy to examine the nature of SiC-SiO₂ interfaces (Li, Burggraf, *et al*, 2000; Burggraf, Weeks, Duan, 2002). Theoretical work has used small quantum mechanical systems embedded in larger molecular mechanics structures to attempt to better understand SiC surfaces and bulk material (Shoemaker, 1999; Shoemaker, 2000). To better understand the chemistry of SiC oxidation, the properties of the

oxides of SiC must be determined. The purpose of this research is to use quantum mechanical calculations to predict properties of small molecular clusters of SiC monoxides. Later research will then be able to use these results to study the oxidation of larger SiC structures and surfaces.

1.2. Background

Previous research on clusters has centered primarily on silicon, silicon oxides, and SiC. Theoretical work on silicon clusters began in the early to mid-1980s. Important early research in this area was done by Dr Raghavachari of AT&T Bell Labs (Raghavachari, 1986). He examined Si_n clusters with $n=2-7, 10$ using Hartree-Fock, Møller-Plesset Fourth Order Perturbation (MP4), and Coupled Cluster (CC) calculations. He considered many isomers of these clusters and successfully identified the ground state geometries and electronic structures.

Numerous other studies have also been done on silicon and silicon oxides. This work includes etching of silicon cations and anions by O_2 (Bergeron and Castleman, 2002), a theoretical study of Si_3O_2 and its anion using CAS-MP2 and QCISD(T) (Dupuis and Nicholas, 1999), a study of small Si_n molecules for $n=2-8$ using DFT/PW and MP4 (Fournier *et al*, 1992), an experimental study of ionization potentials for Si_n $n=2-200$ (Fuke, 1993), experimental studies of the luminescence of small silicon clusters (Kanemitsu *et al*, 1993; Kanemitsu *et al*, 1994; Kanemitsu *et al*, 1995), a theoretical study of oxygen adsorption on silicon surfaces using the semiempirical method MNDO (Oshiro *et al*, 1996), and

theoretical studies of silica clusters using DFT (Pereira *et al*, 1999a; Pereira *et al*, 1999b).

Further applicable work on silicon was done here at AFIT by Jim Shoemaker (Shoemaker, 1999; Shoemaker, 2000). He used *ab initio* clusters buried in a molecular mechanics bulk to investigate the properties of silicon surfaces. This is part of a method to eventually build up to devices. His method, surface integrated molecular orbital molecular mechanics (SIMOMM), will ultimately be used for the SiC clusters studied in this work.

There is extensive work that has been done on SiC clusters including that done by the Gordon group at Iowa State (Rintelman and Gordon, 2001) and our group at AFIT (Duan *et al*, 2002). The most applicable of this work is the 2001 thesis by Ms. Jean Henry (Henry, 2001). She successfully modeled the geometry and energy of Si_mC_n clusters with $m,n \leq 4$ using the AM1 semi-empirical method, Hartree-Fock Self-Consistent-Field theory, and Density Functional Theory. Figure 1 shows a map of the ground state singlet geometries that she produced. This map has since been updated and confirmed by Dr. Xiaofeng Duan using higher levels of theory. By determining the energy of both the neutral and singly charged anion of each molecule, she predicted the adiabatic electron affinity of each molecule. Her predicted electron affinities match those obtained experimentally by Dr. Carl Lineberger at the University of Colorado using photoelectron spectroscopy (Duan *et al*, 2002; Davico *et al*, 2001). A diagram of his experimental setup is shown as Figure 2. He produces Si_mC_n anions using a cold cathode discharge of a SiC rod. After being

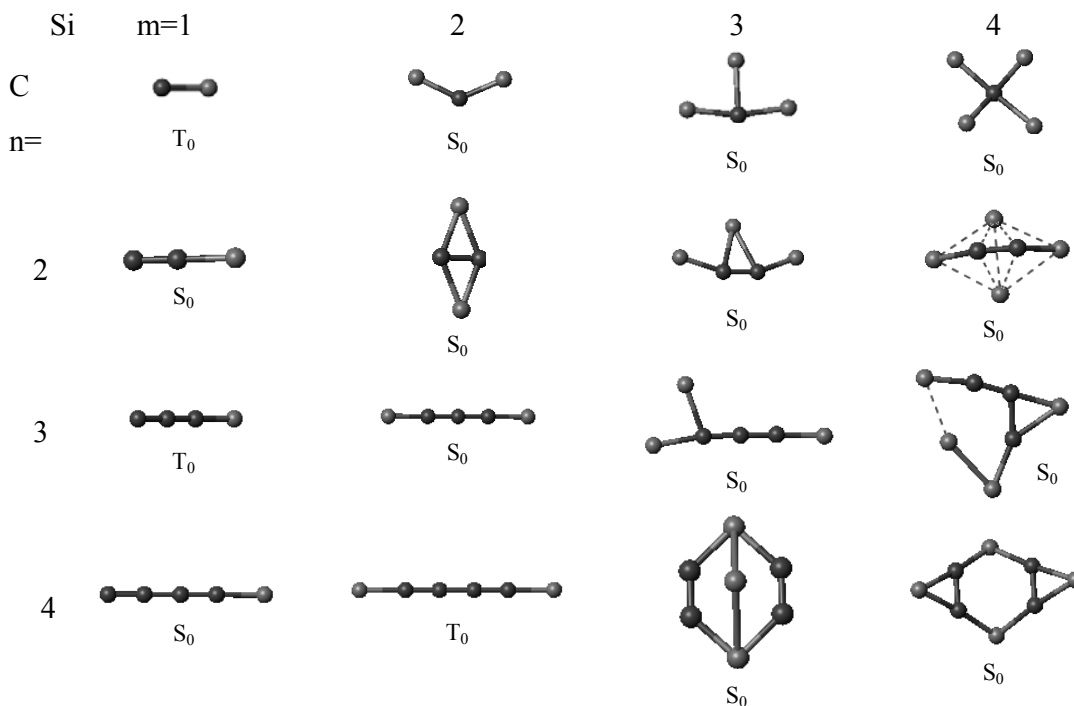


Figure 1. Map of the Ground State Geometries of Si_mC_n Clusters (Henry, 2001:63)

accelerated and mass selected, the anions interact with a laser that ejects a photoelectron and leaves the cluster with no net charge. An example of the photoelectron spectrum produced is shown in Figure 3. Peaks A-G are produced by linear C_3Si . Peak A is produced by a transition between the vibrational ground states of the anion and neutral. Peaks B-G are produced by transitions between the anion's vibrational ground state and higher vibrational states of the neutral. Most of the intensity is in Peak A, showing that the geometries of the anion and neutral are very similar.

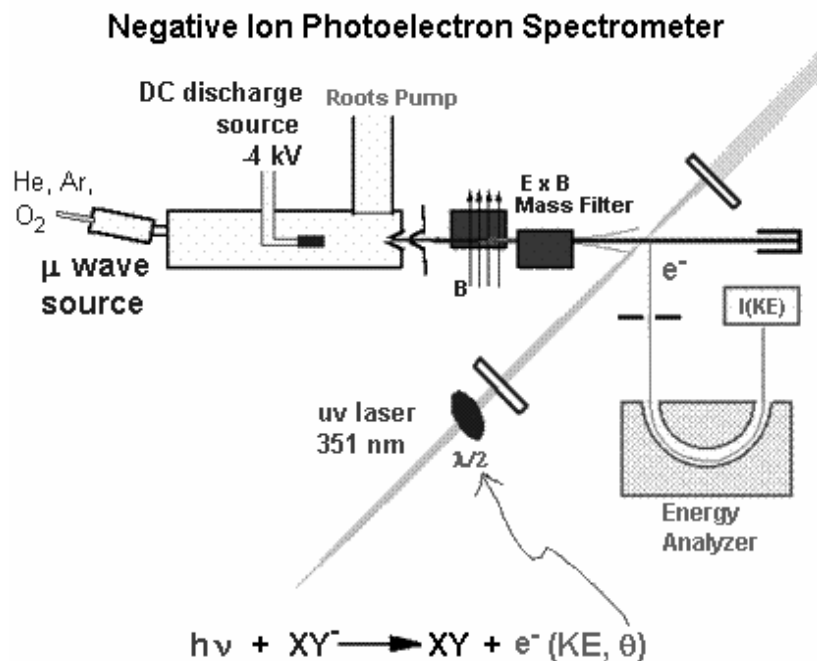


Figure 2. Photoelectron Spectroscopy Experimental Setup (Lineberger, 2002)

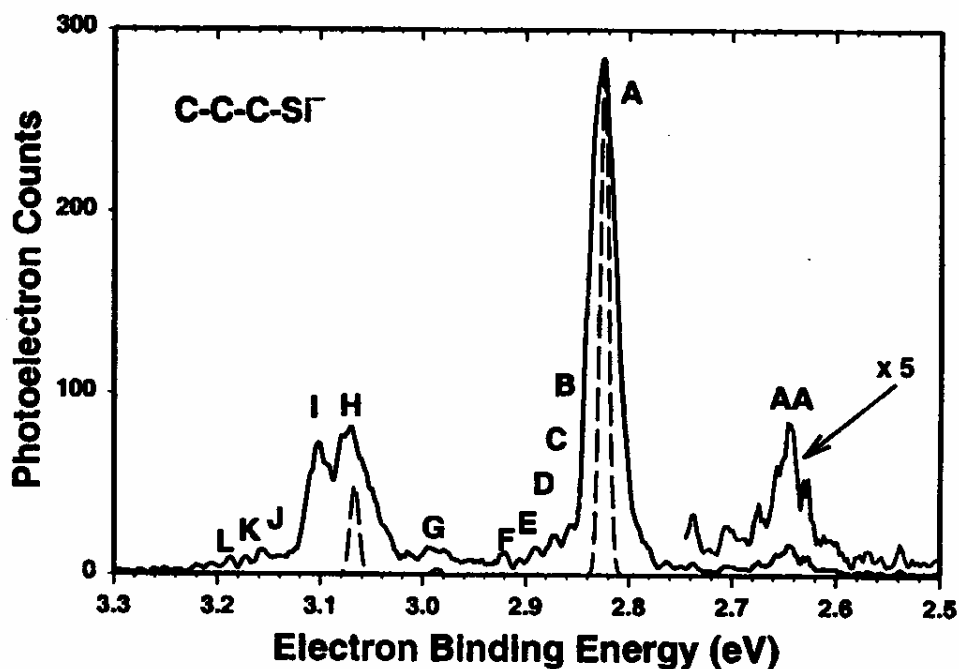


Figure 3. 364 nm photoelectron spectrum of C₃Si⁻ (Davico, 2001:1790).

The only theoretical SiC oxide cluster work has been done by the group led by Dr. Schaefer at the University of Georgia (Petraco *et al*, 2000a; Petraco *et al*, 2000b). They used high level *ab initio* calculations to determine the geometry and energy of the ground and first excited states of neutral SiCO and CSiO. This work provides a useful accuracy check for the smallest cluster that I shall consider. The only other work is unpublished surface and bulk oxidation work done by Dr. Duan at AFIT.

Experimental work on SiC oxides is also fairly limited. This includes two studies of the electron spin resonance and optical spectra of SiCO by Lembke *et al* in 1977 and 1987 (Lembke *et al*, 1977; van Zee *et al*, 1987). To date, no research that I can find has looked at clusters larger than SiCO or at any $\text{Si}_m\text{C}_n\text{O}$ anions.

1.3. Scope

This research examines $\text{Si}_m\text{C}_n\text{O}$ clusters with $0 \leq m, n \leq 4$. For each of these 25 molecules several properties will be determined. First, I will determine whether the neutral, ground state multiplicity is a singlet or triplet. Next, by examining as many isomers as is practical, I will determine the ground state geometry and energy for both the neutral and anion. These ground state geometries will be used to create ground state maps similar to Figure 1. For both the neutral and the anion the ground state, vibrational modes and frequencies will be identified. Finally, I will calculate both the adiabatic and vertical electron affinities. The vertical electron affinities and neutral vibrational frequencies will

then allow us to make some predictions regarding the expected photoelectron spectrum that Dr Lineberger will see. This research will also qualitatively determine preferred geometries, functional groups, and bonding locations.

This theoretical research will support experimental work on SiC oxides being done by Dr. Lineberger. He will use the same method previously described, but will introduce atomized oxygen into the discharge chamber. This oxygen will hopefully react with and attach itself to the silicon-carbide clusters. In this way, Dr. Lineberger will hopefully confirm the electron affinities that this current work will determine.

1.4. Research Approach

I will be using the General Atomic and Molecular Electronic Structure System (GAMESS) to do most calculations (Schmidt *et al*, 1993). Some higher level post-Hartree-Fock calculations will also use Gaussian 98 (Gaussian, 2002). Hartree-Fock calculations will be done using GAMESS and the DZV, cc-pVDZ, and aug-cc-pVDZ basis sets (Dunning and Hay, 1977; Basis sets, 2002; Dunning, 1989; Woon and Dunning, 1993; Kendall *et al*, 1992). These same basis sets will then be used in GAMESS with density functional theory (DFT) B3LYP hybrid method of exchange and correlation functionals (Becke, 1993; Stephens *et al*, 1994; Hertwig and Koch, 1997). For the CSi₂O cluster, post-Hartree-Fock calculations will be done to confirm the accuracy of the DFT calculation. These calculations include Møller-Plesset Second Order

Perturbation (MP2), Configuration Interaction (CI), Multi-Configurational Self-Consistent Field (MCSCF), and Coupled Cluster (CC).

Simple calculations on small clusters were done using my personal computer running an Athlon XP 1800 CPU and 256 Mb of PC2700 RAM using the PC version of GAMESS (Granovsky, 2002). DFT calculations on small clusters were done using an AFIT Silicon Graphics workstation. Calculations on larger clusters were performed at the Aeronautical System Center (ASC) Major Shared Resource Center (MSRC). Calculations at the MSRC were principally run in parallel on a Compaq ES40/ES45

1.5. Thesis Outline

Chapter I: Chapter one is introductory material, including a problem statement, some background material, the scope of the research, and a brief outline of the research approach.

Chapter II: The second chapter presents the theory that will be used in this research. It is divided into basic quantum mechanics, single and many electron atoms, the Hartree-Fock approximation, post-Hartree-Fock methods, and density functional theory.

Chapter III: Chapter three details the research methodology I have used. This chapter uses the Si₂CO cluster as an example of all the steps and calculations used in this research.

Chapter IV: My results are given in the fourth chapter. A map of ground state geometries is presented along with corresponding electron affinities. An analysis of preferred functional groups will also be presented.

Chapter V: The final chapter will present a summary, conclusions, and suggestions for future research.

II. Theory

2.1. Introduction

Since the beginning of the twentieth century, the study of physics and chemistry has become more and more a study of quantum mechanics. By the end of the nineteenth century, scientists studying the fields of atomic and radiation physics had reached the limit of classical physics. This limit was overcome in the first decades of the 1900s by men such as Plank, Einstein, Schrödinger, and Heisenberg who laid the foundations for and discovered quantum mechanics. Since then, quantum mechanics has been found to be the best theory to describe matter.

This chapter will give an overview of quantum mechanics and its application to the simplest atoms. It will then move to more complex polyatomic systems and explain a number of approximations and methods used to describe them. These theories will then be used in Chapter 3 to develop a method of examining the monoxide molecules of silicon carbide that are the focus of this research. The discussion assumes that the reader has a background in calculus and differential equations and has a basic understanding of fundamental physics and chemistry.

2.2. Single Particle Quantum Mechanics

(The primary references for this section are Chapters three and five of Gasiorowicz's Quantum Physics.)

The basic assumption of quantum mechanics is that the behaviors of all particles can be described by a wavefunction, $\psi(\vec{r}, t)$. When $\psi(\vec{r}, t)$ is multiplied by its complex conjugate, $\psi^*(\vec{r}, t)$ (formed by replacing every i in $\psi(\vec{r}, t)$ with $-i$), the probability of finding the particle at position \vec{r} at time t is found. The biggest step in the discovery of quantum mechanics was finding an equation which gives $\psi(\vec{r}, t)$. This was accomplished in 1926 by Erwin Schrödinger.

The fundamental equation of quantum mechanics, showing the space and time relationship of the wavefunction, is known as the Schrödinger Equation. This equation was essentially postulated by Schrödinger and cannot be derived from classical physics. The Schrödinger equation in its full form for a single particle is shown as Equation 1.

$$i\hbar \frac{\partial \psi(\vec{r}, t)}{\partial t} = -\frac{\hbar^2}{2m} \nabla^2 \psi(\vec{r}, t) + V(\vec{r}) \cdot \psi(\vec{r}, t) \quad (1)$$

where

$$\vec{r} = \text{position vector } (x \cdot \hat{i} + y \cdot \hat{j} + z \cdot \hat{k})$$

$$t = \text{time}$$

$$\psi(\vec{r}, t) = \text{probability wave function}$$

$$i = \text{imaginary number } (\sqrt{-1})$$

$$\hbar = \text{Plank's constant}/2\pi$$

$$m = \text{mass of the particle}$$

$$\nabla = \frac{\partial}{\partial x} \hat{i} + \frac{\partial}{\partial y} \hat{j} + \frac{\partial}{\partial z} \hat{k}$$

$$V(\vec{r}) = \text{external potential}$$

If the functional form of $V(\vec{r})$ is known, Schrödinger's equation can, in theory, be solved for $\psi(\vec{r}, t)$. Unfortunately, there are only a few special cases of $V(\vec{r})$ for which an analytical solution for $\psi(\vec{r}, t)$ can be found. In the next section we will look at one of the simplest solvable cases: the single electron atom, the solution of which is basic to approximate multi-electron solutions.

Before we actually solve Schrödinger's equation it will be helpful to first examine a few properties of the wavefunction. As stated earlier, a wavefunction is related to the probability of finding the particle at a certain place and time. This is expressed as a probability $P(\vec{r}, t)d^3\vec{r}$ which is the probability of finding the particle in the cube of space between \vec{r} and $\vec{r} + d^3\vec{r}$ at time t . Mathematically this is

$$P(\vec{r}, t)d^3\vec{r} = \psi^*(\vec{r}, t) \cdot \psi(\vec{r}, t)d^3\vec{r} \quad (2)$$

where

$$P(\vec{r}, t) = \text{Probability Density}$$

The probabilistic interpretation of the wavefunction leads to several restrictions on acceptable wavefunctions. First, for the probability to be sensical, it must be normalized, i.e., the probability of finding the particle somewhere must be unity. Mathematically this is

$$\int \int \int_{-\infty}^{\infty} P(\vec{r}, t)d^3\vec{r} = \int \int \int_{-\infty}^{\infty} \psi^*(\vec{r}, t) \cdot \psi(\vec{r}, t)d^3\vec{r} = 1 \quad (3)$$

Secondly, because the wavefunction appears twice in a product in the middle of Equation 3, it must be square integrable. This requires that it be continuous and equal to zero at its infinite extrema.

An important mathematical tool used extensively in quantum mechanics is operator algebra. An operator is any mathematical entity that operates on another. For instance, $\frac{d}{dx}$ is an operator which takes the derivative of whatever is to the right of it. In quantum mechanics any observable quantity can be expressed as an operator. Notationally, an operator is signified by a “hat” over the operator’s symbol, as in \hat{p} , which may be pronounced as “p hat”. The average value of an observable property represented by an operator for a given wavefunction is found by taking its expectation value. This is defined for a general function $f(x)$ as

$$\langle f(x) \rangle = \int_{-\infty}^{\infty} \psi^*(x,t) f(x) \psi(x,t) dx = \langle \psi(x,t) | f(x) | \psi(x,t) \rangle \quad (4)$$

The middle expression is in the standard integral form. The right expression is in Dirac notation, which is also called bracket notation. Bracket notation is especially useful for the large, cumbersome integrals encountered in quantum mechanics. In this notation $|\psi\rangle$ is called a “ket”. Its complex conjugate, $\langle\psi|$ is called a “bra” (hence the term “bra-ket” or “bracket” notation).

There are several operators that are especially important in using the Schrödinger equation. Their derivations are relatively straightforward and can be found in standard quantum textbooks (Gasiorowicz, 45-46,49-51,54)(Eisberg and Resnick, 144-145). These are the linear momentum (\hat{p}), energy (\hat{E}), and Hamiltonian (\hat{H}) operators given by

$$\hat{p} = -i\hbar\vec{\nabla} \quad (5)$$

$$\hat{E} = i\hbar \frac{\partial}{\partial t} \quad (6)$$

$$\hat{H} = \frac{\hat{p}^2}{2m} + V(\vec{r}) \quad (7)$$

These operators allow us to rewrite the Schrödinger equation in a simpler, more compact form as

$$\hat{H}(\vec{r})\psi(\vec{r}, t) = \hat{E}(t)\psi(\vec{r}, t) \quad (8)$$

where I have explicitly shown the position and time dependence of the operators.

To solve this equation let's assume that the wavefunction is separable in space and time (if this is an incorrect assumption it will merely give us a nonsensical answer or no answer at all):

$$\psi(\vec{r}, t) = \psi(\vec{r}) \cdot \psi(t) \quad (9)$$

Substituting this into Equation 8 gives us

$$\psi(t) \cdot \hat{H}(\vec{r})\psi(\vec{r}) = \psi(\vec{r}) \cdot \hat{E}(t)\psi(t) \quad (10)$$

If we now divide both sides by $\psi(\vec{r}) \cdot \psi(t)$ we get

$$\frac{\hat{H}(\vec{r})\psi(\vec{r})}{\psi(\vec{r})} = \frac{\hat{E}(t)\psi(t)}{\psi(t)} \quad (11)$$

The left side of Equation 11 depends only on position, while the right side depends only on time. Therefore, for the equation to hold for any position independent of time and vice versa, each side must be equal to a constant, which we call E (note the difference between this constant, E , without a hat, and the operator, \hat{E} , which has a hat). The solution of the right side

$$\hat{E}(t)\psi(t) = i\hbar \frac{d}{dt}\psi(t) = E\psi(t) \quad (12)$$

is

$$\psi(t) = C \cdot e^{\frac{iEt}{\hbar}} \quad (13)$$

where C is an undetermined constant. The left side of Equation 11 is

$$\hat{H}\psi(\vec{r}) = E\psi(\vec{r}) \quad (14)$$

or written out

$$-\frac{\hbar^2}{2m}\nabla^2\psi(\vec{r}) + V(\vec{r})\psi(\vec{r}) = E\psi(\vec{r}) \quad (15)$$

Notice that Equations 14 and 15 depend only on position. These are called the time-independent Schrödinger equation. Because the solutions we are looking for are stationary states (i.e., they are not going anywhere), from now on this is the equation that we shall use.

The time-independent Schrödinger equation is what is called an eigenvalue equation. An eigenvalue equation is one in which an operator acts on a function to return a constant, or eigenvalue, multiplied by the original function. This property of the Hamiltonian operator is key to quantum mechanics and leads to the quantization of energy.

2.3. Single Electron Atoms

(The primary references for this section and its subsections are Chapters Ten through Twelve of Gasiorowicz's Quantum Physics, Chapter Seven of

Eisberg and Resnick's Quantum Physics, and lecture notes by Dr. Dave Weeks from Chemistry 662)

We now turn to real world cases of actual atoms. We first look at the simplest case of single electron atoms known as hydrogen-like atoms. A single-electron atom is a two-body system with an electron and a nucleus with a much larger mass. Because of the large mass difference, the system can be treated as an infinitely massive and unmoving nucleus orbited by a reduced mass electron. If the mass of an electron is m and the mass of the nucleus is M , the electron's reduced mass, μ is

$$\mu = \frac{m \cdot M}{m + M} \quad (16)$$

We now have a single particle of mass μ and charge e moving in the spherically symmetric Coulombic potential field created by the nucleus of charge Ze . This creates a potential in spherical coordinates of

$$V(r) = \frac{-Ze^2}{4\pi\epsilon_0 r} \quad (17)$$

where

r = distance between electron and nucleus

Z = atomic charge of nucleus

e = elementary charge

ϵ_0 = permittivity of free space

Before we plug this potential into the Schrodinger equation and attempt to find a wavefunction, we also need to express $\bar{\nabla}^2$ in spherical coordinates to make it easier to separate the variables. The form that we will use is

$$\bar{\nabla}^2 = \frac{1}{r^2} \frac{\partial}{\partial r} \left(r^2 \frac{\partial}{\partial r} \right) + \frac{1}{r^2 \sin \theta} \frac{\partial}{\partial \theta} \left(\sin \theta \frac{\partial}{\partial \theta} \right) + \frac{1}{r^2 \sin^2 \theta} \frac{\partial^2}{\partial \varphi^2} \quad (18)$$

This can be simplified to

$$\bar{\nabla}^2 = \hat{\mathcal{R}}(r) + \frac{1}{r^2} \hat{\mathcal{L}}^2(\theta, \varphi) \quad (19)$$

where

$$\hat{\mathcal{R}}(r) = \frac{1}{r^2} \frac{\partial}{\partial r} \left(r^2 \frac{\partial}{\partial r} \right) \quad (20)$$

$$\hat{\mathcal{L}}^2(\theta, \varphi) = \frac{1}{\sin \theta} \frac{\partial}{\partial \theta} \left(\sin \theta \frac{\partial}{\partial \theta} \right) + \frac{1}{\sin^2 \theta} \frac{\partial^2}{\partial \varphi^2} \quad (21)$$

This now allows us to express the Schrödinger equation as

$$\left(-\frac{\hbar^2}{2\mu} \hat{\mathcal{R}}(r) - \frac{\hbar^2}{2\mu r^2} \hat{\mathcal{L}}^2(\theta, \varphi) - \frac{Ze^2}{4\pi\epsilon_0 r} \right) \Psi(r, \theta, \varphi) = E \Psi(r, \theta, \varphi) \quad (22)$$

We now perform a separation of variables by letting

$$\Psi(r, \theta, \varphi) = R(r)Y(\theta, \varphi) \quad (23)$$

If we substitute this into Equation 22 and multiply by $-\frac{2\mu r^2}{\hbar^2 R(r)Y(\theta, \varphi)}$ we get

$$\frac{r^2 \hat{\mathcal{R}}(r)R(r)}{R(r)} + \frac{2\mu r^2}{\hbar^2} \left(E + \frac{Ze^2}{4\pi\epsilon_0 r} \right) = \frac{-\hat{\mathcal{L}}^2(\theta, \varphi)Y(\theta, \varphi)}{Y(\theta, \varphi)} \quad (24)$$

The left side of this equation depends only on r while the right side depends only on θ and φ . Therefore each side must equal a constant which, for reasons that

will be clear later, we will call $\ell(\ell+1)$ where ℓ is a constant. This gives us two equations

$$\hat{\mathcal{R}}(r)R(r) + \frac{2\mu}{\hbar^2} \left(E + \frac{Ze^2}{4\pi\epsilon_0 r} \right) R(r) = \frac{\ell(\ell+1)R(r)}{r^2} \quad (25)$$

$$\hat{\mathcal{L}}^2(\theta, \varphi)Y(\theta, \varphi) = -\ell(\ell+1)Y(\theta, \varphi) \quad (26)$$

Equation 25 depends only on the radial variable and is called the radial equation.

Equation 26 depends only on the two angular variables and is called the angular equation. We will now solve each of these separately.

2.3.1. Angular Solution

We start the solution of the angular equation by rewriting Equation 26 in its full differential form.

$$\frac{1}{\sin\theta} \frac{\partial}{\partial\theta} \left(\sin\theta \frac{\partial Y(\theta, \varphi)}{\partial\theta} \right) + \frac{1}{\sin^2\theta} \frac{\partial^2 Y(\theta, \varphi)}{\partial\varphi^2} + \ell(\ell+1)Y(\theta, \varphi) = 0 \quad (27)$$

We now perform another separation of variables by letting

$$Y(\theta, \varphi) = \Theta(\theta) \cdot \Phi(\varphi) \quad (28)$$

If we now substitute this into Equation 28 and multiply by $\frac{\sin^2\theta}{\Theta(\theta)\Phi(\varphi)}$ we get

$$\frac{\sin\theta}{\Theta(\theta)} \frac{\partial}{\partial\theta} \left(\sin\theta \frac{\partial\Theta(\theta)}{\partial\theta} \right) + \ell(\ell+1)\sin^2(\theta) = -\frac{1}{\Phi(\varphi)} \frac{\partial^2\Phi(\varphi)}{\partial\varphi^2} \quad (29)$$

Once again the variables are separated and we can set each side equal to a constant we call m^2 . This gives us two equations to solve

$$\frac{d}{d\theta} \left(\sin \theta \frac{d\Theta}{d\theta} \right) + \left(\sin \theta \ell(\ell+1) - \frac{m^2}{\sin^2 \theta} \right) \Theta = 0 \quad (30)$$

$$\frac{d^2 \Phi}{d\varphi^2} + m^2 \Phi = 0 \quad (31)$$

which are called the polar and azimuthal equations.

We next solve the azimuthal equation. By inspection this has the solution

$$\Phi(\varphi) = e^{im\varphi} \quad (32)$$

The allowable values of m are found by using the boundary condition that $\Phi(0) = \Phi(2\pi)$. This works only for positive and negative integers, i.e.,

$$m = 0, \pm 1, \pm 2, \pm 3, \dots \quad (33)$$

Now we solve the polar equation. From Equation 30, the polar equation is significantly more complex than the azimuthal equation. Fortunately, with a simple substitution, the polar equation can be written in a form that is identified as an associated Legendre equation. The solution steps are fairly involved (the interested reader is directed to the references cited at the beginning of the section), and result in the polar equation as

$$\Theta(\theta) = \varepsilon \left[\frac{2\ell+1}{4\pi} \frac{(\ell-|m|)!}{(\ell+|m|)!} \right]^{\frac{1}{2}} P_\ell^m(\cos \theta) \quad (34)$$

where

$$P_\ell^m(w) = (1-w^2)^{\frac{|m|}{2}} \frac{d^{|m|}}{dw^{|m|}} P_\ell(w) \quad (35)$$

$$P_0(w) = 1 \quad (36)$$

$$P_1(w) = w \quad (37)$$

$$P_{\ell+1}(w) = \frac{(2\ell+1)wP_{\ell}(w) - \ell P_{\ell-1}(w)}{\ell+1} \quad (38)$$

$$\varepsilon = \begin{cases} (-1)^m & \text{for } m > 0 \\ 1 & \text{for } m \leq 0 \end{cases} \quad (39)$$

$$\ell = 0, 1, 2, \dots \quad (40)$$

$$m = -\ell, -\ell+1, \dots, 0, \dots, \ell-1, \ell \quad (41)$$

Equation 35 creates the associated Legendre polynomials which are part of the solution in Equation 34. Equation 38 is a recursion relation that uses Equations 36 and 37 to create the Legendre polynomials. Because of the derivative in Equation 35, a further restriction is made on the values of m . The new restriction is shown in Equation 41.

If we now combine the solutions of Equations 32 and 34, we obtain the complete angular solution $Y_m^{\ell}(\theta, \varphi)$. These functions are known as spherical harmonics. It is important to note that for each combination of ℓ and m a new function is obtained which is orthogonal to all other functions with different ℓ 's and m 's. Mathematically this is expressed as

$$\int_0^{2\pi} \int_0^{\pi} Y_{m'}^{\ell'*}(\theta, \varphi) Y_m^{\ell}(\theta, \varphi) \sin \theta d\theta d\varphi = \langle \ell' m' | \ell m \rangle = \delta_{\ell', \ell} \delta_{m', m} \quad (42)$$

where $\delta_{m', m}$ is the Kronekar delta function such that

$$\delta_{m', m} = \begin{cases} 1 & \text{if } m = m' \\ 0 & \text{if } m \neq m' \end{cases} \quad (43)$$

2.3.2. Radial Solution

Having solved the angular dependence of the wavefunction, we now turn to the radial function. In differential form the radial equation is

$$\left(\frac{1}{r^2} \frac{\partial}{\partial r} \left(r^2 \frac{\partial}{\partial r} \right) \right) R(r) + \frac{2\mu}{\hbar^2} \left(E + \frac{Ze^2}{4\pi\epsilon_0 r} \right) R(r) = \frac{\ell(\ell+1)R(r)}{r^2} \quad (44)$$

Simplifying the differential and collecting terms gives

$$\frac{d^2 R(r)}{dr^2} + \frac{2}{r} \frac{dR(r)}{dr} + \frac{2\mu}{\hbar^2} \left(E + \frac{Ze^2}{4\pi\epsilon_0 r} - \frac{\ell(\ell+1)\hbar^2}{2\mu r^2} \right) R(r) = 0 \quad (45)$$

The solution steps of this differential equation are rather involved; the reader interested in seeing the solution is referred to the references cited at the beginning of the section. After making appropriate substitutions and a series expansion, the radial solution is found to be

$$R_{n\ell}(r) = - \left\{ \left(\frac{2Z}{n a_0} \right)^3 \frac{(n-\ell-1)!}{2n[(n+\ell)!]^3} \right\}^{\frac{1}{2}} e^{-\frac{\rho}{2}} \rho^\ell L_{n-\ell-1}^{2\ell+1}(\rho) \quad (46)$$

where

$$a_0 = \frac{4\pi\epsilon_0 \hbar^2}{m e^2} \quad (47)$$

$$\rho = \frac{2Z}{n a_\mu} r \quad (48)$$

$$L_{n-\ell-1}^{2\ell+1}(\rho) = \sum_{k=0}^{\infty} a_k \rho^k \quad (49)$$

$$a_{k+1} = \frac{k+\ell+1-n}{(k+1)(k+2\ell+2)} a_k \quad (50)$$

$$n = 1, 2, 3, \dots \quad (51)$$

$$\ell = 0, 1, \dots, n-1 \quad (52)$$

A portion of the radial solution, shown in Equation 49, is a set of polynomials called the Laguerre polynomials. Equation 50, together with the Bohr radius of Equation 47, provides the recursion relation for the Laguerre polynomials. The solution also limits the allowable values of ℓ to those non-negative integers less than n .

2.3.3. Total Hydrogen-Like Atomic Wave Functions

(In addition to the references at the head of this section, this subsection uses material from Gasiorowicz, Chapter 17)

With Equations 32, 34, and 46 we have solutions that can be combined for a complete set of solutions. Each complete solution is defined by three quantum numbers. The first, n , is called the principal quantum number. This is what defines the energy levels since the energy,

$$E = -\frac{e^2 Z^2}{8\pi\epsilon_0 a_0 n^2} \quad (53)$$

depends only on this quantum number. Within each energy level there are n^2 states that are degenerate or have the same energy. The allowed values of n are all positive integers.

The second quantum number is the orbital quantum number ℓ . Together with the principal quantum number, ℓ determines the shape and number of nodes of the wavefunction. The allowed values of ℓ are non-negative integers less than n . The different values of ℓ are commonly associated with letters

originating in spectroscopy. $\ell = 0,1,2,3,4,5,\dots$ are referred to as s, p, d, f, g, h, ..., respectively.

The third quantum number is m . This is referred to as the magnetic quantum number since the degeneracy of these states is lifted in the presence of a magnetic field. The allowable values of $|m|$ are integers smaller than or equal to ℓ .

As stated previously, the energy states of one electron atoms depend only on n , and not ℓ or m . When other effects are considered or included as corrections to $V(\vec{r})$ in the Hamiltonian, the degeneracy of states with the same n is lifted. The first effect to consider is that the Schrödinger equation does not consider relativistic effects. When the Schrodinger equation is reformulated with relativistic considerations, the Dirac equation is obtained. The Dirac equation includes the fact that particles have a completely non-classical property called spin. As an electron moves around the nucleus its spin interacts with the magnetic field caused by the relative motion of the nucleus from the electron's perspective in an interaction called spin-orbit coupling. This splits the states, or orbitals, based upon their angular momentum which, in part, is determined by the orbitals' ℓ values. This splitting is often called fine structure splitting.

The degeneracy of orbitals with differing ℓ values is completely lifted by the Lamb shift. This is an effect of the electron interacting with its own magnetic field and quantum-vacuum fluctuations. It is an effect of quantum electrodynamics theory.

A final splitting is called hyperfine splitting. This is described by a fourth quantum number m_s , which is the spin of the electron. The allowable values for m_s are $\pm \frac{1}{2}$. Hyperfine splitting splits an orbital based on its value of m_s . This is caused by the interaction of the electron with the spin of the nucleus.

2.4. Many Electron Wave Functions

Having solved the simple case of atoms with a single electron, we now move on to atoms and molecules with two or more electrons. This is known as the many-body problem. Two-body problems such as the one we considered in the previous section are generally able to be solved in a closed analytical fashion. For example, the positions of two bodies in their mutual gravitational field can be predicted for all past and future times using equations developed by Newton. In the late 1800s Henri Poincaré proved that, except for some special cases, this can not be done for three or more bodies. Similarly, the Schrödinger equation can not be solved analytically for systems larger than the hydrogen-like atoms. For these systems we make certain simplifying approximations and find a solution numerically. This section presents these approximations and the tools and methods which will be used to solve many-electron systems.

2.4.1. Atomic Units

From the equations and solutions of the previous section, one may notice that there are a large number of constants complicating the equations. The

situation is greatly simplified by switching to a unit system called atomic units. In atomic units the charge of the electron, e ; the mass of the electron, m_e ; Planck's constant barred, \hbar ; and the dielectric constant, $4\pi\epsilon_0$, are set equal to unity. The unit of length is the bohr which is 0.529 Å. The unit of energy is the hartree which is 27.2 eV or 627.5 kcal/mol (Ratner and Schatz, 2001: back cover). For the rest of this chapter I will use atomic units to simplify the equations. In later chapters, where specific units are not specified, atomic units are assumed.

2.4.2. Many Electron Hamiltonian

(The primary references for this section and its subsections are Chapters Ten through Twelve of Gasiorowicz's Quantum Physics, Chapter Seven of Eisberg and Resnick's Quantum Physics, and lecture notes by Dr. David Weeks from Chemistry 662)

The first step in solving a molecular system using the Schrödinger equation is to define the Hamiltonian for the system. As defined previously, the general Hamiltonian is

$$\hat{H} = -\frac{1}{2m} \nabla^2 + V(\vec{r}) \quad (54)$$

For a general molecular system with N electrons and M nuclei, there are $3(M + N)$ spatial coordinates to which the second derivative must be taken. The total potential is composed of terms formed by the potential between each pair of particles. This gives us a total general Hamiltonian of

$$\hat{H} = \underbrace{-\sum_{i=1}^N \frac{1}{2} \bar{\nabla}_i^2}_{\text{Electronic Kinetic Energy}} - \underbrace{\sum_{A=1}^M \frac{1}{2M_A} \bar{\nabla}_A^2}_{\text{Nuclear Kinetic Energy}} - \underbrace{\sum_{i=1}^N \sum_{A=1}^M \frac{Z_A}{|\vec{r}_i - \vec{R}_A|}}_{\text{Electron-Nuclei Attraction}} + \underbrace{\sum_{i=1}^N \sum_{j>i}^N \frac{1}{|\vec{r}_i - \vec{r}_j|}}_{\text{Electron-Electron Repulsion}} + \underbrace{\sum_{A=1}^M \sum_{B>A}^M \frac{Z_A Z_B}{|\vec{R}_A - \vec{R}_B|}}_{\text{Nuclei-Nuclei Repulsion}} \quad (55)$$

where

$$N = \text{number of electrons} \quad (56)$$

$$M = \text{number of nuclei} \quad (57)$$

$$\bar{\nabla}_i^2 = \text{Laplacian with respect to spatial coordinates of } i \text{ th electron} \quad (58)$$

$$\bar{\nabla}_A^2 = \text{Laplacian with respect to spatial coordinates of } A \text{ th nuclei} \quad (59)$$

$$M_A = \text{mass of } A \text{ th nuclei (in atomic units)} \quad (60)$$

$$Z_A = \text{atomic number of } A \text{ th nuclei} \quad (61)$$

$$\vec{r}_i = \text{spatial position of } i \text{ th electron} \quad (62)$$

$$\vec{R}_A = \text{spatial position of } A \text{ th nuclei} \quad (63)$$

(Szabo and Ostlund, 1996, 40-41).

2.4.3. Born-Oppenheimer Approximation

If we examine Equation 55, we see that the Hamiltonian has a total of

$$3N + 3M + NM + \frac{N^2}{2} + \frac{M^2}{2} \text{ terms for each possible spatial configuration of}$$

electrons and nuclei. To make a solution more manageable, we start by making some approximations to reduce the number of terms.

For the first approximation, we consider the difference in mass between an electron and nucleus. Even the lightest nucleus is more than 1800 times

more massive than an electron. Because of this large difference in mass, nuclei move much slower than electrons. Therefore, we can consider the nuclei to be fixed and immovable with the electrons moving through the field setup by the nuclei. This approximation is called the Born-Oppenheimer approximation.

Since the nuclei are not moving, the second term in Equation 55 is zero. In addition, the fifth term, which gives the nuclear-nuclear repulsion, is a constant. Removing these two terms makes the problem significantly more manageable. The remaining three terms make up what is called the electronic Hamiltonian.

2.4.4. Potential Energy Surfaces

While the Born-Oppenheimer approximation allows us to more easily calculate the energy for a system at a fixed nuclear geometry, we are left with the question of what happens as the nuclear geometry is varied. To examine this, we start by examining the simplest molecular system of H_2^+ . This ion has one electron and two hydrogen nuclei. For this molecule, a single variable, the nuclear separation, can specify the nuclear geometry. The number of variables, or reaction coordinates, required to specify a given nuclear geometry depends on the number of nuclei. In general M nuclei require $3M - 6$ reaction coordinates to completely specify their geometry. For a linear molecule, including all diatoms, $3M - 5$ reaction coordinates are required. If the molecule has symmetry, fewer coordinates are required.

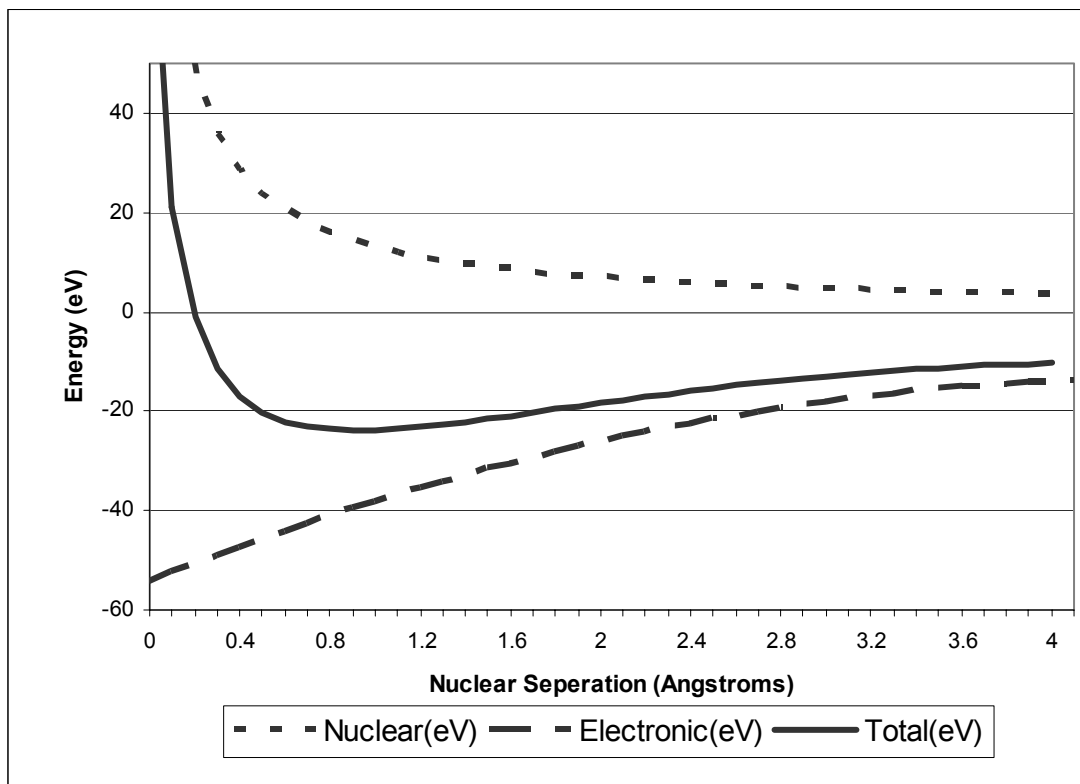


Figure 4. Potential Energy Curve for H_2^+

The energy of H_2^+ is composed of two components shown in Figure 4. The first component is the nuclear-nuclear repulsion energy. When the nuclei are close together the energy is very high. As they get further apart the energy quickly decreases, eventually reaching zero. The second component is the electronic energy. When the nuclei are far apart, the electron is essentially bound to one of them and the energy is simply that of a single hydrogen atom, -13.6 eV. When the nuclei are very close together, they appear to the electron like a helium nucleus and the energy is that of helium, -54.4 eV. When these two components are added together, the curve produced starts out high, quickly

decreases to a minimum around 1 Å, and then gradually increases, asymptotically reaching -13.6 eV. The molecule is most stable when the nuclear separation is such that the energy is minimized, since if it is displaced in either direction from the minima, it will quickly be returned to the minima.

The total curve in Figure 4 is called a potential energy curve. For molecules with more than one reaction coordinate, a potential energy surface is formed. In general, any molecule with more than two nuclei will require more than three dimensions to plot the energy and the reaction coordinates, making it essentially unplottable and unimaginable.

A potential energy curve or surface may have one, many, or no minima. If there is only one, that will be the stable geometry. If there are multiple minima, there will be multiple stable configurations called isomers. In this case the global minimum will be the most stable isomer. If there are none, the molecule is not stable and will dissociate into other molecules and/or atoms.

2.4.5. Molecular Vibration and Rotation

The minima of the potential energy curve is the geometry where the molecule is most stable, but the molecule still has motion at the minima. Due to quantization, the lowest allowable energy level is somewhere above the minima. This energy level is called the zero-point energy. Above this, there are additional energy levels which have their energy stored in nuclear motion.

There are three types of nuclear motion: translational, vibrational, and rotational. The first, translational, is motion of the entire molecule. This is the

kinetic energy of the molecule and is measured only relative to an external point. While this is important for thermodynamics, we are concerned only with energy internal to the molecule's frame of reference.

The second energy is vibrational energy. As its name indicates, this is from the vibration of atoms about the equilibrium point of the potential energy minima. Classically, this motion is analogous to that of a weight on a frictionless, massless spring, since it is approximately symmetric about the minimum. This situation is known as a harmonic oscillator. The harmonic oscillator is one of the few quantum mechanical problems for which a solution is obtainable. From this solution, the allowable energy levels are found to be (in atomic units)

$$E_{vib} \approx \left(n_v + \frac{1}{2} \right) \sqrt{\frac{1}{4M}} \quad (64)$$

(Gasiorowicz, 1996: 338). These levels are generally on the order of tens of meV's. An important thing to note is that the lowest level is with $n_v = 0$ which is slightly above the bottom of the minimum. This is called the zero point energy.

The final form of energy is rotational energy. This is from rotations of the atoms around the bond. For this energy, the molecule is treated as a rigid rotor similar to a dumbbell. The energy obtained is

$$E_{rot} \approx \frac{n_r(n_r + 1)}{4M} \quad (65)$$

(Gasiorowicz, 1996: 336-337). These rotational levels exist for each of the vibrational levels. The energy of the rotational states is in the sub-meV range.

Seeing individual rotational energy levels requires very high resolution spectroscopic equipment. Rotational states are not considered in this research.

2.4.6. Variational Principle

(The primary reference for this subsection is Ratner and Schatz pp 105-106)

An important theorem for the calculation of wavefunctions and quantum mechanical properties is the variational principle. This principle states that if φ is a normalized wavefunction that fits the problem's boundary conditions, but not necessarily an eigenfunction of the Hamiltonian, the energy associated with it, E_{trial} , will be greater than or equal to the ground state energy, E_0 , of the system.

This is shown in Equation 66.

$$E_{trial} = \langle \varphi | \hat{H} | \varphi \rangle \geq E_0 \quad (66)$$

The importance of this theorem is that for any wavefunction, the energy will always be higher than the actual energy unless the wavefunction is the exact wavefunction. This gives us a measure of the quality of a wavefunction: the lower the energy, the better the wavefunction. It also allows a method of improving a given wavefunction. If the wavefunction depends on a parameter α , the best value of α is the one for which E_{trial} is minimized; i.e.,

$$\frac{\partial E_{trial}}{\partial \alpha} = 0 \quad (67)$$

2.4.7. Pauli Exclusion Principle, Aufbau Principle, and Multiplicity

As we have seen, exact solutions to the Schrödinger Equation produce an infinite number of energy levels or orbitals. This presents the question of how electrons fill these orbitals. For atoms, it is easiest and relatively accurate to assume that they have a hydrogen-like orbital structure. Therefore, the orbitals are designated as 1s, 2s, 2p, 3s, 3p, 3d, etc. where there is one 's' orbital per n, three 'p' orbitals per n, five 'd' orbitals per n, and so on. The number of electrons that can be put into a single orbital is determined by the Pauli exclusion principle. This states that for the class of particles called fermions, which includes electrons, only one can be in any given state at a time. Each orbital is defined by the three quantum numbers n , ℓ , and m . In addition to these, there is one remaining quantum number that defines the state of an electron: the spin, m_s .

This has two allowable values of $\pm \frac{1}{2}$. Each orbital can therefore hold up to two electrons of opposite spin.

The order that electrons fill orbitals is determined by the *Aufbau* principle. This states that electrons fill the lowest energy orbitals first. This makes the order of filling orbitals 1s, 2s, 2p, 3s, 3p, 4s, 3d, 4p, etc. This principle is responsible for the shape of the periodic table.

While the *Aufbau* principle holds very well for small atoms, there are some larger atoms and molecules that do not fill orbitals in their *Aufbau* order. For example, copper should have two 4s and nine 3d electrons. Instead, it has one 4s and ten 3d electrons. This is because the full 3d shell in the latter

configuration is slightly lower in energy than a full 4s shell in the former.

Similarly, with molecules, electrons do not always add in pairs or in the order expected. This can affect what is known as the multiplicity of an atom or molecule. Multiplicity is determined by the formula $2s + 1$ where s is the net absolute spin of the atom or molecule. This is determined by adding together the spin of all the orbitals in the atom or molecule. Orbitals that are filled with a pair of electrons have no net spin, since the electrons have opposite spin. Orbitals that have only one electron have net spin of $\frac{1}{2}$. If all of the orbitals are filled with pairs, there is no net spin and the multiplicity is a singlet. If there is a single unpaired electron, the net spin is $\frac{1}{2}$ and the multiplicity is a doublet. For atoms or molecules that have two unpaired electrons the multiplicity is a triplet, and so on. The name comes from the number of possible spin states the atom or molecule can have. For instance, a triplet has total net absolute spin of 1. But there are four ways the two unpaired electrons can be oriented. If they are both spin up ($+\frac{1}{2}$), the spin is 1. If they are both spin down ($-\frac{1}{2}$), the spin is -1. If one is up and the other is down, the spin is 0. In the presence of a magnetic field these three states have different energies and will produce three separate spectroscopic lines.

2.4.8. Perturbation Theory

(The primary references for this subsection are Ratner and Schatz pp 82-83, Bernath pp 96-98, and Gasiorowicz Chapter 16.)

As stated previously, most systems and potentials do not have analytic solutions. In order to obtain relatively accurate estimates for these systems, certain approximation techniques can be used. One of these methods is perturbation theory.

We start by breaking the Hamiltonian into two pieces.

$$\hat{H} = \hat{H}_0 + \lambda \hat{V} \quad (68)$$

The first is \hat{H}_0 which has solutions $\varphi_n^{(0)}$ and energies $E_n^{(0)}$ that can be found.

$$\hat{H}_0 \varphi_n^{(0)} = E_n^{(0)} \varphi_n^{(0)} \quad (69)$$

The next step is to apply a perturbation that is small relative to the first part. λ is a parameter that we use for the method.

Next, we do a series expansion of the actual, exact wavefunction, ψ_n , and energy, E_n , in terms of λ and φ_n :

$$\psi_n = \varphi_n^{(0)} + \lambda \varphi_n^{(1)} + \lambda^2 \varphi_n^{(2)} + \lambda^3 \varphi_n^{(3)} + \dots \quad (70)$$

$$E_n = E_n^{(0)} + \lambda E_n^{(1)} + \lambda^2 E_n^{(2)} + \lambda^3 E_n^{(3)} + \dots \quad (71)$$

Now, we substitute these into

$$\hat{H} \psi_n = E_n \psi_n \quad (72)$$

and equate like powers of λ . This gives us a system of equations

$$\hat{H}_0 \varphi_n^{(0)} = E_n^{(0)} \varphi_n^{(0)} \quad (73)$$

$$\hat{V}\varphi_n^{(0)} + \hat{H}_0\varphi_n^{(1)} = E_n^{(1)}\varphi_n^{(0)} + E_n^{(0)}\varphi_n^{(1)} \quad (74)$$

⋮

$$\hat{V}\varphi_n^{(j-1)} + \hat{H}_0\varphi_n^{(j)} = \sum_{k=0}^j E_n^{(k)}\varphi_n^{(j-k)} \quad (75)$$

Equation 73 is simply our given of Equation 68. To solve Equation 74, we expand $\varphi_n^{(1)}$ in terms of $\varphi_k^{(0)}$:

$$\varphi_n^{(1)} = \sum_{k \neq n} C_{nk}^{(1)}\varphi_k^{(0)} \quad (76)$$

We now substitute Equation 76 into Equation 74, switch to Dirac notation, and multiply by $\langle \varphi_n^{(0)} |$ to get

$$\langle \varphi_n^{(0)} | \hat{V} | \varphi_n^{(0)} \rangle + \langle \varphi_n^{(0)} | \hat{H}_0 \sum_{k \neq n} C_{nk}^{(1)} | \varphi_k^{(0)} \rangle = \langle \varphi_n^{(0)} | E_n^{(1)} | \varphi_n^{(0)} \rangle + \langle \varphi_n^{(0)} | E_n^{(0)} \sum_{k \neq n} C_{nk}^{(1)} | \varphi_k^{(0)} \rangle \quad (77)$$

Since

$$\langle \varphi_n^{(0)} | \varphi_k^{(0)} \rangle = \delta_{n,k} \quad (78)$$

Equation 77 can be simplified to

$$\langle \varphi_n^{(0)} | \hat{V} | \varphi_n^{(0)} \rangle = E_n^{(1)} \quad (79)$$

If we now substitute Equation 76 into Equation 74, switch to Dirac notation, and multiply by $\langle \varphi_j^{(0)} |$, we get

$$\langle \varphi_j^{(0)} | \hat{V} | \varphi_n^{(0)} \rangle + \langle \varphi_j^{(0)} | \hat{H}_0 \sum_{k \neq n} C_{nk}^{(1)} | \varphi_k^{(0)} \rangle = \langle \varphi_j^{(0)} | E_n^{(1)} | \varphi_n^{(0)} \rangle + \langle \varphi_j^{(0)} | E_n^{(0)} \sum_{k \neq n} C_{nk}^{(1)} | \varphi_k^{(0)} \rangle \quad (80)$$

which simplifies to

$$\langle \varphi_j^{(0)} | \hat{V} | \varphi_n^{(0)} \rangle + E_j^{(0)} C_{nj}^{(1)} = E_n^{(0)} C_{nj}^{(1)} \quad (81)$$

This can then be solved for $C_{nj}^{(1)}$

$$C_{nj}^{(1)} = \frac{\langle \varphi_j^{(0)} | \hat{V} | \varphi_n^{(0)} \rangle}{E_n^{(0)} - E_j^{(0)}} \quad \text{for } (j \neq n) \quad (82)$$

Similar methods can be done for the higher order perturbation terms. In general, the more higher order terms that are included, the more accurate the solution.

2.4.9. Self Consistent Field (SCF)

Many of the equations we will develop in the next section are not easily solvable. Obtaining a solution often requires some special mathematical tricks. One of these is the self consistent field method. This is an iterative method where an initial guess is made, the equation is solved, this solution becomes the new guess, the equation is solved, and so on. This process is repeated until the guess and the solution are the same or differ by less than some tolerance.

As an very simple mathematical example, we solve the equation $e^x = 1$. By inspection the solution is $x = 0$, but if we rearrange it and add x to either side to get $x = x - e^x + 1$, we can use an SCF to solve it. We start with a guess of $x = 2$ which we put into the right side of the equation to get $x = -4.389$. The iterations are shown in Table 1. Within ten iterations the correct solution is obtained to within fifteen decimal places.

Many of the methods developed in the following section are solved in a similar manner. In these instances, we guess a set of initial orbitals, and then

Table 1. SCF Iterations for $x = x - e^x + 1$

Iteratio n	x
0	2.0000000000000000
1	-4.389056098930650
2	-3.401468538738610
3	-2.434792834728060
4	-1.522408730867070
5	-0.740594433718539
6	-0.217424820918350
7	-0.022012911758287
8	-0.000240516089578
9	-0.000000028921676
10	0.0000000000000000
11	0.0000000000000000
12	0.0000000000000000

solve iteratively until we reach some tolerance. The result is a wavefunction solution to the equations we are using.

2.4.10. Basis Sets

(The primary reference is class notes prepared for CHEM 662 by Dr Alan Yeates and Ratner and Schatz pp 165-167.)

Another important method to approximating a function that we have already used is expanding it in terms of another set of functions. If the set of other functions, known as a basis set, is a complete set, the function we are looking for can be exactly expressed. As an example, the set of functions $1, x, x^2, x^3, \dots$ is a complete basis set and a function such as e^x can be expanded in terms of these as $e^x = 1 + x + \frac{x^2}{2!} + \frac{x^3}{3!} + \frac{x^4}{4!} + \dots$. Unfortunately, this requires an

infinite number of basis functions to exactly express the other function and is therefore impossible to fully implement for a calculation. While truncating the expansion at some point does not give the exact answer, the answer produced can get relatively close if the expansion is large enough. Therefore, since a larger expansion requires more calculation time and effort, the key is to choose the basis functions such that as few as possible are needed to get an answer that is as accurate as wanted. Toward this end, special sets of functions have been developed which allow accurate calculation of wavefunctions while keeping the size of the expansion reasonable. Once the basis set is chosen, the only remaining problem to solve is to find the coefficient in front of each individual basis function.

The first type of basis set is the Slater-type orbitals (STOs). These have an exponential form of

$$\xi_{nlm} = Nr^{n-1}e^{-\zeta r}Y_{lm}(\theta, \varphi) \quad (83)$$

where

$$\xi = \text{basis function} \quad (84)$$

$$N = \text{normalization constant} \quad (85)$$

$$\zeta = \text{orbital exponent} \quad (86)$$

STOs are similar to hydrogen wavefunctions without the complicated radial nodal structure. Due to the r^{n-1} term, STOs go to infinity at the nucleus, which makes them very difficult to integrate. In general, these do not accurately reproduce the wavefunction near or far from the nucleus.

A second type of basis set is the Gaussian-type orbitals (GTOs). These are Gaussian functions centered on the nucleus of the form

$$\xi_{\zeta} = Nx^a y^b z^c e^{-\zeta r^2} \quad a, b, c > 0 \quad (87)$$

GTOs are much easier to integrate since the product of two or more Gaussians is another gaussian, but a single GTO, known as a primitive gaussian, generally does not accurately reproduce an actual wavefunction. Instead, GTOs are usually put together in linear combinations called a contracted gaussian. The fixed coefficients used to make the linear combination are called contraction coefficients. By choosing the right primitives for the linear combination, a GTO can be made that accurately reproduces actual wavefunctions. GTOs are the most common type of orbitals and the only type used in this research.

While most basis sets use GTOs, the way they are used varies. A minimal basis set uses only one contracted GTO for each atomic shell. Higher zeta basis sets such as the double-zeta or triple-zeta use more contracted GTOs per atomic shell (in these cases two or three).

Many basis sets add extra basis functions to the main part of the set. One of these is polarization functions. These are Gaussian functions with high angular momentum so that electrons involved in a bond between atoms of differing electronegativity are skewed toward the more electronegative atom. The *cc-p* which appears in basis sets such as cc-pVDZ means that correlation-consistent polarization functions with higher angular momentum have been added to an orbital. For instance a p orbital will have d or f functions added to it.

Another type of function often added to a basis set is diffuse functions. These are Gaussian functions with small exponential coefficients, ζ , which allow for electron densities far from the nuclei. These are especially important for anions and electronically excited states. The *aug-* which appears in basis sets such as aug-cc-pVDZ means that diffuse functions have been added.

The contraction coefficients and orbital exponents are variationally optimized for each element. Once this is done, sets of basis sets for groups of elements are published for general use. Favorite sets are the STO-#G (which use contracted GTOs to approximate STOs), Pople sets, Atomic Natural Orbitals (ANOs) (good for post-Hartree-Fock calculations), and Dunning sets. In this research, I use Dunning sets exclusively. Collections of basis sets can be found online at <http://www.emsl.pnl.gov:2080/forms/basisform.html>.

2.4.11. Spin Orbitals

(The primary references for this subsection are Ratner and Schatz pp 110-129 and Szabo and Ostlund pp 46-53.)

The final topic we must look at before examining the calculational theory that we will use is the type of orbitals that we will use. The first thing we must note is the presence of electron spin and the Pauli Exclusion Principle. We have already noted that electrons can be either spin up or spin down. Mathematically, we denote these respectively as α_n and β_n , where the subscript indicates which electron it is applied to. As an example, we consider the He atom. This has two electrons whose spatial wavefunctions in the He ground state can be

represented by hydrogen-like 1s orbitals. As previously stated, the Pauli Exclusion Principle requires that these two electrons have differing spin. This gives two possible total wavefunctions:

$$\Psi = \varphi_{1s}(1)\alpha_1\varphi_{1s}(2)\beta_2 \quad (88)$$

$$\Psi = \varphi_{1s}(1)\beta_1\varphi_{1s}(2)\alpha_2 \quad (89)$$

where the number in parentheses after the spatial wavefunctions indicates the electron to which they apply. Unfortunately, neither of these two wavefunctions satisfy another requirement of the Pauli Exclusion Principle. This requires that for a fermion, such as an electron, exchanging two particles changes the sign of the wavefunction. A proper wavefunction can be made from Equations 88 and 89 by a process called antisymmetrization. This produces a wavefunction of the form

$$\Psi = \frac{1}{\sqrt{2}} \varphi_{1s}(1)\varphi_{1s}(2)(\alpha_1\beta_2 - \beta_1\alpha_2) \quad (90)$$

For larger systems, antisymmetrization is easily done with a Slater determinant. This is the determinant of a matrix formed with the possible states making up the different columns and each electron in a different row. As an example of a larger system, the Be ground state produces a wavefunction

$$\Psi(Be) = \frac{1}{\sqrt{4!}} \begin{vmatrix} \varphi_{1s}(1)\alpha_1 & \varphi_{1s}(1)\beta_1 & \varphi_{2s}(1)\alpha_1 & \varphi_{2s}(1)\beta_1 \\ \varphi_{1s}(2)\alpha_2 & \varphi_{1s}(2)\beta_2 & \varphi_{2s}(2)\alpha_2 & \varphi_{2s}(2)\beta_2 \\ \varphi_{1s}(3)\alpha_3 & \varphi_{1s}(3)\beta_3 & \varphi_{2s}(3)\alpha_3 & \varphi_{2s}(3)\beta_3 \\ \varphi_{1s}(4)\alpha_4 & \varphi_{1s}(4)\beta_4 & \varphi_{2s}(4)\alpha_4 & \varphi_{2s}(4)\beta_4 \end{vmatrix} \quad (91)$$

The determinant in Equation 91 will also be denoted in the simpler notation

$$\Psi(Be) = \frac{1}{\sqrt{4!}} |\varphi_{1s} \bar{\varphi}_{1s} \varphi_{2s} \bar{\varphi}_{2s}| \quad (92)$$

where the bar over a wavefunction denotes that it is a β spin state.

2.5. Hartree-Fock (HF) Approximation

(The primary references for this section are Ratner and Schatz pp 130-134, Szabo and Ostlund pp 108-131, and class notes prepared for CHEM 662 by Dr Alan Yeates.)

We are now prepared to develop the theories we will use in the calculations. We start with the electronic Hamiltonian that we developed in Section 2.4.3.

$$\hat{H} = \sum_{i=1}^n h_i + \frac{1}{2} \sum_{i \neq j=1}^n \frac{1}{r_{ij}} \quad (93)$$

where

$$h_i = -\frac{1}{2} \bar{\nabla}_i^2 - \sum_{A=1}^M \frac{Z_A}{|\vec{r}_i - \vec{R}_A|} \quad (94)$$

$$r_{ij} = |\vec{r}_i - \vec{r}_j| \quad (95)$$

We now consider a three electron wavefunction

$$\Psi(1,2,3) = \frac{1}{\sqrt{3!}} |a \ b \ c| \quad (96)$$

$$\Psi(1,2,3) = \frac{1}{\sqrt{6}} \begin{bmatrix} a(1)b(2)c(3) + b(1)c(2)a(3) + c(1)a(2)b(3) \\ -c(1)b(2)a(3) - b(1)a(2)c(3) - a(1)c(2)b(3) \end{bmatrix} \quad (97)$$

By definition the energy of this system is

$$E = \langle \Psi(1,2,3) | \hat{H} | \Psi(1,2,3) \rangle \quad (98)$$

We first consider the h_i terms. The wavefunction on each side of the Hamiltonian in Equation 98 has six terms, while there are three h_i s. This gives 108 separate integrals that must be performed. For simplicity, we start by considering only $i = 1$. This gives us

$$\langle h_1 \rangle \equiv \langle \Psi(1,2,3) | \hat{h}_1 | \Psi(1,2,3) \rangle \quad (99)$$

$$\langle h_1 \rangle = \frac{1}{6} \left[\begin{array}{l} \langle a(1)b(2)c(3) | h_1 | a(1)b(2)c(3) \rangle + \langle a(1)b(2)c(3) | h_1 | b(1)c(2)a(3) \rangle \\ + \langle a(1)b(2)c(3) | h_1 | c(1)a(2)b(3) \rangle - \langle a(1)b(2)c(3) | h_1 | c(1)b(2)a(3) \rangle \\ - \dots \end{array} \right] \quad (100)$$

Because h_i operates only on wavefunctions of electron one, the terms in the bracket can be simplified by separating the integrals of each term by electron. For the first term this gives us

$$\langle a(1)b(2)c(3) | h_1 | a(1)b(2)c(3) \rangle = \langle a(1) | h_1 | a(1) \rangle \langle b(2) | b(2) \rangle \langle c(3) | c(3) \rangle \quad (101)$$

The right side of this simplifies to

$$\langle a(1) | h_1 | a(1) \rangle \equiv h_a \quad (102)$$

For the second h_i term,

$$\langle a(1)b(2)c(3) | h_1 | b(1)c(2)a(3) \rangle = \langle a(1) | h_1 | b(1) \rangle \langle b(2) | c(2) \rangle \langle c(3) | a(3) \rangle \quad (103)$$

The second and third integral on the right side of this are both zero. Similarly all terms that do not couple terms of the same electron are zero. Since h_a can also be obtained from the

$$\langle a(1)c(2)b(3) | h_1 | a(1)c(2)b(3) \rangle = \langle a(1) | h_1 | a(1) \rangle \langle c(2) | c(2) \rangle \langle b(3) | b(3) \rangle \quad (104)$$

term and h_b and h_c terms also survive

$$\langle h_1 \rangle = \frac{1}{6}[2h_a + 2h_b + 2h_c] \quad (105)$$

Now we look at the other $\langle h_i \rangle$'s. These all have the same form as $\langle h_1 \rangle$.

Therefore,

$$\langle h_1 \rangle = \langle h_2 \rangle = \langle h_3 \rangle \quad (106)$$

and

$$\langle \Psi(1,2,3) | \sum_{i=1}^3 h_i | \Psi(1,2,3) \rangle = \frac{1}{6}[6h_a + 6h_b + 6h_c] \quad (107)$$

Next we turn to the $\frac{1}{r_{ij}}$ term in the Hamiltonian. We start by looking at

$$\frac{1}{r_{12}}.$$

$$\langle r_{12}^{-1} \rangle \equiv \langle \Psi(1,2,3) | \frac{1}{r_{12}} | \Psi(1,2,3) \rangle \quad (108)$$

$$\langle r_{12}^{-1} \rangle = \frac{1}{6} \left[\begin{aligned} & \langle a(1)b(2)c(3) | \frac{1}{r_{12}} | a(1)b(2)c(3) \rangle + \langle a(1)b(2)c(3) | \frac{1}{r_{12}} | b(1)c(2)a(3) \rangle \\ & + \langle a(1)b(2)c(3) | \frac{1}{r_{12}} | c(1)a(2)b(3) \rangle - \langle a(1)b(2)c(3) | \frac{1}{r_{12}} | c(1)b(2)a(3) \rangle \\ & - \dots \end{aligned} \right] \quad (109)$$

Because r_{12}^{-1} operates only on wavefunctions of electrons one and two, the terms in the bracket can be simplified by again separating the integrals of each term by electron. For the first term this gives us

$$\langle a(1)b(2)c(3) | r_{12}^{-1} | a(1)b(2)c(3) \rangle = \langle a(1)b(2) | r_{12}^{-1} | a(1)b(2) \rangle \langle c(3) | c(3) \rangle \quad (110)$$

The right side of this simplifies to

$$\langle a(1)b(2) | r_{12}^{-1} | a(1)b(2) \rangle \equiv T_{12}(ab|ab) \quad (111)$$

For the second h_i term,

$$\langle a(1)b(2)c(3) | h_1 | b(1)c(2)a(3) \rangle = \langle a(1)b(2) | r_{12}^{-1} | b(1)c(2) \rangle \langle c(3) | a(3) \rangle \quad (112)$$

The final integral on the right side of this is zero. Similarly all terms that do not couple terms of the same electron are zero. $T_{12}(ab|ab)$ can also be obtained from the

$$\langle b(1)a(2)c(3) | r_{12}^{-1} | b(1)a(2)c(3) \rangle = \langle b(1)a(2) | r_{12}^{-1} | b(1)a(2) \rangle \langle c(3) | c(3) \rangle \quad (113)$$

term. It is important to note that

$$\langle a(1)b(2)c(3) | r_{12}^{-1} | b(1)a(2)c(3) \rangle = \langle a(1)b(2) | r_{12}^{-1} | b(1)a(2) \rangle \langle c(3) | c(3) \rangle \equiv T_{12}(ab|ba) \quad (114)$$

is a different term and is not the same as $T_{12}(ab|ab)$. The standard notation for these is

$$T_{12}(ab|ab) \equiv J_{ab} \quad (115)$$

which is called the Coulomb integral and

$$T_{12}(ab|ba) \equiv K_{ab} \quad (116)$$

which is called the exchange integral.

As before, T_{bc} and T_{ac} terms also survive. Since all r_{ij}^{-1} all have the same form

as r_{12}^{-1} ,

$$\langle r_{12}^{-1} \rangle = \langle r_{23}^{-1} \rangle = \langle r_{13}^{-1} \rangle \quad (117)$$

In addition,

$$J_{ab} = J_{ba}, \quad K_{ab} = K_{ba}, \quad \text{and} \quad J_{aa} = K_{aa} \quad (118)$$

This gives us

$$\langle \Psi(1,2,3) | \sum_{i \neq j=1}^3 r_{ij}^{-1} | \Psi(1,2,3) \rangle = \frac{1}{2} \frac{1}{6} [6J_{ab} + 6J_{bc} + 6J_{ac} - 6K_{ab} - 6K_{bc} - 6K_{ac}] \quad (119)$$

$$\langle \Psi(1,2,3) | \sum_{i \neq j=1}^3 r_{ij}^{-1} | \Psi(1,2,3) \rangle = \frac{1}{2} \sum_{m,n} (J_{mn} - K_{mn}) \quad \text{for } m,n = a,b,c \quad (120)$$

For the general case

$$E = \sum_{i=1}^n \langle \varphi_i | h_i | \varphi_i \rangle + \sum_{i=1}^n \sum_{j>i}^n (J_{ij} - K_{ij}) \quad (121)$$

For an individual orbital φ_i , we can define an operator, which we call the Fock operator

$$\hat{f}(i) \equiv h(i) + \sum_j [J_j(i) - \hat{K}_j(i)] \quad (122)$$

This allows us to create an eigenvalue equation

$$\hat{f}|\varphi_i\rangle = \varepsilon_i|\varphi_i\rangle \quad (123)$$

which is called the Hartree-Fock equation. Unfortunately, this is not a standard eigenvalue equation since the Fock operator itself depends on the orbitals used. This makes it a highly nonlinear equation. To solve the Hartree-Fock equation, basis sets are used to create a set of initial wavefunctions. The equation is then solved using the SCF method.

The method exactly as described above is called an unrestricted Hartree-Fock or UHF calculation. UHF calculations have the problem of orbitals differing only by their spin ending up with different energies. This result is generally

incorrect and is called spin contamination. To correct this, another method called restricted Hartree-Fock or RHF forces orbitals differing only by their spin to have the same energy. RHF works only for singlet states but the more general restricted open-shell Hartree-Fock or ROHF works for all multiplicities.

2.6. Post-Hartree-Fock Methods

The Hartree-Fock method produces energies and properties that are reasonably accurate for some uses, which is good since it is a fairly fast calculation to perform (fast, of course, being a relative term). Unfortunately, the Hartree-Fock equation does not calculate all of the energy of a system. To get more accurate results, other methods can be used which generally build upon the Hartree-Fock theory. As a class, these methods are called Post-Hartree-Fock methods.

The difference in the exact energy, which we are looking for, and the Hartree-Fock energy is called the correlation energy:

$$E_{corr} = E_{exact} - E_{HF} \quad (124)$$

Correlation is what results from the probability of a particular event depending on another event. For orbitals, the probability density for one electron depends on the probability density of every other electron. This is taken into account by using a complete set of orbitals. For example, in the Be atom that we used earlier, the wavefunction must include not only the 1s and 2s orbitals, but the 2p, 3s, 3p, 3d, 4s, etc. orbitals. For a basis set of N orbitals used to describe n

electrons, an atom will have $\frac{n}{2}$ occupied orbitals and $N - \frac{n}{2}$ unoccupied or virtual orbitals. Important terms related to these orbitals are the Highest Occupied Molecular Orbital or HOMO and the Lowest Unoccupied Molecular Orbital or LUMO. In excited states electrons from the occupied orbitals are moved into the virtual orbitals. Including at least some of these is necessary for retrieving part of the correlation energy. Notation for these excited states is Ψ_0 for the ground state, Ψ_a^r for a singly excited state where an electron is moved from orbital a to orbital r , Ψ_{ab}^{rs} for a doubly excited state where an electron is moved from orbital a to orbital r and another electron from orbital b to orbital s , etc.

When working with excited states, an important theorem is Brillouin's Theorem which states that singly excited states do not mix with Hartree-Fock ground states (Szabo and Ostlund, 1996: 128-129). In addition, states that are triply or more excited do not mix with the ground state since the Hamiltonian only includes one and two electron operators which causes highly excited states to produce only integrals involving orthogonal states which are zero. While excited states other than doubles do not directly interact with the ground state, they do indirectly by interacting with the doubly excited states and including them can be important.

There are four types of Post-Hartree-Fock calculations that we will look at. In this research these methods will be used only rarely to compare with DFT results. Therefore, we will look only briefly at each of them.

2.6.1. Møller-Plesset Second Order Perturbation Theory (MP2)

(The primary references for this section are Szabo and Ostlund pp 350-353, Ratner and Schatz pg 171, and class notes prepared for CHEM 662 by Dr Alan Yeates.)

The first and computationally easiest Post-Hartree-Fock method is MP2. As the name indicates, MP2 uses the second order of the perturbation theory described in Section 2.4.8. This is based on Hartree-Fock in that the HF Hamiltonian is used as H_0 where

$$H_0 = \sum_i f(i) = \sum_i [h(i) + v^{HF}(i)] \quad (125)$$

The perturbation, V , is set to

$$V = \sum_{i<j} r_{ij}^{-1} - V^{HF} = \sum_{i<j} r_{ij}^{-1} - \sum_i v^{HF}(i) \quad (126)$$

The second order correction to the Hartree-Fock energy is found to be

$$E_0^{(2)} = \sum_{\substack{a<b \\ r<s}} \frac{\left| \langle \Psi_0 | \sum_{i<j} r_{ij}^{-1} | \Psi_{ab}^{rs} \rangle \right|^2}{\epsilon_a + \epsilon_b - \epsilon_r - \epsilon_s} \quad (127)$$

The derivation of this can be found in Szabo and Ostlund pp 350-352.

MP2 is a fast calculation that can be done with relatively small computational resources. But, the results tend not to be extraordinarily accurate.

2.6.2. Configuration Interaction (CI)

(The primary references for this section are Szabo and Ostlund pp 231-245, Ratner and Schatz pg 172, and class notes prepared for CHEM 662 by Dr Alan Yeates.)

The second type of Post-Hartree-Fock calculation is Configuration Interaction. The CI method incorporates excited states by including them in a wavefunction which includes all possible states. The wavefunction is of the form

$$\Psi = c_0 D_0 + \sum_{a,r} c_a^r D_a^r + \sum_{a,b,r,s} c_{ab}^{rs} D_{ab}^{rs} + \dots \quad (128)$$

where the D 's are Slater determinants with the excitations shown in the subscripts and superscripts and the c 's are coefficients which are variationally optimized. A full CI, which includes all possible excitations, is the exact energy for a system in the given basis set.

If there are $2K$ single electron spin orbitals and N electrons, there are

$$\binom{2K}{N} = \frac{(2K)!}{N!(2K-N)!} \text{ terms in the wavefunction. For even a relatively small}$$

molecule and a reasonably small basis set, the number of terms in a full CI is such that a calculation will take many years of CPU time to obtain an answer.

For this reason, CI expansions are generally truncated at some level. Common truncations include those that include up to doubles, called CISD, and those that have up to triples, called CISDT. While these do not recover all of the correlation energy, as a full CI does, they generally recover most of it. These CI's usually

recover more correlation energy than MP2, but take considerably more computational time.

2.6.3. Multi-Configuration Self-Consistent Field (MCSCF)

(The primary references for this section are Szabo and Ostlund pp 258-259 and Ratner and Schatz pp 172-173.)

MCSCF is a method that is very similar to CI. Like CI the wavefunction is composed of a sum of determinants truncated at some level of excitation. The important difference between MCSCF and CI is that instead of variationally optimizing just the expansion coefficients, the orbitals that make up each of the determinants are also variationally optimized. This added step increases the complexity and time required considerably beyond the large amount of time already required for a CI calculation. This is helped somewhat by reducing the number of orbitals that electrons can be excited from and to. These orbitals make up what is called the active space. A calculation where the active space includes all orbitals is called a Complete Active Space SCF (CASSCF). MCSCF generally produces results that are better than CI, but can take considerably more computational time.

2.6.4. Coupled Cluster (CC) Theory

(The primary references for this section are Szabo and Ostlund pp 286-296 and Ratner and Schatz pg 173.)

The final type of Post-Hartree-Fock calculation considered is coupled cluster theory. This uses a wavefunction of the form

$$\Psi_{CC} = e^T \Psi_0 \quad (129)$$

where

$$T = T_1 + T_2 \quad (130)$$

$$T_1 = \sum_{ra} c_a^r \tilde{a}_r a_a \quad (131)$$

$$T_2 = \frac{1}{4} \sum_{abrs} c_{ab}^{rs} \tilde{a}_r \tilde{a}_s a_b a_a \quad (132)$$

and where a_a is an operator that removes an electron from orbital a . \tilde{a}_s is an operator that puts an electron in orbital s . The utility of this method is shown by

expanding part of the exponential as $e^x = 1 + x + \frac{1}{2}x^2 + \dots$ to give

$$e^{T_2} = 1 + \frac{1}{4} \sum_{abrs} c_{ab}^{rs} \tilde{a}_r \tilde{a}_s a_b a_a + \frac{1}{32} \sum_{\substack{abcd \\ rstu}} c_{ab}^{rs} c_{cd}^{tu} \tilde{a}_r \tilde{a}_s a_b a_a \tilde{a}_t \tilde{a}_u a_c a_d + \dots \quad (133)$$

and similarly for e^{T_1} . Therefore, a coupled cluster expansion includes at least some contribution from all possible excitations.

CC produces results that are generally better than the other methods and, time-wise, is roughly comparable to MCSCF.

An important characteristic of HF, CC, and MP2 but not of CI or MCSCF is size extensivity. Size extensive, or size consistent, theories produces the same level of accuracy regardless of the size of the system. For instance, for a set of

two identical systems infinitely far apart, a size extensive theory produces a result that is exactly twice that of a single system.

2.7. Density Functional Theory (DFT)

The final theory that we will look at, and, along with HF, the method that this research will focus upon, is Density Functional Theory (DFT). All of the methods that we have looked at so far are what are called *ab initio* theories. These are theories that are developed and calculated completely from first principles of physics. In theory, DFT is also an *ab initio* method. Unfortunately, as we shall see, DFT is, in practice, a semi-empirical method. Empirical methods are the opposite of *ab initio* methods. These use some set of known experimental data as a given and extrapolate unknown data based upon this. A semi-empirical method is derived from first principles, but is then somehow fit to some known data. This is the case for DFT.

2.7.1. Early DFT Theory

(The primary references for this section are Koch and Holthausen pp 29-32 and class notes prepared for CHEM 662 by Dr Alan Yeates.)

The most important difference between DFT and the other methods is that the principle variable is the electron density rather than the wavefunction. The initial DFT theory was developed by Thomas and Fermi in 1927. They developed an energy functional (a function of a function) of the form

$$E_{TF}[\rho(\vec{r})] = \underbrace{\frac{3}{10}(3\pi^2)^{\frac{2}{3}} \int \rho(\vec{r})^{\frac{5}{3}} d^3r}_{\text{kinetic energy functional}} - \underbrace{Z \int \frac{\rho(\vec{r})}{\vec{r}} d^3r}_{\text{nuclear-electron potential energy}} + \underbrace{\frac{1}{2} \iint \frac{\rho(\vec{r}_1)\rho(\vec{r}_2)}{|\vec{r}_1 - \vec{r}_2|} d^3r_1 d^3r_2}_{\text{electron-electron repulsion energy}} \quad (134)$$

A few years later in 1930, Dirac introduced an exchange term to the Thomas-Fermi model to give

$$E_{TFD}[\rho(\vec{r})] = E_{TF}[\rho] - K_D[\rho] \quad (135)$$

$$K_D[\rho] = \frac{3}{4} \left(\frac{3}{\pi}\right)^{\frac{1}{3}} \int \rho(\vec{r})^{\frac{4}{3}} d^3r \quad (136)$$

Unfortunately, this Thomas-Fermi-Dirac theory worked even worse than the original. This was helped in 1935 by Weisacker who added gradient correction terms to the Thomas-Fermi kinetic energy functional of the form

$$T_w[\rho] = \frac{1}{8} \int \frac{|\nabla \rho(\vec{r})|^2}{\rho(\vec{r})} d^3r \quad (137)$$

to account for nonlocal effects in a nonuniform density.

A final early addition to the theory was in 1951 by Slater. In this method, called the X_α method, a semi-empirical constant, α , is added to Dirac's exchange term to make it

$$K_{DS}[\rho] = \frac{9}{8} \left(\frac{3}{\pi}\right)^{\frac{1}{3}} \alpha \int \rho(\vec{r})^{\frac{4}{3}} d^3r \quad (138)$$

Typical values of α are between $\frac{2}{3}$ and 1 (Koch and Holthausen, 2001: 32).

2.7.2. Hohenberg-Kohn Theorems

(The primary references for this section are Koch and Holthausen pp 33-40, class notes prepared for CHEM 662 by Dr Alan Yeates and the 1964 Hohenberg and Kohn paper.)

Modern DFT theory is based on two theorems developed by Hohenberg and Kohn in 1964. The first Hohenberg-Kohn theorem states that “the external potential $V_{ext}(\vec{r})$ is (to within a constant) a unique functional of $\rho(\vec{r})$; since, in turn $V_{ext}(\vec{r})$ fixes \hat{H} we see that the full many particle ground state is a unique functional of $\rho(\vec{r})$ ” (Hohenberg and Kohn, 1964: B865). Essentially, this states that no two external potentials that differ by more than a constant will produce the same electron density.

The proof of this theorem is fairly straightforward. Two different external potentials produce two different Hamiltonians which are associated with two different ground state wavefunctions and energies. By taking the Hamiltonians of each of these wavefunctions and assuming that they can produce the same electron density, the inequality

$$E_0 + E_0' < E_0' + E_0 \quad (139)$$

is obtained, which leads to $0 < 0$. This is obviously wrong and therefore, by *reduction ad absurdum* the theorem is proven. The consequence of this theorem is that once the electron density is determined, the ground state properties of the system are uniquely determined. This now leaves us with the question of how to find the ground state density. This is handled by the second theorem.

The second Hohenberg-Kohn theorem is the equivalent of the variational principle applied to densities rather than wavefunctions. This states that if $E_{HK}[\rho]$ is the ground state energy functional, $\rho(\vec{r})$ is the exact ground state density, and $\rho'(\vec{r})$ is an approximate density that satisfies the boundary conditions of $\rho'(\vec{r}) \geq 0$ and $\int \rho'(\vec{r}) d^3r = N$, then

$$E_{HK}[\rho] \leq E_{HK}[\rho'] \quad (140)$$

The consequence of this is that since the energy is broken down as

$$E_{HK}[\rho] = E_{electron}[\rho] + V_{ext}[\rho] \quad (141)$$

and $V_{ext}[\rho]$ completely fixes the Hamiltonian, $E_{electron}[\rho]$ is a universal functional.

If we know the form of this functional we can find the exact ground state density, $\rho_g(\vec{r})$ by the variational principle, i.e.,

$$\left. \frac{\delta E_{HK}[\rho]}{\delta \rho} \right|_{\rho=\rho_g} = 0 \quad (142)$$

2.7.3. Kohn-Sham Approach

(The primary references for this section are Koch and Holthausen pp 41-64, class notes prepared for CHEM 662 by Dr Alan Yeates, and the 1965 Kohn and Sham paper.)

The Hohenberg-Kohn theorems showed that an electron density can be used to find the energy and properties of a system if the energy functional is known. The basic modern form of this functional was put forward by Kohn and Sham in 1965.

The Hohenberg-Kohn theorems lead to an expression for the energy of the form

$$E_0 = \min_{\rho \rightarrow N} \left(F[\rho] + \int \rho(\vec{r}) V_{Ne} d^3 r \right) \quad (143)$$

where V_{Ne} is the external potential produced by the nuclei. $F[\rho]$ is the universal energy functional

$$F[\rho(\vec{r})] = T[\rho(\vec{r})] + J[\rho(\vec{r})] + E_{nc}[\rho(\vec{r})] \quad (144)$$

where $T[\rho(\vec{r})]$ is the kinetic energy, $J[\rho(\vec{r})]$ the classical Coulomb interaction, and $E_{nc}[\rho(\vec{r})]$ the non-classical effects which include electron self-interaction, electron exchange, and electron correlation.

An important step Kohn and Sham made was to make an analogy between DFT and HF. They introduced the use of a Slater determinant to describe the electron density. The orbitals that make up the determinant are related to the electron density by

$$\rho(\vec{r}) = N \int |\psi(\vec{r}_1, \vec{r}_2, \dots, \vec{r}_N)|^2 d^3 \vec{r}_2 \dots d^3 \vec{r}_N \quad (145)$$

$$\rho(\vec{r}) = \sum_{i=1}^N |\varphi_i(\vec{r})| \quad (146)$$

Using these orbitals we can now begin to examine the individual functionals. First, we look at the kinetic energy functional. As a start, we use the HF form of the kinetic energy for non-interacting electrons:

$$T_s[\rho] = -\frac{1}{2} \sum_{i=1}^N \langle \varphi_i | \nabla^2 | \varphi_i \rangle \quad (147)$$

This does not include contributions due to correlation of the electron motions, which will be handled in another term.

Likewise, the classical Coulomb term is

$$J[\rho] = \frac{1}{2} \iint \frac{\rho(\vec{r}_1)\rho(\vec{r}_2)}{|\vec{r}_1 - \vec{r}_2|} d^3r_1 d^3r_2 \quad (148)$$

This is only the classical electron-electron repulsion and does not include electron exchange or correlation. It also includes electron self-interaction which must be removed.

The key to the Kohn-Sham approach is the redefinition of the functional as

$$F[\rho(\vec{r})] = T[\rho(\vec{r})] + J[\rho(\vec{r})] + E_{xc}[\rho(\vec{r})] \quad (149)$$

$E_{xc}[\rho(\vec{r})]$, called the exchange-correlation functional, includes the non-classical effects from Equation 144, as well as the exchange, correlation, and removal of self-interaction effects that are missing from Equations 147 and 148.

If we now set the functional derivative of the energy to zero, we get the Kohn-Sham equations:

$$\left(-\frac{1}{2} \nabla^2 + V_{eff}(\vec{r}) \right) \phi_i = \varepsilon_i \phi_i \quad (150)$$

$$V_{eff}(\vec{r}) = \int \frac{\rho(\vec{r}')}{|\vec{r} - \vec{r}'|} d^3r' + V_{xc}(\vec{r}) - \sum_A \frac{Z_A}{r_A} \quad (151)$$

$$V_{xc}(\vec{r}) = \frac{\delta E_{xc}[\rho]}{\delta \rho} \quad (152)$$

2.7.4. Exchange-Correlation Functional

(The primary references for this section are Koch and Holthausen pp 65-92 and class notes prepared for CHEM 662 by Dr Alan Yeates.)

If we knew the form of the exchange-correlation functional, the Kohn-Sham equations would give us an exact solution for the ground state of the system. Unfortunately, to date, no exact form of this functional has been found. Since the introduction of the Kohn-Sham approach, theoretical work has focused on developing approximations for it. There are three types of approximations that we will look at.

The first type of approximation for the exchange-correlation functional is called the local density approximation or LDA. It is also known as the SVWN method, for Slater, Vosko, Wilk, and Nusair, whose work it is based upon. This method uses a form for the functional of

$$E_{XC}^{LDA}[\rho] = \int \rho(\vec{r}) \varepsilon_{XC}[\rho(\vec{r})] d^3 r \quad (153)$$

where

$$\varepsilon_{XC}[\rho] = \varepsilon_X[\rho(\vec{r})] + \varepsilon_C[\rho(\vec{r})] \quad (154)$$

The right side of Equation 154 has two components. The first is the exchange part. For this, the exchange energy of a uniform electron gas is used:

$$\varepsilon_X^{LDA}[\rho] = -\frac{3}{4} \sqrt[3]{\frac{3\rho(\vec{r})}{\pi}} \quad (155)$$

This is the same term that Dirac introduced to the Thomas-Fermi model.

The second component of Equation 154 is the correlation term. There is no explicit expression for this. Instead, LDA uses a functional fit to numerical

quantum Monte-Carlo simulations of a uniform electron gas. Examples of LDA functionals include VWN and VWN5.

The second type of approximation for the functional are the generalized gradient approximations or GGA. Like LDA, GGA is spit into two pieces:

$$\varepsilon_{XC}^{GGA}[\rho] = \varepsilon_X^{GGA}[\rho(\vec{r})] + \varepsilon_C^{GGA}[\rho(\vec{r})] \quad (156)$$

The exchange term is

$$\varepsilon_X^{GGA}[\rho(\vec{r})] = \varepsilon_X^{LDA}[\rho(\vec{r})] - \sum_{\sigma} \int F(s_{\sigma}) \rho_{\sigma}(\vec{r})^{\frac{4}{3}} d^3r \quad (157)$$

where the local inhomogeneity parameter s_{σ} is

$$s_{\sigma}(\vec{r}) = \frac{|\vec{\nabla} \rho_{\sigma}(\vec{r})|}{\rho_{\sigma}(\vec{r})^{\frac{4}{3}}} \quad (158)$$

The function F is determined empirically and there are several methods and many fits available. One important class of fits was developed by Becke in 1988 who created the B or B88 functional

$$F^B = \frac{\beta s_{\sigma}^2}{1 + 6\beta s_{\sigma} \sinh^{-1} s_{\sigma}} \quad (159)$$

where β is found to be 0.0042 by a least squares fit to rare gas exchange energies. Other functionals that are similar are FT97, PW91, CAM(A), and CAM(B). A second class of exchange functionals includes B86, P, LG, P86, or PBE. The F for P86 has the form

$$F^{P86} = \left(1 + 1.296 \left(\frac{s_{\sigma}}{\sqrt[3]{24\pi^2}} \right)^2 + 14 \left(\frac{s_{\sigma}}{\sqrt[3]{24\pi^2}} \right)^4 + 0.2 \left(\frac{s_{\sigma}}{\sqrt[3]{24\pi^2}} \right)^6 \right)^{\frac{1}{15}} \quad (160)$$

GGA correlation functionals are similar to, but more complicated than the exchange functionals and will not be explicitly shown. Popular functionals include P86, PW91, and LYP.

Complete GGA functionals combine an exchange functional with a correlation functional. Common combinations are B88 and P86 to give BP86, B88 and LYP to give BLYP, and B88 and PW91 to give BPW91.

The final type of functional is hybrid functionals. These combine GGA functionals with exact HF exchange. An example, which will be the only functional that we will use in this research, is B3LYP. This has a functional form of

$$\varepsilon_{XC}^{B3LYP}[\rho] = (1-a)\varepsilon_X^{LSD} + a\varepsilon_{XC}^{\lambda=0} + b\varepsilon_X^{B88} + c\varepsilon_C^{LYP} + (1-c)\varepsilon_C^{LSD} \quad (161)$$

where $a = 0.20$, $b = 0.72$, and $c = 0.81$ are parameters that found by Becke to fit a set of experimental data. Other examples of hybrid functionals are BPW91, B1B95, B97 and B98.

III. Methodology

3.1. Introduction

As stated in Chapter 2, quantum mechanical calculations of molecular systems are not solvable analytically. They require specialized computer programs, usually running on fast computers with large amounts of memory, to numerically solve the millions of integrals each calculation requires. One of these programs, and the major one I have used for this research, is the General Atomic and Molecular Electronic Structure System (GAMESS) (Schmidt *et al*, 1993). In addition, the program Gaussian 98 has been used for CC calculations (Gaussian, 2002).

In this chapter I will present the method that I have used in a stepwise fashion. I will begin by giving an example of GAMESS input and output files and explanations of each. I will then give a step-by-step explanation of the method that I have used for each of the molecules that I have examined. A list of all the steps is shown in Table 2. For illustrative purposes, I will use the Si₂CO molecule as an example.

This chapter presents the general method of calculations and assumes that no problems are encountered. For various reasons, not all calculations successfully produce a result. Some troubleshooting methods that I have used to complete problematic calculations are presented in Appendix E.

Table 2. Steps used in my method for determining ground state geometries of C_mSi_nO , $m, n \leq 4$, molecules.

1	Identify all possible isomers
2	Optimize geometry using GAMESS, ROHF, and VDZ basis set for singlet and triplet neutral as well as doublet anion
3	Identify all stable isomers and rank order by increasing energy
4	Choose lowest energy structures and neutral multiplicity (if possible)
5	Optimize geometry using GAMESS, ROHF, and cc-pVDZ basis set
6	Identify all stable isomers and rank order by increasing energy
7	Choose lowest energy structures and neutral multiplicity (if possible/necessary)
8	Optimize geometry using GAMESS, ROHF, and aug-cc-pVDZ basis set
9	Identify all stable isomers and rank order by increasing energy
10	Choose lowest energy structures and neutral multiplicity (if possible/necessary)
11	Optimize geometry using GAMESS, DFT, and VDZ basis set
12	Identify all stable isomers and rank order by increasing energy
13	Choose lowest energy structures and neutral multiplicity (if possible/necessary)
14	Optimize geometry using GAMESS, DFT, and cc-pVDZ basis set
15	Identify all stable isomers and rank order by increasing energy
16	Choose lowest energy structures and neutral multiplicity (if possible/necessary)
17	Optimize geometry using GAMESS, DFT, and aug-cc-pVDZ basis set
18	Identify all stable isomers and rank order by increasing energy
19	Choose lowest energy structures and neutral multiplicity (if necessary)
20	Calculate Hessian using GAMESS, DFT, and aug-cc-pVDZ basis set
21	Confirm structures are minima by looking for imaginary frequencies
22	Assign vibrational frequencies to respective modes
23	If suspect or "interesting" geometry, continue; otherwise skip to Step 26
24	Calculate geometry and energy using aug-cc-pVDZ basis set and post-HF methods
25	Compare geometries from different methods/determine "best" geometry
26	Calculate single point energy of neutral using ground geometry of doublet
27	Determine electron affinities

3.2. GAMESS Input

Figure 5 shows an example of a GAMESS input file. The input file is contained within the box with dots (·) representing spaces. For illustrative purposes, line numbers appear on the left of the input. The order of keyword

```

1  . $DATA
2  SiCO . . ROHF / aug-cc-pVDZ
3  C1 . . 1
4  . O . . . . 8.0 . . . . 0.0 . . . . 0.0 . . . -1.2
5  . C . . . . 6.0 . . . . 0.0 . . . . 0.0 . . . 0.0
6  . Si . . 14.0 . . . . 0.0 . . . . 0.0 . . . 2.2
7  . $END
8
9  ! . $BASIS . . GBASIS=DZV . . $END
10 ! . $BASIS . . GBASIS=CPVDZ . . EXTFIL=.T . . $END
11 . $BASIS . . GBASIS=ACPVDZ . . EXTFIL=.T . . $END
12
13 ! . $DFT . DFTTYP=B3LYP . NRAD=128 . NTHE=32 . NPHI=64 . NRAD0=32 . NTHE0=24 . NPHI0=48 . $END
14
15 . $CONTRL
16 ICHARG=-1
17 MULT=2
18 RUNTYP=OPTIMIZE
19 SCFTYP=ROHF
20 COORD=UNIQUE . . NZVAR=0 . . UNITS=ANGS
21 MAXIT=200
22 ! . . . . EXETYP=CHECK
23 . $END
24
25 . $SCF . . MAXVT=50 . . SHIFT=.T . . $END
26
27 . $SYSTEM . . TIMLIM=10000 . . MWORDS=100 . . $END
28
29 . $STATPT . . NSTEP=100 . . HESS=CALC . . IHREP=0 . . HSEND=.T . . $END
30
31 . $GUESS . . GUESS=HUCKEL . . $END
32

```

Figure 5. Sample GAMESS input. Calculation shown is HF/aug-cc-pVDZ for a SiCO doublet anion. Line numbers are shown only for illustrative purposes (“.” represent spaces)

sections (those preceded by a dollar sign) is unimportant. The order shown here is simply the one that I have personally found to be most useful. I will here be explaining only the basic input used for HF and DFT calculations. Additions to the input file for doing post-HF calculations will be addressed later in this chapter. I will only be explaining those keywords and sections that I have had to use. There are a great many more that I have either not used, or the default value was sufficient. For these and further explanations, please see the GAMESS User Manual, the most recent version of which can be found at the GAMESS website at <http://www.msg.ameslab.gov/games/gamess.html>.

(NOTE: For ease of understanding, throughout this chapter, words which are taken from the example input appear in the `COURIER` font.)

All sections start with a "\$" in the second column, followed immediately by the keyword label for the section. Each section is ended by a `$END` which may appear anywhere on a line. Any line that starts with an exclamation point or that is outside of a section and does not have a dollar sign in the second column is treated as a comment and is not processed. Blank lines between sections are not needed, but are useful for readability.

The first seven lines of the example input are the data section. This is where information is placed about the atoms making up the molecule of interest. Line 1 is the data tag. Line 2 gives the title of the calculation. This has no bearing on the actual calculation to be done, but is useful when reading output files. Line 3 gives the symmetry. For most calculations I have used C1 symmetry (i.e., no symmetry) as shown here. If any symmetry other than C1 is used, the next line must be blank. Lines 4 through 6 give atomic information. The input shown uses Cartesian coordinates, though a z-matrix may also be used instead. The first column gives an atomic label. This label can be anything and has no effect on the actual calculation. For obvious reasons, I have always used the chemical symbol of the atom. The second column is the nuclear charge of the atom. This is what tells the program what atom to use. Columns 3 through 5 give the x, y, and z Cartesian coordinates of the atom. Finally, Line 7 ends the data section.

Lines 9 through 11 give the basis set. After the \$BASIS section label, two keywords are used. The first, GBASIS, gives the name of the basis set to be used. If this is not a built-in basis set, EXTFIL= .T. must be included to tell the program to get the basis set from an external file given by the external environment variable EXTBAS. In the example, three basis options are given. Before running the input, two of these must be commented out (in this case, Lines 9 and 10). Uncommenting Line 9 gives Dunning's VDZ basis set which is built-into GAMESS. Using Line 10 tells GAMESS to use the user-defined basis set CPVDZ which, in this case, is Dunning's cc-pVDZ basis set given in an external basis set file. In the example, Line 11 is processed doing the calculation with Dunning's aug-cc-pVDZ basis set.

Line 13 gives the parameters for doing a DFT calculation. The example input is for a HF calculation, so Line 13 is commented out. The first keyword in this section, DFTTYP, gives the DFT functional to be used. The functional in the example is the B3LYP functional that I have used for all DFT calculations and which was described in Chapter 2. The next six keywords give the number of grid points to use for the DFT calculation. Each atom will be spherically surrounded by NRAD*NTHE*NPHI grid points. NRAD0, NTHE0, and NPHI0 give an initial grid to be used. Once the change between iterations of the density matrix falls below some threshold value (3.0E-4 is the default) the finer grid given by NRAD, NTHE, and NPHI is used. As with basis sets, the computed energy depends on the size of the DFT grid used. Therefore calculations done with different size grids cannot be compared.

Lines 15 through 23 are the `$CONTRL` section which tells GAMESS what to do. Lines 16 and 17 give the charge and multiplicity of the molecule, in this case, a doublet anion. Line 18 specifies the type of calculation. In the example, `OPTIMIZE` tells the program to find the optimized molecular geometry. This is the option that I used most often. Other options that I used were `ENERGY`, which computes the molecule's single point energy with no geometry change, and `HESSIAN`, which calculates the single point energy and does a vibrational analysis. Line 19 specifies the type of wavefunction to use. I set this to `ROHF` for all HF and DFT calculations. Line 20 gives several coordinate options. `COORD` sets the type of coordinates to be used in the `$DATA` section. The example specifies `UNIQUE` which requires only the symmetry unique atoms to be specified in Cartesian coordinates. The only other option I used here was `ZMT` which allows the input of the molecule using a z-matrix. `NZVAR` specifies what type of internal coordinates to use. Here 0 means Cartesian coordinates. `UNITS` gives the type of distance units to use. I have used Angstroms throughout. `MAXIT` gives the maximum number of SCF iterations before nonconvergence is declared. The default is 30, but to allow for some particularly troublesome molecules I have set this to 200, which is the maximum allowable setting at the MSRC, where I did most of my calculations. The final line within the `$CONTRL` section is `EXETYP=CHECK`. For actual calculation runs, this is left commented out. If this line is uncommented, the program will set up the calculation but not actually do it. This allows for making sure a complex or lengthy calculation is properly setup before potentially wasting time running an incorrect input. I have

found this particularly useful for checking non-C1 symmetry inputs to ensure that I have chosen the correct symmetry and that there are no extra atoms being added.

Line 25 gives parameters for the SCF routine. `MAXVT` sets the maximum number of iterations within each SCF step. I have increased the number to 50 from the default of 20. `SHIFT=.T.` tells the program to shift levels in the Fock matrix that are close together. This helps to prevent convergence problems.

Line 27 gives system control information. `TIMLIM` gives the maximum time the calculation is allowed to take in minutes. `MWORDS` gives the maximum amount of memory to use in 8Mb units. Both of these are set to large values to prevent problems or a premature abort of the program. At the MSRC, these values are reset by user input at job submittal time.

The `$STATPT` group on line 29 controls the optimization search. `NSTEP` gives the maximum number of geometry optimization steps to take. I have set this to 100 rather than the default of 20. `HESS` selects what type of Hessian matrix to start with. Setting this to `GUESS` uses a positive definite diagonal matrix. Setting this to `CALC`, as in the example, tells it to compute the initial matrix. `IHREP` specifies how many steps to take before recomputing the Hessian. Setting this to 0 means that only the initial Hessian is calculated. `HSEND=.T.` is a flag which tells GAMESS to calculate the Hessian at the optimized geometry and to output the vibrational analysis.

The final line, the `$GUESS` section, specifies the initial orbitals to use. `GUESS=HUCKEL` uses a calculated guess as the initial orbitals. Replacing this

with `GUESS=MOREAD` allows for reading in orbitals from a previous run. If `MOREAD` is used, `NORB` must also be specified. `NORB` gives the number of orbitals to be read. Also, if `MOREAD` is used, a `$VEC` group must be given. This is a formatted group that is taken from the `.dat` file of a previous run and is not editable by the user.

3.3. GAMESS Output

The output produced by even a small GAMESS calculation is extremely large. Running the input from Figure 5 with the built-in VDZ basis set produces 38 pages of output.

The beginning of the output file starts with a citation for the program and some information about the computer on which it is running. Then are several pages of setup options and variable definitions. Once the calculation is setup, a single point energy calculation is done, the eigenvectors are output, and the gradient at the initial geometry is determined. If an optimization is being done, there will then be a series of optimization steps. One of the important parts of the output is at the end of the optimization after the keyword `***** EQUILIBRIUM GEOMETRY LOCATED *****`. Here is the optimized geometry and energy. The optimized orbitals are next. After the orbitals is some bond information. Finally at the end, if requested, is Hessian information, including vibrational information and thermodynamic data.

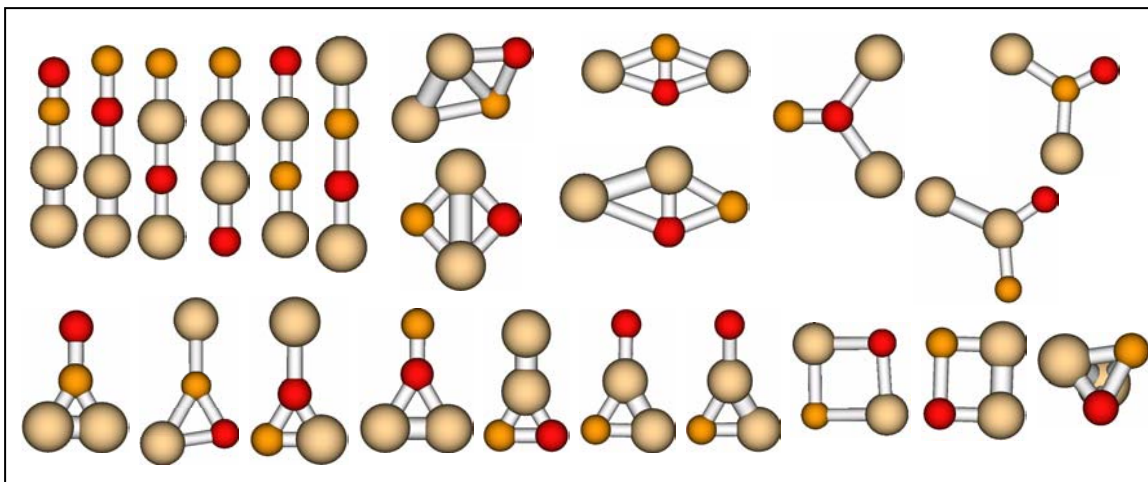


Figure 6. Initial 23 isomers for Si_2CO calculation. These isomers were calculated at HF/VDZ level. Tan atoms are silicon, orange atoms are carbon, and red atoms are oxygen. All but the last are planar

3.4. Step 1: Identify Isomers

The first step in optimizing a molecule's geometry is to identify the possible isomers. For small molecules such as Si_2CO this is relatively simple and all possible isomers can be examined. But for larger molecules the number of possible isomers is too large to allow examination of all of them. For Si_2CO I examined the 23 isomers shown in Figure 6. Once the isomers are identified, the initial Cartesian coordinates of each must be assigned. The rules I have used for this are Si-Si bonds are 2.2\AA , Si-C bonds are 1.8\AA , Si-O bonds are 1.5\AA , C-C bonds are 1.2\AA , C-O bonds are 1.2\AA , and the molecules should be as symmetric as possible. These bond lengths are approximately those that are normally seen for bonds between those atoms. If the atoms are not reordered in some way, the final bond lengths are expected to be about these values.

3.5. Steps 2-10: Hartree-Fock Optimization

Once the input files are prepared, the first calculations can be performed. The initial calculations are done with the Hartree-Fock method using the VDZ basis set. The calculated final energy is then extracted from each output file. For small numbers of output files this can be done by manually searching through each output file for the message “EQUILIBRIUM GEOMETRY LOCATED” and copying the following total energy. For larger numbers of output files, I have created a small batch file that automatically extracts the energy from all the output files in a directory. This batch file, and a further description of its use, is included in Appendix D. Once all the energies are extracted, they are sorted from lowest to highest. The final geometry for each unique energy is then determined by reading the output files into the visualization program Molden (Schaffenaar and Noordik: 2000) running on a PC with an X-Windows emulator. Depending on the number of stable isomers found, either all stable isomers will be identified or only those that are lowest in energy. For Si₂CO there are nine anion and thirteen neutral stable geometries. These are shown with their energies and multiplicities in Figure 7.

The next step is to identify which isomers will continue on for further calculations. First, singlet and triplet energies for similar geometries are compared. If there is a significant difference in energy, the lower energy multiplicity can be declared the ground state neutral multiplicity. What constitutes a significant energy difference is subjective. Generally, at low levels of theory, I used around 0.5 eV. At higher levels of theory, I used around 0.2 eV.

Anion			Neutral		
Isomer	Energy (Hartrees)		Isomer	Energy (Hartrees)	Multiplicity
	-690.417	D ₀		-690.371	S ₀
	-690.414	D ₀		-690.365	S ₀
	-690.387	D ₀		-690.356	S ₀
	-690.383	D ₀		-690.354	T ₀
<hr/>			<hr/>		
	-690.381	D ₀		-690.353	S ₀
	-690.373	D ₀		-690.353	T ₀
	-690.369	D ₀		-690.344	T ₀
	-690.369	D ₀		-690.336	S ₀
	-690.362	D ₀		-690.327	S ₀
				-690.327	T ₀
				-690.309	T ₀
				-690.295	T ₀
				-690.175	S ₀

Figure 7. Stable isomers for Si₂CO calculation using HF/VDZ. Isomers are ordered with most stable at the top. Isomers above the line proceeded to the next level of calculation. Tan atoms are silicon, orange atoms are carbon, and red atoms are oxygen. All are planar.

The stable isomers with the lowest neutral and anion energies are then selected for the next step. In Figure 7 this cutoff is shown by the lines. For Si_2CO , four isomers in both singlet and triplet were chosen.

Once the isomers for the next set of calculations are chosen, the input files are prepared. Each of the candidate isomers is calculated in all remaining multiplicities. The files are the same as those prepared earlier except that line nine is now commented out and line ten is uncommented. This sets up a Hartree-Fock calculation using the cc-pVDZ basis set. As before, the calculations are performed, the energies are extracted and sorted, and the stable isomers are identified. Figure 8 shows the results of these calculations. There were four anion and seven neutral stable geometries. The cc-pVDZ calculations produced five distinct geometries all of which were selected to continue to the next level of calculations.

For the third set of calculations input files are prepared with line ten commented and line eleven uncommented to give a Hartree-Fock calculation with the aug-cc-pVDZ basis set. Again, the calculations are done and analyzed. The results are shown in Figure 9. For Si_2CO there were five anion and eight neutral stable isomers. At this point I was able to identify the neutral ground multiplicity as a singlet and narrow the geometry to four isomers.

3.6. Steps 11-19: Density Functional Theory Optimization

The next step is to perform density functional theory calculations. The input files are prepared the same as in the beginning with line nine

Anion			Neutral		
Isomer	Energy (Hartrees)	Multiplicity	Isomer	Energy (Hartrees)	Multiplicity
	-690.533	D ₀		-690.502	S ₀
	-690.520	D ₀		-690.481	S ₀
	-690.481	D ₀		-690.473	T ₀
	-690.465	D ₀		-690.449	T ₀
<hr/>				-690.427	S ₀
				-690.408	T ₀
				-690.346	T ₀
			<hr/>		

Figure 8. Stable isomers for Si₂CO calculation using HF/cc-pVDZ. Isomers are ordered with most stable at the top. Isomers above the line proceeded to the next level of calculation. Tan atoms are silicon, orange atoms are carbon, and red atoms are oxygen. The four-membered rings are slightly non-planar. All others are planar.

uncommented to use the VDZ basis set and line thirteen uncommented to perform a DFT calculation. For Si₂CO, five isomers were calculated in the singlet and doublet multiplicities. The results of these calculations are shown in Figure 10. There were four doublet and three singlet stable geometries. The top two of each were chosen for the next level of calculation.

The next set of calculations is then prepared by uncommenting lines ten and thirteen giving a DFT calculation using the cc-pVDZ basis set. Four isomers

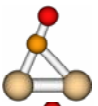
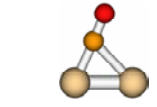
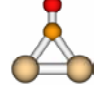
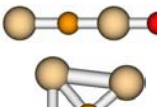
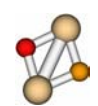
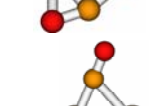
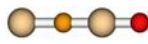
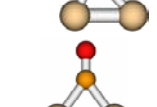
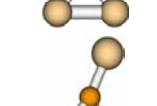
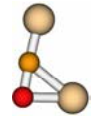
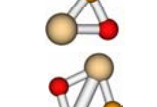
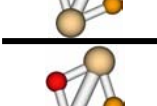
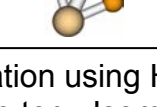
Anion			Neutral		
Isomer	Energy (Hartrees)		Isomer	Energy (Hartrees)	Multiplicity
	-690.554	D ₀		-690.512	S ₀
	-690.551	D ₀		-690.497	S ₀
	-690.547	D ₀		-690.494	S ₀
	-690.489	D ₀		-690.485	T ₀
<hr/>				-690.483	T ₀
	-690.463	D ₀		-690.464	T ₀
				-690.448	S ₀
			<hr/>		
				-690.388	T ₀

Figure 9. Stable isomers for Si₂CO calculation using HF/aug-cc-pVDZ. Isomers are ordered with most stable at the top. Isomers above the line proceeded to the next level of calculation. Tan atoms are silicon, orange atoms are carbon, and red atoms are oxygen. The four-membered rings are slightly non-planar. All others are planar.

were calculated in the singlet and doublet multiplicities giving the results shown in Figure 11. There were four doublet and three singlet stable geometries.

The final DFT calculations were prepared by uncommenting lines eleven and thirteen giving a DFT calculation using the aug-cc-pVDZ basis set. This calculation resulted in two doublet and three singlet stable geometries as shown in Figure 12.

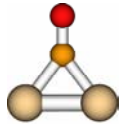
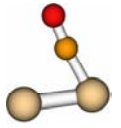
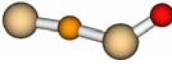
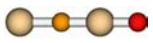
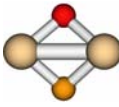
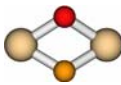
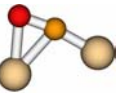
Anion			Neutral		
Isomer	Energy (Hartrees)	Multiplicity	Isomer	Energy (Hartrees)	Multiplicity
	-692.08574	D ₀		-692.01824	S ₀
	-692.07931	D ₀		-692.01152	S ₀
<hr/>			<hr/>		
	-692.04887	D ₀		-691.98392	S ₀
	-692.04634	D ₀			

Figure 10. Stable isomers for Si₂CO calculation using DFT/B3LYP/VDZ. Isomers are ordered with most stable at the top. Isomers above the line proceeded to the next level of calculation. Tan atoms are silicon, orange atoms are carbon, and red atoms are oxygen. The four-membered rings are slightly non-planar. All others are planar.

At this point, a ground state geometry for each multiplicity can be identified. For the doublet anion the ground state geometry is a symmetric three-membered ring composed of two silicons and one carbon. The oxygen is bonded to the carbon nearly symmetrically (7° off of symmetric). For the neutral singlet, the ground state geometry also has a three-membered ring of two silicons and a carbon, but one of the carbon-silicon bonds is shorter than the other. Also different for the singlet is that the oxygen bonds to the carbon so that the oxygen-carbon bond and the shorter carbon-silicon bond is nearly linear (177.6°).

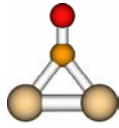
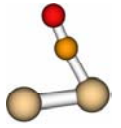
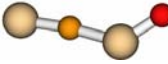
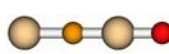
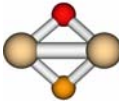
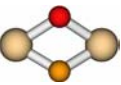
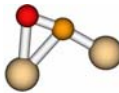
Anion			Neutral		
Isomer	Energy (Hartrees)	Multiplicity	Isomer	Energy (Hartrees)	Multiplicity
	-692.08574	D ₀		-692.01824	S ₀
	-692.07931	D ₀		-692.01152	S ₀
<hr/>			<hr/>		
	-692.04887	D ₀		-691.98392	S ₀
	-692.04634	D ₀			

Figure 11. Stable isomers for Si₂CO calculation using DFT/B3LYP/cc-pVDZ. Isomers are ordered with most stable at the top. Isomers above the line proceeded to the next level of calculation. Tan atoms are silicon, orange atoms are carbon, and red atoms are oxygen. The four-membered rings are slightly non-planar. All others are planar.

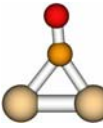
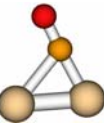
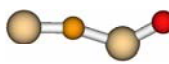
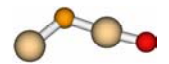
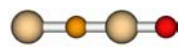
Anion			Neutral		
Isomer	Energy (Hartrees)	Multiplicity	Isomer	Energy (Hartrees)	Multiplicity
	-692.18919	D ₀		-692.12616	S ₀
<hr/>			<hr/>		
	-692.17652	D ₀		-692.10906	S ₀
				-692.10855	S ₀

Figure 12. Stable isomers for Si₂CO calculation using DFT/B3LYP/aug-cc-pVDZ. Isomers are ordered with most stable at the top. Isomers above the line proceeded to the next level of calculation. Tan atoms are silicon, orange atoms are carbon, and red atoms are oxygen. All are planar.

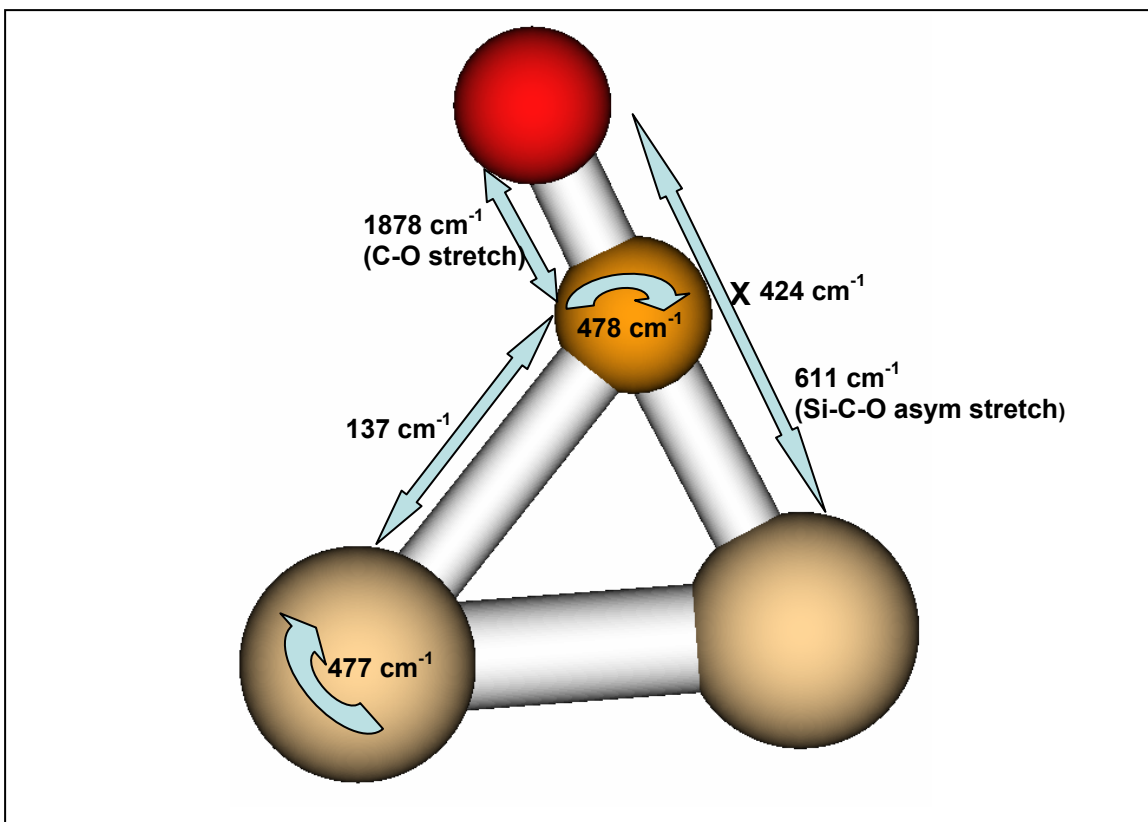


Figure 13. Vibrational modes of Si₂CO using DFT/B3LYP/aug-cc-pVDZ. Tan atoms are silicon, orange atoms are carbon, and red atoms are oxygen. An “X” indicates a mode into the plane.

3.7. Steps 20-22: Vibrational Analysis

The next step is to perform a vibrational analysis and confirm that the ground state structures are minima. This is done by preparing an input file as before with DFT and the aug-cc-pVDZ basis set, the final ground state geometry, and changing line eighteen to “RUNTYPE=HESSIAN”. This will compute a Hessian and vibrational analysis at the given geometry.

Once the calculation is performed, the vibrational frequencies near the end of the output file are examined. If all of the frequencies are real numbers, the geometry is a minima. If one of the frequencies is imaginary and all of the

others are real, the geometry is a transition state. If more than one frequency is imaginary, the geometry is not a stationary point. For Si₂CO, both the doublet and singlet were minima.

If the identified ground state geometry is a minima, the vibrational frequencies can then be assigned to vibrational modes. This is done by reading the output file into Molden and looking at each vibrational frequency/mode. The results of this for the ground state singlet are shown in Figure 13.

3.8. Steps 23-25: Post-Hartree-Fock Analysis

The next set of calculations is done only if the ground geometries are suspect or interesting. For Si₂CO these were done because of the difference in geometries between the singlet and doublet and the asymmetry of the singlet.

The first post-Hartree-Fock calculation is Møller-Plesset Second Order Perturbation Theory (MP2). This is done in GAMESS by adding "MPLEVL=2" and "CITYP=NONE" to the \$CONTRL group and adding a line reading " \$CIDRT GROUP=C1 IEXCIT=2 NFZC=7 NDOC=14 NALP=0 NVAL=20 mxnint=10000000 \$END". For descriptions of the contents of the \$CIDRT group, please see the GAMESS manual. An MP2 geometry optimization can only be done for the singlet since GAMESS does not have an ROHF MP2 gradient.

The next post-Hartree-Fock calculation is Configuration Interaction (CI). Two CI calculations can be done: a CISD and a CISDT. The CISD is done in GAMESS by adding "CITYP=GUGA" to the \$CONTRL group and adding a line

reading “ \$CIDRT GROUP=C1 IEXCIT=2 NFZC=7 NDOC=14 NALP=0
NVAL=87 mxnint=10000000 \$END”. The CISDT input would be the same
except “IEXCIT=2” in the \$CIDRT group is changed to “IEXCIT=3”. For Si₂CO,
I did only the CISD since CISDT requires a very significant amount of processor
time. Like MP2, CI optimization can only be done for the singlet since GAMESS
does not have an ROHF CI gradient implemented.

The third post-Hartree-Fock calculation to be done is Multi-Configuration
Self Consistent Field (MCSCF). MCSCF is started by doing a single point
Hartree-Fock energy calculation at the DFT ground state geometry using the
aug-cc-pVDZ basis set. Then, by examining the orbitals in the output file and
using the Molden visualization software to view the orbitals, each orbital is
identified as being an unbonded electron pair, a sigma bond, or a pi bond. The
decision must then be made as to how large an active space you want and which
electrons to include in this active space. As the active space is made larger, the
time required for the calculation grows exponentially. For Si₂CO, the six pi-like
valence orbitals and the six corresponding pi-like virtual orbitals were selected for
the active space. This was found to be about the largest practical size for the
active space. The next calculation was done to produce a set of modified virtual
orbitals. To do this, “MVOQ=6” was added to the \$SCF group of a standard
Hartree-Fock/aug-cc-pVDZ single-point energy calculation. In addition,
“GUESS=MOREAD” and “IORDER(27)=28 , 27” in the \$GUESS group are used to
read in the vectors from the previous Hartree-Fock calculation and reorder them
so that the active space orbitals are contiguous. The modified virtual method

uses a highly charged cation (in this case a +6 charge) to obtain the virtual orbitals. This produces virtual orbitals that are much cleaner looking and more well-behaved (Bauschlicher, 1980). For the actual MCSCF calculation, several modifications must be made to the standard input file. First, the SCFTYP in the \$CONTRL group is set to "SCFTYP=MCSCF". Next, the lines

```
$DRT GROUP=C1 FORS=.T. NMCC=15 NDOC=6 NVAL=6 $END
$DET NCORE=15 NACT=12 NELS=12 $END
$MCSCF CISTEP=GUGA SOSCF=.T. $END
```

are added to the input. Again, for a description of these keywords, see the GAMESS User Manual. Finally, "GUESS=MOREAD" is used to read in the properly reordered vectors from the modified-virtual calculation. MCSCF can be done for both the singlet and doublet.

The final post-Hartree-Fock calculation is Coupled-Cluster (CC). Similar to CI, CC can be done as either a CCSD or CCSD(T) calculation but for reliable results CCSD(T) should be done. CC calculations must be done using Gaussian. A sample input is shown in Figure 14. For a description of the Gaussian input format, please see the Gaussian manual or website.

Once all of the post-Hartree-Fock calculations are done, the geometry results are compared and a "best" geometry is selected. The singlet geometry results for all of the levels of calculation using the aug-cc-pVDZ basis set are shown in Figure 15. The highest level and therefore the most reliable calculation is the CCSD(T) which is in relatively good agreement with the DFT results. This confirms that the DFT results are reliable.

```

1 %nproc=4
2 %mem=64mw
3 %chk=gaussian-CCSDT.chk
4 #n·ccsd(t)/aug-cc-pVDZ opt
5 nosym
6
7 CCSD-T·for·cyc3_C-Si-Si_O.singlet
8
9 0··1
10 C
11 Si··1··r1
12 Si··2··r2··1··a1
13 O···1··r3··3··a2··2··d1
14
15 r1=1.808810
16 r2=2.277107
17 r3=1.204345
18 a1=61.103436
19 a2=110.535
20 d1=180.000000

```

Figure 14. Sample Gaussian 98 input for Coupled Cluster calculation. Calculation shown is CCSD(T)/aug-cc-pVDZ for a Si₂CO singlet neutral. Line numbers are shown only for illustrative purposes. (“·” represent spaces)

3.9. Steps 26-27: Determine Electron Affinities

The final steps are to calculate the molecule’s electron affinities. The adiabatic electron affinity is the difference in the anion and neutral ground states. This is calculated by subtracting the DFT/aug-cc-pVDZ ground energy of the singlet from the doublet. The vertical electron affinity is the difference in energies at the anion geometry. The first step to find this is to perform a single-point DFT energy calculation for the singlet using the ground doublet geometry and the aug-cc-pVDZ basis set. The DFT/aug-cc-pVDZ ground energy of the doublet is then subtracted from this energy. Once this is done, this map point is complete and the process is repeated for each molecule.

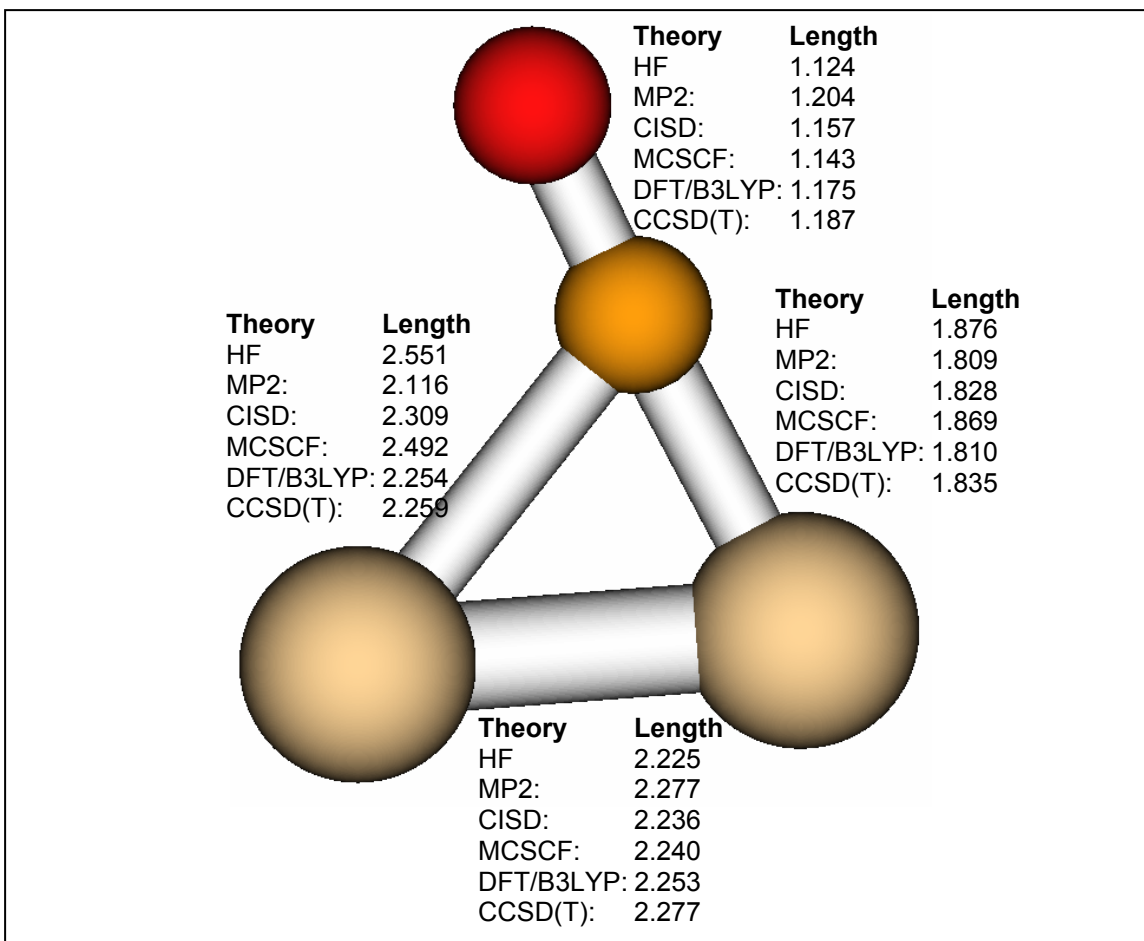


Figure 15. Geometry comparison for Si₂CO at several levels of theory. All calculations use aug-cc-pVDZ basis set. Tan atoms are silicon, orange atoms are carbon, and red atoms are oxygen.

IV. Results and Analysis

4.1. Introduction

Having explored some theories and methods of computational quantum chemistry in Chapter 2 and developed a method of calculation using these theories in Chapter 3, we are now prepared to examine the results I have obtained. The method described in the previous chapter was applied to 25 molecules of the formula C_mSi_nO where $m, n \leq 4$. This chapter will begin by examining each molecule individually. For each of these molecules, I will present my calculated values for the ground state geometry, multiplicity, and vibrational analysis for both the neutral and anion. I will then present the adiabatic electron affinity and vertical electron affinity for the molecule. Where experimental results are available, I will compare my results with these.

Each molecule's section will be accompanied by a figure which will graphically show the ground state geometry, bond lengths, and multiplicity for both the neutral and anion. In addition for small molecules, non-scaled arrows (or X's for movement in/out of the paper) are used to show vibrational modes. Associated with each arrow is the frequency for that mode. When room allows, the IR intensity is shown in parentheses beneath the frequency in units of $\text{Debye}^2/\text{AMU} \cdot \text{\AA}^2$. As before, in the figures, oxygen atoms are red, carbon atoms are orange, and silicon atoms are tan.

After examining all of the molecules in detail, the next section of this chapter will examine several trends and chemical preferences including functional groups, geometries, and electron affinities.

Finally, the last section presents the results of thermodynamics calculations. Here, I examine the heats of formation for both silicon carbide and monoxides of silicon carbide and the enthalpies of reaction for 15 important reactions.

Throughout this chapter the results presented are, unless otherwise noted, calculated with the DFT method using the B3LYP functional and aug-cc-pVDZ basis set since this has been shown to produce accurate results for the similar C_nSi_m clusters (Duan, 2002). Energy values produced by GAMESS are output to ten decimal places in hartrees. Bond lengths are output to seven decimal places in Å. While these numbers are exact to this many decimal places given the method and basis set, the accuracy to the actual value is significantly less. For the sake of consistency, I will report electron affinities to three significant figures and bond lengths to three decimal places. For vibrational frequencies, I will report them to the nearest wavenumber. Data for all calculations performed is included in Appendix C. In Appendix B are figures showing all isomers that were examined for each molecule.

4.2. O, CO, and SiO

The first three molecules I looked at were the simplest, in that there is only one isomer per molecule. The simplest molecule I examined was $m,n = 0$ which

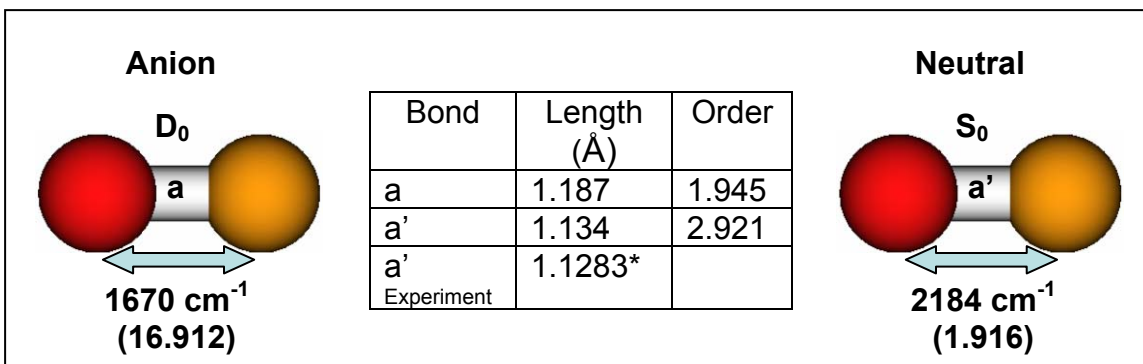


Figure 16. Calculated geometry and vibrational modes for ground state CO neutral and anion. Performed with DFT/B3LYP/aug-cc-pVDZ. Numbers in parentheses are vibrational IR intensities in Debye²/AMU-Å². Experimental data from Huber and Herzberg.

is atomic oxygen. The ground state multiplicities of oxygen are doublet and triplet for the anion and neutral respectively. Because atoms have no reaction coordinates, the adiabatic and vertical electron affinities are the same. Using DFT-B3LYP/aug-cc-pVDZ, I found the oxygen triplet electron affinity to be 1.59 eV. The experimental value from the NIST Webbook is 1.46198 ± 0.00043 eV (Hotop and Lineberger, 1985: 731).

The first *molecule* I examined was CO, carbon-monoxide. Like an atom, a diatom has only one geometric isomer. This geometry and the calculated parameters are shown in Figure 16. The neutral bond length differs from experiment by about 0.006 Å which is relatively good agreement. Also shown in the figure are the vibrational frequencies. The frequency of 2184 cm^{-1} is in good agreement with the experimental value of 2169.8 cm^{-1} (Huber and Herzberg, 1979). I calculated the adiabatic electron affinity to be -1.16 eV and the vertical electron affinity to be -1.01 eV. This compares to an experimental adiabatic

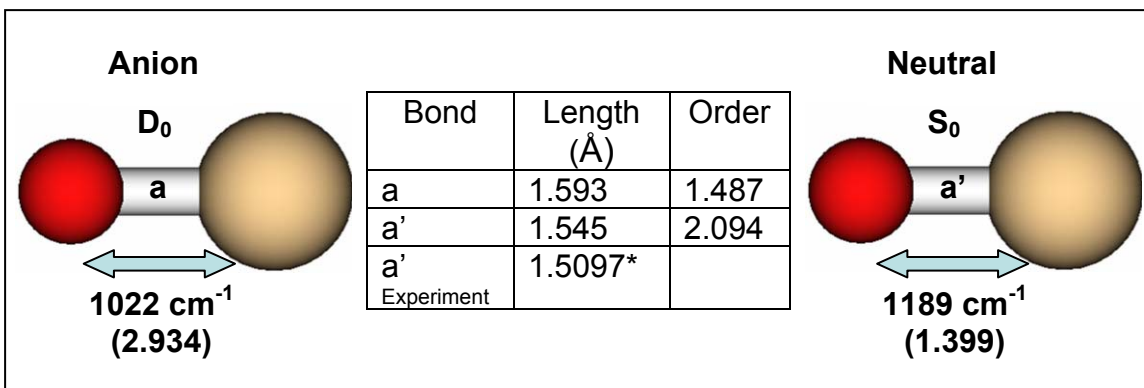


Figure 17. Calculated geometry and vibrational modes for ground state SiO neutral and anion. Performed with DFT/B3LYP/aug-cc-pVDZ. Numbers in parentheses are vibrational IR intensities in Debye²/AMU- Å². Experimental data from Huber and Herzberg.

value of -1.3261 eV (Refaey and Franklin, 1976: 19). As expected, this predicts that CO⁻ is not stable.

The next molecule that I looked at was SiO or silicon-monoxide. Again, this has only one isomer. The calculated data for this molecule is shown in Figure 17. The calculated bond length for the neutral is off significantly: over 0.035 Å. However, the vibrational frequency of 1189 cm⁻¹ is fairly close to the experimental value of 1241.6 cm⁻¹ (Huber and Herzberg, 1979). The calculated adiabatic electron affinity is 0.188 eV. The vertical electron affinity is 0.245 eV. The difference in bond length between the anion and neutral is about 0.05 Å, which is reasonably small.

4.3. CSiO

The next molecule examined was CSiO. For this, I examined all four possible isomers: O-centered, C-centered, Si-centered, and a three-membered

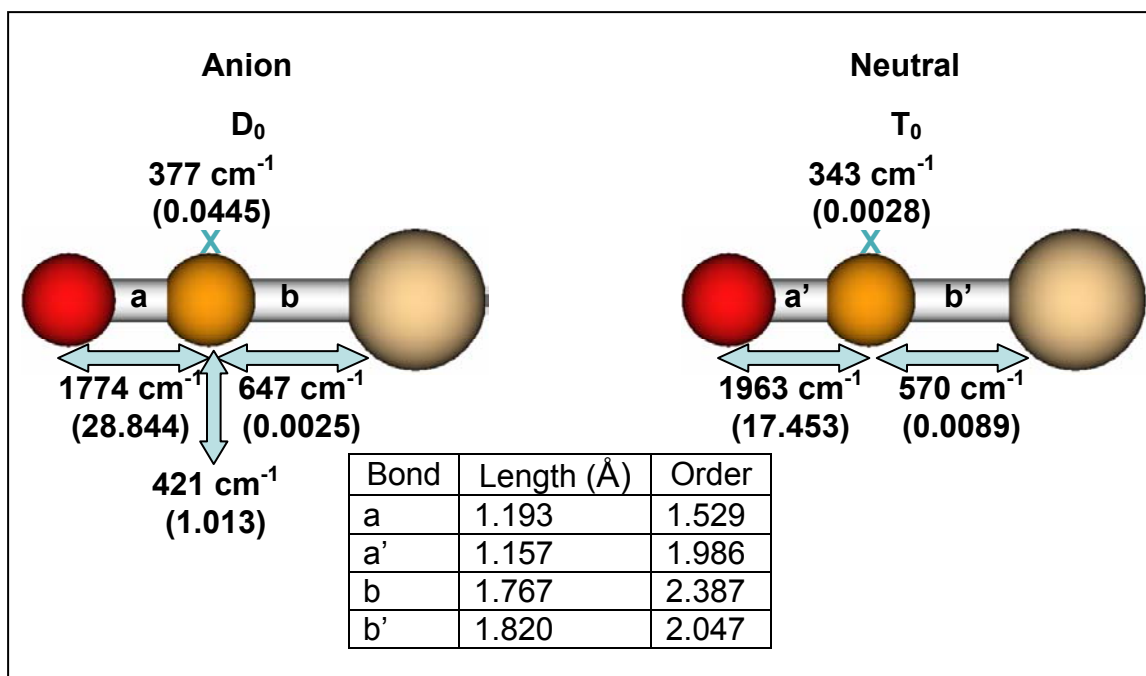


Figure 18. Calculated geometry and vibrational modes for ground state SiCO neutral and anion. Performed with DFT/B3LYP/aug-cc-pVDZ. Numbers in parentheses are vibrational IR intensities in Debye²/AMU-Å².

ring. This molecule was calculated very early in the research using the VTZ family of basis sets. This was done so that the results could be compared with the published results of the Schaefer group (Petraco, et al, 2000b). My ground state results for this molecule, which matched Schaefer's well, are shown in Figure 18. The ground state for both the anion and neutral is a linear arrangement with carbon in the middle, which gives it the name *silaketenyldene*. The ground state neutral is a triplet. This isomer is significantly lower in energy than the other isomers. Using DFT-B3LYP and the aug-cc-pVTZ basis set, the C-O vibrational stretch frequency of 1963 cm⁻¹ is in agreement with experimental results of 1898.1 cm⁻¹. However, the 570 cm⁻¹ prediction for the Si-C vibrational mode is off of the estimated actual value of 800 cm⁻¹ (Petraco, et al, 2000b).

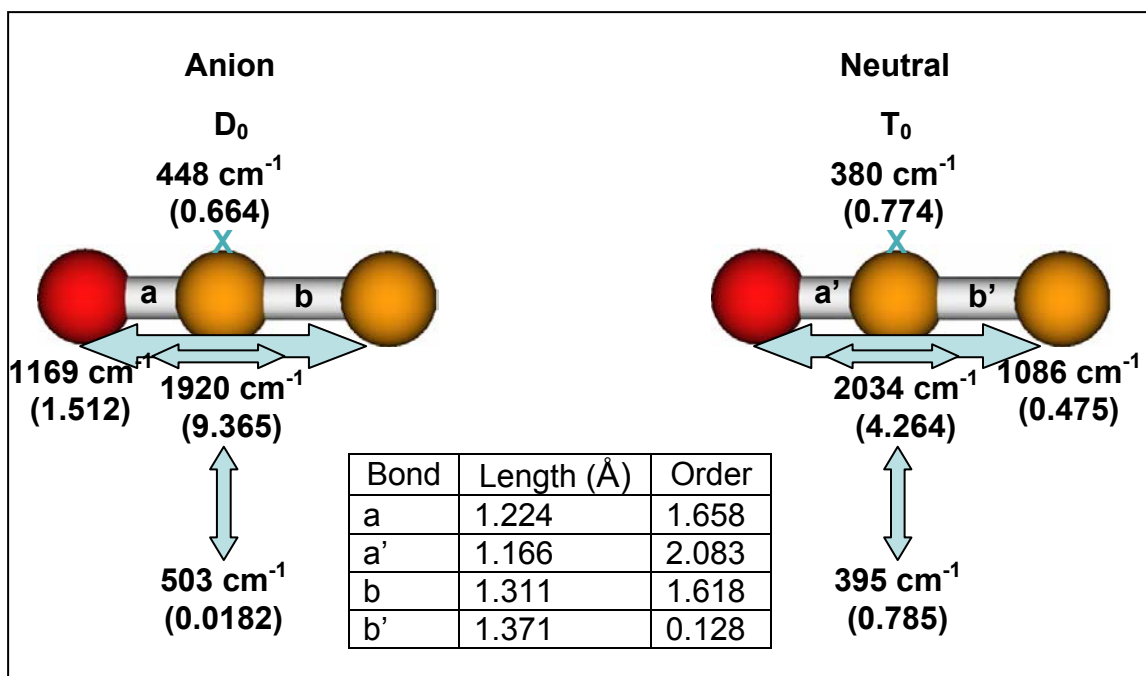


Figure 19. Calculated geometry and vibrational modes for ground state C_2O neutral and anion. Performed with DFT/B3LYP/aug-cc-pVDZ. Numbers in parentheses are vibrational IR intensities in $\text{Debye}^2/\text{AMU} \cdot \text{\AA}^2$.

The adiabatic electron affinity is calculated to be 1.38 eV. The vertical electron affinity is 1.46 eV. Again the differences in bond lengths are relatively small.

4.4. C_2O

C_2O was the next molecule I looked at. I examined all three possible isomers: C-centered, O-centered, and a three-membered ring. The ground state, shown in Figure 19, is a linear isomer with oxygen terminal. For the ground state the multiplicity is triplet. Other isomers and multiplicities are significantly higher in energy. The calculated vibrational frequencies are extremely close to experimental values: 2034 cm^{-1} vs 1970.86 cm^{-1} for the asymmetric stretch (Pitts, 1981), 1086 cm^{-1} vs 1063 cm^{-1} for the symmetric stretch (Pitts, 1981), 380 cm^{-1}

vs 379.53 cm^{-1} (Ohashi, 1993), and 395 cm^{-1} vs 381 cm^{-1} (Jacox, 1965) for the bent modes. The calculated adiabatic electron affinity is 2.22 eV. This is in good agreement with the experimental value of $2.289 \pm 0.018\text{ eV}$ (Zengin, 1996). The predicted vertical electron affinity is 2.42 eV. The bond lengths for the neutral and anion are significantly different with the C-C bond changing by over 0.2 Å. The chemical name for the ground state geometry is *ketenylidene*.

4.5. Si₂O

Next, I looked at Si₂O. Again, I examined all three possible isomers. As shown in Figure 20, the anion and neutral have different ground state geometries. For the neutral, the ground geometry is a linear, symmetric isomer with oxygen in the middle and triplet multiplicity. This is 0.45 eV lower in energy than the isomer with oxygen terminal. For the anion, the linear isomer with oxygen terminal is the ground state. This is 0.92 eV lower in energy than the O-centered isomer. For Si-O-Si, the adiabatic electron affinity is 0.609 eV. The vertical electron affinity is 0.616 eV. For Si-Si-O, the adiabatic electron affinity is 1.98 eV. Its vertical electron affinity is 2.05 eV. Si-O-Si has only small differences in geometry between the neutral and anion. However, Si-Si-O has large geometry differences.

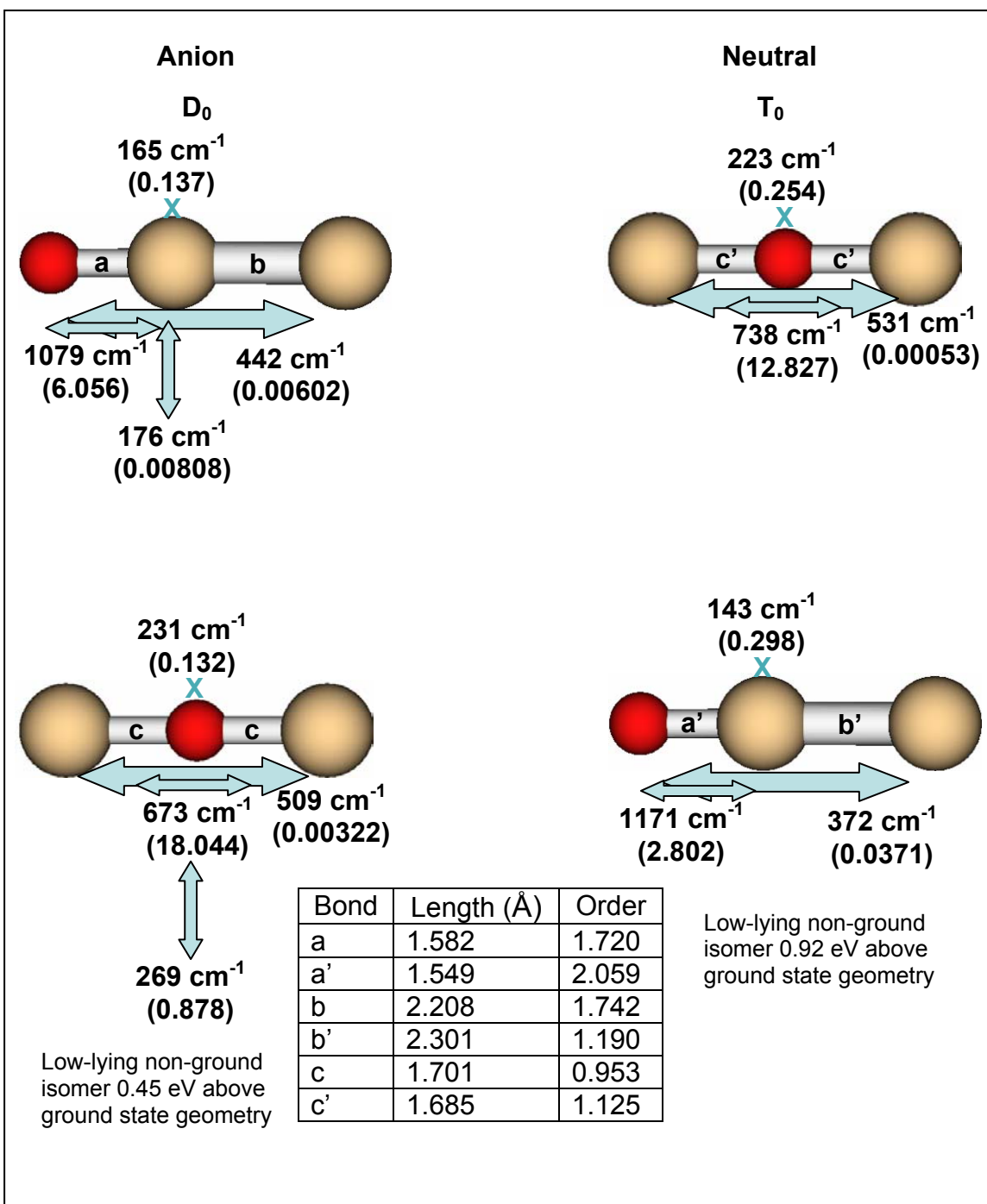


Figure 20. Calculated geometry and vibrational modes for ground state Si_2O neutral and anion. Performed with DFT/B3LYP/aug-cc-pVDZ. Numbers in parentheses are vibrational IR intensities in $\text{Debye}^2/\text{AMU} \cdot \text{\AA}^2$.

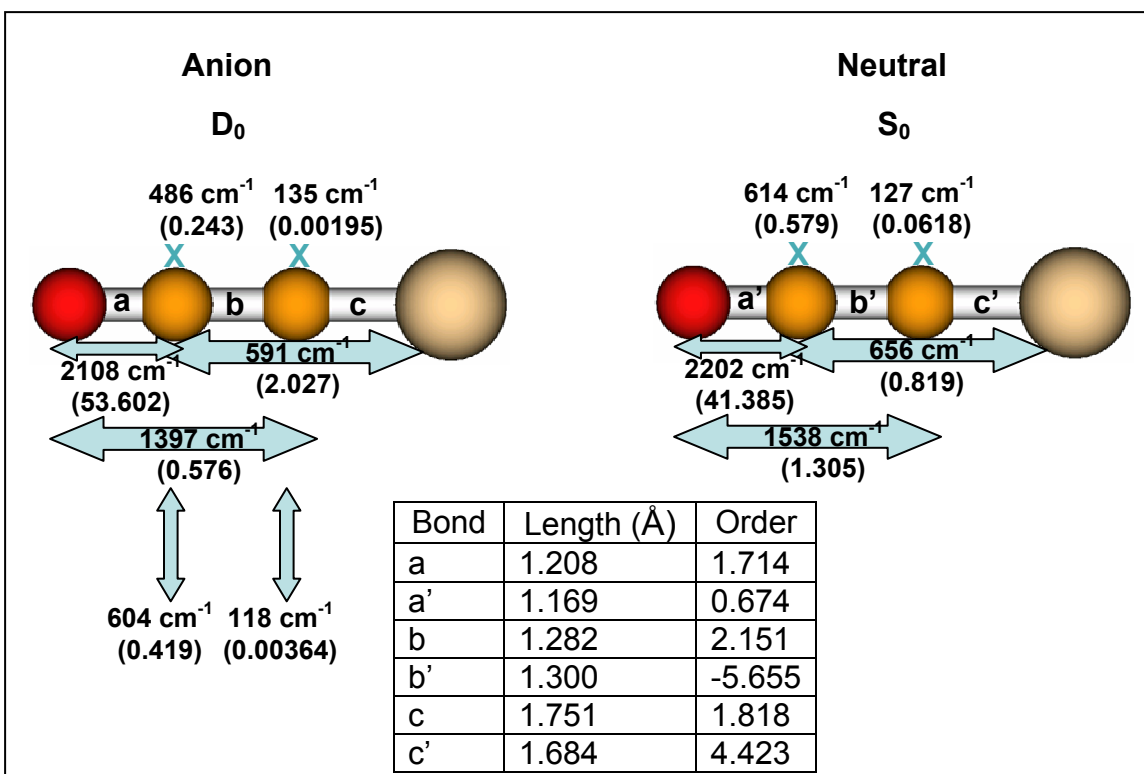


Figure 21. Calculated geometry and vibrational modes for ground state C_2SiO neutral and anion. Performed with DFT/B3LYP/aug-cc-pVDZ. Numbers in parentheses are vibrational IR intensities in $\text{Debye}^2/\text{AMU} \cdot \text{\AA}^2$.

4.6. C_2SiO

C_2SiO was the next molecule examined. I examined 25 different initial isomers. The ground state isomer was found to be a linear molecule with an oxygen and silicon terminal and singlet neutral multiplicity. Other isomers and multiplicities were significantly higher in energy. Figure 21 shows the ground state geometry and vibrational data. The adiabatic electron affinity is calculated to be 0.907 eV and the vertical electron affinity is 1.05 eV. The geometries of the anion and neutral have significant differences in their bond lengths, particularly for the C-Si bond which is over 0.06 Å longer for the anion.

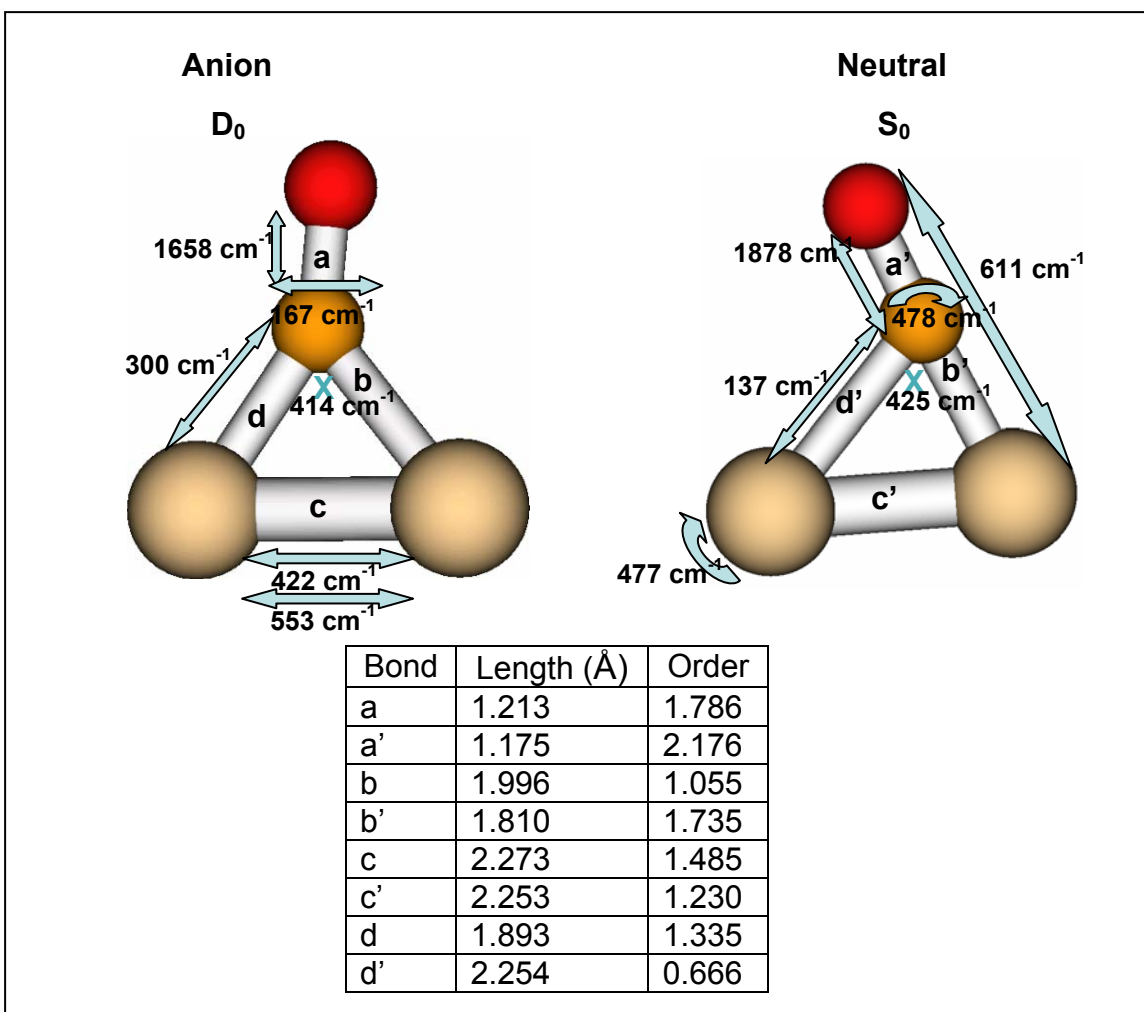


Figure 22. Calculated geometry and vibrational modes for ground state CSi_2O neutral and anion. Performed with DFT/B3LYP/aug-cc-pVDZ. Both molecules are planar.

4.7. CSi_2O

Figure 22 shows CSi_2O , the next molecule that was calculated. This molecule was calculated at 23 different initial isomer geometries. The ground state geometry for both the neutral and anion was found to be a three-membered ring of two silicons and one carbon with a carbonyl oxygen attached to the carbon. A bent-linear isomer of Si-C-Si-O was found to also be relatively low in

energy. For the doublet, this was 0.34 eV higher than the ground isomer. The singlet bent-linear was 0.46 eV higher than the singlet ground isomer. Other isomers and multiplicities were higher in energy. For the lowest energy molecule, I calculated the adiabatic electron affinity to be 1.75 eV and the vertical electron affinity to be 2.55 eV. The adiabatic electron affinity was also calculated using CCSD(T) and the aug-cc-pVDZ basis set and found to be 1.60 eV.

For the ground state geometries, there are significant differences between the doublet and singlet. The doublet is much more symmetric with the oxygen bond only 7° off of symmetric. For the singlet, the oxygen-carbon bond is nearly co-linear with one of the carbon-silicon bonds (177.6°). This is due, in part, to the presence of a strong pi bonding in the singlet. This is not as strong in the doublet due to the extra electron causing the pi bonds to be weaker.

These geometries were also optimized with post-Hartree-Fock methods. This was done both because of the interesting difference in geometry between the neutral and anion and as a small test case to evaluate the accuracy of DFT. The singlet was optimized with MP2, CISD, MCSCF, CCSD, and CCSD(T). The doublet was optimized with CCSD(T). All these calculations produced results similar to DFT-B3LYP. In particular, for the highest level results, CCSD(T), the geometry was in good agreement with DFT. Figure 15 from the previous chapter shows the results for the singlet using the various methods.

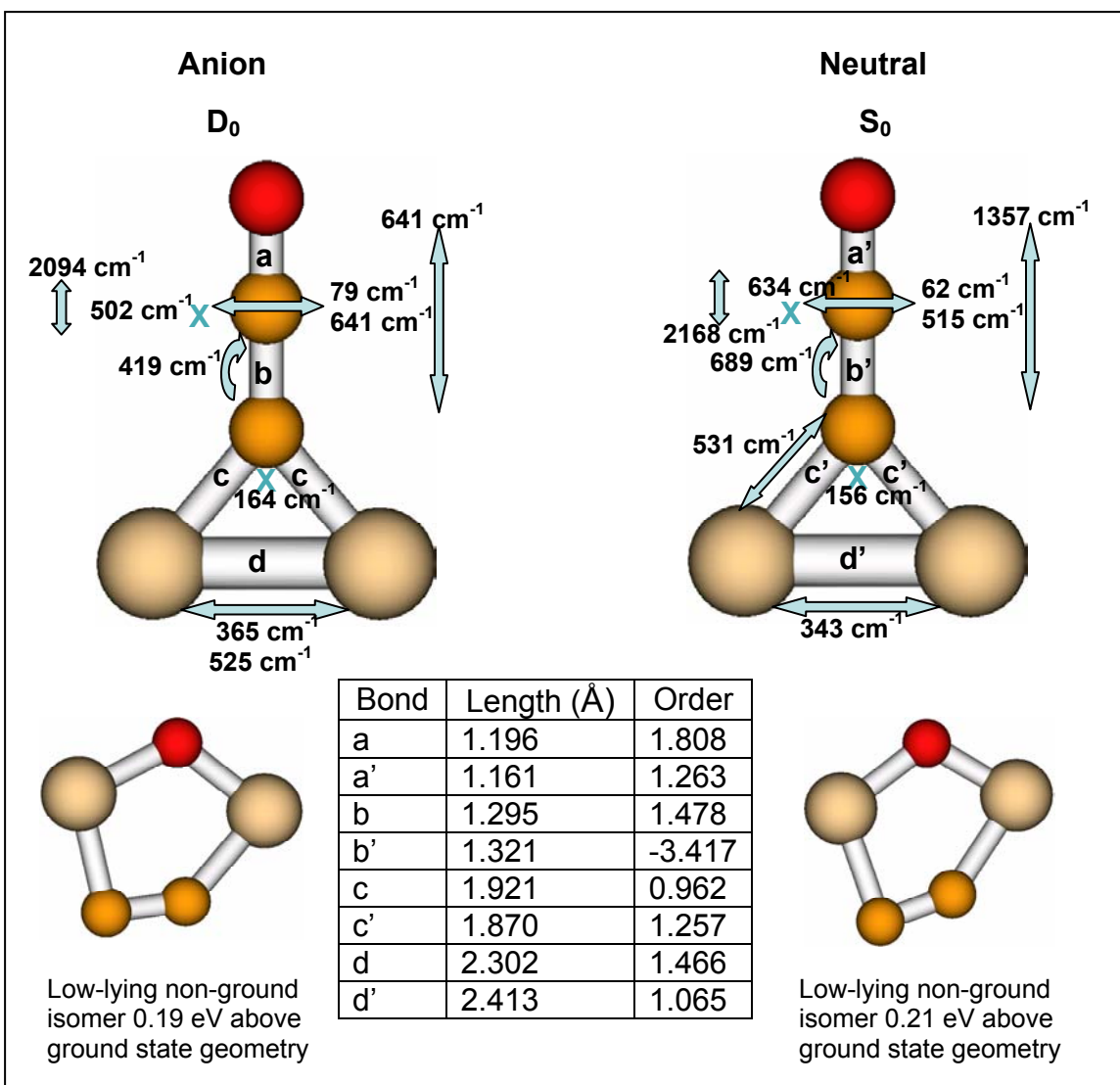


Figure 23. Calculated geometry and vibrational modes for ground state C_2Si_2O neutral and anion. Performed with DFT/B3LYP/aug-cc-pVDZ. Also shown is a low-lying non-ground isomer. All molecules are planar.

4.8. C_2Si_2O

For C_2Si_2O , I started with 167 different initial isomers. The lowest energy isomers for these calculations are shown in Figure 23. The neutral ground state multiplicity is a singlet. The ground state geometry for both the neutral and anion has a three-membered ring of two silicons and one carbon with $=C=O$ attached

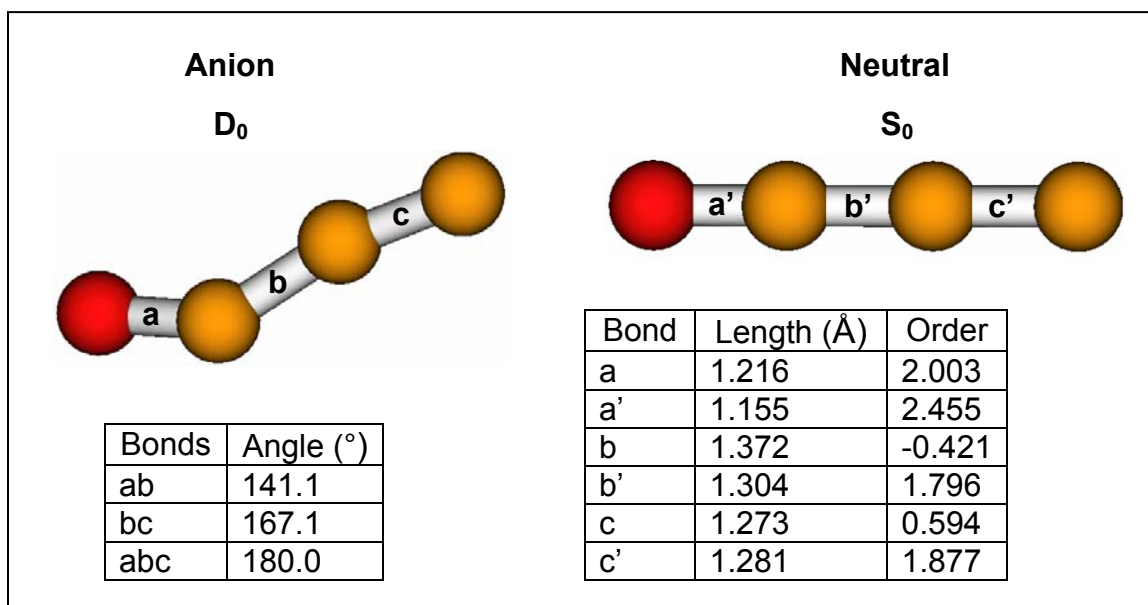


Figure 24. Calculated geometry for ground state C_3O neutral and anion. Performed with DFT/B3LYP/aug-cc-pVDZ. Both molecules are planar.

to the carbon. In both cases the geometry is symmetric. There is also a low energy, asymmetric, five-membered ring that is a stable isomer. This geometry has the oxygen situated between the two silicons and the two carbons opposite the oxygen. A view of this isomer is also shown in Figure 23. For the ground state, my calculations show that the adiabatic electron affinity is 1.68 eV and the vertical electron affinity is 1.86 eV.

4.9. C_3O

Next I looked at C_3O . For this molecule I started with eight different initial isomers. The results of these calculations are shown in Figure 24 and Table 3. The neutral ground state multiplicity is a singlet. The ground state geometries for the neutral and anion are significantly different. The neutral ground state is

Table 3. Vibrational analysis for C₃O. Calculated with DFT/B3LYP/aug-cc-pVDZ. Neutral modes one and three are doubly degenerate.

Anion Ground			Neutral Ground		
Mode	Frequency (cm ⁻¹)	IR Intensity (Debye ² /AMU-Å ²)	Mode	Frequency (cm ⁻¹)	IR Intensity (Debye ² /AMU-Å ²)
1	208	0.147	1	137	0.150
2	241	0.126	2		
3	533	0.0856	3	590	0.530
4	916	0.103	4	962	0.0592
5	1755	8.802	5	1964	0.700
6	1957	11.122	6	2331	38.160

linear with an oxygen terminal. However, the anion ground state is a bent-linear structure with a terminal oxygen. My calculations show that the bent neutral and non-bent anion are not stable isomers. For the ground state geometries, my calculations show that the adiabatic electron affinity is 1.12 eV which is relatively close to an experimental value of 1.34 ± 0.15 eV (Oakes and Ellison, 1986: 6263). The vertical electron affinity that I obtained is 2.24 eV. The large difference between the electron affinities is due to the very large difference in geometry.

4.10. Si₃O

I next looked at Si₃O. For this molecule I started with eight different initial isomers. The lowest energy isomers for these calculations are shown in Figure 25 and Table 4. The neutral ground state multiplicity is a triplet. The ground state geometry for both the anion and neutral is a three-membered ring of silicons with the oxygen bonded to two of the silicons in an epoxide-like fashion.

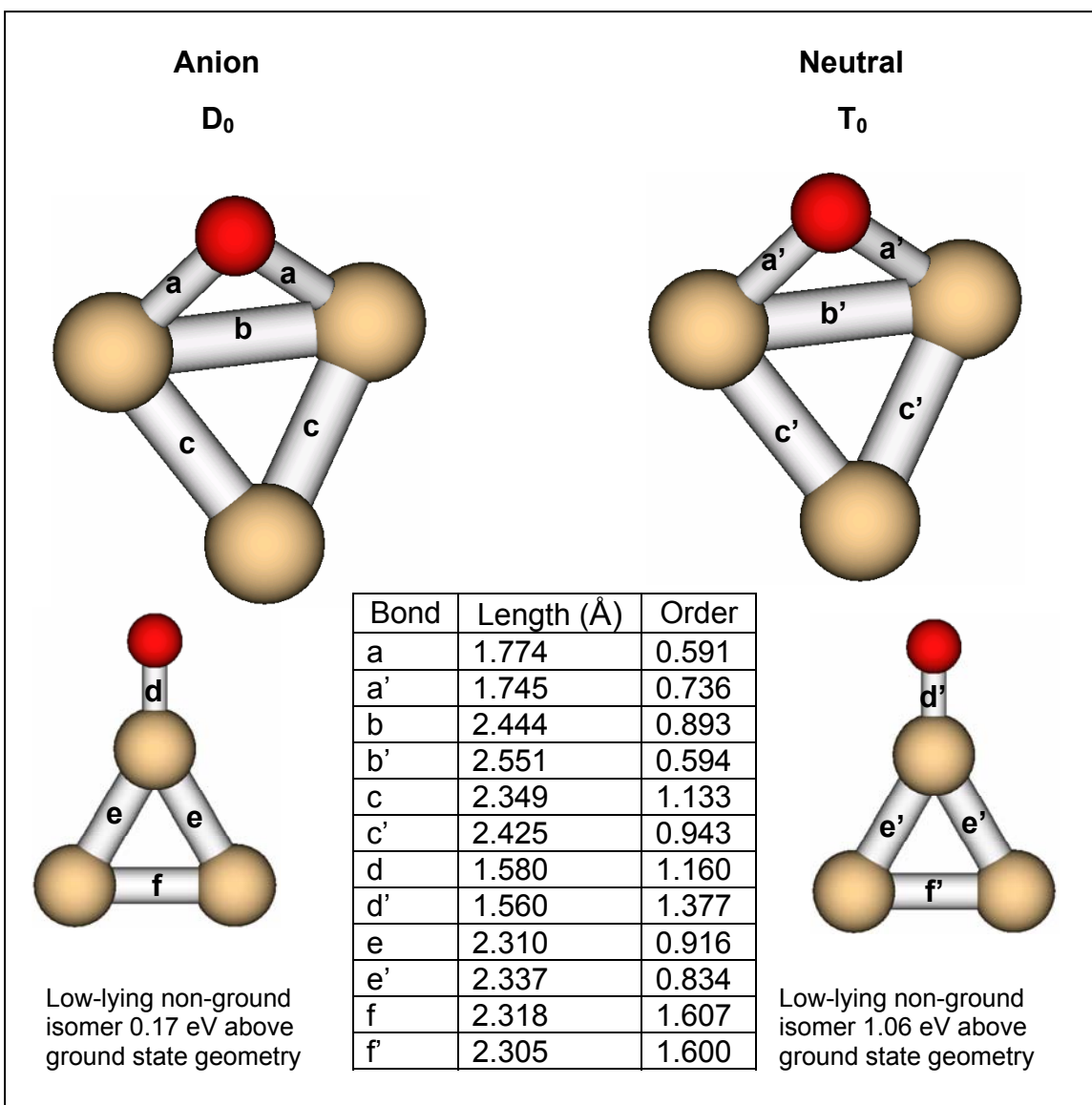


Figure 25. Calculated geometry for ground state Si_3O neutral and anion. Performed with DFT/B3LYP/aug-cc-pVDZ. Also shown is a low-lying non-ground isomer. The ground state isomer is non-planar. The low-lying isomer is planar.

For the anion, there is also another isomer that is only 0.17 eV higher in energy. This is a three-membered ring of silicons with the oxygen attached to one of them. For the ground state, this second isomer is over an electron-volt higher in energy. While these two isomers are very similar, and the reaction coordinate

Table 4. Vibrational analysis for Si₃O. Calculated with DFT/B3LYP/aug-cc-pVDZ.

Anion Ground			Neutral Ground		
Mode	Frequency (cm ⁻¹)	IR Intensity (Debye ² /AMU-Å ²)	Mode	Frequency (cm ⁻¹)	IR Intensity (Debye ² /AMU-Å ²)
1	159	0.0516	1	213	0.0865
2	305	0.389	2	270	0.145
3	375	0.324	3	328	0.143
4	451	0.483	4	408	0.379
5	464	0.0417	5	580	0.0188
6	725	2.487	6	756	1.822

between them is very simple, my calculations show that they are both stable geometries. For the ground state, my calculations show that the adiabatic electron affinity is 2.16 eV and the vertical electron affinity is 2.39 eV. For the second isomer the adiabatic electron affinity is 3.06 eV and the vertical electron affinity is 3.07 eV. The electron affinities of the second isomer are very close due to their similar geometries.

4.11. C₃SiO

C₃SiO, with 47 different initial isomers, was the next molecule I examined. The lowest energy isomer for these calculations is shown in Figure 26 and Table 5. The neutral ground state multiplicity is a triplet. The ground state geometries for the neutral and anion are fairly similar. They are both linear molecules with the oxygen and silicon terminal, differing only slightly in bond lengths. All other geometries and multiplicities are significantly higher in energy. For the ground

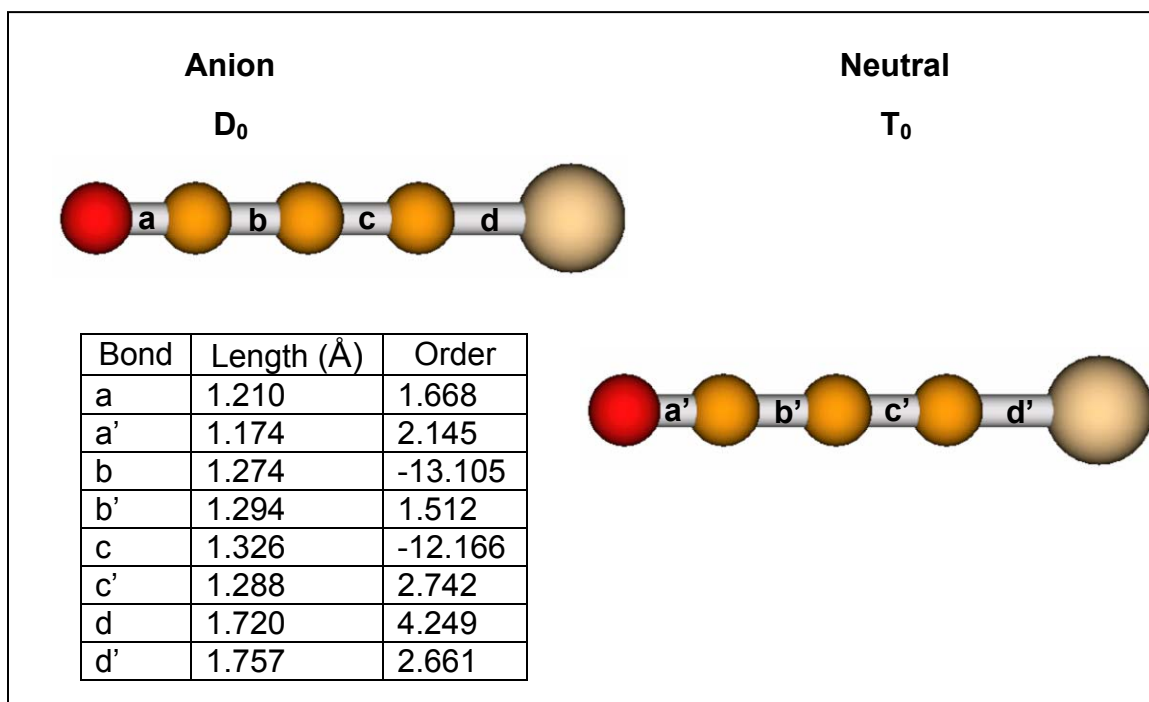


Figure 26. Calculated geometry for ground state C_3SiO neutral and anion. Performed with DFT/B3LYP/aug-cc-pVDZ.

Table 5. Vibrational analysis for C_3SiO . Calculated with DFT/B3LYP/aug-cc-pVDZ. Modes one through three are doubly degenerate.

Anion Ground			Neutral Ground		
Mode	Frequency (cm ⁻¹)	IR Intensity (Debye ² /AMU-Å ²)	Mode	Frequency (cm ⁻¹)	IR Intensity (Debye ² /AMU-Å ²)
1	114	0.00688	1	105	0.00156
2	371	0.159	2	335	0.0703
3	537	0.166	3	495	0.233
4	428	0.266	4	520	0.204
5	1122	5.640	5	1105	0.527
6	1700	1.198	6	1862	0.896
7	2209	64.970	7	2268	54.909

state geometries, my calculations show that the adiabatic electron affinity is 2.01 eV. The vertical electron affinity that I obtained is 2.11 eV.

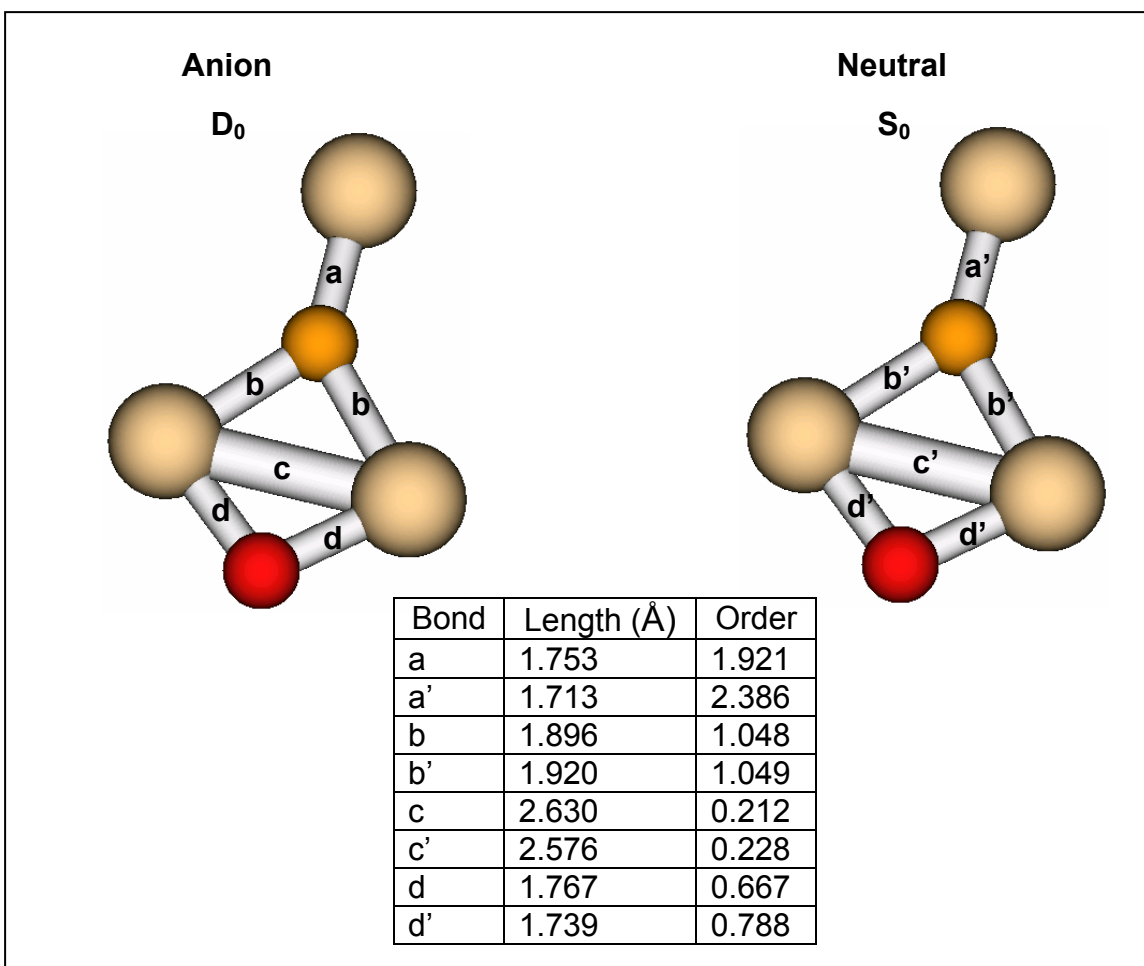


Figure 27. Calculated geometry for ground state CSi_3O neutral and anion. Performed with DFT/B3LYP/aug-cc-pVDZ. Singlet is planar. Doublet is non-planar with a planar four-membered ring.

4.12. CSi_3O

For the CSi_3O molecule, I started with 47 different initial isomers. The lowest energy isomer for these calculations is shown in Figure 27 and Table 6. The neutral ground state multiplicity is a singlet. The ground state geometries for the neutral and anion are similar geometries but have significantly differing bond lengths. They are both four-membered rings with the silicons opposite each other and only weakly bonded, the oxygen between the two silicons, a carbon

Table 6. Vibrational analysis for CSi_3O . Calculated with DFT/B3LYP/aug-cc-pVDZ. Mode five is doubly degenerate.

Anion Ground			Neutral Ground		
Mode	Frequency (cm ⁻¹)	IR Intensity (Debye ² /AMU-Å ²)	Mode	Frequency (cm ⁻¹)	IR Intensity (Debye ² /AMU-Å ²)
1	74	0.158	1	74	0.00013
2	102	0.0870	2	132	0.00363
3	223	0.260	3	233	0.0319
4	428	0.0293	4	379	0.0803
5	549	0.177	5	474	0.572
6	622	0.619	6	728	6.500
7	701	0.987	7	759	2.778
8	938	0.804	8	1161	8.897

between the two silicons and the final silicon outside the ring and bonded to the carbon. All other geometries and multiplicities are significantly higher in energy. For the ground state geometries, my calculations show that the adiabatic electron affinity is 1.06 eV. The vertical electron affinity that I obtained is 1.38 eV. Once again the relatively large difference in electron affinities is due to significant differences in bond lengths.

4.13. $\text{C}_3\text{Si}_2\text{O}$

Next, I looked at $\text{C}_3\text{Si}_2\text{O}$. For this molecule, I started with 195 different initial isomers. The lowest energy isomers for these calculations are shown in Figure 28 and Table 7. The neutral ground state multiplicity is a singlet. The ground state geometries for the neutral and anion are different isomers. For the doublet, the ground state is a four-membered ring with oxygen between the two silicons, a carbon opposite the oxygen, and the remaining two carbons linearly

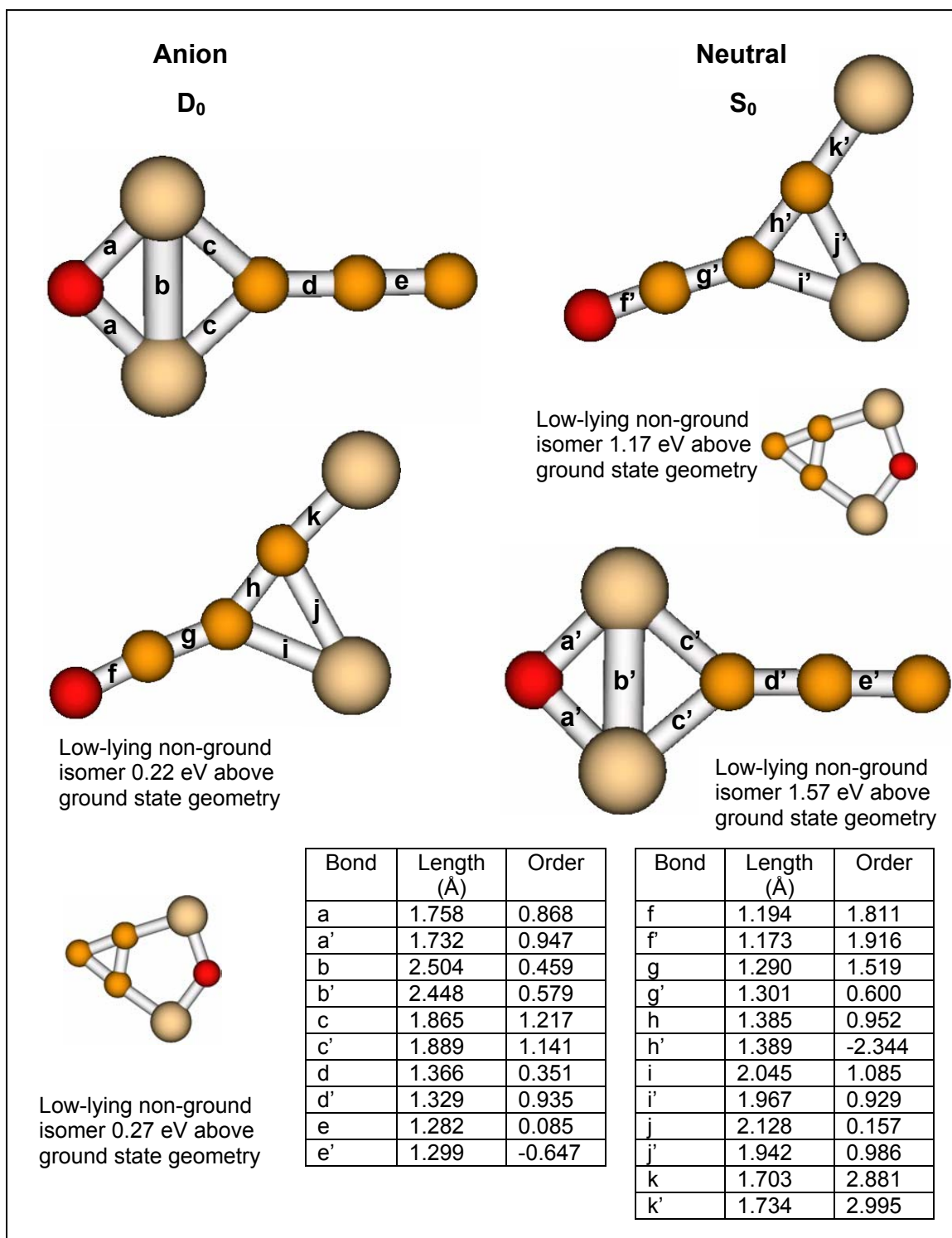


Figure 28. Calculated geometry for ground state C_3Si_2O neutral and anion. Performed with DFT/B3LYP/aug-cc-pVDZ. Since the ground state isomers differ, the corresponding isomer is also shown. Another low-lying non-ground isomer is also shown. Singlet four-membered ring isomer is non-planar with a planar ring. All other isomers shown are planar.

Table 7. Vibrational analysis for C₃Si₂O. Calculated with DFT/B3LYP/aug-cc-pVDZ.

Anion Ground			Neutral Ground		
Mode	Frequency (cm ⁻¹)	IR Intensity (Debye ² /AMU-Å ²)	Mode	Frequency (cm ⁻¹)	IR Intensity (Debye ² /AMU-Å ²)
1	80	0.00199	1	94	0.0181
2	126	0.174	2	116	0.0151
3	174	0.105	3	233	0.0157
4	371	0.00396	4	350	0.0309
5	430	0.322	5	373	0.692
6	445	0.0100	6	444	0.283
7	463	0.223	7	507	0.755
8	525	0.120	8	653	1.268
9	706	3.184	9	695	0.709
10	741	2.417	10	1089	0.391
11	1238	0.156	11	1597	0.157
12	1918	8.206	12	2213	52.848

attached to the carbon within the ring. The ground state geometry for the neutral has a linear body of O-C-C-C-Si which is bent at the center carbon, and the remaining silicon attached to both the second and third carbon. The anion isomer which corresponds to the neutral ground geometry is 0.22 eV lower than the ground. There is also a third anion isomer which is low-lying in energy. This a symmetric, five-membered ring with oxygen between two silicons, two carbons opposite the oxygen, and the remaining carbon attached to both the carbons in the ring. This isomer is 0.27 eV above the doublet ground state. The corresponding singlet isomer is the second lowest neutral geometry, 1.17 eV above the neutral ground state. The neutral isomer which corresponds to the anion ground geometry is the third lowest singlet state at 1.57 eV above ground. For the four-membered ring, anion ground state, my calculations show that the

adiabatic electron affinity is 2.95 eV and the vertical electron affinity is 3.04 eV. For the neutral ground geometry isomer the adiabatic electron affinity is 1.19 eV and the vertical electron affinity is 1.48 eV. Finally, for the five-membered ring, the adiabatic electron affinity is 2.29 eV and the vertical electron affinity is 2.38 eV

4.14. C₂Si₃O

The next molecule examined was C₂Si₃O. For this, I started with 195 different initial isomer geometries. The lowest energy isomer for these calculations is shown in Figure 29 and Table 8. The neutral ground state multiplicity is a singlet. The ground state geometries for the neutral and anion are similar geometries but have moderately differing bond lengths. They are both planar five-membered rings with the oxygen between two silicons and the carbons together opposite the oxygen. The carbons together with the third silicon form a planar three-membered ring. All other geometries and multiplicities are significantly higher in energy. For the ground state geometries, my calculations show that the adiabatic electron affinity is 1.90 eV. The vertical electron affinity that I obtained is 1.99 eV.

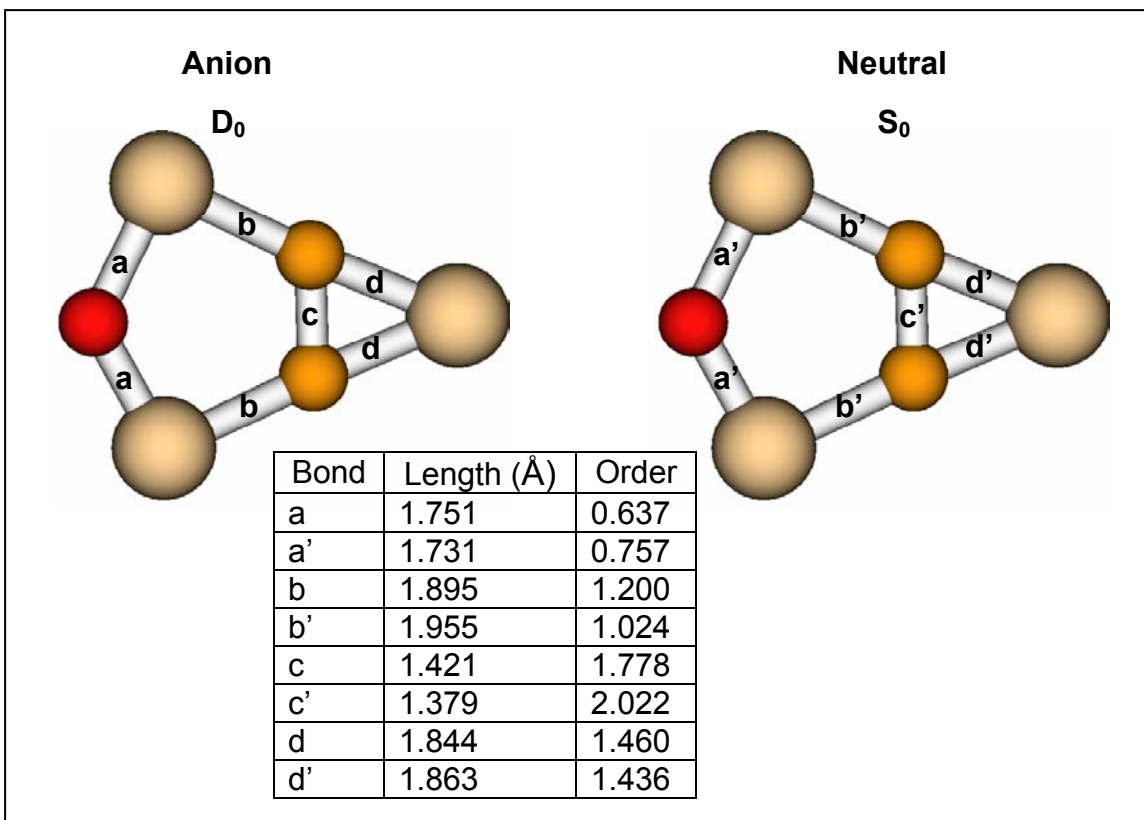


Figure 29. Calculated geometry for ground state C_2Si_3O neutral and anion. Performed with DFT/B3LYP/aug-cc-pVDZ. Both molecules are planar.

Table 8. Vibrational analysis for C_2Si_3O . Calculated with DFT/B3LYP/aug-cc-pVDZ.

Anion Ground			Neutral Ground		
Mode	Frequency (cm ⁻¹)	IR Intensity (Debye ² /AMU-Å ²)	Mode	Frequency (cm ⁻¹)	IR Intensity (Debye ² /AMU-Å ²)
1	144	0.00628	1	118	0.00227
2	246	0.0185	2	145	0.0365
3	257	0.122	3	225	0.00010
4	336	0.00001	4	238	0.00668
5	389	0.0732	5	378	0.0150
6	437	0.490	6	412	0.916
7	449	0.427	7	453	1.361
8	588	0.725	8	633	1.682
9	608	1.133	9	764	4.737
10	852	2.305	10	842	3.825
11	931	3.558	11	925	3.403
12	1223	0.0500	12	1402	1.846

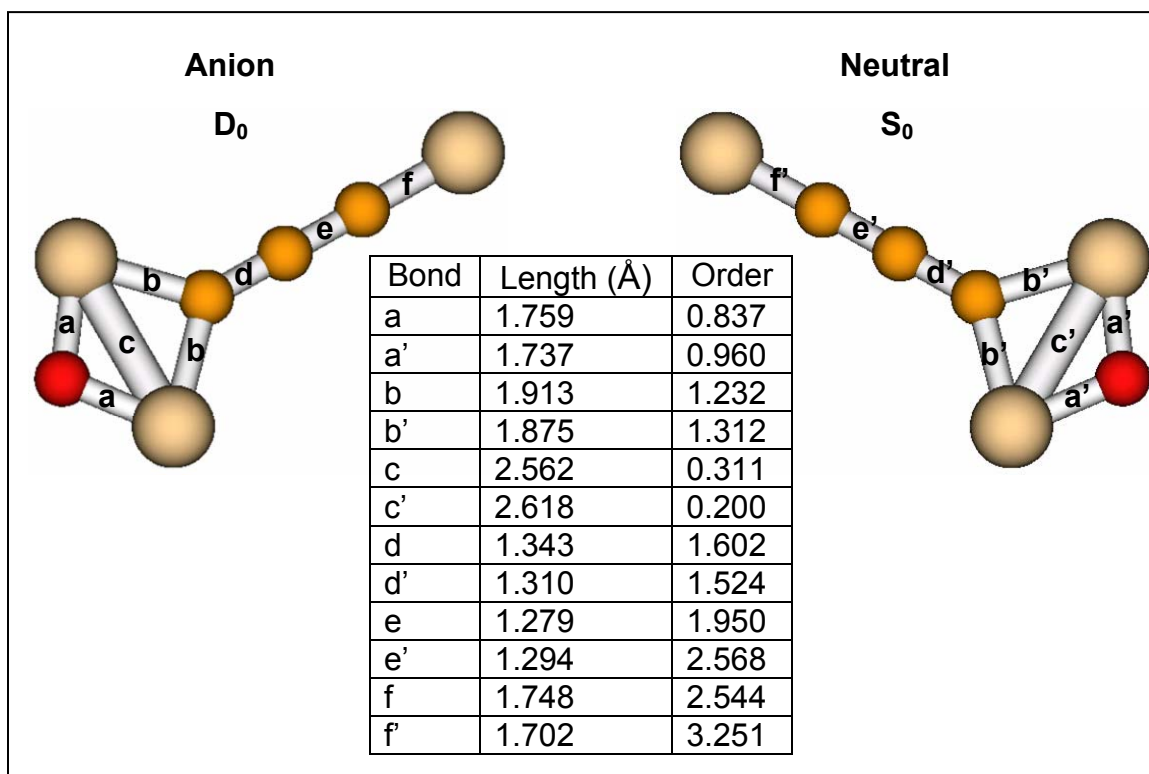


Figure 30. Calculated geometry for ground state C_3Si_3O neutral and anion. Performed with DFT/B3LYP/aug-cc-pVDZ. Both molecules are planar.

4.15. C_3Si_3O

For the C_3Si_3O molecule, I started with 1315 different initial isomer geometries. The lowest energy isomer for these calculations is shown in Figure 30 and Table 9. The neutral ground state multiplicity is a singlet. The ground state geometries for the neutral and anion are very similar geometries differing only slightly in their bond lengths. They both have four-membered rings with the oxygen between two silicons and a carbon opposite the oxygen; the remaining two carbons are bonded linearly to the carbon in the ring; and the third silicon terminating the linear carbon branch. All other geometries and multiplicities are significantly higher in energy. For the ground state geometries, my calculations

Table 9. Vibrational analysis for C_3Si_3O , calculated with DFT/B3LYP/aug-cc-pVDZ.

Anion Ground			Neutral Ground		
Mode	Frequency (cm ⁻¹)	IR Intensity (Debye ² /AMU-Å ²)	Mode	Frequency (cm ⁻¹)	IR Intensity (Debye ² /AMU-Å ²)
1	59	0.00075	1	59	0.0745
2	63	0.0639	2	60	0.00730
3	89	0.0568	3	149	1.032
4	190	0.0109	4	188	0.154
5	249	0.0621	5	211	0.0343
6	322	0.0481	6	322	0.579
7	442	0.470	7	435	0.379
8	475	0.0135	8	458	0.873
9	476	0.216	9	547	0.157
10	528	0.00219	10	606	0.00302
11	697	3.388	11	743	16.020
12	735	1.965	12	753	6.747
13	742	3.290	13	789	4.359
14	1380	1.863	14	1487	0.502
15	1833	9.704	15	1990	66.335

show that the adiabatic electron affinity is 1.58 eV. The vertical electron affinity that I obtained is 1.69 eV.

4.16. C₄O

Next, I looked at C₄O. For this molecule, I started with 17 different initial isomers. The lowest energy isomer for these calculations is shown in Figure 31 and Table 10. The neutral ground state multiplicity is a triplet. The ground state geometries for the neutral and anion are similar geometries but have moderately differing bond lengths. They are both linear molecules with a terminal oxygen. All other geometries and multiplicities are significantly higher in energy. For the

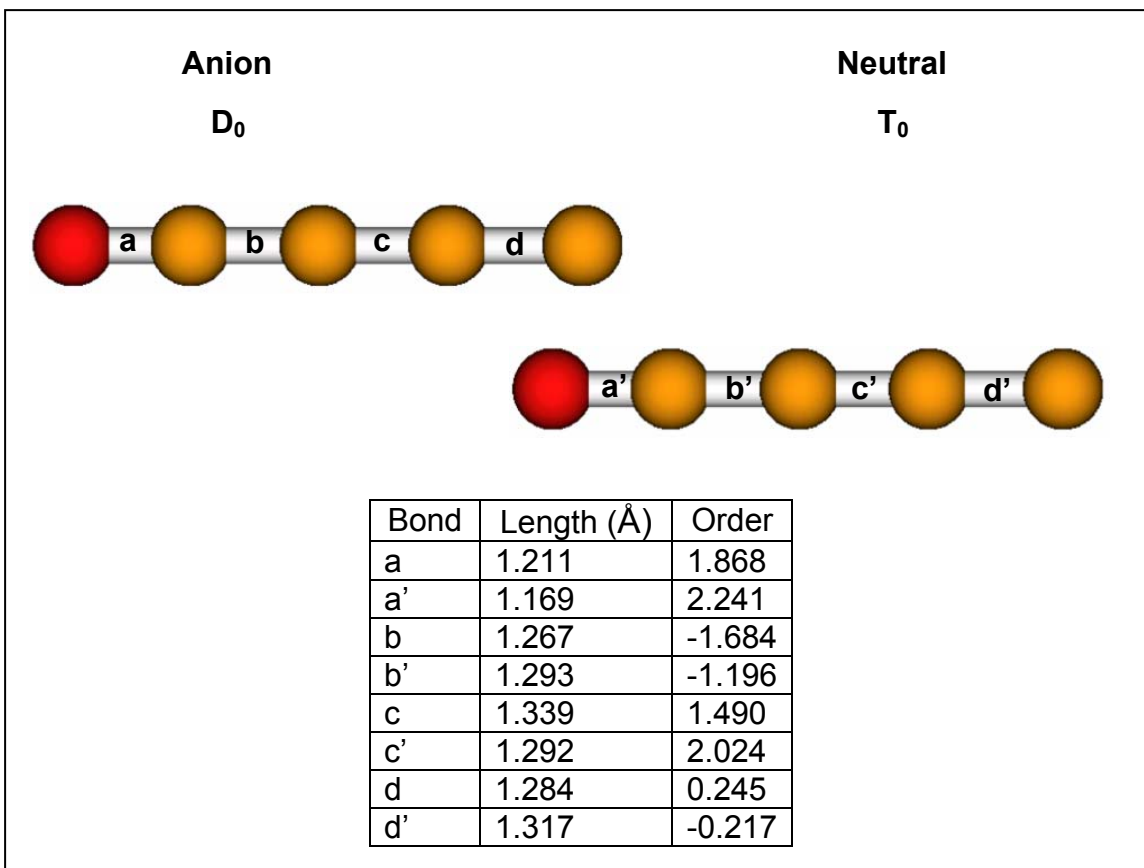


Figure 31. Calculated geometry for ground state C_4O neutral and anion. Performed with DFT/B3LYP/aug-cc-pVDZ.

ground state geometries, my calculations show that the adiabatic electron affinity is 2.87 eV, which is significantly higher than the experimental value of 2.05 ± 0.15 (Oakes and Ellison, 1986: 6263). The vertical electron affinity that I obtained is 3.05 eV.

4.17. Si_4O

Figure 32 and Table 11 show the lowest energy isomers for Si_4O . For this molecule, I started with 17 different initial isomers. The neutral ground state

Table 10. Vibrational analysis for C₄O, calculated with DFT/B3LYP/aug-cc-pVDZ. Modes one through three are doubly degenerate.

Anion Ground			Neutral Ground		
Mode	Frequency (cm ⁻¹)	IR Intensity (Debye ² /AMU-Å ²)	Mode	Frequency (cm ⁻¹)	IR Intensity (Debye ² /AMU-Å ²)
1	132	0.184	1	131	0.165
2	382	0.104	2	351	0.127
3	492	0.0942	3	494	0.258
4	751	0.211	4	771	0.126
5	1458	2.973	5	1460	0.472
6	1940	8.881	6	1979	8.969
7	2260	21.315	7	2304	20.427

multiplicity is a triplet. The ground state geometries for the neutral and anion are both five-membered rings. For both, there are two conformations that are very close in energy. For the doublet, the ground state is a planar, asymmetric conformation. The second doublet conformation, only 0.11 eV above the ground isomer, has three silicons which form a central three-membered ring; the oxygen is bonded to two of these and bent up from the plane of the three-membered ring by about 10°; and the fourth silicon is bent up from the three-membered ring by about 75°. The ground state singlet is similar to the ground state doublet except that one of the silicons opposite the oxygen is bent about 18° up from the oxygen and silicons next to it and the silicon furthest from the oxygen is bent about 21.5° up from the oxygen and the silicons next to it. The second singlet conformation is a symmetric ring with the silicons not bonded to the oxygen having dihedral angles of +21.3° and -21.3°. All other geometries and multiplicities are significantly higher in energy. For the ground state geometries, my calculations

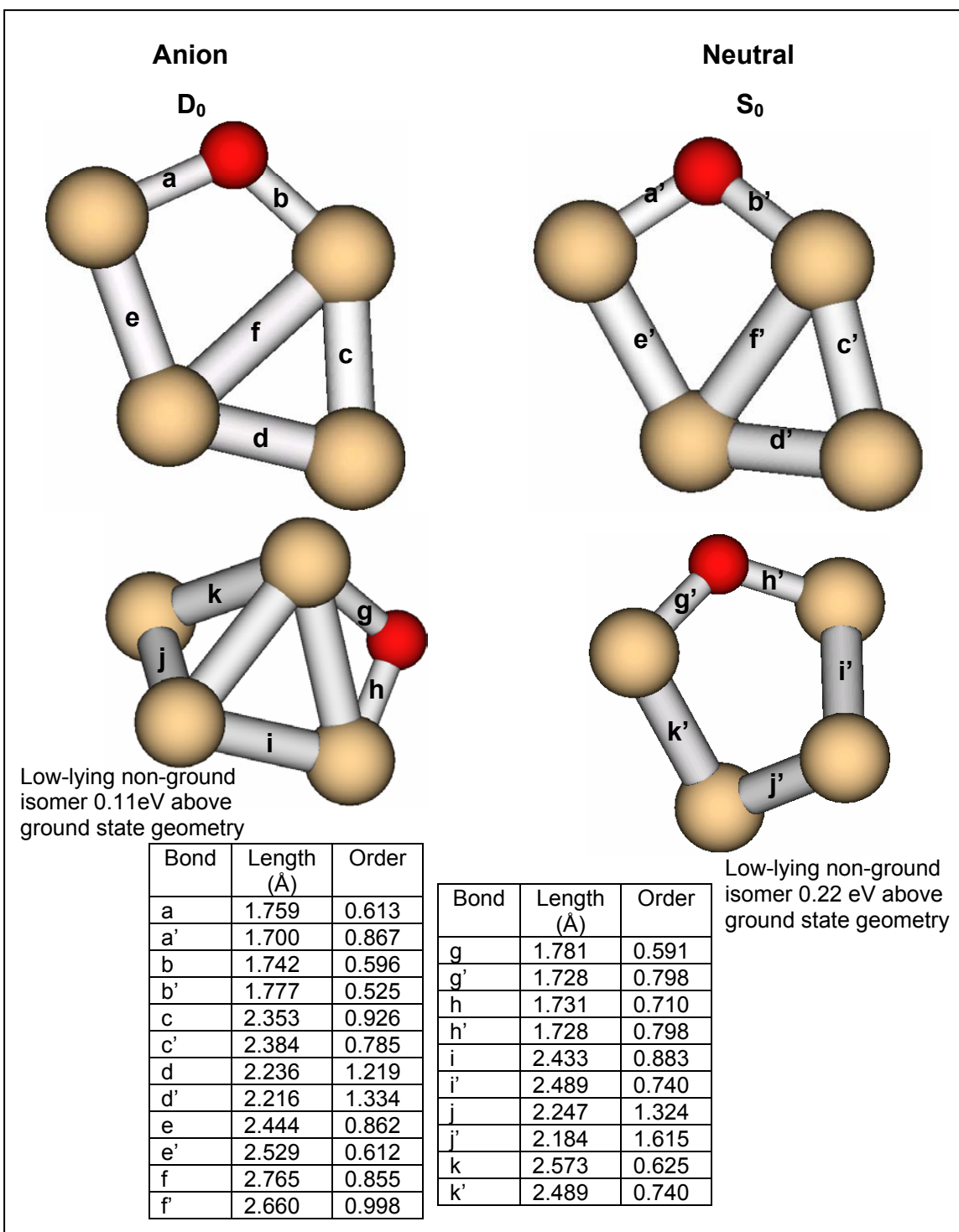


Figure 32. Calculated geometry for ground state Si_4O neutral and anion. Performed with DFT/B3LYP/aug-cc-pVDZ. Also shown is a second conformal isomer that is low-lying in energy. The doublet ground state is planar. All others are non-planar.

Table 11. Vibrational analysis for Si₄O, calculated with DFT/B3LYP/aug-cc-pVDZ.

Anion Ground			Neutral Ground		
Mode	Frequency (cm ⁻¹)	IR Intensity (Debye ² /AMU-Å ²)	Mode	Frequency (cm ⁻¹)	IR Intensity (Debye ² /AMU-Å ²)
1	96	0.0442	1	78	0.0323
2	183	0.287	2	132	0.0378
3	189	0.00928	3	155	0.155
4	213	0.326	4	224	0.0821
5	317	0.0894	5	293	0.649
6	339	0.206	6	330	0.442
7	499	0.0176	7	526	0.572
8	621	0.00664	8	624	1.936
9	661	1.401	9	752	0.438

show that the adiabatic electron affinity is 1.89 eV. The vertical electron affinity that I obtained is 2.00 eV. For the low-lying conformation, my calculations show that the adiabatic electron affinity is 2.00 eV and the vertical electron affinity is 2.44 eV.

4.18. C₄SiO

C₄SiO, with 128 different initial isomers, was the next molecule I looked at. The lowest energy isomer for these calculations is shown in Figure 33 and Table 12. The neutral ground state multiplicity is a singlet. The ground state geometries for the neutral and anion are both linear with a terminal oxygen and silicon. The bond lengths are roughly similar, as well. All other geometries and multiplicities are significantly higher in energy. For the ground state geometries,

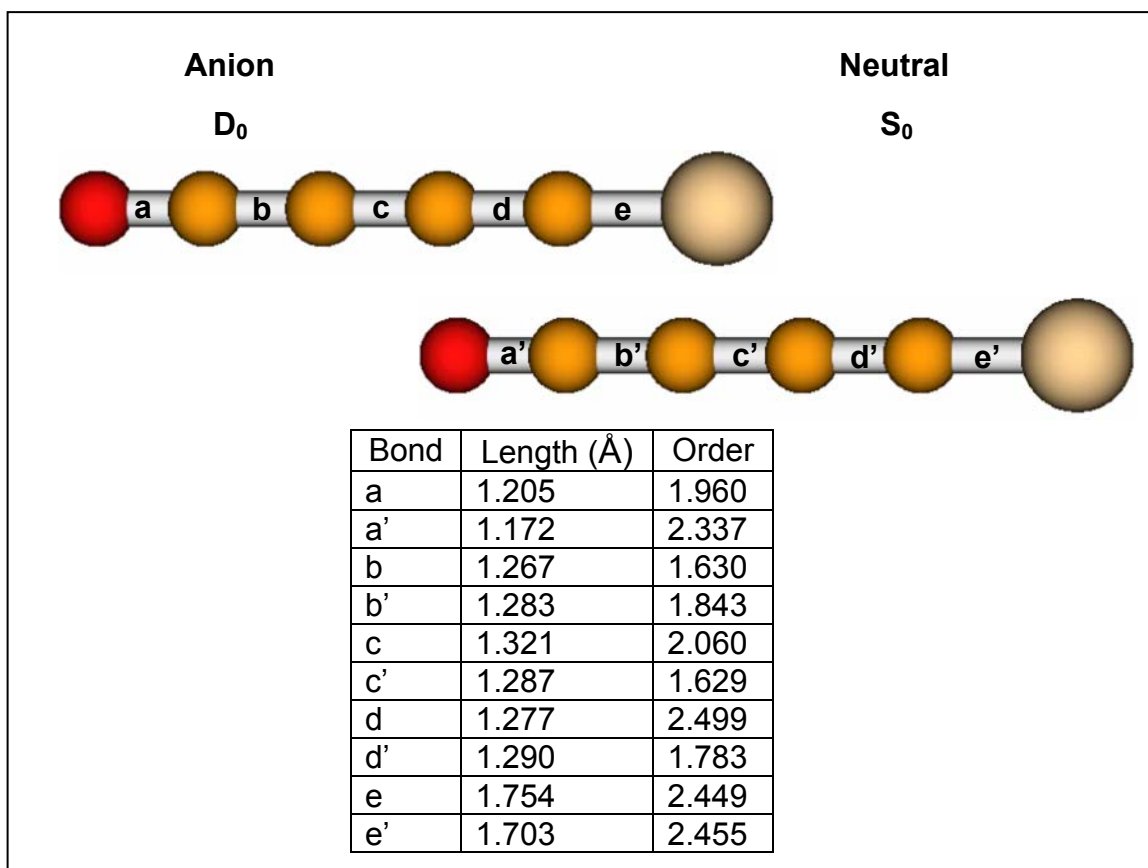


Figure 33. Calculated geometry for ground state C_4SiO neutral and anion. Performed with DFT/B3LYP/aug-cc-pVDZ.

Table 12. Vibrational analysis for C_4SiO , calculated with DFT/B3LYP/aug-cc-pVDZ. Modes one through four are doubly degenerate.

Anion Ground			Neutral Ground		
Mode	Frequency (cm ⁻¹)	IR Intensity (Debye ² /AMU-Å ²)	Mode	Frequency (cm ⁻¹)	IR Intensity (Debye ² /AMU-Å ²)
1	80	0.107	1	67	0.0142
2	196	0.00428	2	153	0.0370
3	434	0.196	3	487	0.377
4	529	0.263	4	548	0.230
5	469	1.015	5	503	0.604
6	939	0.310	6	1025	0.424
7	1540	12.184	7	1641	12.722
8	1977	4.534	8	2106	8.883
9	2249	95.946	9	2312	109.535

my calculations show that the adiabatic electron affinity is 1.61 eV. The vertical electron affinity that I obtained is 1.73 eV.

4.19. CSi₄O

I next looked at CSi₄O. For this molecule I started with 128 different initial isomer geometries. The lowest energy isomer for these calculations is shown in Figure 34 and Table 13. The neutral ground state multiplicity is a singlet. The ground state geometries are similar shapes but with several very different bond lengths. They are both a combination of a five-membered ring and a three-membered ring. The five-membered ring has an oxygen at its top between two silicons. At the bottom are a silicon and carbon which, together with the final silicon, are also part of the three-membered ring. All other geometries and multiplicities are significantly higher in energy. For the ground state geometries, my calculations show that the adiabatic electron affinity is 2.08 eV. The vertical electron affinity that I obtained is 2.23 eV.

4.20. C₄Si₂O

Next I looked at C₄Si₂O. For this molecule I started with 28 different initial isomers. The isomers chosen as initial points are not exhaustive, but were chosen based upon all previous results. The lowest energy isomer for these calculations is shown in Figure 35 and Table 14. The neutral ground state multiplicity is a singlet. The ground state geometries are similar shapes but with several very different bond lengths. They are both four-membered rings with the

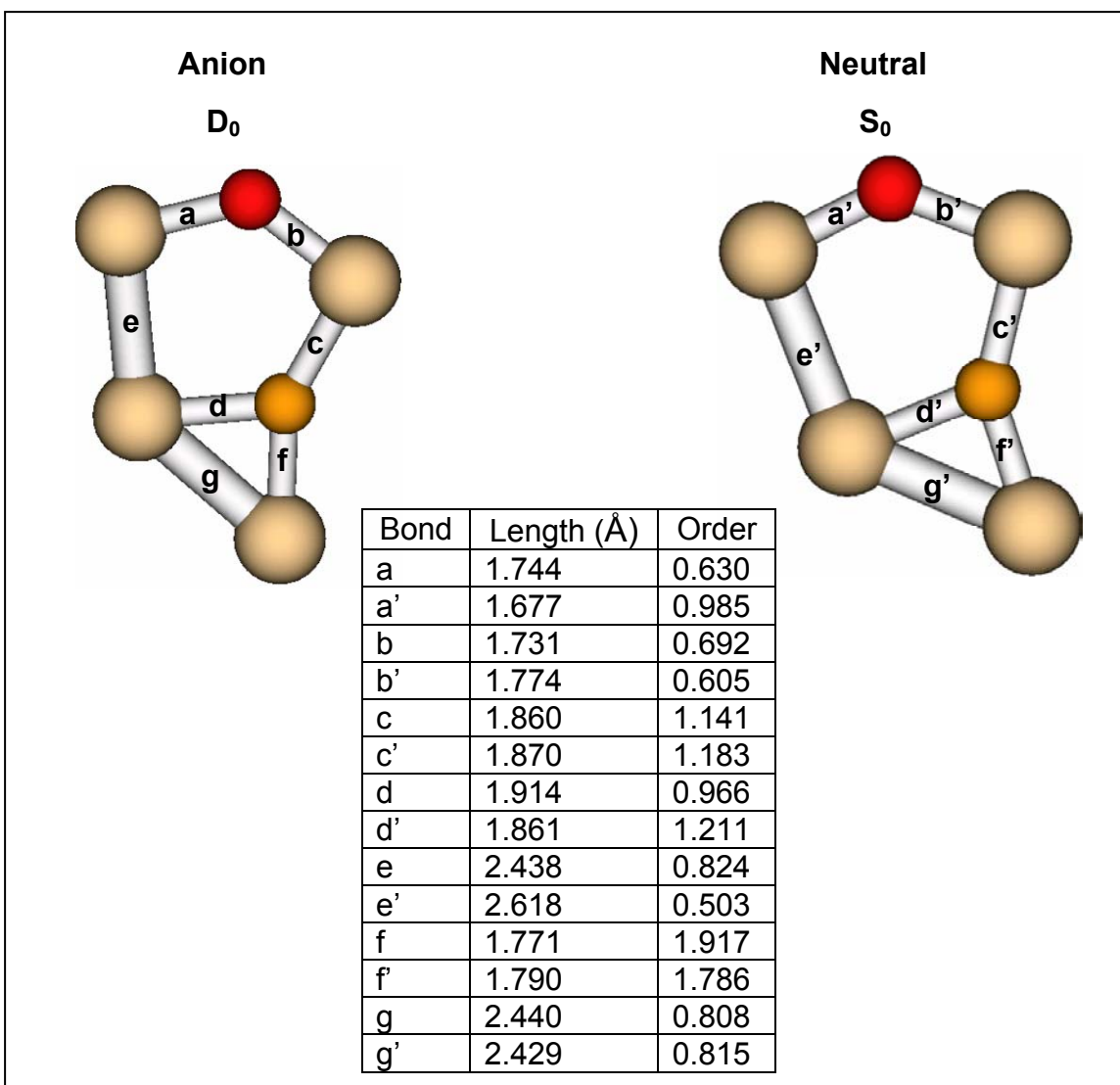


Figure 34. Calculated geometry for ground state CSi_4O neutral and anion. Performed with DFT/B3LYP/aug-cc-pVDZ. The doublet molecule is planar. The singlet molecule is non-planar.

oxygen between two silicons and a carbon opposite the oxygen; the remaining three carbons are bonded linearly to the carbon in the ring. The singlet is planar. However, the oxygen in the doublet is bent up 35° from the plane of the ring. All other geometries and multiplicities are significantly higher in energy. For the ground state geometries, my calculations show that the adiabatic electron affinity

Table 13. Vibrational analysis for CSi_4O , calculated with DFT/B3LYP/aug-cc-pVDZ.

Anion Ground			Neutral Ground		
Mode	Frequency (cm^{-1})	IR Intensity ($\text{Debye}^2/\text{AMU}\cdot\text{\AA}^2$)	Mode	Frequency (cm^{-1})	IR Intensity ($\text{Debye}^2/\text{AMU}\cdot\text{\AA}^2$)
1	74	0.00137	1	29	0.0109
2	181	0.00290	2	82	0.00103
3	185	0.0445	3	156	0.0656
4	210	0.00686	4	185	0.0120
5	253	0.0376	5	234	0.151
6	340	0.136	6	318	0.226
7	387	0.791	7	389	1.433
8	456	0.640	8	465	0.709
9	589	1.014	9	569	1.228
10	625	0.344	10	706	0.650
11	699	0.193	11	805	1.191
12	1059	4.693	12	1041	6.271

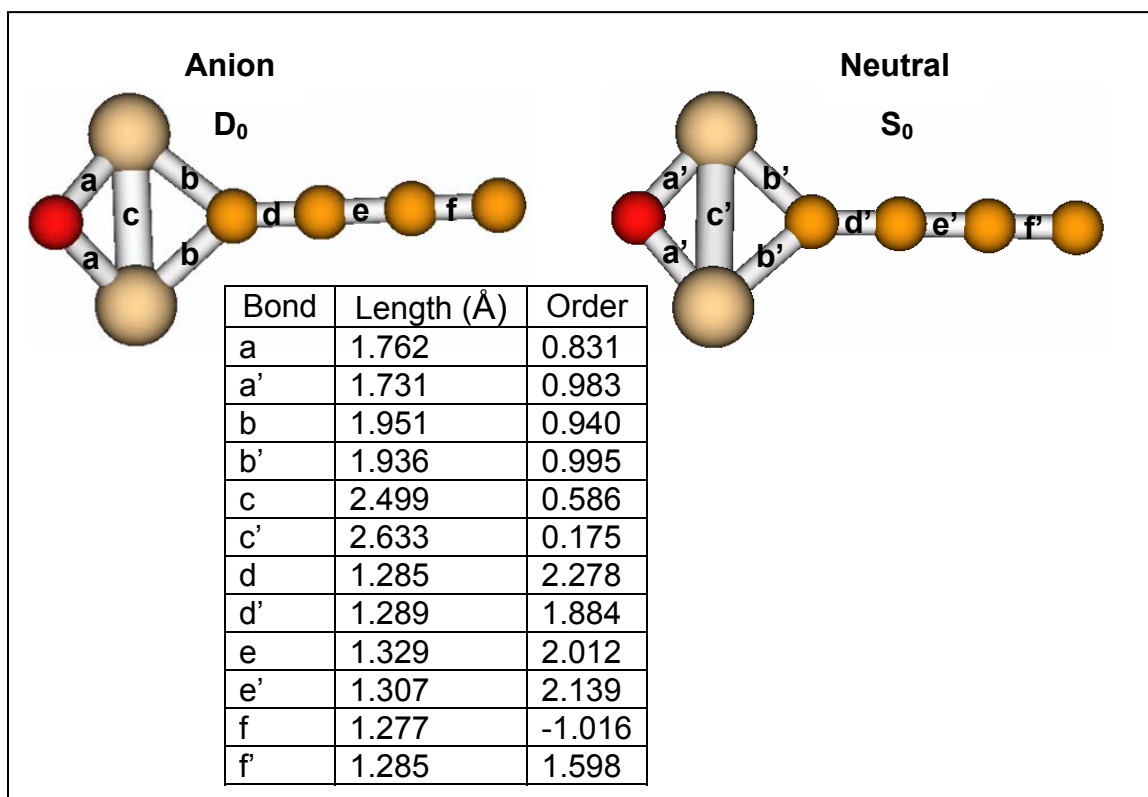


Figure 35. Calculated geometry for ground state $\text{C}_4\text{Si}_2\text{O}$ neutral and anion. Performed with DFT/B3LYP/aug-cc-pVDZ. The doublet is non-planar. The singlet is non-planar with a planar ring.

Table 14. Vibrational analysis for C₄Si₂O, calculated with DFT/B3LYP/aug-cc-pVDZ.

Anion Ground			Neutral Ground		
Mode	Frequency (cm ⁻¹)	IR Intensity (Debye ² /AMU-Å ²)	Mode	Frequency (cm ⁻¹)	IR Intensity (Debye ² /AMU-Å ²)
1	76	0.0350	1	77	0.144
2	91	0.147	2	84	0.122
3	157	0.0618	3	139	0.0110
4	189	0.373	4	184	0.0290
5	257	0.0596	5	219	0.0284
6	344	0.775	6	367	0.700
7	363	0.506	7	391	0.562
8	377	0.641	8	459	1.216
9	421	1.392	9	465	0.113
10	478	0.223	10	564	0.177
11	565	0.112	11	752	7.095
12	736	2.686	12	761	2.791
13	1013	0.176	13	1065	2.333
14	1790	4.139	14	1828	3.196
15	2005	21.599	15	2149	66.400

is 1.89 eV. The vertical electron affinity that I obtained is 2.26 eV.

4.21. C₂Si₄O

For C₂Si₄O, I started with 170 different initial isomers. The lowest energy isomers for these calculations are shown in Figure 36 and Table 15. The neutral ground state multiplicity is a singlet. The ground state geometries for the neutral and anion are very similar geometries differing only slightly in their bond lengths. They are both five-membered rings with the oxygen between two silicons and the carbons together opposite the oxygen. The carbons, together with the remaining two silicons, form a four-membered ring with one silicon 30° out of the five-

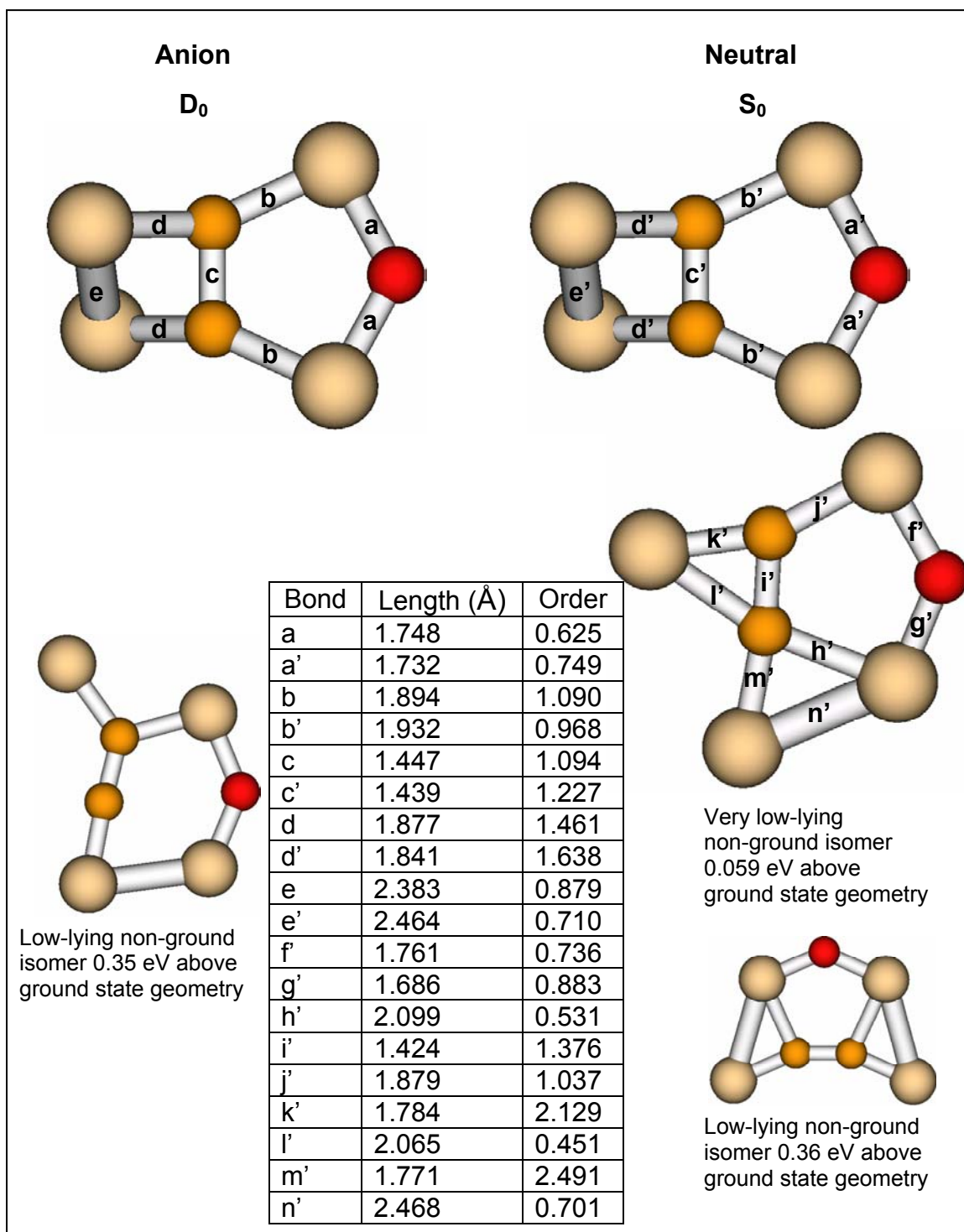


Figure 36. Calculated geometry for ground state C_2Si_4O neutral and anion. Performed with DFT/B3LYP/aug-cc-pVDZ. Several other low-lying non-ground isomers are also shown. Of particular note is the very low-lying non-ground singlet isomer at 0.06 eV above ground. Ground state isomers are non-planar. All low-lying isomers are planar.

Table 15. Vibrational analysis for C₂Si₄O, calculated with DFT/B3LYP/aug-cc-pVDZ.

Anion Ground			Neutral Ground		
Mode	Frequency (cm ⁻¹)	IR Intensity (Debye ² /AMU-Å ²)	Mode	Frequency (cm ⁻¹)	IR Intensity (Debye ² /AMU-Å ²)
1	80	0.0708	1	79	0.0487
2	86	0.0690	2	103	0.0177
3	178	0.184	3	175	0.00224
4	241	0.00416	4	192	0.00409
5	250	0.0107	5	249	0.244
6	366	0.223	6	346	0.00187
7	378	0.138	7	372	0.166
8	403	0.0619	8	419	0.436
9	488	1.454	9	507	1.267
10	491	1.026	10	530	1.201
11	608	1.066	11	628	1.428
12	631	0.107	12	754	2.988
13	784	0.305	13	824	0.915
14	914	1.827	14	954	2.464
15	1097	0.531	15	1148	5.037

membered ring's plane and the other 30° into the plane. There is also another very low-lying singlet isomer only 0.059 eV above the ground. This has a five membered ring like the ground state, but with one silicon asymmetrically bonded to the two carbons and the other bonded to a carbon and silicon of the ring. Another low-lying singlet, at 0.36 eV above ground, is a symmetric five membered ring like the ground state, but with the two remaining silicons bonded to a carbon and silicon on either side of the ring. The reaction coordinate connecting these three isomers is very simple, but at the B3LYP/aug-cc-pVDZ level of theory, they are all stable states. Neither of the two low-lying, non-ground singlet states appears to have corresponding stable anion isomers. There is a low-lying anion isomer 0.35 eV above the ground state. This is a six

membered ring with the oxygen between two silicons; one of the silicons is bonded to another silicon; the two carbons are opposite the oxygen; and the remaining silicon is outside the ring bonded to the carbon nearer the oxygen. This isomer does not appear to have a corresponding stable neutral isomer. For the ground state geometries, my calculations show that the adiabatic electron affinity is 1.84 eV. The vertical electron affinity that I obtained is 1.95 eV. I also obtained a vertical electron affinity for the six-membered ring of 2.16 eV.

4.22. Functional Group Analysis

Now that we have examined each of the molecules in detail, we are prepared to examine the overall picture. We start with Figures 40 and 41. Respectively, these are the complete maps for the ground state isomers of the neutral and anion.

By looking at these maps, we can determine what bonds and functional groups are preferred. First we look at oxygen placement. Among stable, low-energy isomers, only three oxygen configurations exist. The rarest of these is a sila-ketene, where the oxygen is terminally bonded to a silicon ($R - Si \equiv O$). Other than silicon-monoxide, where it is the only option, this appears in a ground state isomer only once: for the Si_2O anion. For all other molecules, this is a high energy structure.

The next most common oxygen configuration is a ketene, where the oxygen is terminally bonded to a carbon ($R = C = O$). This is the most stable bond for molecules with zero or one silicon. It is also seen as a ground state in

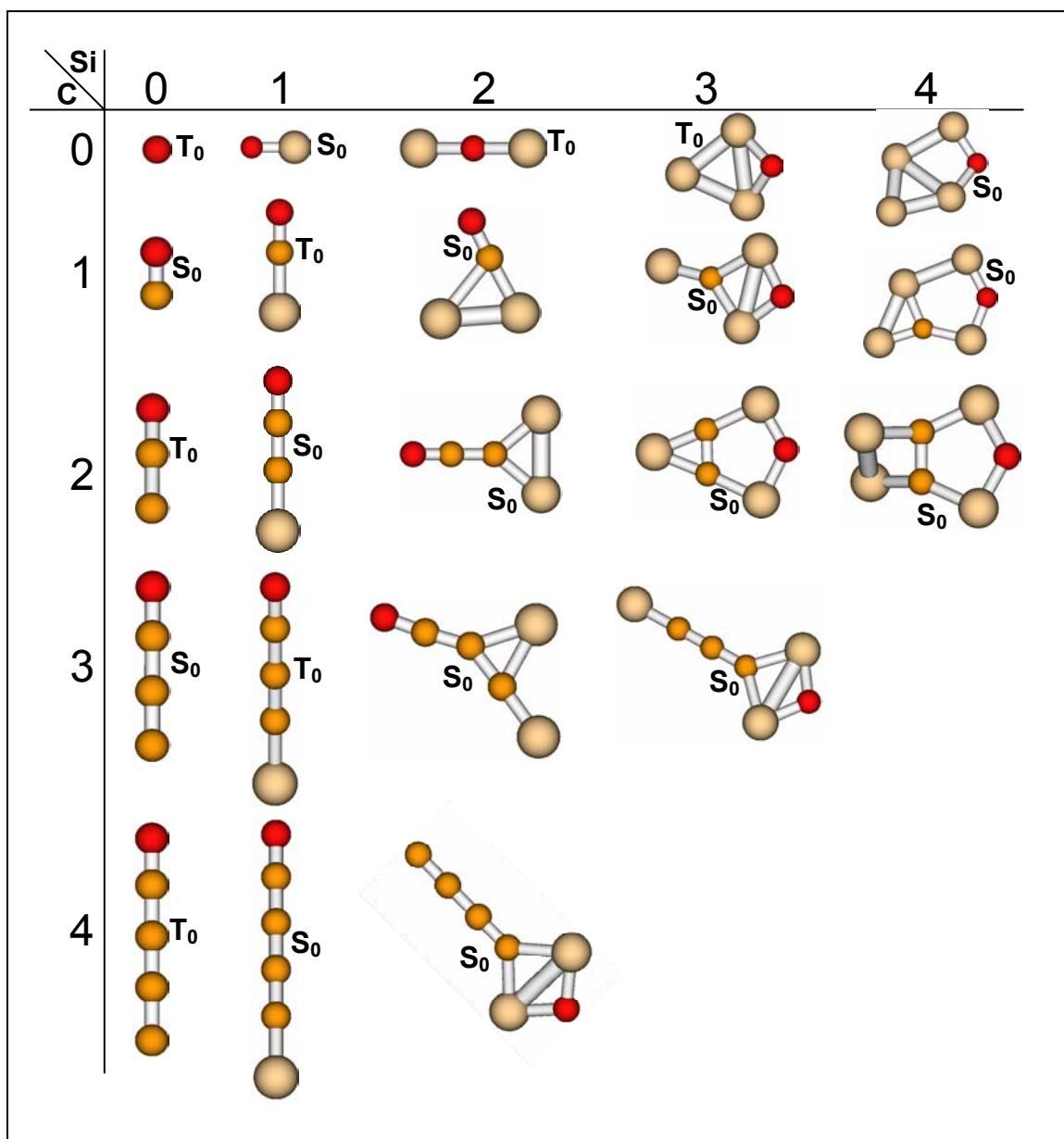


Figure 37. Neutral ground state isomers for C_mSi_nO , $m, n \leq 4$ with DFT/B3LYP/aug-cc-pVDZ

some molecules with two silicons and three or fewer carbons. For other molecules, this is a stable structure, but tends to be relatively high in energy.

The most common oxygen bond is a disilyl-ether, where the oxygen is bonded between two silicon atoms ($R-Si-O-Si-R'$). For molecules with three

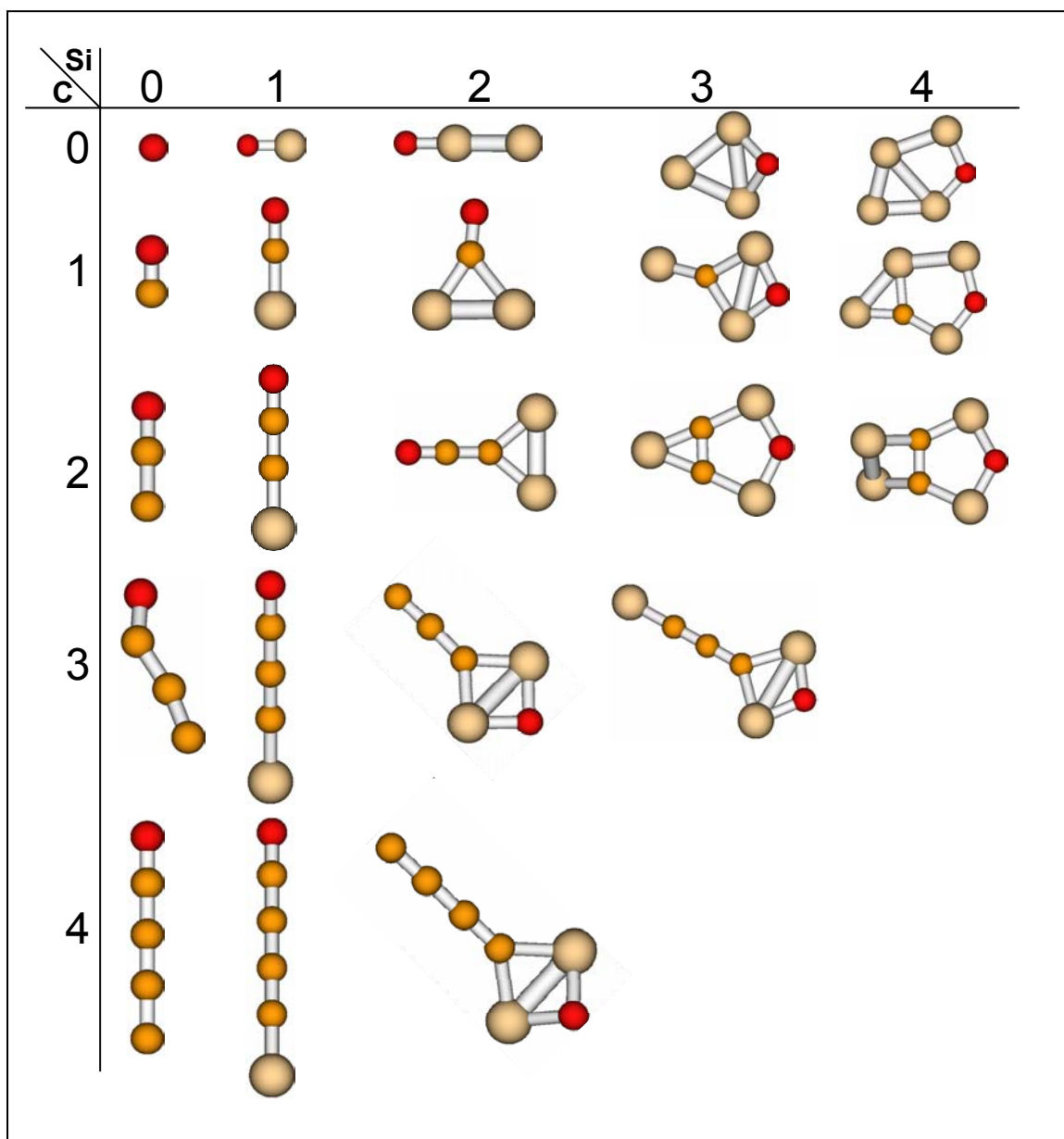


Figure 38. Anion ground state isomers for C_mSi_nO , $m, n \leq 4$ with DFT/B3LYP/aug-cc-pVDZ. All anion ground states have doublet multiplicity.

or more silicons, this is the most stable and only ground state configuration. The $Si-O-Si$ three atom group occurs in three primary configurations. First, is a linear configuration which occurs when one of the silicon atoms is terminal. While stable, this is not generally a very low-energy structure. The next most

common configuration is as part of a four-membered ring. In these isomers, $Si-O-Si$ has a characteristic angle of about 95° . This is usually a ground or low-lying configuration for molecules with two or three silicons. The final and most common configuration is as part of a five-membered ring. In five-membered ring isomers, $Si-O-Si$ has a characteristic angle of about 125° . For molecules with three or more silicons this is generally a stable and very low-lying isomer or the ground state.

Stable isomers with other oxygen configurations such as ethers ($R-O-R'$), silyl-ethers ($R-Si-O-R'$), ketones ($>C=O$), and strange configurations such as an oxygen with three separate bonding sites exist, but these are rare and always very high in energy. Calculations with an initial ether or silyl-ether configuration almost always dissociate and form a ketene.

Next, we can look at bonds not involving oxygen. Looking at the ground state isomers and other low-lying isomers that have been shown throughout this chapter, it can quickly be seen that carbon atoms are never separated from each other in low-lying isomers. In addition, carbon atoms preferentially form linear chains over bent or cyclic structures. With the single exception of the bent C_3O doublet, the ground state of molecules with zero or one silicon is always a ketene, with the silicon, if present, terminal on the end opposite the oxygen. For molecules with two or more silicons, the carbon atoms tend to form linear chains terminated on one end by silicon-oxygen cyclic structure.

Looking at the ground state structures, we can also see that silicons tend to avoid bonding with other silicons. Silicon generally only bonds to another

silicon when the silicon to carbon ratio is high enough that it must, or when it forms a weak bond across a cyclic structure.

In addition to individual atom trends, there are also several larger scale functional trends among ground state isomers. As previously stated, silicon poor molecules tend to be linear with an oxygen and silicon on opposite ends of a carbon chain. In molecules with two or more silicons, there are two particularly common functional groups. The first is a four membered ring with the oxygen between two silicons and a carbon opposite the oxygen. In these molecules, other atoms are bonded to the carbon. The second is a five-membered ring with the oxygen between two silicons and two carbons opposite the oxygen. In these molecules other atoms bond to the carbons or sometimes bridge-bond to a carbon and silicon.

Another point of analysis that can be examined is bond lengths. For this I used all of the bonds tabulated in this chapter's figures and found the average bond length for each bond combination. For carbon-oxygen bonds, the span of bond lengths is relatively narrow, from 1.155 Å to 1.244 Å. The average is 1.187 Å. Silicon-oxygen-silicon bonds had a bit more span varying from 1.677 Å to 1.781 Å and averaging 1.739 Å. There were only four silicon-oxygen bonds, but these averaged 1.568 Å. Carbon-carbon bonds had a wider variance of lengths. They varied from 1.267 Å to 1.447 Å and averaged 1.321 Å. For these, the length was very dependent on second-nearest neighbors. When the second nearest neighbors were silicons, the carbon-carbon bonds were longer than if the second nearest neighbors were carbons or oxygens. Carbon-silicon bonds had a

very large variance of from 1.684 Å to 2.254 Å. They averaged 1.869 Å. Silicon-silicon bonds also had a very large span. They varied from 2.184 Å up to 2.765 Å. The average silicon-silicon bond was 2.418 Å.

Also important, is the arrangement of electrons in the ground state neutral isomers. This is what determines the multiplicity. There are two separate multiplicity trends for two types of molecules. The first is for nonlinear molecules. These are, with the single exception of Si_3O , singlets. The second is for linear molecules. These depend on the number of atoms. If the total number of atoms is odd, the molecule is a ground state triplet. If the total number of atoms is even, the molecule is a ground state singlet.

Finally, we can also look at electron affinities for trends. Tables 16 and 17 show all of the adiabatic and vertical electron affinities, respectively. While there are no trends in the electron affinities, most of them are in a fairly small range. Most of the adiabatic electron affinities are between 0.9 eV and 2.25 eV, while most of the vertical electron affinities are between 1.0 eV and 2.55 eV.

4.23. Vibrational Analysis Accuracy

Before presenting the final set of thermodynamic results, we must first consider the accuracy of the vibrational analysis. This must be done because thermodynamics properties are derived from the vibrational states through a partition function. The vibrational frequencies for which experimental data is available are shown in Table 18. As can be seen, the calculated values are consistently two to four percent high. According to Dr. Xiaofeng Duan, it is

Table 16. Adiabatic electron affinities for C_mSi_nO , $m, n \leq 4$ calculated with DFT/B3LYP/aug-cc-pVDZ. For cells with two values, top value is for anion ground geometry to corresponding neutral isomer, bottom value is for neutral ground geometry to corresponding anion isomer.

		Number of silicon atoms				
Number of carbon atoms	eV	0	1	2	3	4
	0	1.59	0.188	1.98	2.16	1.89
				0.609		
	1	-1.16	1.38	1.75	1.06	2.08
	2	2.22	0.907	1.68	1.90	1.84
	3	1.12	2.01	2.95	1.58	
1.19						
4	2.87	1.61	1.89			

standard practice to multiply B3LYP vibrational frequencies by a factor of 0.97 to obtain accurate values. If this is done to the values that I calculated, the corrected frequencies match experiment very closely.

4.24. Thermodynamics

The final set of results we can obtain from the calculations performed is some thermodynamics properties. When a Hessian calculation is performed by GAMESS, along with the vibrational modes, it also outputs the standard enthalpy (H_0), Gibb's standard energy (G_0), heat capacities (C_v , C_p), and standard entropy (S_0). These calculations were done using DFT with the B3LYP functional and

Table 17. Vertical electron affinities for C_mSi_nO , $m, n \leq 4$ calculated with DFT/B3LYP/aug-cc-pVDZ. For cells with two values, top value is for anion ground geometry to corresponding neutral isomer, bottom value is for neutral ground geometry to corresponding anion isomer.

		Number of silicon atoms				
Number of carbon atoms	eV	0	1	2	3	4
	0	1.59	0.245	2.05	2.39	2.00
				0.616		
	1	-1.01	1.46	2.55	1.38	2.23
	2	2.42	1.05	1.86	1.99	1.95
	3	2.24	2.11	3.04	1.69	
				1.48		
4	3.05	1.73	2.26			

the aug-cc-pVDZ basis set. The values obtained assume an ideal gas partition function at 298.15 K. The complete data obtained from these calculations are shown in Appendix F. Here I will focus on two important quantities that can be obtained from this data: heat of formation ($\Delta_f H_g^0$) and heat of reaction ($\Delta_r H_g^0$).

Heat of formation is “the heat evolved when a substance is formed from the elements in their standard states” (Brown, LeMay, and Bursten, 1991: G-8). The reactions of formation for silicon carbide monoxides and silicon carbide are shown in Equations 162 and 163 respectively.



Table 18. Comparison of calculated vibrational frequencies with experimental values. Calculated values were obtained using DFT/B3LYP/aug-cc-pVDZ. Experimental values are from webbook.nist.gov database.

Molecule	mode	Calculated Frequency (cm ⁻¹)	Experimental Frequency (cm ⁻¹)	Relative Error (%)
CO	OC stretch	2184	2169.8	+0.65
CCO	OC stretch	2034	1970.86	+2.77
CCO	CC stretch	1086	1063	+2.16
CCO	bend	387	379.53	+2.10
SiCO	OC stretch	1963	1898.1	+3.42
CCCO	C2-C3 stretch	962	939.1	+2.44
CCCO	C1-C2 stretch	1964	1907.0	+2.99
CCCO	C2-C3 asy stretch	2331	2243	+3.92
CCCO	C3 bend	590	580	+1.72
CCCCO	C2-C4 stretch	771	774.8	-0.49
CCCCO	O-C3 stretch	1460	1431.5	+1.99
CCCCO	C3-C4 stretch	2304	2221.7	+3.70
CCCCO	O-C2 asy stretch	1979	1922.7	+2.93
CCCCO	C4 bend	494	484.0	+2.07



The calculated values of the heats of formation for silicon carbide monoxides and silicon carbide are shown in Tables 19 and 20 respectively. Available experimental values are shown in parentheses.

If those heats of formation that have experimental values are compared to the calculated values, it can be seen that, except for the atoms and diatoms, the calculated values are consistently seven to twelve percent high. This is due to the vibrational frequencies being consistently high. The spread of accuracy is larger here than it was in the vibrational frequencies because of the complicated exponentials in the ideal gas partition function.

Table 19. Ideal gas phase enthalpies of formation for C_mSi_nO neutral ground states at 298.15K calculated with DFT/B3LYP/aug-cc-pVDZ. Experimental values from webbook.nist.gov in parentheses. All values are in kJ/mol.

		Number of silicon atoms				
Number of carbon atoms	kJ/mol	0	1	2	3	4
	0	248.8 (249.18)	-46.62 (-100.42)	248.1	362.6	487.2
	1	-92.51 (-110.53)	204.8	351.5	375.4	569.6
	2	365.1 (286.60)	220.4	402.9	526.8	671.2
	3	329.9	452.8	546.3	581.2	
	4	576.9	474.3	678.0		

Table 20. Ideal gas phase enthalpies of formation for C_mSi_n neutral ground states at 298.15K calculated with DFT/B3LYP/aug-cc-pVDZ. Experimental values from webbook.nist.gov in parentheses. All values are in kJ/mol.

		Number of silicon atoms				
Number of carbon atoms	kJ/mol	0	1	2	3	4
	0		449.2 (450.0)	590.9 (589.94)	685.9 (636.0)	729.6
	1	716.7 (716.68)	765.5 (719.65)	601.6 (535.55)	700.7	866.7
	2	978.2 (837.74)	683.8 (615.05)	771.8	850.2	939.6
	3	(820.06)	891.7	810.2	998.1	1202
	4	1036 (970.69)	912.1	983.1	1168	1313

Table 21. Ideal gas phase reaction enthalpies for atomic oxidation of C_mSi_n neutral ground states at 298.15K calculated with DFT/B3LYP/aug-cc-pVDZ. All values are in kJ/mol.

Top value: $C_nSi_m + O \rightarrow C_nSi_mO$ Middle value: $C_nSi_m + O \rightarrow C_{n-1}Si_m + CO$ Bottom value: $C_nSi_m + O \rightarrow C_nSi_{m-1}O + Si$						
Number of silicon atoms						
Number of carbon atoms	kJ/mol	0	1	2	3	4
	0	0.0	-738	-584	-563	-485
	1	-1045	738	151	330	321
	2	0.0	-796	-487	-566	-539
	3	-852	146	139	211	62.8
	4	249	146	297	423	252
5	-852	-693	-603	-563	-508	
6	249	436	92.8	73.4	95.1	
7	542	582	263	325	300	
8	-671	-502	-655			
9	122	120	167			
10	321	351	412			
11	-690	-669	-545			
12	307	35.0				
13	542	249				

LEGEND:

- Most favored reaction
- Second most favored reaction
- Third most favored reaction
- Not all data available

The second set of thermodynamics values we can obtain are reaction enthalpies. There are 15 important reactions I have chosen to examine. The first three reactions are shown in Table 21 and are for the atomic oxidation of silicon carbide. Table 22 shows six reactions for the molecular oxidation of silicon carbide. These reactions show that, for atomic oxidation, the formation of a monoxide of silicon carbide is the preferred reaction. Formation of carbon monoxide or oxidation with loss of a silicon is endothermic. For molecular

Table 22. Ideal gas phase reaction enthalpies for molecular oxidation of C_mSi_n neutral ground states at 298.15K calculated with DFT/B3LYP/ug-cc-pVDZ. All values are in kJ/mol.

Top value: $C_nSi_m + \frac{1}{2}O_2 \rightarrow C_nSi_mO$ Middle value: $C_nSi_m + \frac{1}{2}O_2 \rightarrow C_{n-1}Si_m + CO$ Bottom value: $C_nSi_m + \frac{1}{2}O_2 \rightarrow C_nSi_{m-1}O + Si$							
Number of silicon atoms							
Number of carbon atoms	kJ/mol	0	1	2	3	4	
	0	252	-486	-332	-311	-233	
			252	-181	18.3	88.8	
	1	-793	-544	-235	-314	-287	
		-793	-398	-96.3	-103	-224	
	2	-600	-398	62.2	109	-35.2	
-351		-442	-258	-238	-256		
3		141	-87.8	13.8	-161		
		-419	-250	-403	-351		
4		-297	-130	-236	-163		
		-98.5	101.5	8.86	-351		
4	-438	-417	-293	-255	-197		
		-110	-258	-31.3			
		125	-44.2				

LEGEND:

Most favored reaction

Second most favored reaction

Third most favored reaction

Not all data available

Top value: $C_nSi_m + O_2 \rightarrow C_nSi_mO + O$ Middle value: $C_nSi_m + O_2 \rightarrow C_{n-1}Si_m + CO_2$ Bottom value: $C_nSi_m + O_2 \rightarrow C_nSi_{m-1} + SiO_2$							
Number of silicon atoms							
Number of carbon atoms	kJ/mol	0	1	2	3	4	
	0	504	-234	-80.3	-59.5	19.3	
			-614	-310	-264	-214	
	1	-541	-292	16.7	-61.9	-34.9	
		-1075	-680	-378	-384	-506	
	2	-348	-220	-7.42	-270	-336	
-633		-190	-99.2	-59.1	-4.50		
3		-287	-540	-520	-443		
		126	-260	-249	-259		
4		-167	2.18	-151	-633		
		-579	-412	-518	-374		
4	-186	-165	-93.2	-356	-374		
		-392	-41.4	-537	-478		
		-51.4	-241	-352	-316		

Table 23. Ideal gas reaction enthalpies for one-atom dissociation of C_mSi_n neutral ground states at 298.15K calculated with DFT/B3LYP/aug-cc-pVDZ. All values are in kJ/mol.

Top value: $C_nSi_m \rightarrow C_{n-1}Si_m + C$						
Bottom value: $C_nSi_m \rightarrow C_nSi_{m-1} + Si$						
		Number of silicon atoms				
Number of carbon atoms	kJ/mol	0	1	2	3	4
	0		0	305	351	400
	1	0	395	697	690	569
	2	442	788	535	555	632
	3		496	663	557	442
	4		683	535	538	596
		563	373	262	298	

LEGEND:

Most favored reaction
 Second most favored reaction
 Not all data available

oxidation, the preferred reaction is to form carbon dioxide. Formation of silicon dioxide is also usually preferred over forming a monoxide of silicon carbide which is usually only slightly endothermic. This tells us that in order to create monoxides of silicon carbide from silicon carbide, the oxygen should be atomized before the reaction takes place.

The second type of reaction I looked at was dissociation. First, I looked at single-atom dissociation of silicon carbide. The two possible reaction routes are shown in Table 23. These reactions are all very endothermic. This tells us that silicon carbide is stable at standard temperatures.

Table 24. Ideal gas reaction enthalpies for dissociation of C_mSi_nO neutral ground states at 298.15K calculated with DFT/B3LYP/aug-cc-pVDZ. All values are in kJ/mol.

Top value: $C_nSi_mO \rightarrow C_{n-1}Si_mO + C$ Top middle value: $C_nSi_mO \rightarrow C_{n-1}Si_m + CO$ Bottom middle value: $C_nSi_mO \rightarrow C_nSi_{m-1}O + Si$ Bottom value: $C_nSi_mO \rightarrow C_nSi_{m-1} + SiO$							
		Number of silicon atoms					
Number of carbon atoms	kJ/mol	0	1	2	3	4	
	0			738 0	151 151	330 176	321 147
	1	0 0	395 146 146 454	697 139 297 356	690 211 423 173	569 62.8 252 79.9	
	2	442 249	788 436 582 696	535 92.8 263 219	555 73.4 325 190	632 95.1 300 126	
	3	542	496 122 321	663 120 351 285	557 167 412 176	442	
	4		683 307 542 495	535 35.0 249 181	538	596	

LEGEND:

- Most favored reaction
- Second most favored reaction
- Third favored
- Fourth favored
- Not all data available

The final set of reactions I looked at was dissociation of monoxides of silicon carbide. The results of these calculations are shown in Table 24. These calculations show that monoxides of silicon carbide are also stable at standard temperatures. However, for some molecules, the loss of carbon monoxide is

only barely endothermic. At higher temperatures, these molecules would be expected to begin dissociating into silicon carbide and carbon monoxide.

V. Conclusions and Recommendations

5.1. Conclusions

The previous chapter presented the results that I have obtained in the course of this research. As a conclusion, we now turn to a discussion of these results and the meaning they have with respect to experimental confirmation. In particular, we are concerned with the outcome of Dr Lineberger's PES experiments that were described in Chapter 1. There are several questions that can be asked in regard to this experiment. This section will address these.

The first question we can ask is *What C_mSi_nO anions will he produce?* The method of producing anions is to first produce a C_mSi_n cluster, which is then oxidized. The C_mSi_n clusters produced are expected to be the ground state isomers found by Jean Henry and shown in her C_mSi_n map, an expanded version of which is shown as Figure 42. If this map is compared with my C_mSi_nO maps shown in Figures 40 and 41, it is seen that the ground state isomers of C_mSi_n do not necessarily correspond to the ground state isomers of C_mSi_nO . Therefore, if the oxidation process is a very gentle one, the C_mSi_nO cluster produced may not be the ground state isomer. If, on the other hand, the process is more energetic, the oxidation process is likely to cause atomic rearrangement. But even in this case, it is not guaranteed that the final cluster formed will be the lowest-energy state. If other low-lying isomers have a simpler reaction coordinate from the C_mSi_n ground state, are close in energy to the C_mSi_nO ground state, and have a relatively high activation barrier to the C_mSi_nO ground state, the final cluster

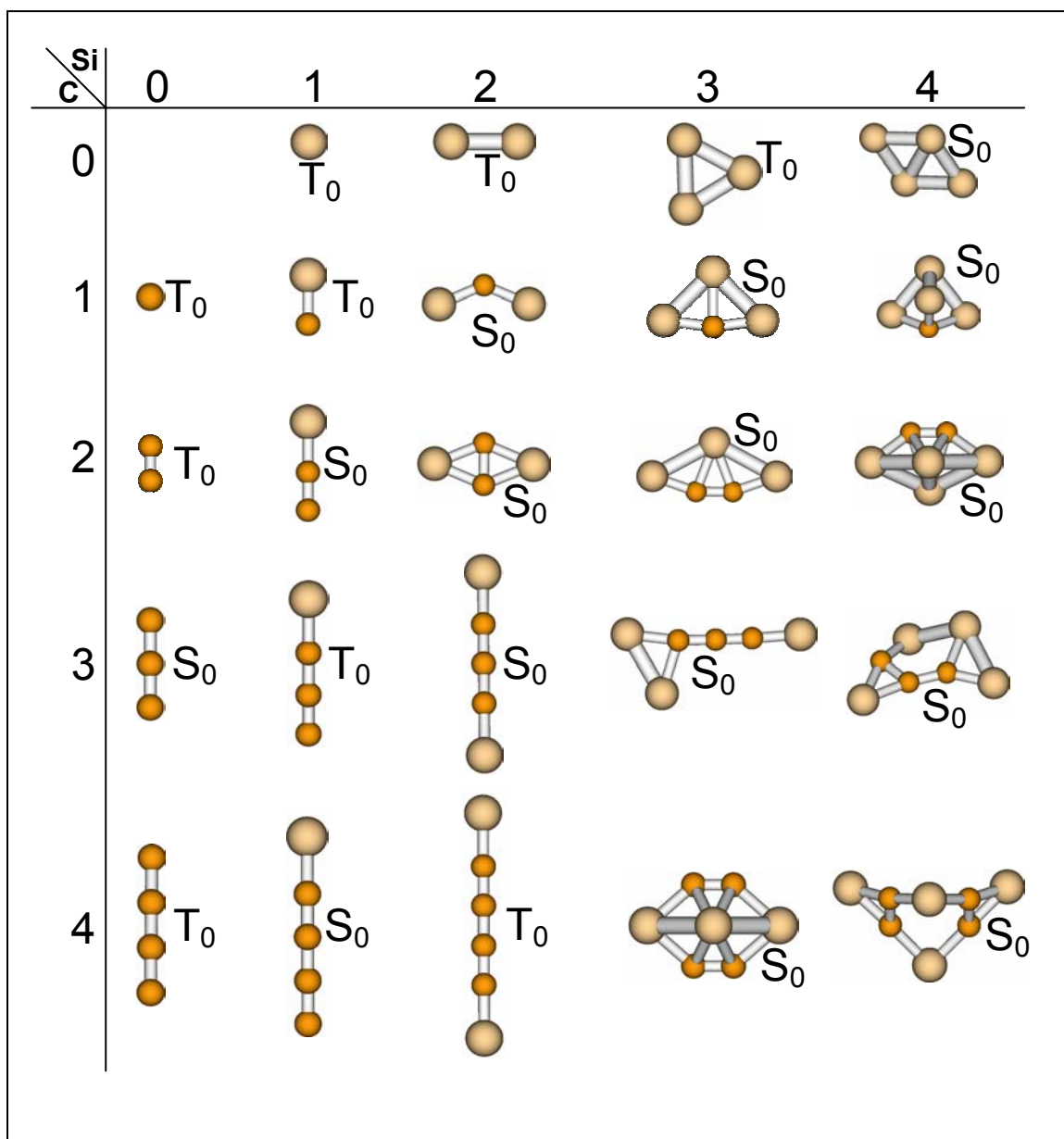


Figure 39. Neutral ground state isomers for C_mSi_n , $m, n \leq 4$ with DFT/B3LYP/aug-cc-pVDZ. Based on work by Henry; updated and expanded by Duan and the author.

produced may not be the ground state isomer. Therefore the answer to our question is *It depends*. If the C_mSi_n ground state is similar to the C_mSi_nO ground state or the oxidation process is an energetic one, the C_mSi_nO ground state

isomer will be produced. Otherwise, it will depend on the energy of the reaction, where the oxygen attaches, and many other factors.

Once we have produced a C_mSi_nO cluster we can ask the next question: *What will the photoelectron spectrum look like?* This question is answered by comparing the neutral and anion maps of Figures 40 and 41 and the electron affinities of Tables 4 and 5. From these, it can be seen that C_mSi_nO , unlike C_mSi_n , has significant differences in geometry between the anion and neutral. Therefore, when the electron is removed from the anion, the neutral cluster that is left will be in a very vibrationally excited state. If the anion and neutral geometries are exactly the same, the vertical and adiabatic electron affinities are the same and the photoelectron spectrum will be a large peak at this energy and maybe some smaller vibrational peaks at lower energies. For our case, the geometries differ, sometimes very significantly. We therefore expect there to be a peak at the vertical electron affinity, vibrational peaks going up from there to the adiabatic electron affinity, and vibrational peaks down from there. The relative intensity of the peaks will, in a complicated way, be dependent on the intensities of the various vibrational modes of the neutral cluster. The spectrum is complicated even more by the fact that for some molecules, the ground anion isomer is not the ground neutral isomer, and for other molecules there are other low-lying isomers that the ground state may end up in. Therefore, the vibrational structure seen in the spectrum may not be simply be that of a single isomer, but may be a superposition of the vibrational states of many modes of two or more

isomers. The result is that, for many molecules, the photoelectron spectrum will be very complex with a large number of peaks.

5.2. Recommendations for Future Work

For almost any scientific endeavor, the work is never totally completed and there is always further work to do and questions to answer. This work is no different. Therefore, I will here present several avenues for future research based upon this work.

The first type of further research would be a further analysis of the calculations that I have performed. During this research, I have performed over 12,000 calculations (not including instances where a calculation had to be repeated to obtain a final result), collected over five gigabytes of data, and used over ten years of CPU time. In the timeframe of this research project, it would be impossible to fully analyze this data. There are several analysis projects that could be undertaken. First, a further functional analysis could be done. The functional analysis that I presented at the end of Chapter 4 was primarily based on ground state isomers. The contribution of other isomers was only qualitative and based on the experience I have received while doing this research. Further research could be done to determine not only what structures are ground states, but what structures are stable at all. Using graph theory and an examination of how the energy changes with geometry and bonds, a more complete list of functional groups and characteristic energies could be developed. As part of

this, or as a separate endeavor, the effects of second-nearest neighbor atoms on bond lengths, stability, and energy could be determined.

The second type of further research is new calculations based on my results. This is the next step in eventually being able to model silicon-carbide semiconductor devices. The next steps are to build larger and larger C_mSi_nO clusters and to embed these into a molecular mechanics framework. This will allow for the study of the properties of silicon-carbide bulk and surface materials. In addition, having oxygen present will allow for the study of defects in these materials.

Hopefully this research and future research will eventually result in the development of high-band-gap silicon-carbide semiconductors which can be used for devices in high radiation and temperature environments.

Appendix A. Glossary

AFIT—Air Force Institute of Technology

ASC—Aeronautical System Center

aug-cc-pVDZ—double zeta valence basis set with correlation consistent and diffuse functions added (Dunning and Hay, 1977; Basis sets, 2002; Dunning, 1989; Woon and Dunning, 1993; Kendall *et al*, 1992)

CC—Coupled Cluster

cc-pVDZ—double zeta valence basis set with correlation consistent functions added (Dunning and Hay, 1977; Basis sets, 2002; Dunning, 1989; Woon and Dunning, 1993; Kendall *et al*, 1992)

CI—configuration interaction

DFT—density functional theory

DZV—double zeta valence basis set (same as VDZ) (Dunning and Hay, 1977; Basis sets, 2002; Dunning, 1989; Woon and Dunning, 1993; Kendall *et al*, 1992)

GAMESS—General Atomic and Molecular Electronic Structure System (Schmidt *et al*, 1993)

GTO—Gaussian Type Orbital

HF—Hartree-Fock

MCSCF—multi-configurational self-consistent field

MOSFET—metal-oxide semiconductor field effect transistor

MP2—Møller-Plesset second order perturbation

MP4—Møller-Plesset fourth order perturbation

MSRC—Major Shared Resource Center; large, parallel computing facility located at Wright-Patterson AFB

PES—photoelectron spectroscopy

SCF—self-consistent field

SIMOMM—surface integrated molecular orbital molecular mechanics

STO—Slater Type Orbital

VDZ— valence double zeta basis set (Dunning and Hay, 1977; Basis sets, 2002; Dunning, 1989; Woon and Dunning, 1993; Kendall *et al*, 1992)

Appendix B. Initial Isomers for HF/VDZ Calculations

This appendix is a series of figures which show the initial isomers used for HF/VDZ calculations. Those molecules which are not shown are those for which there were few isomers and the name in the tables of Appendix B should be self-explanatory.

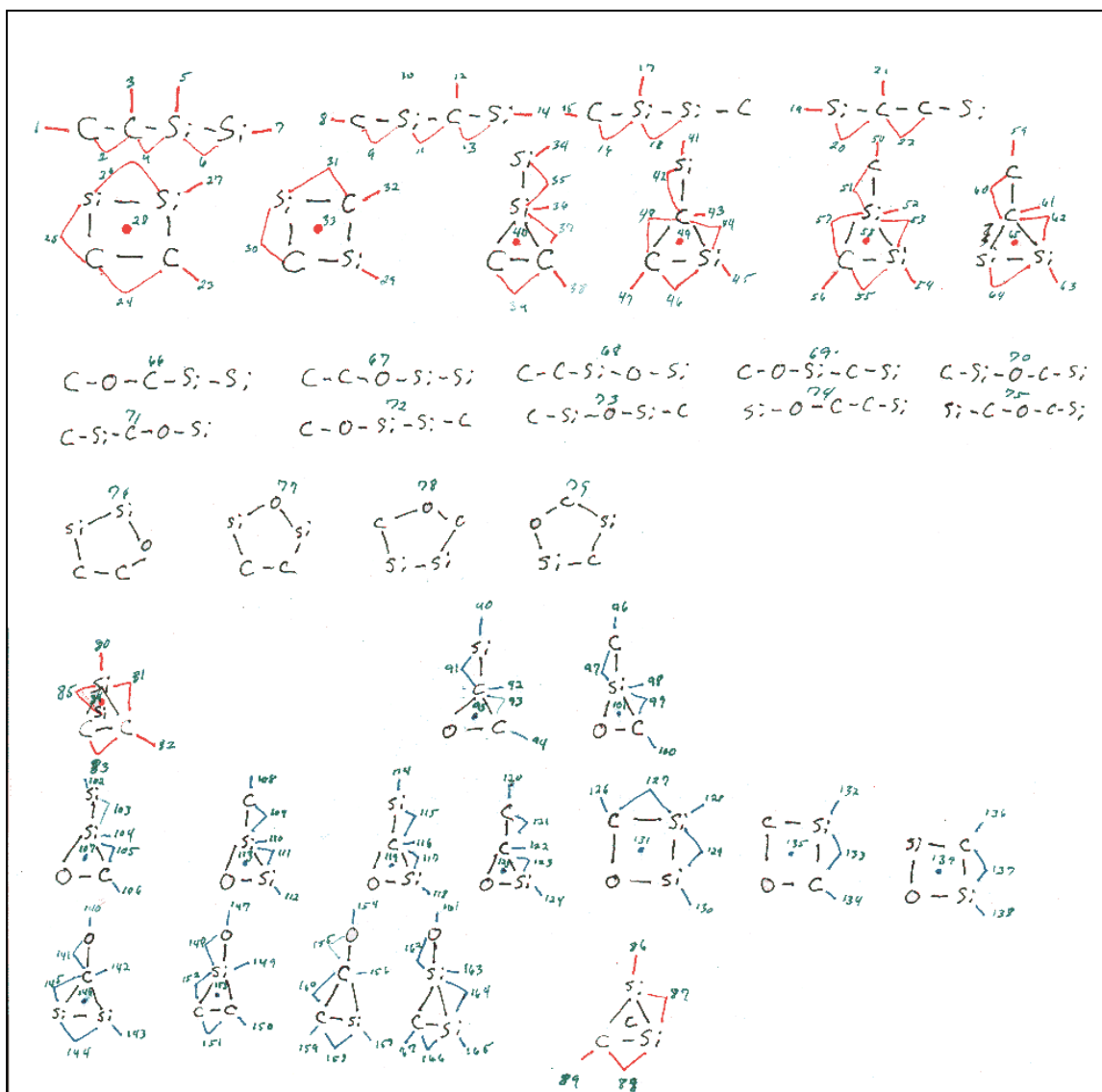


Figure 40. Initial isomers for C_2Si_2O calculations with HF/VDZ. Red marks are oxygen positions. Blue marks are silicon positions

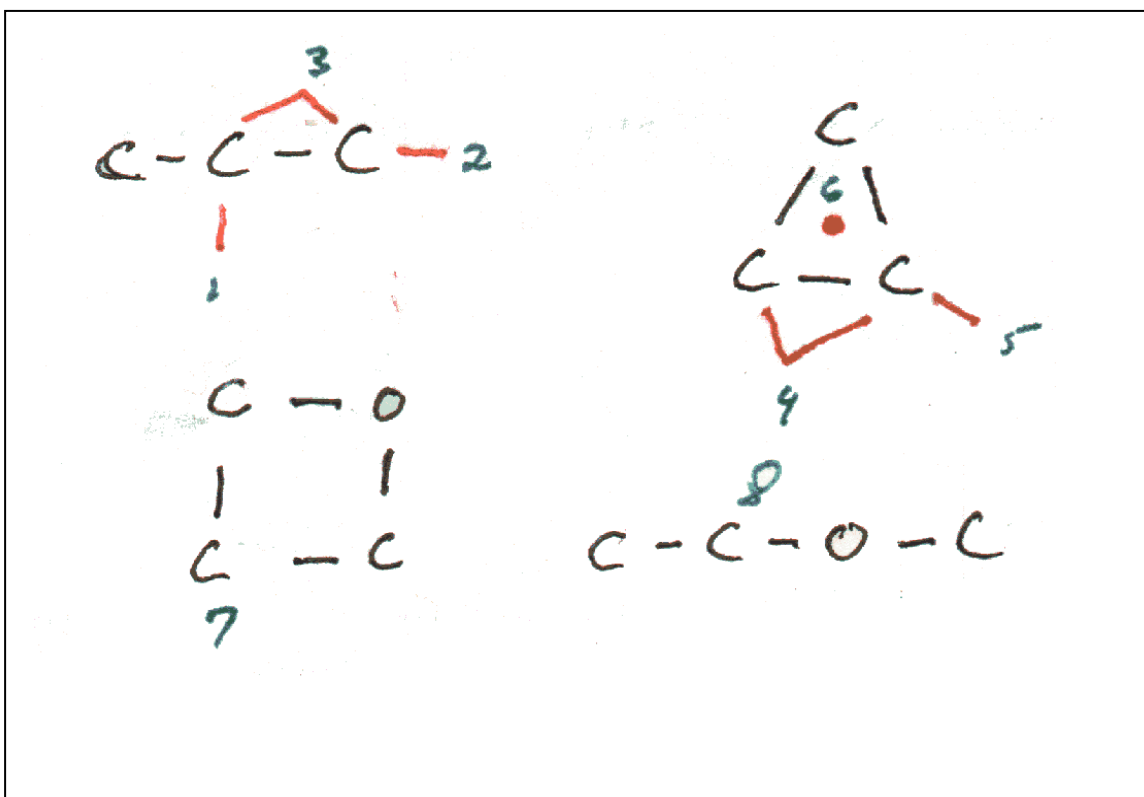


Figure 41. Initial isomers for C_3O and Si_3O calculations with HF/VDZ. Red marks are oxygen positions. Si_3O isomers are formed by replacing C with Si.

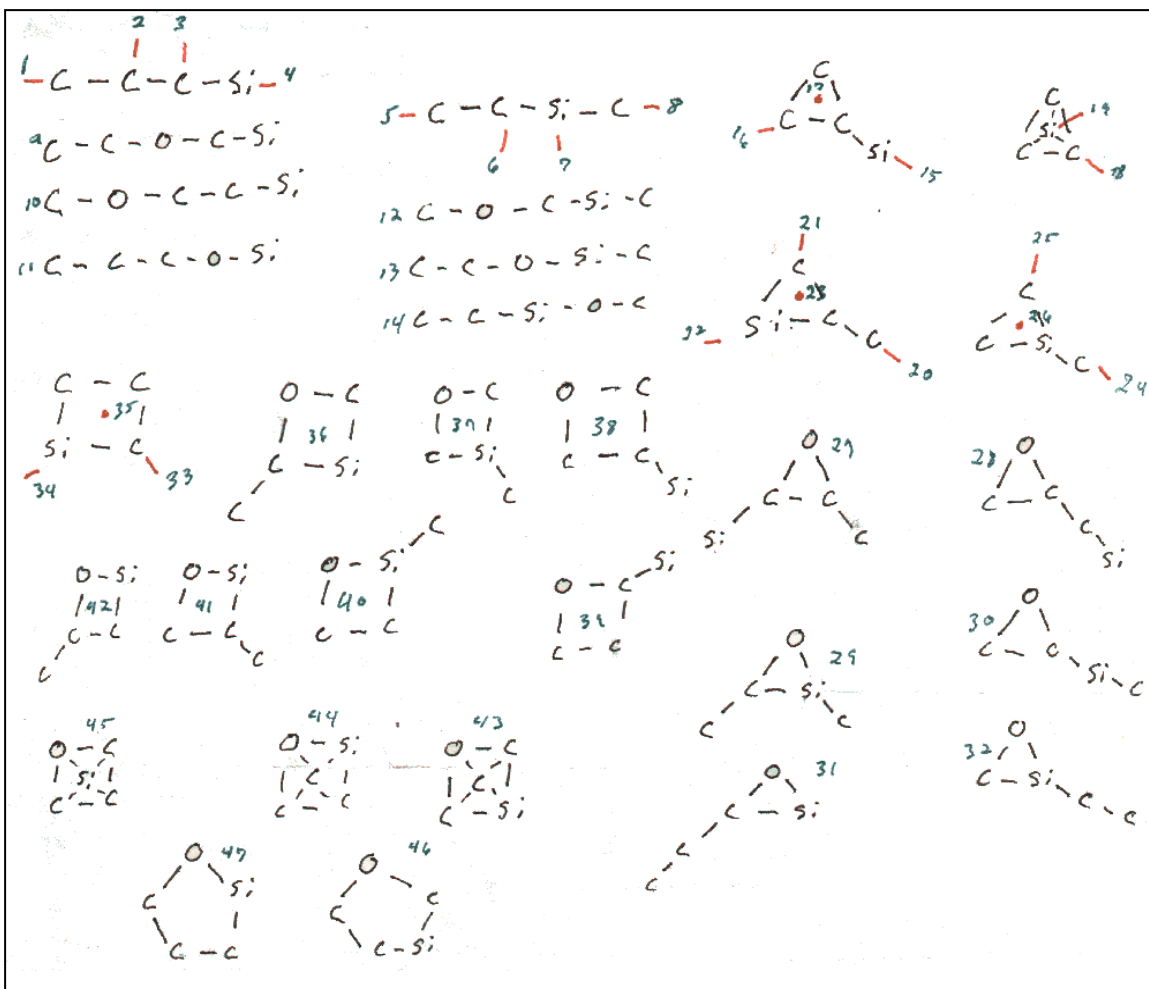


Figure 42. isomers for C_3SiO and CSi_3O calculations with HF/VDZ. Red marks are oxygen positions. CSi_3O isomers are formed by switching C and Si.

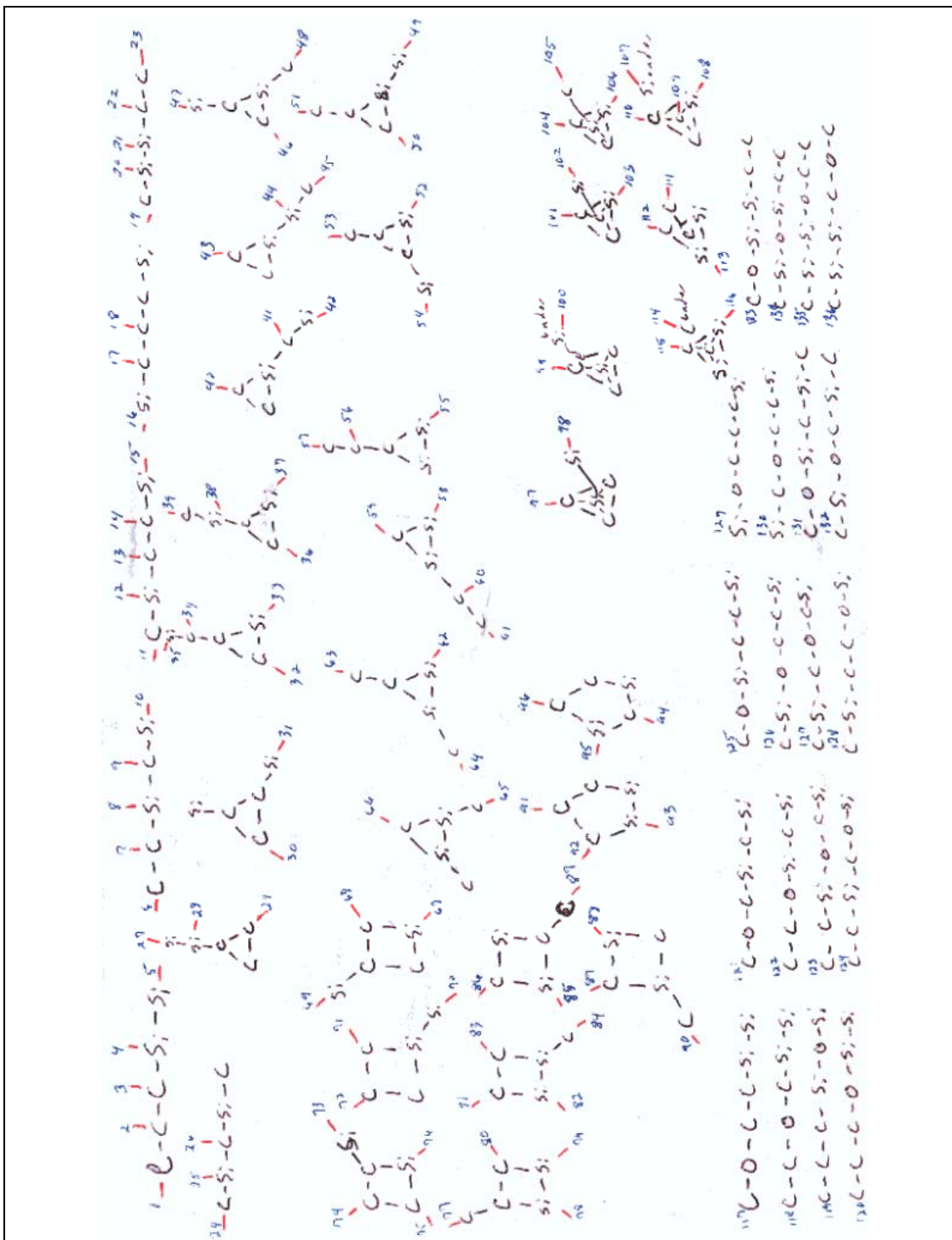


Figure 43. Initial isomers for C_3Si_2O and C_2Si_3O calculations with HF/VDZ. Red marks are oxygen positions. C_2Si_3O isomers are formed by switching C and Si.

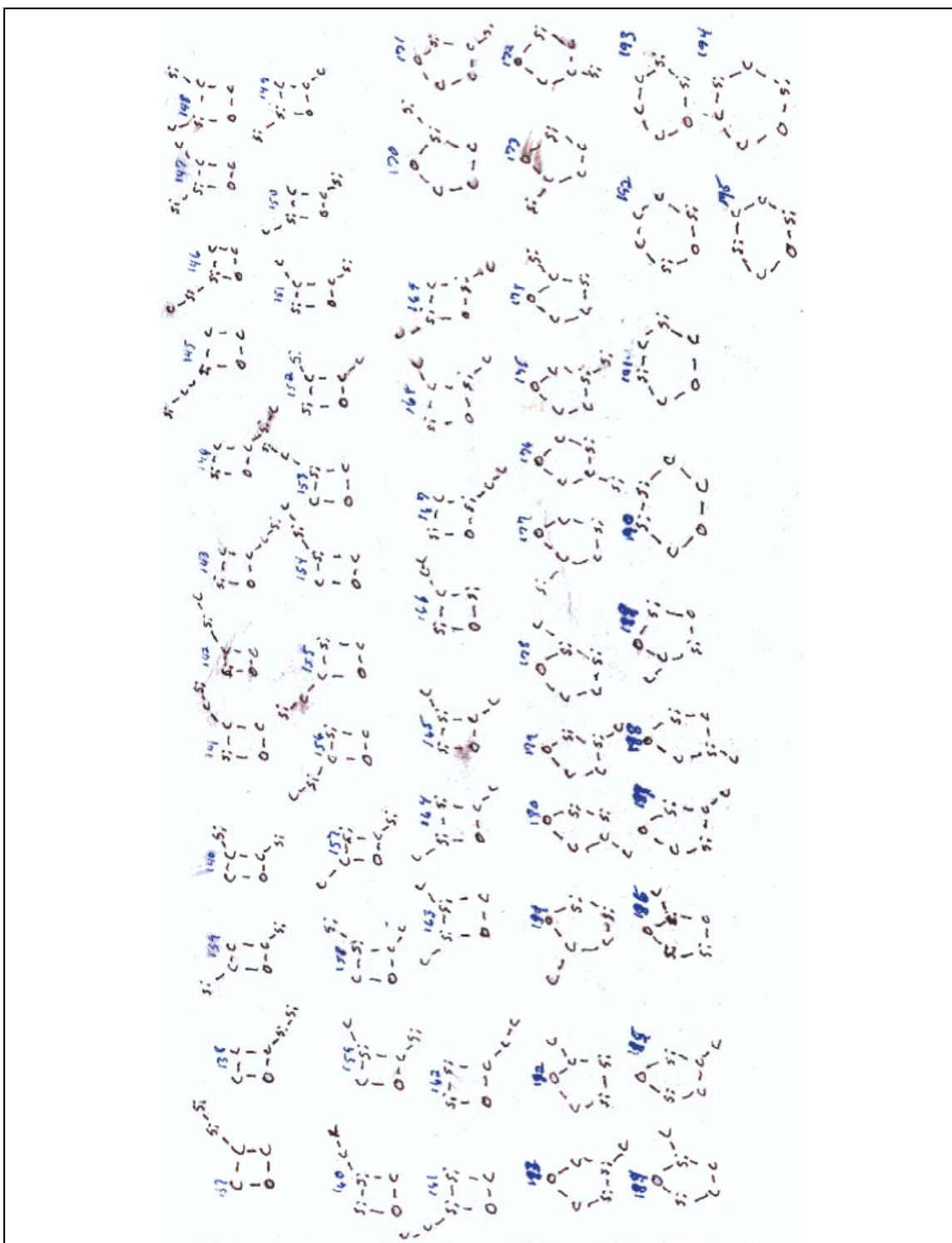


Figure 43. (Continued). Initial isomers for C_3Si_2O and C_2Si_3O calculations with HF/VDZ. Red marks are oxygen positions. C_2Si_3O isomers are formed by switching C and Si.

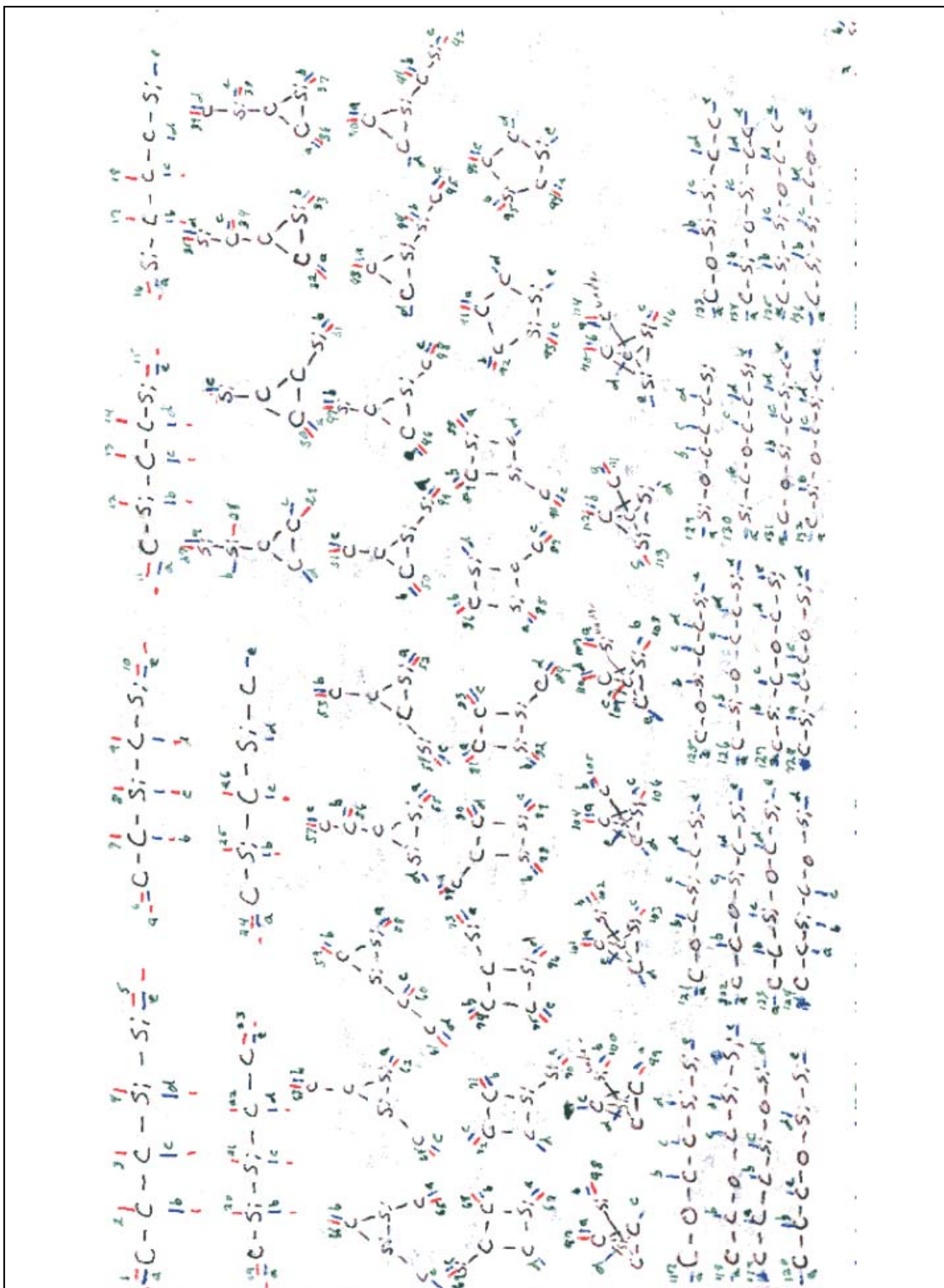


Figure 44. Initial isomers for C_3Si_3O calculations with HF/VDZ. Red marks are oxygen positions. Blue marks are silicon positions.

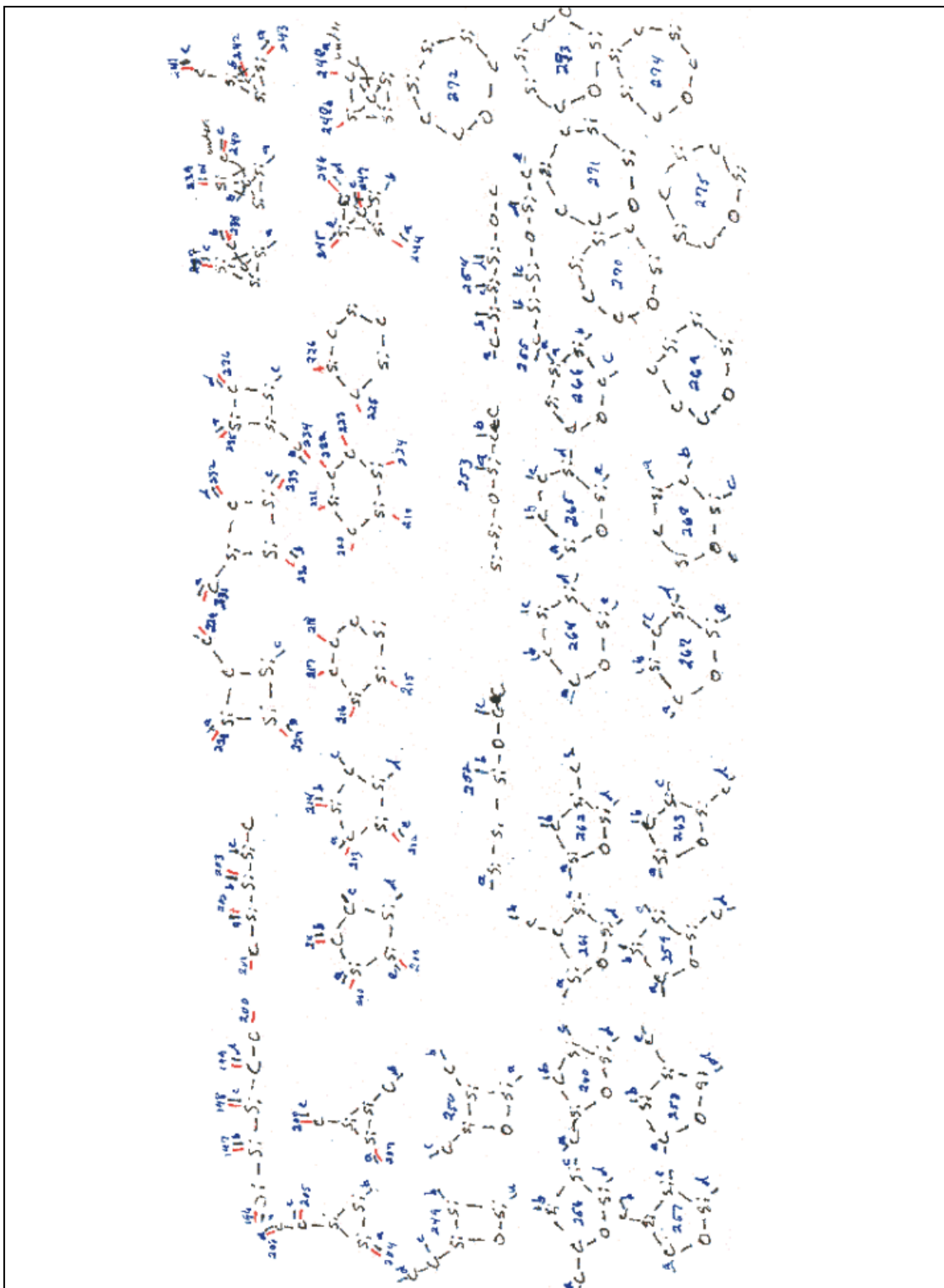


Figure 44. (Continued). Initial isomers for C_3Si_3O calculations with HF/VDZ. Red marks are oxygen positions. Blue marks are silicon positions.

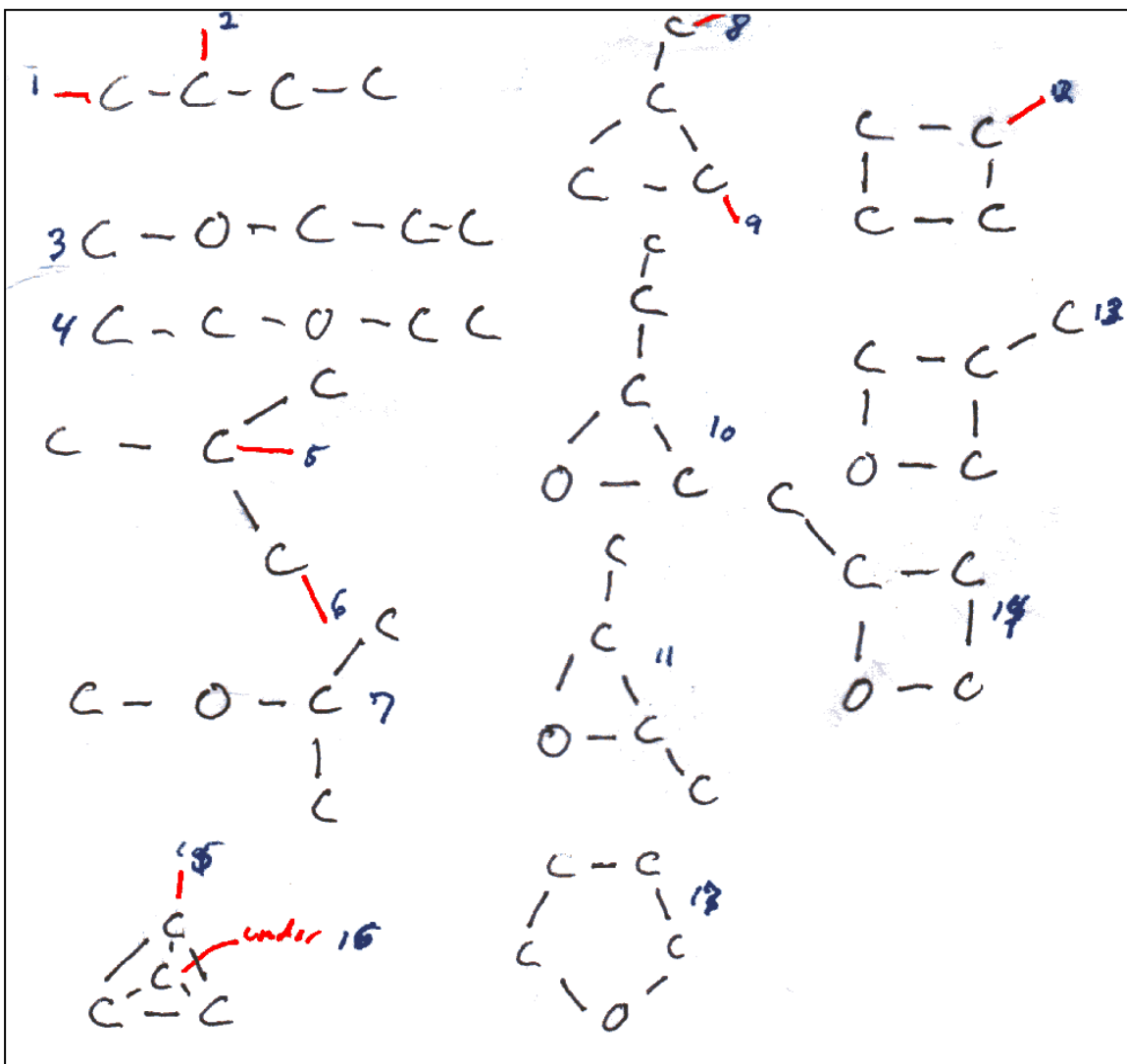


Figure 45. Initial isomers for C_4O and Si_4O calculations with HF/VDZ. Red marks are oxygen positions. Si_4O isomers are formed by switching C and Si.

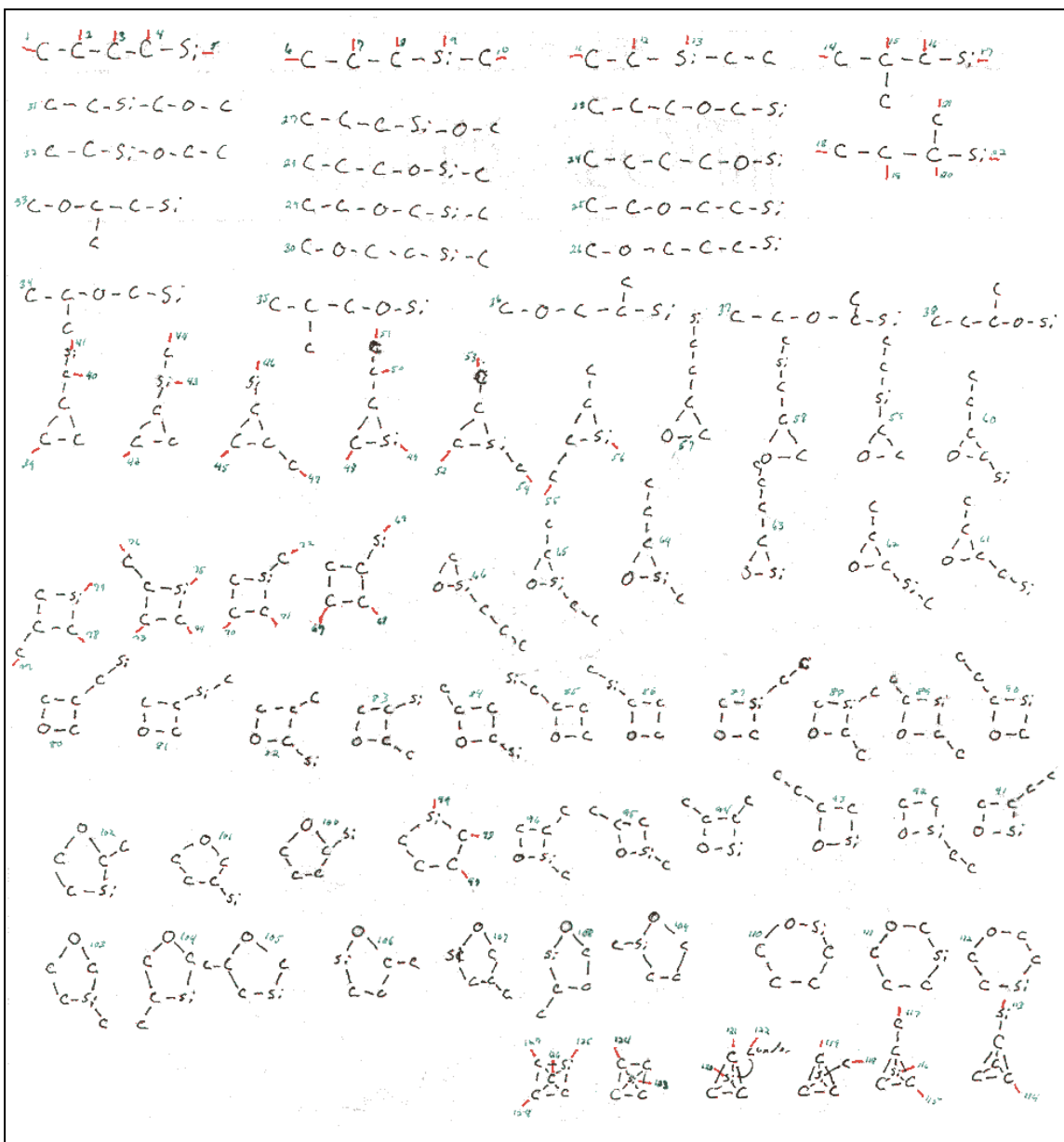


Figure 46. Initial isomers for C_4SiO and CSi_4O calculations with HF/VDZ. Red marks are oxygen positions. CSi_4O isomers are formed by switching C and Si.

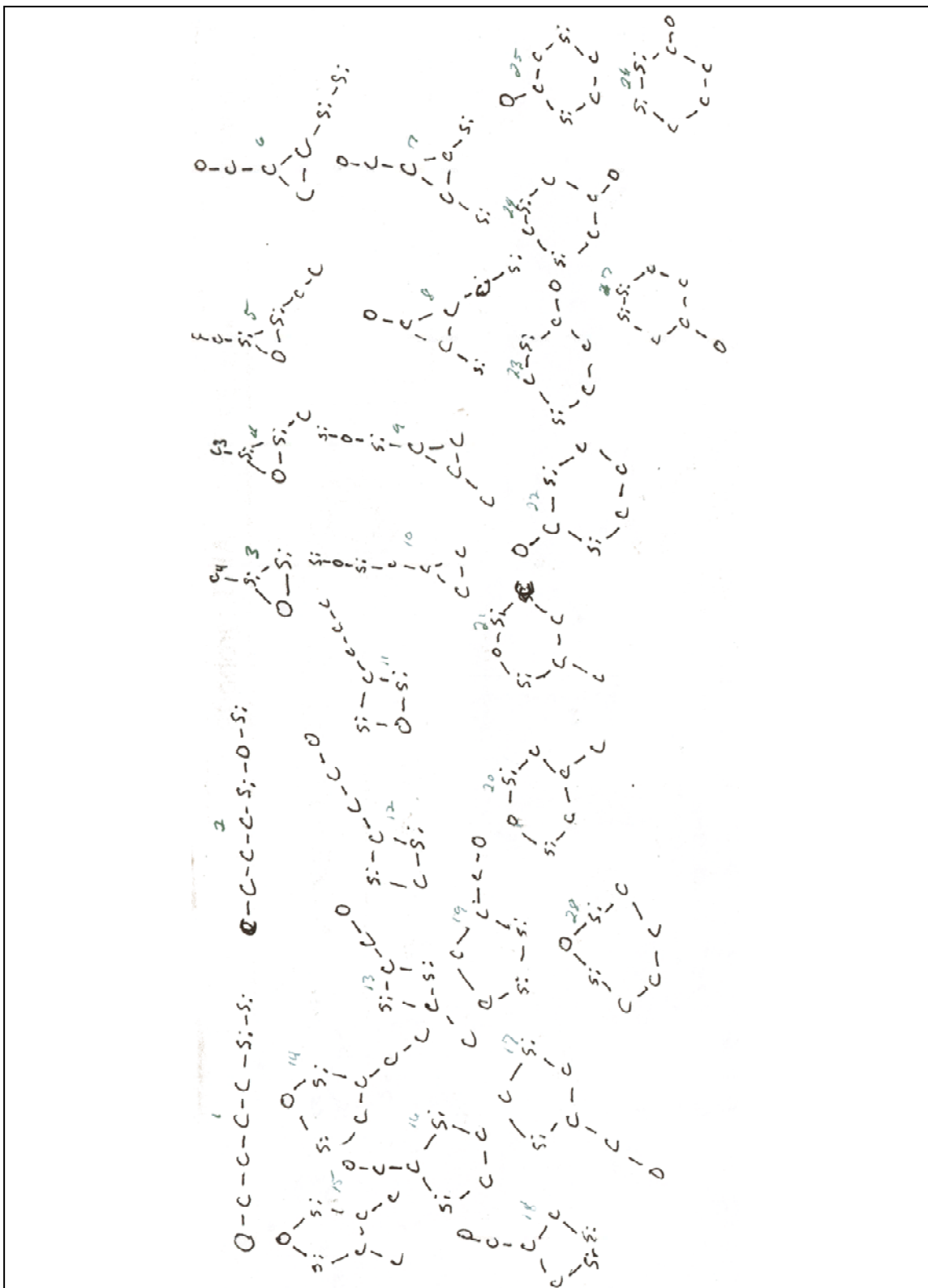


Figure 47. Initial isomers for C_4Si_2O calculations with HF/VDZ.

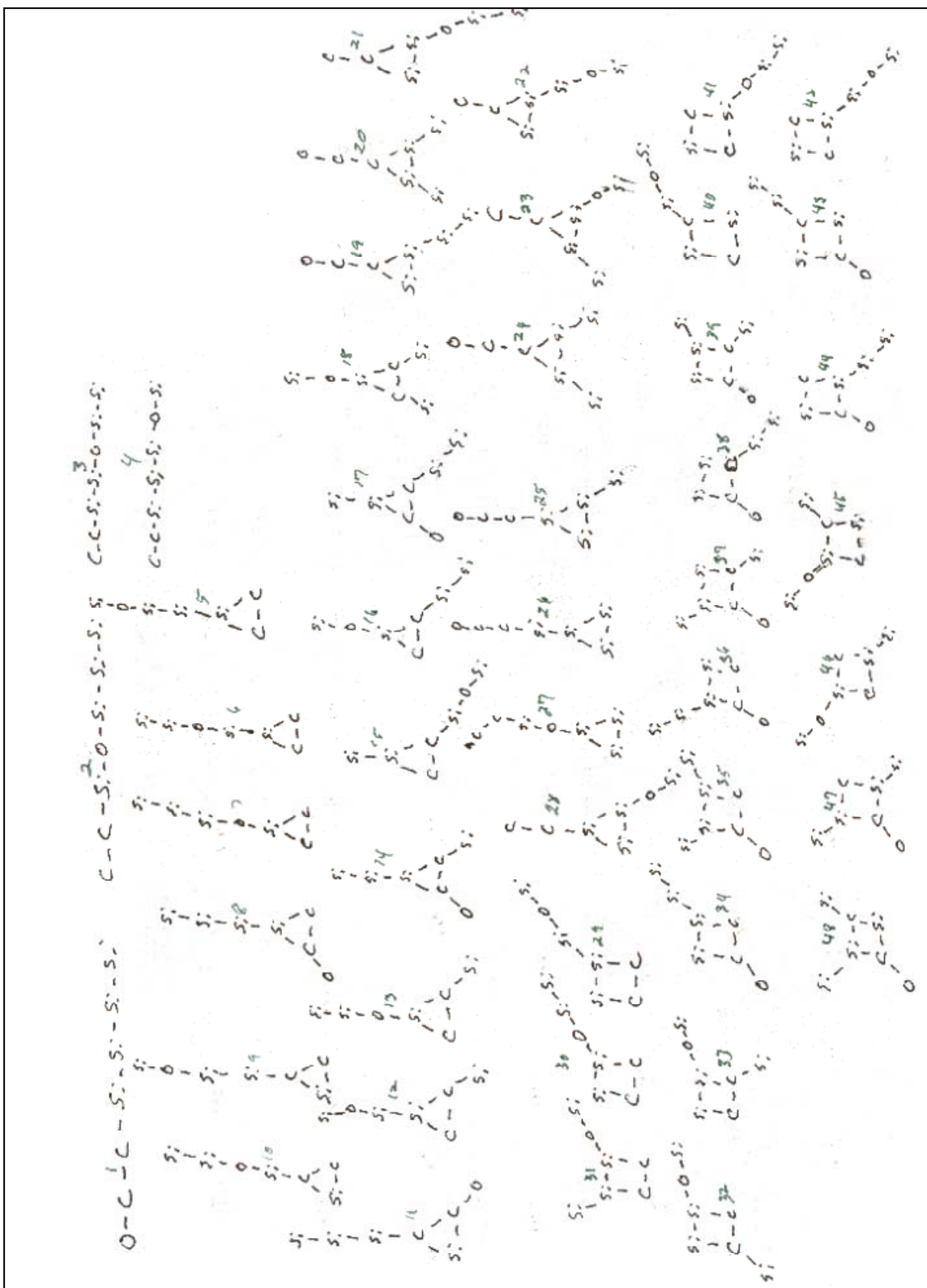


Figure 48. Initial isomers for C_2Si_4O calculations with HF/VDZ.

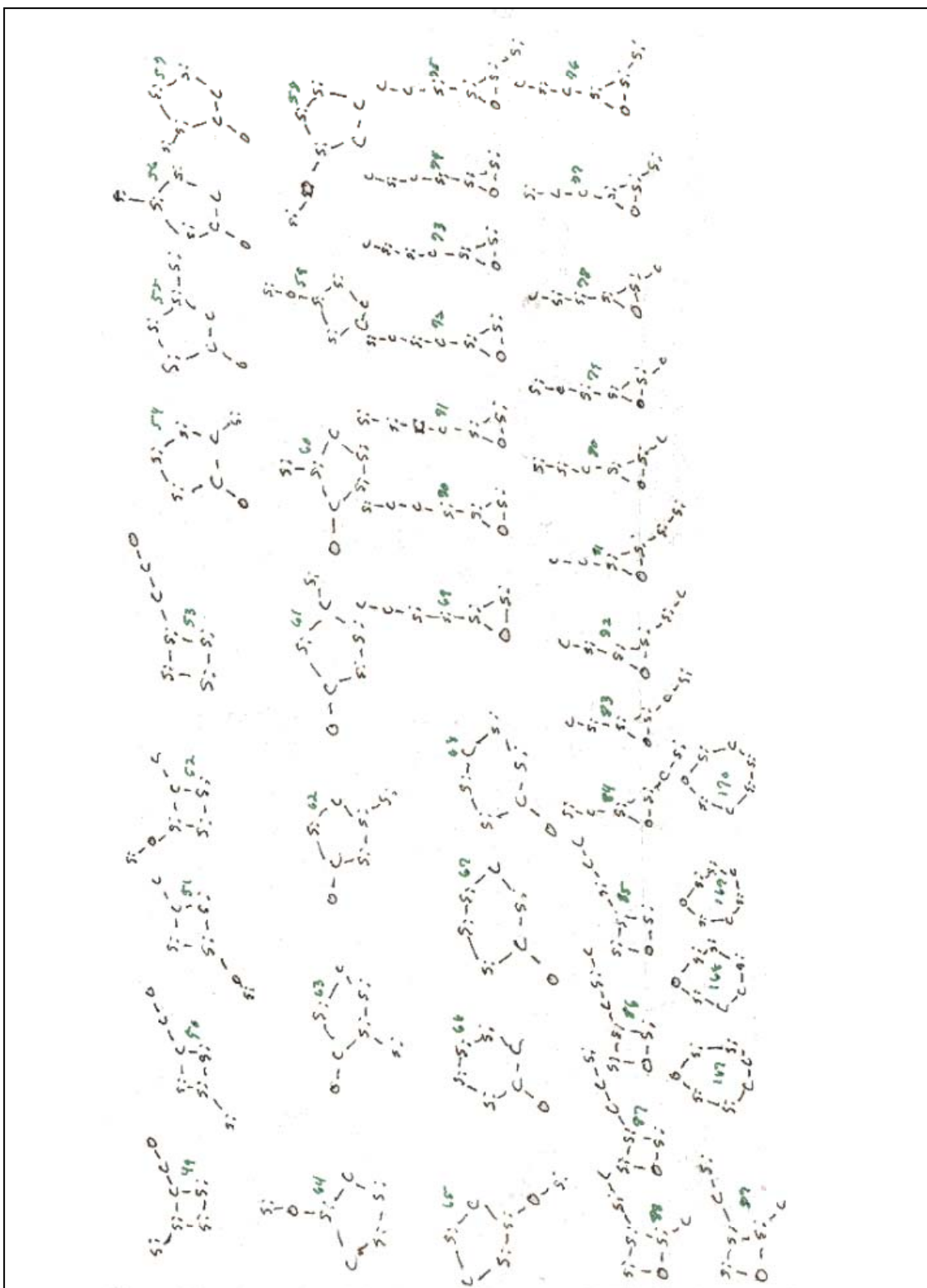


Figure 48. (Continued) Initial isomers for C_2Si_4O calculations with HF/VDZ.

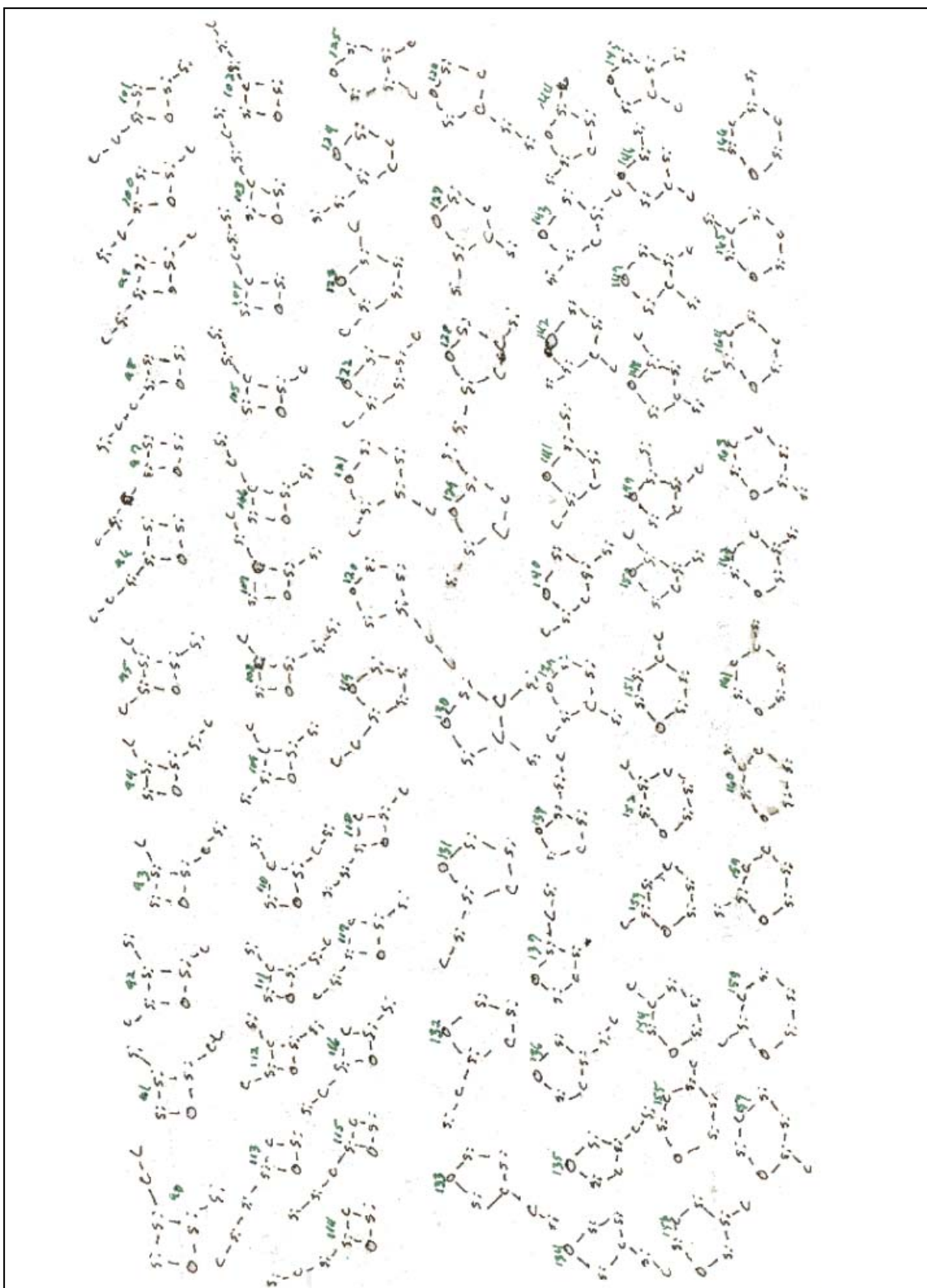


Figure 48. (Continued) Initial isomers for C_2Si_4O calculations with HF/VDZ.

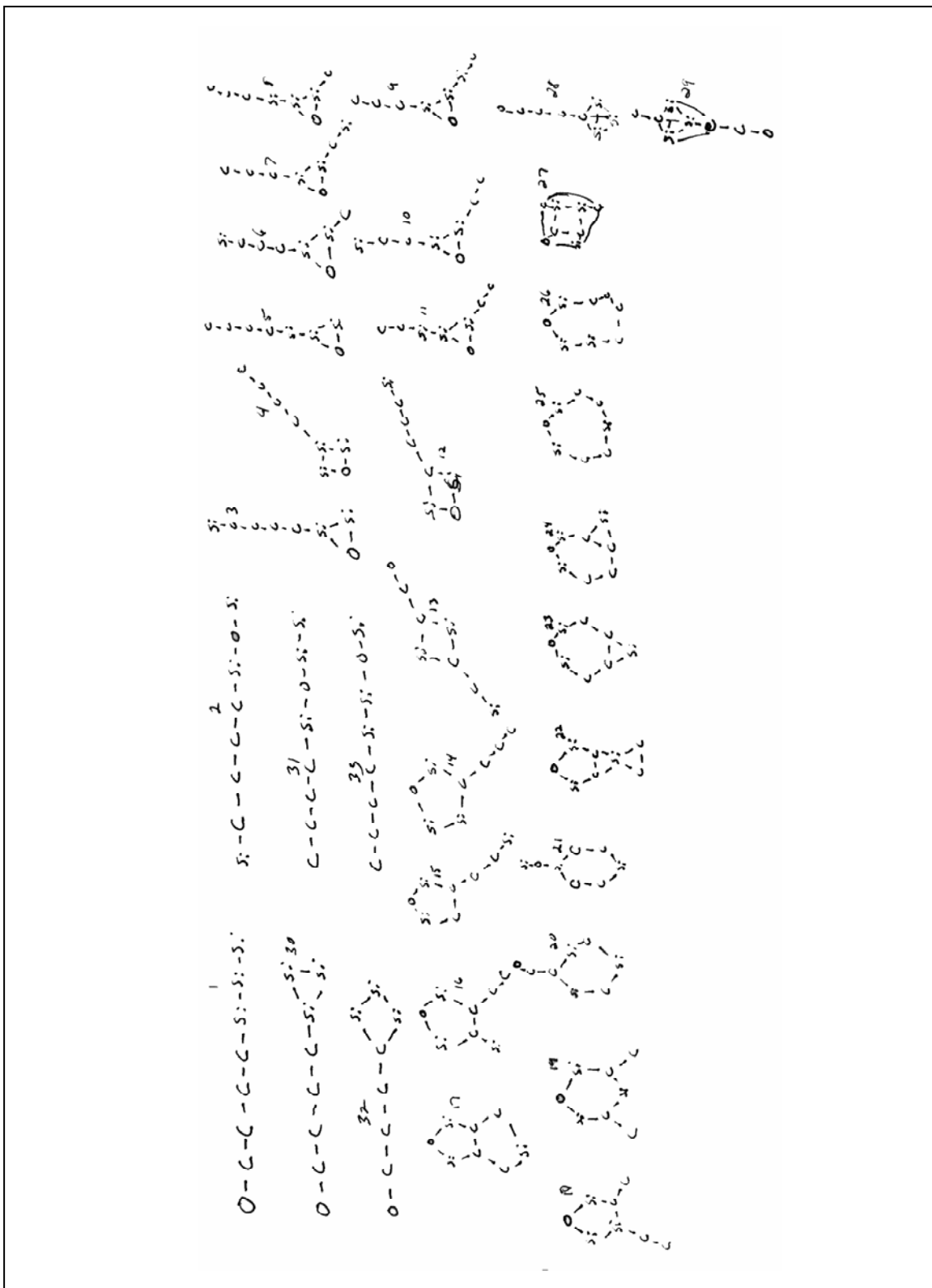


Figure 49. Initial isomers for C_4Si_3O calculations with HF/VDZ

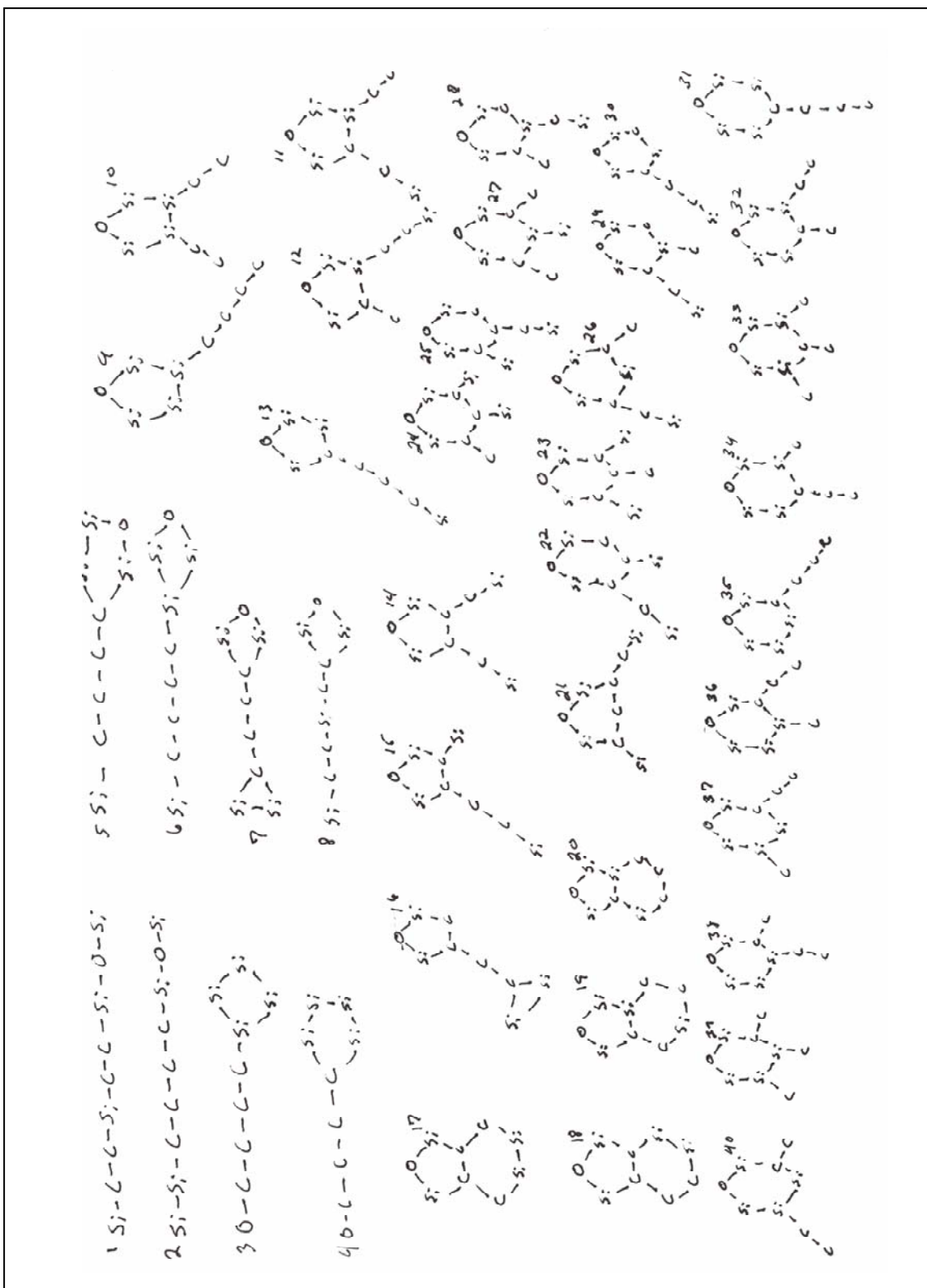


Figure 51. Initial isomers for C_4Si_4O calculations with HF/VDZ

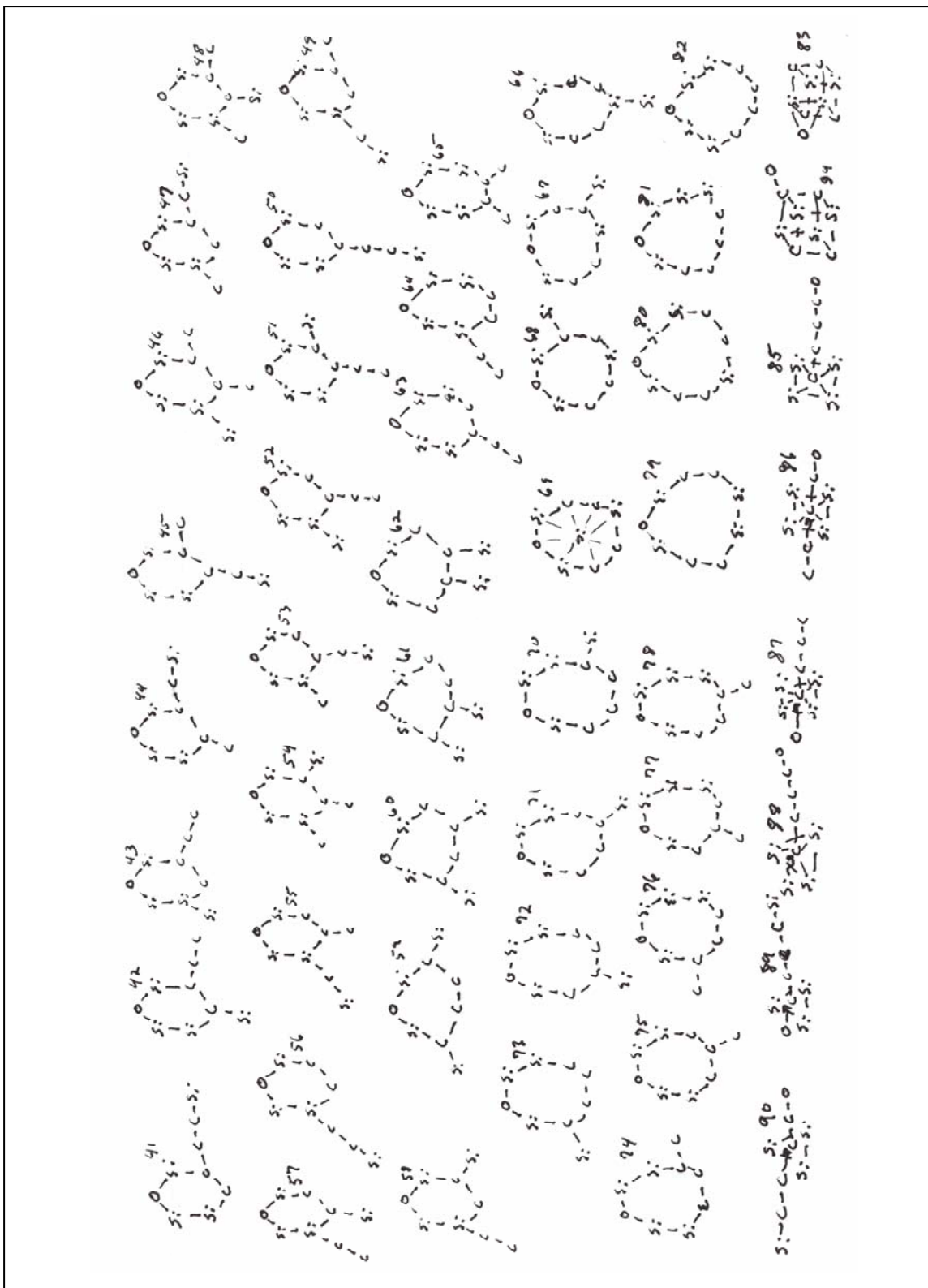


Figure 51. (Continued) Initial isomers for C_4Si_4O calculations with HF/VDZ

Appendix C. Detailed Calculation Data

This appendix is a series of tables detailing most of the calculations that I have done in the course of this research. The only calculations not shown are the initial HF/VDZ calculations done for the larger molecules. These are left out due to their extremely large number.

C.1. O

Table 25. Detailed Calculation Data for O

Charge	Mult	Basis Set	Final Energy (hart)	EA (eV)
0	3	DVZ	-74.80054632	1.252341
-1	2	DVZ	-74.75450439	
0	1	DVZ	-74.67855885	
-1	4	DVZ	-74.06201896	
0	3	cc-pVDZ	-74.78757634	1.870789
-1	2	cc-pVDZ	-74.71879734	
0	3	aug-cc-pVDZ	-74.79148377	0.499922
-1	2	aug-cc-pVDZ	-74.77310426	
-1	2	DFT/VDZ	-75.06245897	-0.30453
0	3	DFT/VDZ	-75.05126304	
-1	2	DFT/cc-pVDZ	-75.02098178	0.467356
0	3	DFT/cc-pVDZ	-75.03816398	
-1	2	DFT/aug-cc-pVDZ	-75.10534915	-1.58715
0	3	DFT/aug-cc-pVDZ	-75.04699806	

C.2. CO

Table 26. Detailed Calculation Data for CO

Charge	Mult	Basis Set	Final Energy (hart)	EA (eV)	ZPE (hart)	EA (eV) w/ZPE
0	1	DVZ	-112.6850703739	2.02121		
-1	2	DVZ	-112.6107611990			
0	3	DVZ	-112.5057371985			
0	1	cc-pDVZ	-112.7505418517	3.153106		
-1	2	cc-pDVZ	-112.6346188333			
0	1	aug-cc-pDVZ	-112.7564277478	2.164022		
-1	2	aug-cc-pDVZ	-112.6768681116			
0	1	DFT/DVZ	-113.2256492384	1.535123		
-1	2	DFT/DVZ	-113.1692108993			
0	1	DFT/cc-pDVZ	-113.2709811734	2.520233		
-1	2	DFT/cc-pDVZ	-113.1783255567			
0	1	DFT/aug-cc-pDVZ	-113.2809150378	1.191161	0.00497 5	1.15933 7
-1	2	DFT/aug-cc-pDVZ	-113.2371223526		0.00380 5	

C.3. SiO

Table 27. Detailed Calculation Data for SiO

Charge	Mult	Basis Set	Final Energy (hart)	EA (eV)	ZPE (hart)	EA (eV) w/ZPE
0	1	DVZ	-363.7341927429	0.617643		
-1	2	DVZ	-363.7114852831			
0	3	DVZ	-363.6274052707			
0	1	cc-pVDZ	-363.7905917065	1.06279		
-1	2	cc-pVDZ	-363.7515185471			
0	1	aug-cc-pVDZ	-363.8029257588	0.30346		
-1	2	aug-cc-pVDZ	-363.7917691446			
0	1	DFT/VDZ	-364.6152100352	0.390889		
-1	2	DFT/VDZ	-364.6008391089			
0	1	DFT/cc-pVDZ	-364.6533132241	0.6767		
-1	2	DFT/cc-pVDZ	-364.6284345568			
-1	2	DFT/aug-cc-pVDZ	-364.6731376581	-0.17747	0.00232 8	-0.18781
0	1	DFT/aug-cc-pVDZ	-364.6666129350		0.00270 8	

C.4. CSiO

Table 28. Detailed Calculation Data for CSiO

Q	M	Input Geometry	Output Geometry	Basis Set	Final Energy (hart)	EA (eV)	ZPE (hart)	EA (eV) w/ZPE
-1	2	O-C-Si Linear	O-C-Si Linear	DZV	-401.5363	-0.26656		
-1	2	O-C-Si cyc3	O-C-Si Linear	DZV	-401.5363			
0	3	O-C-Si Linear	O-C-Si Linear	DZV	-401.5265			
0	3	C-O-Si Linear	Dissociated	DZV	-401.5177			
-1	4	O-C-Si Linear	O-C-Si Linear	DZV	-401.4989			
-1	4	C-O-Si Linear	Dissociated	DZV	-401.4976			
0	1	O-C-Si cyc3	O-C-Si Linear	DZV	-401.4868			
0	1	C-O-Si Linear	Dissociated	DZV	-401.4579			
0	3	O-C-Si cyc3	O-C-Si cyc3	DZV	-401.42			
-1	2	O-Si-C Linear	O-Si-C Linear	DZV	-401.384			
0	3	O-Si-C Linear	O-Si-C Linear	DZV	-401.3406			
0	1	O-Si-C Linear	O-Si-C Linear	DZV	-401.1909			
0	1	O-C-Si Linear	O-C-Si Linear	DZV	-401.1805			
-1	2	C-O-Si Linear	Dissociated	DZV	N/A			
-1	4	O-Si-C Linear	unconverged	DZV				
-1	4	O-C-Si cyc2	unconverged	DZV				
-1	2	O-C-Si Linear	O-C-Si Linear	cc-pVTZ	-401.6566	-0.08976		
0	3	O-C-Si Linear	O-C-Si Linear	cc-pVTZ	-401.6533			
0	3	C-O-Si Linear	Dissociated	cc-pVTZ	-401.6357			
-1	4	O-C-Si Linear	O-C-Si Linear	cc-pVTZ	-401.6349			
0	1	O-C-Si Linear	O-C-Si Linear	cc-pVTZ	-401.6113			
0	1	O-C-Si cyc4	O-C-Si Linear	cc-pVTZ	-401.6113			
-1	4	O-C-Si cyc3	C-O-Si bent	cc-pVTZ	-401.6011			
-1	4	C-O-Si Linear	C-O-Si Linear	cc-pVTZ	-401.5899			

Table 28. Detailed Calculation Data for CSiO (continued)

Q	M	Input Geometry	Output Geometry	Basis Set	Final Energy (hart)	EA (eV)	ZPE (hart)	EA (eV) w/ZPE
0	1	C-O-Si Linear	Dissociated	cc-pVTZ	-401.5784			
0	3	O-C-Si cyc3	O-C-Si cyc3	cc-pVTZ	-401.5601			
-1	2	O-Si-C Linear	O-Si-C Linear	cc-pVTZ	-401.531			
0	3	O-Si-C Linear	O-Si-C Linear	cc-pVTZ	-401.4996			
0	1	O-Si-C Linear	O-Si-C Linear	cc-pVTZ	-401.3549			
-1	2	C-O-Si Linear	Dissociated	cc-pVTZ	N/A			
-1	2	O-C-Si cyc4	unconverged	cc-pVTZ				
-1	4	O-Si-C Linear	unconverged	cc-pVTZ				
-1	2	O-C-Si Linear	O-C-Si Linear	DZV(DFT)	-402.6557	-1.26208		
0	3	O-C-Si Linear	O-C-Si Linear	DZV(DFT)	-402.6093			
-1	2	O-C-Si Linear	O-C-Si Linear	cc-pVTZ(DFT)	-402.7534	-1.19952		
0	3	O-C-Si Linear	O-C-Si Linear	cc-pVTZ(DFT)	-402.7093			
-1	2	O-C-Si Linear	O-C-Si Linear	DFT/aug-cc-pVDZ	-402.7630095	-1.38288	0.00733	-1.38296
0	3	O-C-Si Linear	O-C-Si Linear	DFT/aug-cc-pVDZ	-402.7121685		0.00734	
0	3	O-C-Si Linear	O-C-Si Linear	SP	-402.7094935	-1.45564	0.00734	-1.45572

C.5. C₂O

Table 29. Detailed Calculation Data for C₂O

Q	M	Input Geometry	Output Geometry	Basis Set	Final Energy (hart)	EA (eV)	ZPE (hart)	EA (eV) w/ZPE
0	3	cyc3_CCO_	CCO	DVZ	-150.3907498	0.02268 3		
-1	2	CCO	CCO	DVZ	-150.3899159			
0	3	CCO	CCO	DVZ	-150.3519609			
-1	2	cyc3_CCO_	cyc3_CCO_	DVZ	-150.3321428			
0	1	cyc3_CCO_	cyc3_CCO_	DVZ	-150.2854233			
0	3	COC	COC	DVZ	-150.267869			
-1	2	COC	COC	DVZ	-150.2380572			
0	1	COC	COC	DVZ	-150.2294428			
0	1	CCO	CCO	DVZ	-150.132271			
-1	2	CCO	CCO	cc-pVDZ	-150.4346856	-0.41057		
0	3	CCO	CCO	cc-pVDZ	-150.4195912			
-1	2	CCO	CCO	aug-cc-pVDZ	-150.4580926	-0.84043		
0	3	CCO	CCO	aug-cc-pVDZ	-150.4271943			
-1	2	CCO	CCO	DFT/DVZ	-151.2309427	-2.19028		
0	3	CCO	CCO	DFT/DVZ	-151.1504177			
-1	2	CCO	CCO	DFT/cc-pVDZ	-151.2598639	-1.63126		
0	3	CCO	CCO	DFT/cc-pVDZ	-151.1998909			
-1	2	CCO	CCO	DFT/aug-cc-pVDZ	-151.2922503	-2.23011	0.00920 2	-2.22116

C.6. Si₂O

Table 30. Detailed Calculation Data for Si₂O

Q	M	Input Geometry	Output Geometry	Basis Set	Final Energy (hart)	EA (eV)	ZPE (hart)	EA (eV) w/ZPE
0	3	cyc3_SiSiO_	SiOSi	DVZ	-652.6341929	1.38459 5		
0	3	SiOSi	SiOSi	DVZ	-652.5989505			
-1	2	SiSiO	SiSiO	DVZ	-652.5832887			
0	1	cyc3_SiSiO_	SiOSi	DVZ	-652.5681732			
0	1	SiOSi	SiOSi	DVZ	-652.5681732			
0	3	SiSiO	Dissociated SiO Si	DVZ	-652.5640412			
-1	2	SiOSi	SiOSi	DVZ	-652.5550341			
-1	2	cyc3_SiSiO_	cyc3_SiSiO_	DVZ	-652.54925			
0	1	SiSiO	SiSiO	DVZ	-652.2826507			
-1	2	SiSiO	SiSiO	cc-pDVZ	-652.6809203	-0.77526		
0	3	SiSiO	SiSiO	cc-pDVZ	-652.652418			
0	3	SiOSi	SiOSi	cc-pDVZ	-652.6492582			
-1	2	SiOSi	SiOSi	cc-pDVZ	-652.6077423	1.12923 2		
-1	2	SiSiO	SiSiO	aug-cc-pDVZ	-652.705904	-1.07228		
0	3	SiOSi	SiOSi	aug-cc-pDVZ	-652.6666006	-0.86456		
0	3	SiSiO	SiSiO	aug-cc-pDVZ	-652.666482			
-1	2	SiOSi	SiOSi	aug-cc-pDVZ	-652.6348153			
-1	2	SiSiO	SiSiO	DFT/VDZ	-654.0223633	-1.71274		
-1	2	SiOSi	SiOSi	DFT/VDZ	-654.0135768	-0.12645		
0	3	SiOSi	SiOSi	DFT/VDZ	-654.0089279			

Table 30. Detailed Calculation Data for Si₂O (continued)

Q	M	Input Geometry	Output Geometry	Basis Set	Final Energy (hart)	EA (eV)	ZPE (hart)	EA (eV) w/ZPE
-1	2	SiSiO	SiSiO	DFT/cc-pVDZ	-654.0916116	-1.61878		
-1	2	SiOSi	SiOSi	DFT/cc-pVDZ	-654.0615291	-0.17967		
0	3	SiOSi	SiOSi	DFT/cc-pVDZ	-654.0549235			
0	3	SiSiO	SiSiO	DFT/cc-pVDZ	-654.0320977			
-1	2	SiSiO	SiSiO	DFT/aug-cc-pVDZ	-654.1183805	-1.98365	0.00424 1	-1.98167
-1	2	SiOSi	SiOSi	DFT/aug-cc-pVDZ	-654.0841303	-0.60684	0.00383 1	-0.60902
0	3	SiOSi	SiOSi	DFT/aug-cc-pVDZ	-654.0618199		0.00391 1	
0	3	SiSiO	SiSiO	DFT/aug-cc-pVDZ	-654.045452		0.00416 8	
0	3	SiOSi	SP	DFT/aug-cc-pVDZ	-654.061552	-0.61413	0.00391 1	-0.6163
0	3	SiSiO	SP	DFT/aug-cc-pVDZ	-654.0429145	-2.05267	0.00416 8	-2.05069

C.7. C₂SiO

Table 31. Detailed Calculation Data for C₂SiO

Q	M	Input Geometry	Output Geometry	Basis Set	Final Energy (hart)	EA (eV)	ZPE (hart)	EA (eV) w/ZPE
-1	2	Si-C2-O	Si-C2-O	cc-pVDZ	-439.473	-0.06577		
-1	2	cyc3_C-Si-O_C	Si-C2-O	cc-pVDZ	-439.473			
0	1	cyc3_C-Si-O_C	Si-C2-O	cc-pVDZ	-439.47			
0	1	Si-C2-O	Si-C2-O	cc-pVDZ	-439.47			
-1	2	bent_C2-Si- O	bent_C2-Si-O	cc-pVDZ	-439.435			
0	3	Si-C2-O	Si-C2-O	cc-pVDZ	-439.403			
0	1	bent_C2-Si- O	cyc3_Si-C2_O	cc-pVDZ	-439.376			
-1	2	bent_C2-O- Si	bent_C2-O- Si	cc-pVDZ	-439.374			
0	3	bent_C2-Si- O	bent_C2-Si-O	cc-pVDZ	-439.323			
0	3	bent_C2-O- Si	bent_C2-O- Si	cc-pVDZ	-439.317			
0	3	cyc3_C-Si-O_C	bent_C2-O- Si	cc-pVDZ	-439.31			
0	1	bent_C2-O- Si	C2-O-Si	cc-pVDZ	-439.304			
-1	2	bent_C2-Si-O	bent_C2-Si-O	aug-cc-pVDZ	1.250/1.608			
0	1	bent_C2-Si-O	cyc3_Si-C2_O	aug-cc-pVDZ	1.269/2.648			
0	3	bent_C2-Si-O	bent_C2-Si-O	aug-cc-pVDZ	1.202/-2.644			
0	1	Si-C2-O		aug-cc-pVDZ				
-1	2	Si-C2-O		aug-cc-pVDZ				
0	3	Si-C2-O		aug-cc-pVDZ				

Table 31. Detailed Calculation Data for C₂SiO (continued)

Q	M	Input Geometry	Output Geometry	Basis Set	Final Energy (hart)	EA (eV)	ZPE (hart)	EA (eV) w/ZPE
-1	2	Si-C2-O	Si-C2-O	VDZ-DFT	-440.7246226409	-0.76489		
0	1	Si-C2-O	Si-C2-O	VDZ-DFT	-440.6965018574			
-1	2	bent_C2-Si-O	bent_C2-Si-O	VDZ-DFT	-440.6839179849			
0	3	Si-C2-O	Si-C2-O	VDZ-DFT	-440.6055188272			
0	1	bent_C2-Si-O	Si-C2-O	VDZ-DFT	-440.5810485241			
-1	2	Si-C2-O	Si-C2-O	cc-pVDZ-DFT	-440.7789754434	-0.47811		
0	1	Si-C2-O	Si-C2-O	cc-pVDZ-DFT	-440.7613978973			
-1	2	Si-C2-O	Si-C2-O	aug-cc-pVDZ-DFT	-440.8050340469	-0.88029	0.01239	
0	1	Si-C2-O	Si-C2-O	aug-cc-pVDZ-DFT	-440.7726703307		3	-0.90741
							0.01339	
0	1	Si-C2-O	Si-C2-O	aug-cc-pVDZ-DFT	-440.7672547346	-1.0276	0.01339	-1.05472

C.8. CSi₂O

Table 32. Detailed Calculation Data for CSi₂O

Q	M	Input Geometry	Output Geometry	Basis Set	Final Energy (hart)	EA (eV)	ZPE (hart)	EA (eV) w/ZPE
-1	2	cyc3_C-Si-Si_O	cyc3_C-Si-Si_O	cc-pVDZ	-690.533			
-1	2	cyc4_Si-C-Si-O_	cyc4_Si-C-Si-O_	cc-pVDZ	-690.52			
-1	2	Si-C-Si-O	Si-C-Si-O	cc-pVDZ	-690.481			
-1	2	cyc3_C-Si-O_Si	cyc3_C-Si-O_Si	cc-pVDZ	-690.465			
0	1	cyc3_C-Si-O_Si	bent_O-C-Si-Si_	cc-pVDZ	-690.502			
0	1	cyc3_C-Si-Si_O	bent_O-C-Si-Si_	cc-pVDZ	-690.502			
0	1	Si-C-Si-O	Si-C-Si-O	cc-pVDZ	-690.481			
0	3	cyc3_C-Si-Si_O	cyc3_C-Si-Si_O	cc-pVDZ	-690.473			
0	3	cyc3_C-Si-O_Si	cyc3_C-Si-O_Si	cc-pVDZ	-690.449			
0	1	cyc4_Si-C-Si-O_	cyc4_Si-C-Si-O_	cc-pVDZ	-690.427			
0	3	Si-C-Si-O	Si-C-Si-O	cc-pVDZ	-690.408			
0	3	cyc4_Si-C-Si-O_	cyc4_Si-C-Si-O_	cc-pVDZ	-690.346			
-1	2	bent_O-C-Si-Si_	bent_O-C-Si-Si_	aug-cc-pVDZ	-690.554	-1.1424		
-1	2	cyc3_C-Si-Si_O	cyc3_C-Si-Si_O	aug-cc-pVDZ	-690.551			
-1	2	cyc4_Si-C-Si-O_	cyc4_Si-C-Si-O_	aug-cc-pVDZ	-690.547			
-1	2	Si-C-Si-O	Si-C-Si-O	aug-cc-pVDZ	-690.489			
-1	2	cyc3_C-Si-O_Si	cyc3_C-Si-O_Si	aug-cc-pVDZ	-690.463			
-1	2	Si-Si-C-O	unconverged	aug-cc-pVDZ				
0	1	bent_O-C-Si-Si_	bent_O-C-Si-Si_	aug-cc-pVDZ	-690.512			
0	1	cyc3_C-Si-Si_O	bent_O-C-Si-Si_	aug-cc-pVDZ	-690.512			
0	1	Si-C-Si-O	Si-C-Si-O	aug-cc-pVDZ	-690.497			
0	1	cyc3_C-Si-O_Si	O- C-Si -Si	aug-cc-pVDZ	-690.494			
0	3	bent_O-C-Si-Si_	bent_O-C-Si-Si_	aug-cc-pVDZ	-690.485			
0	3	cyc3_C-Si-Si_O	cyc3_C-Si-Si_O	aug-cc-pVDZ	-690.483			

Table 32. Detailed Calculation Data for CSi₂O (Continued)

Q	M	Input Geometry	Output Geometry	Basis Set	Final Energy (hart)	EA (eV)	ZPE (hart)	EA (eV) w/ZPE
0	3	cyc3_C-Si-O_Si	cyc3_C-Si-O_Si	aug-cc-pVDZ	-690.464			
0	1	Si-Si-C-O	Si-Si-C-O	aug-cc-pVDZ	-690.459			
0	3	Si-Si-C-O	Si-Si-C-O	aug-cc-pVDZ	-690.449			
0	1	cyc4_Si-C-Si-O	cyc4_Si-C-Si-O	aug-cc-pVDZ	-690.448			
0	3	Si-C-Si-O	Si-C-Si-O	aug-cc-pVDZ	-690.424			
0	3	cyc4_Si-C-Si-O	cyc4_Si-C-Si-O	aug-cc-pVDZ	-690.388			
-1	2	cyc3_C-Si-Si_O	cyc3_C-Si-Si_O	DFT-VDZ	-692.085737			
-1	2	bent_O-C-Si-Si	cyc3_C-Si-Si_O	DFT-VDZ	-692.085737			
-1	2	Si-C-Si-O	bent_O-Si-C-Si	DFT-VDZ	-692.079307			
-1	2	cyc4_Si-C-Si-O	cyc4_Si-C-Si-O	DFT-VDZ	-692.048867			
-1	2	O- C-Si -Si	cyc3_C-Si-O_Si	DFT-VDZ	-692.046336			
0	1	bent_O-C-Si-Si	bent_O-C-Si-Si	DFT-VDZ	-692.018244			
0	1	O- C-Si -Si	bent_O-C-Si-Si	DFT-VDZ	-692.018244			
0	1	cyc3_C-Si-Si_O	bent_O-C-Si-Si	DFT-VDZ	-692.018244			
0	1	Si-C-Si-O	Si-C-Si-O	DFT-VDZ	-692.011524			
0	1	cyc4_Si-C-Si-O	cyc4_Si-C-Si-O	DFT-VDZ	-691.983917			

Table 32. Detailed Calculation Data for CSi₂O (Continued)

Q	M	Input Geometry	Output Geometry	Basis Set	Final Energy (hart)	EA (eV)	ZPE (hart)	EA (eV) w/ZPE
-1	2	cyc3_C-Si-Si_O	cyc3_C-Si-Si_O	DFT-aug-cc-pVDZ	-692.189193			
-1	2	bent_O-C-Si-Si_	cyc3_C-Si-Si_O	DFT-aug-cc-pVDZ	-692.189193	-1.714528		
-1	2	Si-C-Si-O	bent_O-Si-C-Si_	DFT-aug-cc-pVDZ	-692.17652	-1.834780		
-1	2	bent_O-Si-C-Si_	bent_O-Si-C-Si_	DFT-aug-cc-pVDZ	-692.17652			
0	1	bent_O-C-Si-Si_	cyc3_C-Si-Si_O	DFT-aug-cc-pVDZ	-692.126159			
0	1	bent_O-Si-C-Si_	bent_O-Si-C-Si_	DFT-aug-cc-pVDZ	-692.109065			
0	1	cyc3_C-Si-Si_O	Si-C-Si-O	DFT-aug-cc-pVDZ	-692.108549			
0	1	Si-C-Si-O	Si-C-Si-O	DFT-aug-cc-pVDZ	-692.108549			
0	1	cyc3_C-Si-Si_O	Single Point	CISD-aug-cc-pVDZ	-690.961661			
0	1	cyc3_C-Si-Si_O-sym	Single Point	CISD-aug-cc-pVDZ	-690.840537			
0	1	cyc3_C-Si-Si_O		CISD-aug-cc-pVDZ	-690.962291			
0	1	cyc3_C-Si-Si_O		MP2-aug-cc-pVDZ	-690.497138			
0	1	cyc3_C-Si-Si_O		MCSCF-aug-cc-pVDZ	-690.668297			
-1	2	cyc3_C-Si-Si_O	cyc3_C-Si-Si_O	CCSD(T)-aug-cc-pVDZ	-691.117416	-1.599442		
0	1	cyc3_C-Si-Si_O	cyc3_C-Si-Si_O	CCSD(T)-aug-cc-pVDZ	-691.058613			
-1	2	cyc3_C-Si-Si_O	cyc3_C-Si-Si_O	DFT-aug-cc-pVDZ	-692.189193	-1.714535	0.00801	-1.745
0	1	cyc3_C-Si-Si_O	cyc3_C-Si-Si_O	DFT-aug-cc-pVDZ	-692.126159		0.00913	
0	1	cyc3_C-Si-Si_O	SP	DFT-aug-cc-pVDZ	-692.09662	-2.517991	0.00913	-2.54846

C.9. C₂Si₂O

Table 33. Detailed Calculation Data for C₂Si₂O

Q	M	Input Geometry	Output Geometry	Basis Set	Final Energy (hart)	EA (eV)	VDZ input
-1	2	cyc3_Si-C-(O)C-(Si)_	cyc3_C-Si2_-C-O	cc-pVDZ	-728.4058767916	0.59610 1	0
-1	2	cyc3_C-Si2_-C-O	cyc3_C-Si2_-C-O	cc-pVDZ	-728.4058767902		146
-1	2	O-C-C-(Si)(Si)	cyc3_C-Si2_-C-O	cc-pVDZ	-728.4058767857		0
-1	2	C-cyc4_C-Si-O-Si_	cyc4_Si-(C)-C-Si-O_	cc-pVDZ	-728.4044572886	0.66434 2	64
-1	2	cyc5_C-Si-O-Si-C_	cyc4_Si-(C)-C-Si-O_	cc-pVDZ	-728.4044572882		0
-1	2	bent_C2_-Si-bent_O-Si_	cyc5_Si-C2-Si-O_	cc-pVDZ	-728.3965437324		6
-1	2	cyc3_C-Si2_-bent_C-O_	cyc3_C-Si2_-bent_C-O_	cc-pVDZ	-728.3861431730		60
0	1	cyc3_C-Si2_-bent_C-O_	cyc3_C-Si2_-C-O	cc-pVDZ	-728.3839613074		0
0	1	cyc3_C-Si2_-C-O	cyc3_C-Si2_-C-O	cc-pVDZ	-728.3839613038		146
0	1	O-C-C-(Si)(Si)	cyc3_C-Si2_-C-O	cc-pVDZ	-728.3839613022		0
0	1	cyc3_Si-C-(O)C-(Si)_	cyc3_C-Si2_-C-O	cc-pVDZ	-728.3839613000		32
-1	2	Si2-C2-O	Si2-C2-O	cc-pVDZ	-728.3831980908		0
0	1	bent_Si-C2-Si_-O	cyc4_Si-(C)-C-Si-O_	cc-pVDZ	-728.3800329413		0
0	1	cyc5_C-Si-O-Si-C_	cyc4_Si-(C)-C-Si-O_	cc-pVDZ	-728.3800329071		121
0	1	C-cyc4_C-Si-O-Si_	C-cyc4_C-Si-O-Si_	cc-pVDZ	-728.3788991870		6
-1	2	bent_Si-C2-Si_-O	bent_Si-C2-Si_-O	cc-pVDZ	-728.3758955907		45
0	3	O-C-C-(Si)(Si)	cyc3_C-Si2_-C-O	cc-pVDZ	-728.3516846292		158
0	3	cyc3_C-Si2_-bent_C-O_	cyc3_C-Si2_-C-O	cc-pVDZ	-728.3516846243		88
0	3	cyc3_C-Si2_-C-O	cyc3_C-Si2_-C-O	cc-pVDZ	-728.3516846175		0
0	3	Si2-C2-O	Si2-C2-O	cc-pVDZ	-728.3406012015		1
0	3	cyc5_C-Si-O-Si-C_	cyc4_Si-(C)-C-Si-O_	cc-pVDZ	-728.3249548962		137
0	3	bent_Si-C2-Si_-O	bent_Si-C2-Si_-O	cc-pVDZ	-728.3185631870		153
0	3	C-cyc4_C-Si-O-Si_		cc-pVDZ	-728.3173459754		0

Table 33. Detailed Calculation Data for C₂Si₂O (continued)

Q	M	Input Geometry	Output Geometry	Basis Set	Final Energy (hart)	EA (eV)	ZPE (hart)	EA (eV) w/ZPE
0	1	Si2-C2-O	Si2-C2-O	cc-pVDZ	-728.3009235116		56	
0	3	bent_C2_-Si-bent_O-Si_		cc-pVDZ	-728.2948571487		87	
-1	2	Si-C2-O-Si	Si-C2-bent_O-Si_	cc-pVDZ	-728.2800723089		76	
0	1	Si-C2-O-Si	Dissociated	cc-pVDZ	-728.2615217268		0	
0	1	bent_C2_-Si-bent_O-Si_	Rot	cc-pVDZ			0	
-1	2	cyc4_Si-(C)-C-Si-O_	cyc4_Si-(C)-C-Si-O_	aug-cc-pVDZ	-728.4289846652	-0.842589		
0	1	cyc4_Si-(C)-C-Si-O_	cyc4_Si-(C)-C-Si-O_	aug-cc-pVDZ	-728.3980071355			
0	1	cyc3_C-Si2_-C-O	cyc3_C-Si2_-C-O	aug-cc-pVDZ	-728.3922256877	0.391364		
-1	2	cyc3_C-Si2_-C-O	cyc3_C-Si2_-C-O	aug-cc-pVDZ	-728.3778373112			
-1	2	cyc3_C-Si2_-C-O	cyc3_C-Si2_-C-O	DFT-VDZ	-730.1565649507	-1.519037		
-1	2	cyc4_Si-(C)-C-Si-O_	cyc5_Si-C2-Si-O_	DFT-VDZ	-730.1508537272	-1.816903		
0	1	cyc3_C-Si2_-C-O	cyc3_C-Si2_-C-O	DFT-VDZ	-730.1007179945			
0	1	cyc4_Si-(C)-C-Si-O_	cyc5_Si-C2-Si-O_	DFT-VDZ	-730.0840558126			
-1	2	cyc3_C-Si2_-C-O	cyc3_C-Si2_-C-O	DFT-cc-pVDZ	-730.2487599817	-1.346664		
-1	2	cyc5_Si-C2-Si-O_	cyc5_Si-C2-Si-O_	DFT-cc-pVDZ	-730.2396750495	-1.448241		
0	1	cyc3_C-Si2_-C-O	cyc3_C-Si2_-C-O	DFT-cc-pVDZ	-730.1992502917			
0	1	cyc5_Si-C2-Si-O_	cyc5_Si-C2-Si-O_	DFT-cc-pVDZ	-730.1864309006			
-1	2	cyc3_C-Si2_-C-O	cyc3_C-Si2_-C-O	DFT-aug-cc-pVDZ	-730.2714063102	-1.657738	0.013921	-1.67945
-1	2	cyc5_Si-C2-Si-O_	cyc5_Si-C2-Si-O_	DFT-aug-cc-pVDZ	-730.2644589529	-1.672923		
0	1	cyc3_C-Si2_-C-O	cyc3_C-Si2_-C-O	DFT-aug-cc-pVDZ	-730.2104600762		0.014708	
0	1	cyc5_Si-C2-Si-O_	cyc5_Si-C2-Si-O_	DFT-aug-cc-pVDZ	-730.2029544188			

C.10. C₃O

Table 34. Detailed Calculation Data for C₃O

Q	M	Input Geometry	Output Geometry	Basis Set	Final Energy (hart)	EA (eV)	ZPE (hart)	EA (eV) w/ZPE
-1	2	cyc3_CCC_ep_O	bent_C3O	DVZ	-188.2861796	-0.74038		
-1	2	CCCO	CCCO	DVZ	-188.2725308			
0	1	CCCO	CCCO	DVZ	-188.2589598			
0	1	cyc3_CCC_O	CCCO	DVZ	-188.2589598			
-1	2	cyc3_CCC_O	cyc3_CCC_O	DVZ	-188.2289756			
-1	2	CCC_2-O	cyc3_CCC_O	DVZ	-188.2289756			
-1	2	pyr_CCCO	cyc3_CCC_O	DVZ	-188.2289755			
0	3	CCCO	CCCO	DVZ	-188.1688034			
0	3	cyc3_CCC_ep_O	bent_C3O	DVZ	-188.1660215			
-1	2	CCOC	CCOC	DVZ	-188.149131			
-1	2	cyc3_CCO_C	cyc3_CCO_C	DVZ	-188.1354337			
0	3	cyc3_CCC_O	cyc3_CCC_O	DVZ	-188.1321634			
-1	2	cyc4_CCCO	cyc4_CCCO	DVZ	-188.1141592			
0	1	CCOC	CCOC	DVZ	-188.0871662			
0	1	cyc4_CCCO	cyc3_CCO_C	DVZ	-188.0841369			
0	1	pyr_CCCO	cyc3_CCO_C	DVZ	-188.0841369			
0	3	CCC_2-O	C-(C)(C)(O)	DVZ	-188.0645197			
0	3	CCOC	CCOC	DVZ	-188.0609266			
0	3	cyc3_CCO_C	cyc3_CCO_C	DVZ	-188.0343991			
0	3	cyc4_CCCO	cyc4_CCCO	DVZ	-188.02696			
0	1	CCC_2-O	C-(C)(C)(O)	DVZ	-188.0213933			
0	1	cyc3_CCC_ep_O	C- CC -O	DVZ	-188.0210255			
0	3	pyr_CCCO	pyr_CCCO	DVZ	-187.9521937			
0	1	cyc3_CCO_C	Dissociated C2O C	DVZ	-187.949104			

Table 34. Detailed Calculation Data for C₃O (continued)

Q	M	Input Geometry	Output Geometry	Basis Set	Final Energy (hart)	EA (eV)	ZPE (hart)	EA (eV) w/ZPE
-1	2	bent_C3O_	bent_C3O_	cc-pVDZ	-188.3494177	-0.09678		
0	1	bent_C3O_	CCCO	cc-pVDZ	-188.3458594			
0	1	CCCO	CCCO	cc-pVDZ	-188.3458594			
-1	2	CCCO	CCCO	cc-pVDZ	-188.335889			
-1	2	bent_C3O_	bent_C3O_	aug-cc-pVDZ	-188.3718727	-0.50276		
0	1	bent_C3O_	CCCO	aug-cc-pVDZ	-188.3533888			
0	1	CCCO	CCCO	aug-cc-pVDZ	-188.3533882			
-1	2	CCCO	CCCO	aug-cc-pVDZ	-188.3041838			
-1	2	CCCO	bent_C3O_	DFT/VDZ	-189.2958625	-1.04539		
-1	2	bent_C3O_	bent_C3O_	DFT/VDZ	-189.2958625			
0	1	CCCO	bent_C3O_	DFT/VDZ	-189.2574292			
0	1	bent_C3O_	bent_C3O_	DFT/VDZ	-189.2574292			
-1	2	bent_C3O_	bent_C3O_	DFT/cc-pVDZ	-189.3348112	-0.46935		
-1	2	CCCO	bent_C3O_	DFT/cc-pVDZ	-189.3348112			
0	1	CCCO	CCCO	DFT/cc-pVDZ	-189.3175558			
0	1	bent_C3O_	CCCO	DFT/cc-pVDZ	-189.3175558			
-1	2	bent_C3O_	bent_C3O_	DFT/aug-cc-pVDZ	-189.3663855			
-1	2	CCCO	bent_C3O_	DFT/aug-cc-pVDZ	-189.3663855	-1.05221	0.01278	
0	1	bent_C3O_	CCCO	DFT/aug-cc-pVDZ	-189.3277014		1	-0.70456
0	1	CCCO	CCCO	DFT/aug-cc-pVDZ	-189.3277014		0.01528	
							9	
							0.01528	

C.11. Si₃O

Table 35. Detailed Calculation Data for Si₃O

Q	M	Input Geometry	Output Geometry	Basis Set	Final Energy (hart)	EA (eV)	ZPE (hart)	EA (eV) w/ZPE
-1	2	cyc4_SiSiSiO	cyc4_SiSiSiO	DVZ	-941.5054098	-0.55374		
-1	2	cyc3_SiSiO_Si	SiOSi-bent_Si	DVZ	-941.4913147			
-1	2	pyr_SiSiSiO	SiOSi-bent_Si	DVZ	-941.4913147			
-1	2	SiSiSi_2-O	SiOSi-bent_Si	DVZ	-941.4913147			
-1	2	SiSiOSi	SiSiOSi	DVZ	-941.4866073			
-1	2	cyc3_SiSiSi_ep_O	cyc4_SiSiSiO	DVZ	-941.4850519			
0	3	cyc4_SiSiSiO	cyc4_SiSiSiO	DVZ	-941.4824867			
0	3	pyr_SiSiSiO	cyc3_OSiSi_-Si	DVZ	-941.4768068			
0	3	SiSiSi_2-O	bent_SiOSiSi	DVZ	-941.4755949			
0	1	cyc4_SiSiSiO	cyc4_SiSiSiO	DVZ	-941.4557649			
0	1	pyr_SiSiSiO	cyc4_SiSiSiO	DVZ	-941.4557649			
0	3	cyc3_SiSiSi_ep_O	cyc4_SiSiSiO	DVZ	-941.4551004			
0	3	SiSiOSi	SiSiOSi	DVZ	-941.4532985			
0	3	cyc3_SiSiO_Si	Si2OSi	DVZ	-941.4517468			
0	3	cyc3_SiSiSi_O	SiOSi-bent_Si	DVZ	-941.4322079			
-1	2	SiSiSiO	SiSiSiO	DVZ	-941.423246			
0	1	cyc3_SiSiSi_O	cyc4_SiSiSiO	DVZ	-941.4216268			
0	1	cyc3_SiSiSi_ep_O	cyc4_SiSiSiO	DVZ	-941.4216258			
0	1	cyc3_SiSiO_Si	cyc3_SiOSi_-Si	DVZ	-941.4186426			
0	1	SiSiOSi	SiSiOSi	DVZ	-941.4098155			
0	1	SiSiSiO	SiSiSiO	DVZ	-941.3680657			
0	3	SiSiSiO	SiSiSiO	DVZ	-941.3531966			
-1	2	cyc3_SiSiSi_O		DVZ				
0	1	SiSiSi_2-O		DVZ				

Table 35. Detailed Calculation Data for Si₃O (continued)

Q	M	Input Geometry	Output Geometry	Basis Set	Final Energy (hart)	EA (eV)	ZPE (hart)	EA (eV) w/ZPE
-1	2	SiSiSiO	SiSiSiO	cc-pVDZ	-941.5939432	-0.42353		
-1	2	bent_SiSiOSi_	bent_SiSiOSi_	cc-pVDZ	-941.5875403			
-1	2	cyc3_OSiSi_-Si	cyc3_OSiSi_-Si	cc-pVDZ	-941.5849289			
-1	2	SiSiOSi	SiSiOSi	cc-pVDZ	-941.5816963			
0	3	cyc3_OSiSi_-Si	cyc3_OSiSi_-Si	cc-pVDZ	-941.5693578			
0	3	SiSiOSi	SiSiOSi	cc-pVDZ	-941.552833			
-1	2	cyc4_SiSiSiO_	cyc4_SiSiSiO_	cc-pVDZ	-941.5054098			
0	3	SiSiSiO	Dissociated Si2 SiO	cc-pVDZ	-941.4919576			
0	3	cyc4_SiSiSiO_	cyc4_SiSiSiO_	cc-pVDZ	-941.4824866			
0	3	bent_SiSiOSi_		cc-pVDZ				
-1	2	SiSiSiO	Dissociated Si2 SiO	aug-cc-pVDZ	-941.6181058	-0.95596		
-1	2	cyc3_OSiSi_-Si	bent_SiSiOSi_	aug-cc-pVDZ	-941.6130745			
-1	2	SiSiOSi	bent_SiSiOSi_	aug-cc-pVDZ	-941.6130741			
-1	2	bent_SiSiOSi_	bent_SiSiOSi_	aug-cc-pVDZ	-941.6130741			
0	3	cyc3_OSiSi_-Si	cyc3_OSiSi_-Si	aug-cc-pVDZ	-941.5779288			
0	3	SiSiSiO	Dissociated Si2 SiO	aug-cc-pVDZ	-941.5655282			
0	3	SiSiOSi	SiSiOSi	aug-cc-pVDZ	-941.564174			
0	3	bent_SiSiOSi_		aug-cc-pVDZ				
-1	2	SiSiSiO	bent_SiSiSiO_	DFT/VDZ	-943.4498909	-1.81807		
-1	2	bent_SiSiOSi_	SiSiOSi	DFT/VDZ	-943.4417407			
-1	2	SiSiOSi	SiSiOSi	DFT/VDZ	-943.4417405			
-1	2	cyc3_OSiSi_-Si	cyc3_OSiSi_-Si	DFT/VDZ	-943.441451			
0	3	cyc3_OSiSi_-Si	cyc3_OSiSi_-Si	DFT/VDZ	-943.3893895			
0	3	bent_SiSiOSi_	bent_SiSiOSi_	DFT/VDZ	-943.38305			
0	3	SiSiOSi	SiSiOSi	DFT/VDZ	-943.3708201			

Table 35. Detailed Calculation Data for Si₃O (continued)

Q	M	Input Geometry	Output Geometry	Basis Set	Final Energy (hart)	EA (eV)	ZPE (hart)	EA (eV) w/ZPE
-1	2	SiSiSiO	cyc3_Si3_-O	DFT/cc-pVDZ	-943.5751547	-1.73022		
-1	2	cyc3_OSiSi_-Si	cyc3_OSiSi_-Si	DFT/cc-pVDZ	-943.5208019			
-1	2	bent_SiSiOSi_	SiSiOSi	DFT/cc-pVDZ	-943.5201904			
-1	2	SiSiOSi	SiSiOSi	DFT/cc-pVDZ	-943.5201904			
0	3	SiSiSiO	cyc3_Si-Si-(O)-Si_	DFT/cc-pVDZ	-943.5115435			
0	3	cyc3_OSiSi_-Si	cyc3_OSiSi_-Si	DFT/cc-pVDZ	-943.46778			
0	3	SiSiOSi	SiSiOSi	DFT/cc-pVDZ	-943.4524174			
0	3	bent_SiSiOSi_		DFT/cc-pVDZ	SCF			
-1	2	cyc3_Si-Si-(O)-Si_	cyc3_Si-Si-(O)-Si_	DFT/aug-cc-pVDZ	-943.6047101	-2.15669	0.16675 4	
-1	2	cyc3_Si3_-O	cyc3_Si3_-O	DFT/aug-cc-pVDZ	-943.5985795	-3.04999		
-1	2	SiSiSiO	cyc3_Si3_-O	DFT/aug-cc-pVDZ	-943.5985795			
0	3	cyc3_Si-Si-(O)-Si_	cyc3_Si-Si-(O)-Si_	DFT/aug-cc-pVDZ	-943.52542		1.06005 5	
0	3	SiSiSiO	cyc3_Si-Si-(O)-Si_	DFT/aug-cc-pVDZ	-943.52542			
0	3	cyc3_Si3_-O	cyc3_Si3_-O	DFT/aug-cc-pVDZ	-943.4864474			
-1	2	cyc3_Si-Si-(O)-Si_	cyc3_Si-Si-(O)-Si_	DFT/aug-cc-pVDZ	-943.6047101	-2.15669	0.00564 7	-2.1614
-1	2	cyc3_Si3_-O	cyc3_Si3_-O	DFT/aug-cc-pVDZ	-943.5985795	-3.04999	0.00573 8	-3.05698
0	3	cyc3_Si-Si-(O)-Si_	cyc3_Si-Si-(O)-Si_	DFT/aug-cc-pVDZ	-943.52542		0.00582	
0	3	cyc3_Si3_-O	cyc3_Si3_-O	DFT/aug-cc-pVDZ	-943.4864474		0.00599 5	
0	3	cyc3_Si-Si-(O)-Si_	SP	DFT/aug-cc-pVDZ	-943.517053	-2.38427	0.00582	-2.38898
0	3	cyc3_Si3_-O	SP	DFT/aug-cc-pVDZ	-943.4858618	-3.06592	0.00599 5	-3.07291

C.12. C₃SiO

Table 36. Detailed Calculation Data for C₃SiO

Q	M	Input Geometry	Output Geometry	Basis Set	Final Energy (hart)	EA (eV)	ZPE (hart)	EA (eV) w/ZPE
-1	2	SiC3O	SiC3O	cc-pVDZ	-477.2962659	-0.90218		
0	3	SiC3O	SiC3O	cc-pVDZ	-477.2630976			
0	1	SiC3O	SiC3O	cc-pVDZ	-477.2407726			
-1	2	SiC3O		aug-cc-pVDZ	SOLVCG	#VALUE!		
0	3	SiC3O	SiC3O	aug-cc-pVDZ	-477.2711914			
-1	2	SiC3O	SiC3O	DFT/VDZ	-478.7732458	-1.94615		
0	3	SiC3O	SiC3O	DFT/VDZ	-478.701696			
-1	2	SiC3O	SiC3O	DFT/cc-pVDZ	-478.8390397	-1.67685		
0	3	SiC3O	SiC3O	DFT/cc-pVDZ	-478.7773906			
-1	2	SiC3O	SiC3O	DFT/aug-cc-pVDZ	-478.8617754	-2.00055	0.01709 1	-2.0082
0	3	SiC3O	SiC3O	DFT/aug-cc-pVDZ	-478.7882256		0.01737 2	
0	3	SiC3O	SP	DFT/aug-cc-pVDZ	-478.7845069	-2.1017	0.01737 2	-2.10935

C.13. CSi₃O

Table 37. Detailed Calculation Data for CSi₃O

Q	M	Input Geometry	Output Geometry	Basis Set	Final Energy (hart)	EA (eV)	ZPE (hart)	EA (eV) w/ZPE
-1	2	cyc4_CSiOSi_-Si	cyc4_CSiOSi_-Si	cc-pVDZ	-979.4896934	-0.1675162		
0	1	bent_SiCSiOSi_	cyc4_CSiOSi_-Si	cc-pVDZ	-979.4835347			
0	1	cyc4_CSiOSi_-Si	cyc4_CSiOSi_-Si	cc-pVDZ	-979.4835347			
-1	2	bent_SiCSiOSi_	cyc4_CSiOSi_-Si	cc-pVDZ	-979.4791341			
0	3	cyc4_CSiOSi_-Si	cyc4_CSiOSi_-Si	cc-pVDZ	-979.4209231			
0	3	bent_SiCSiOSi_	bent_SiCSiOSi_	cc-pVDZ	-979.4090203			
-1	2	cyc4_CSiOSi_-Si	cyc4_CSiOSi_-Si	aug-cc-pVDZ	-979.5287503	-0.7274689		
0	1	cyc4_CSiOSi_-Si	cyc4_CSiOSi_-Si	aug-cc-pVDZ	-979.5020051			
-1	2	cyc4_CSiOSi_-Si	cyc4_CSiOSi_-Si	DFT/VDZ	-981.5321682	-0.8552515		
0	1	cyc4_CSiOSi_-Si	cyc4_CSiOSi_-Si	DFT/VDZ	-981.5007252			
-1	2	cyc4_CSiOSi_-Si	cyc4_CSiOSi_-Si	DFT/cc-pVDZ	-981.6340063	-0.7237068		
0	1	cyc4_CSiOSi_-Si	cyc4_CSiOSi_-Si	DFT/cc-pVDZ	-981.6073994			
-1	2	cyc4_CSiOSi_-Si	cyc4_CSiOSi_-Si	DFT/aug-cc-pVDZ	-981.6629961	-1.0439950	0.00953 6	-1.05819
0	1	cyc4_CSiOSi_-Si	cyc4_CSiOSi_-Si	DFT/aug-cc-pVDZ	-981.6246139		0.01005 8	
0	1	cyc4_CSiOSi_-Si	SP	DFT/aug-cc-pVDZ	-981.6128696	-1.3634417	0.01005 8	-1.37764

C.14. C₃Si₂O

Table 38. Detailed Calculation Data for C₃Si₂O

Q	M	Input Geometry	Output Geometry	Basis Set	Final Energy (hart)	EA (eV)	ZPE (hart)	EA (eV) w/ZPE
-1	2	cyc4_CSiOSi_-C2	cyc4_CSiOSi_-C2	cc-pVDZ	-766.2402089430			
-1	2	cyc5_Si-C-(C)-C-Si-O_	cyc5_Si-C-(C)-C-Si-O_	cc-pVDZ	-766.2330599676			
-1	2	cyc5_CSiOSiC_-C	cyc6_C3SiOSi_*	cc-pVDZ	-766.2314663063			
-1	2	cyc3_C-C_Si_-Si_-CO	cyc3_C-C(Si)-Si_-CO	cc-pVDZ	-766.2181803430			
0	1	cyc3_C-C_Si_-Si_-CO	cyc3_C-C_Si_-Si_-CO	cc-pVDZ	-766.2016281967			
0	1	cyc5_Si-C-(C)-C-Si-O_	cyc5_Si-C-(C)-C-Si-O_	cc-pVDZ	-766.1947137406			
0	3	cyc5_CSiOSiC_-C	cyc6_C3SiOSi_	cc-pVDZ	-766.1817321078			
0	3	cyc4_CSiOSi_-C2	cyc4_CSiOSi_-C2	cc-pVDZ	-766.1701501448			
0	1	cyc4_CSiOSi_-C2	cyc4_CSiOSi_-C2	cc-pVDZ	-766.1644350621			
0	3	cyc5_Si-C-(C)-C-Si-O_	cyc5_Si-C-(C)-C-Si-O_	cc-pVDZ	-766.1522722035			
0	1	cyc5_CSiOSiC_-C	cyc5_CSiOSiC_-C*	cc-pVDZ	-766.1224928064			
0	3	cyc3_C-C_Si_-Si_-CO	cyc3_C-C_Si_-Si_-CO*	cc-pVDZ	-766.1080737179			
-1	2	cyc5_Si-C-(C)-C-Si-O_	cyc5_Si-C-(C)-C-Si-O_	aug-cc-pVDZ	-766.2553573714	-1.21		
-1	2	cyc3_C-C_Si_-Si_-CO	cyc3_C-C_Si_-Si_-CO	aug-cc-pVDZ	-766.2352200354			
0	1	cyc3_C-C_Si_-Si_-CO	cyc3_C-C_Si_-Si_-CO	aug-cc-pVDZ	-766.2118013825			
0	1	cyc5_Si-C-(C)-C-Si-O_	cyc5_Si-C-(C)-C-Si-O_	aug-cc-pVDZ	-766.2108703100			
0	1	cyc4_CSiOSi_-C2	cyc4_CSiOSi_-C2	aug-cc-pVDZ	-766.1837713475			
-1	2	cyc4_CSiOSi_-C2		aug-cc-pVDZ	SCF			
-1	2	cyc3_C-C_Si_-Si_-CO	cyc3_C-C_Si_-Si_-CO	DFT/VDZ	-768.1792071041	-1.387		
-1	2	cyc4_CSiOSi_-C3	cyc4_CSiOSi_-C3	DFT/VDZ	-768.1742903741			
-1	2	cyc5_Si-C-(C)-C-Si-O_	cyc5_Si-C-(C)-C-Si-O_	DFT/VDZ	-768.1676939635			
0	1	cyc3_C-C_Si_-Si_-CO	cyc3_C-C_Si_-Si_-CO	DFT/VDZ	-768.1282138376			
0	1	cyc5_Si-C-(C)-C-Si-O_	cyc5_Si-C-(C)-C-Si-O_	DFT/VDZ	-768.0832866069			
0	1	cyc4_CSiOSi_-C2	cyc4_CSiOSi_-C2	DFT/VDZ	-768.0800613076	0		

Table 38. Detailed Calculation Data for C₃Si₂O (continued)

Q	M	Input Geometry	Output Geometry	Basis Set	Final Energy (hart)	EA (eV)	ZPE (hart)	EA (eV) w/ZPE
-1	2	cyc3_C-C_Si_-Si_-CO	cyc3_C-C_Si_-Si_-CO	DFT/cc-pVDZ	-768.2799760370	-0.9021		
-1	2	cyc4_CSiOSi_-C2	cyc4_CSiOSi_-C2	DFT/cc-pVDZ	-768.2780676269			
-1	2	cyc5_Si-C-(C)-C-Si-O_	cyc5_Si-C-(C)-C-Si-O_	DFT/cc-pVDZ	-768.2768322216			
0	1	cyc3_C-C_Si_-Si_-CO	cyc3_C-C_Si_-Si_-CO	DFT/cc-pVDZ	-768.2468101308			
0	1	cyc5_Si-C-(C)-C-Si-O_	cyc5_Si-C-(C)-C-Si-O_	DFT/cc-pVDZ	-768.2005457777			
0	1	cyc4_CSiOSi_-C2	cyc4_CSiOSi_-C2	DFT/cc-pVDZ	-768.1787150209			
-1	2	cyc4_CSiOSi_-C2	cyc4_CSiOSi_-C2	DFT/aug-cc-pVDZ	-768.3105024769	-2.9488		
-1	2	cyc3_C-C_Si_-Si_-CO	cyc3_C-C_Si_-Si_-CO	DFT/aug-cc-pVDZ	-768.3026184818		-0.21444	
-1	2	cyc5_Si-C-(C)-C-Si-O_	cyc5_Si-C-(C)-C-Si-O_	DFT/aug-cc-pVDZ	-768.3007494270		-0.26528	
0	1	cyc3_C-C_Si_-Si_-CO	cyc3_C-C_Si_-Si_-CO	DFT/aug-cc-pVDZ	-768.2597437463	-1.1662		
0	1	cyc5_Si-C-(C)-C-Si-O_	cyc5_Si-C-(C)-C-Si-O_	DFT/aug-cc-pVDZ	-768.2167181116		-1.1703	
0	1	cyc4_CSiOSi_-C2	cyc4_CSiOSi_-C2	DFT/aug-cc-pVDZ	-768.2020919690		-1.56813	
-1	2	cyc4_CSiOSi_-C2	cyc4_CSiOSi_-C2	DFT/aug-cc-pVDZ	-768.3105024769	-2.9488	0.01644 2	-2.95315
-1	2	cyc3_C-C_Si_-Si_-CO	cyc3_C-C_Si_-Si_-CO	DFT/aug-cc-pVDZ	-768.3026184819	-1.1662	0.01817 7	-1.19005
-1	2	cyc5_Si-C-(C)-C-Si-O_	cyc5_Si-C-(C)-C-Si-O_	DFT/aug-cc-pVDZ	-768.3007494270	-2.2857	0.01658 7	-2.28826
0	1	cyc3_C-C_Si_-Si_-CO	cyc3_C-C_Si_-Si_-CO	DFT/aug-cc-pVDZ	-768.2597437463		0.01905 4	
0	1	cyc5_Si-C-(C)-C-Si-O_	cyc5_Si-C-(C)-C-Si-O_	DFT/aug-cc-pVDZ	-768.2167181116		0.01668 3	
0	1	cyc4_CSiOSi_-C2	cyc4_CSiOSi_-C2	DFT/aug-cc-pVDZ	-768.2020919690		0.01660 3	

C.15. C₂Si₃O

Table 39. Detailed Calculation Data for C₂Si₃O

Q	M	Input Geometry	Output Geometry	Basis Set	Final Energy (hart)	EA (eV)	ZPE (hart)	EA (eV) w/ZPE
-1	2	cyc5_Si-C-(Si)-C-Si-O	cyc5_Si-C-(Si)-C-Si-O	cc-pVDZ	-1017.352561059	-0.63		
-1	2	cyc4_CSiOSi -CSi	cyc4_CSiOSi -CSi	cc-pVDZ	-1017.332433795			
0	1	cyc5_Si-C-(Si)-C-Si-O	cyc5_Si-C-(Si)-C-Si-O	cc-pVDZ	-1017.329398018			
-1	2	cyc6_Si2C2SiO	cyc6_Si2C2SiO	cc-pVDZ	-1017.325276057			
-1	2	bent_SiC2-SiOSi	cyc6_Si2C2SiO	cc-pVDZ	-1017.325275982			
0	3	cyc4_CSiOSi -CSi	cyc4_CSiOSi -CSi	cc-pVDZ	-1017.294892659			
0	3	cyc5_Si-C-(Si)-C-Si-O	cyc5_Si-C-(Si)-C-Si-O	cc-pVDZ	-1017.288587248			
0	3	cyc6_Si2C2SiO	cyc6_Si2C2SiO	cc-pVDZ	-1017.285975530			
0	1	cyc4_CSiOSi -CSi	cyc4_CSiOSi -CSi	cc-pVDZ	-1017.284715853			
0	3	bent_SiC2-SiOSi	bent_SiC2-SiOSi	cc-pVDZ	-1017.276869643			
0	1	cyc6_Si2C2SiO	cyc5_Si-C-C-(Si)-Si-O	cc-pVDZ	-1017.267754584			
0	1	bent_SiC2-SiOSi	cyc5_Si-C-C-(Si)-Si-O	cc-pVDZ	-1017.267754549			
-1	2	cyc5_Si-C-(Si)-C-Si-O	cyc5_Si-C-(Si)-C-Si-O	aug-cc-pVDZ	-1017.373958779	-0.8149		
0	1	cyc5_Si-C-(Si)-C-Si-O	cyc5_Si-C-(Si)-C-Si-O	aug-cc-pVDZ	-1017.344000595			
-1	2	cyc5_Si-C-(Si)-C-Si-O	cyc5_Si-C-(Si)-C-Si-O	DFT/VDZ	-1019.603466838	-1.8024		
0	1	cyc5_Si-C-(Si)-C-Si-O	cyc5_Si-C-(Si)-C-Si-O	DFT/VDZ	-1019.537200793			
-1	2	cyc5_Si-C-(Si)-C-Si-O	cyc5_Si-C-(Si)-C-Si-O	DFT/cc-pVDZ	-1019.718118008	-1.6877		
0	1	cyc5_Si-C-(Si)-C-Si-O	cyc5_Si-C-(Si)-C-Si-O	DFT/cc-pVDZ	-1019.656068851			
-1	2	cyc5_Si-C-(Si)-C-Si-O	cyc5_Si-C-(Si)-C-Si-O	DFT/aug-cc-pVDZ	-1019.740053078	-1.8912	0.01471 4	-1.89581
							0.01488	

C.16. C₃Si₃O

Table 40. Detailed Calculation Data for C₃Si₃O

Q	M	Input Geometry	Output Geometry	Basis Set	Final Energy (hart)	EA (eV)	ZPE (hart)	EA (eV) w/ZPE
-1	2	cyc4_CSiOSi_-CCSi	cyc4_CSiOSi_-CCSi	cc-pVDZ	-1055.202749368	1.009717 7		
-1	2	cyc6_CSiOSiCC_-Si	cyc6_CSiOSiCC_-Si	cc-pVDZ	-1055.180315713	0.801819 2		
0	1	cyc4_CSiOSi_-CCSi	cyc4_CSiOSi_-CCSi	cc-pVDZ	-1055.165627392			
0	1	cyc6_CSiOSiCC_-Si	cyc6_CSiOSiCC_-Si	cc-pVDZ	-1055.150837065			
-1	2	cyc4_CSiOSi_-CCSi		aug-cc-pVDZ	SCF	#VALUE!		
0	1	cyc4_CSiOSi_-CCSi		aug-cc-pVDZ	SCF			
-1	2	cyc4_CSiOSi_-CCSi		DFT/VDZ	SCF	#VALUE!		
0	1	cyc4_CSiOSi_-CCSi	cyc4_CSiOSi_-CCSi	DFT/VDZ	-1057.609190431			
-1	2	cyc4_CSiOSi_-CCSi	cyc4_CSiOSi_-CCSi	DFT/cc-pVDZ	-1057.782504370	1.290224 7		
0	1	cyc4_CSiOSi_-CCSi	cyc4_CSiOSi_-CCSi	DFT/cc-pVDZ	-1057.735069636			
-1	2	cyc4_CSiOSi_-CCSi	cyc4_CSiOSi_-CCSi	DFT/aug-cc-pVDZ	-1057.810959018	1.545696 3	0.01886 4	-1.57766
0	1	cyc4_CSiOSi_-CCSi	cyc4_CSiOSi_-CCSi	DFT/aug-cc-pVDZ	-1057.754131945		0.02003 9	

C.17. C₄O

Table 41. Detailed Calculation Data for C₄O

Q	M	Input Geometry	Output Geometry	Basis Set	Final Energy (hart)	EA (eV)	ZPE (hart)	EA (eV) w/ZPE
-1	2	C4O	C4O	cc-pVDZ	-226.2014801812	-1.8174387		
0	3	C4O	C4O	cc-pVDZ	-226.1346625808			
-1	2	C4O		aug-cc-pVDZ	SCF	#VALUE!		
0	3	C4O		aug-cc-pVDZ	SCF			
-1	2	C4O	C4O	DFT/VDZ	-227.3623072854	-2.8797322		
0	3	C4O	C4O	DFT/VDZ	-227.2564347756			
-1	2	C4O	C4O	DFT/cc-pVDZ	-227.4164335846	-2.4571667		
0	3	C4O	C4O	DFT/cc-pVDZ	-227.3260965730			
-1	2	C4O	C4O	DFT/aug-cc-pVDZ	-227.4429976092	-2.8683524	0.019186	-2.87121
0	3	C4O	C4O	DFT/aug-cc-pVDZ	-227.3375434764		0.019291	
0	3	C4O	SP	DFT/aug-cc-pVDZ	-227.3308137613	-3.0514006	0.019291	-3.05426

C.18. Si₄O

Table 42. Detailed Calculation Data for Si₄O

Q	M	Input Geometry	Output Geometry	Basis Set	Final Energy (hart)	EA (eV)	ZPE (hart)	EA (eV) w/ZPE
-1	2	cyc3 Si3 -OSi	cyc3 Si3 -OSi	cc-pVDZ	-1230.551636241	-1.141		
-1	2	bent Si3OSi	cyc4 Si-Si-(Si)-Si-O	cc-pVDZ	-1230.550178068			
0	1	bent Si3OSi	cyc5 Si4O	cc-pVDZ	-1230.509686342			
0	1	cyc5 Si4O	cyc5 Si4O	cc-pVDZ	-1230.507863039			
0	1	cyc4 SiSiOSi -Si	cyc4 SiSiOSi -Si*	cc-pVDZ	-1230.497529217			
0	3	cyc5 Si4O	cyc5 Si4O	cc-pVDZ	-1230.493085175			
0	1	cyc3 Si3 -OSi	cyc3 Si3 -OSi	cc-pVDZ	-1230.472303917			
0	3	bent Si3OSi	bent Si3OSi	cc-pVDZ	-1230.471588539			
0	3	cyc4 SiSiOSi -Si	cyc4 SiSiOSi -Si	cc-pVDZ	-1230.466258136			
-1	2	cyc4 SiSiOSi -Si		cc-pVDZ	SCF			
-1	2	cyc5 Si4O		cc-pVDZ	SCF			
0	3	cyc3 Si3 -OSi		cc-pVDZ	SCF			
-1	2	cyc5 Si4O	cyc5 Si4O	aug-cc-pVDZ	-1230.572904503	-0.0282		
-1	2	cyc3 Si3 -OSi	cyc3 Si3 -OSi	aug-cc-pVDZ	-1230.572644300			
-1	2	cyc4 SiSiOSi -Si	cyc4 Si-Si-(Si)-Si-O	aug-cc-pVDZ	-1230.571867920			
-1	2	cyc4 Si-Si-(Si)-Si-O	cyc4 Si-Si-(Si)-Si-O	aug-cc-pVDZ	-1230.571867749			
0	1	cyc4 Si-Si-(Si)-Si-O	cyc4 Si-Si-(Si)-Si-O	aug-cc-pVDZ	-1230.525309990			
0	1	cyc5 Si4O	cyc5 Si4O	aug-cc-pVDZ	-1230.522764218			
0	1	cyc4 SiSiOSi -Si	cyc4 SiSiOSi -Si*	aug-cc-pVDZ	-1230.512242280			
0	3	cyc4 Si-Si-(Si)-Si-O	cyc4 Si-Si-(Si)-Si-O	aug-cc-pVDZ	-1230.493993531			
0	1	cyc3 Si3 -OSi	cyc3 Si3 -OSi	aug-cc-pVDZ	-1230.484036479			
0	3	cyc4 SiSiOSi -Si		aug-cc-pVDZ	SCF			
0	3	cyc5 Si4O		aug-cc-pVDZ	SOLVCG			
0	3	cyc3 Si3 -OSi		aug-cc-pVDZ	SOLVCG			

Table 42. Detailed Calculation Data for Si₄O (continued)

Q	M	Input Geometry	Output Geometry	Basis Set	Final Energy (hart)	EA (eV)	ZPE (hart)	EA (eV) w/ZPE
-1	2	cyc4_Si-Si-(Si)-Si-O	cyc5_Si4O	DFT/VDZ	-1232.902573564	-1.9549		
-1	2	cyc5_Si4O	cyc5_Si4O	DFT/VDZ	-1232.902573495			
-1	2	cyc3_Si3_-OSi	cyc3_Si3_-OSi	DFT/VDZ	-1232.883204930			
0	1	cyc5_Si4O	cyc5_Si4O	DFT/VDZ	-1232.830703510			
0	1	cyc4_Si-Si-(Si)-Si-O	cyc5_Si4O	DFT/VDZ	-1232.829923645			
0	3	cyc5_Si4O	cyc3_Si3_-OSi	DFT/VDZ	-1232.811207913			
0	1	cyc3_Si3_-OSi	cyc3_Si3_-OSi	DFT/VDZ	-1232.808207605			
0	3	cyc4_Si-Si-(Si)-Si-O	cyc5_Si4O	DFT/VDZ	-1232.801041979			
0	3	cyc3_Si3_-OSi	cyc5_Si4O	DFT/VDZ	-1232.797300612			
-1	2	cyc5_Si4O	cyc5_Si4O	DFT/cc-pVDZ	-1233.034871105	-1.8883		
0	1	cyc5_Si4O	cyc5_Si4O	DFT/cc-pVDZ	-1232.965447158			
-1	2	cyc5_Si4O	cyc5_Si4O	DFT/aug-cc-pVDZ	-1233.055475883	-1.8884	0.0071	-1.88811
-1	2	cyc5_Si4O_dih	cyc5_Si4O_dih	DFT/aug-cc-pVDZ	-1233.051336881	-1.9919	0.00686 8	-1.99819
0	1	cyc5_Si4O	cyc5_Si4O	DFT/aug-cc-pVDZ	-1232.986051144		0.00709 1	
0	1	cyc5_Si4O_dih	cyc5_Si4O_dih	DFT/aug-cc-pVDZ	-1232.978104959		0.00709 9	
0	1	cyc5_Si4O	SP	DFT/aug-cc-pVDZ	-1232.981828762	-2.0032	0.00709 1	-2.00296
0	1	cyc5_Si4O_dih	SP	DFT/aug-cc-pVDZ	-1232.961716065	-2.4377	0.00709 9	-2.44397

C.19. C₄SiO

Table 43. Detailed Calculation Data for C₄SiO

Q	M	Input Geometry	Output Geometry	Basis Set	Final Energy (hart)	EA (eV)	ZPE (hart)	EA (eV) w/ZPE
-1	2	SiC4O	SiC4O	cc-pVDZ	-515.1669635393	1.0423203	-	
0	1	SiC4O	SiC4O	cc-pVDZ	-515.1286429386			
-1	2	SiC4O	SiC4O	aug-cc-pVDZ	-515.1840078605	1.2658726	-	
0	1	SiC4O	SiC4O	aug-cc-pVDZ	-515.1374684255			
-1	2	SiC4O	SiC4O	DFT/VDZ	-516.8427935304	1.5288184	-	
0	1	SiC4O	SiC4O	DFT/VDZ	-516.7865869690			
-1	2	SiC4O	SiC4O	DFT/cc-pVDZ	-516.9190990263	1.2654844	-	
0	1	SiC4O	SiC4O	DFT/cc-pVDZ	-516.8725738641			
-1	2	SiC4O	SiC4O	DFT/aug-cc-pVDZ	-516.9421080680	1.5773054	0.02182	
0	1	SiC4O	SiC4O	DFT/aug-cc-pVDZ	-516.8841188985		0.02300	-1.60932
0	1	SiC4O	SP	DFT/aug-cc-pVDZ	-516.8797925839	1.6949811	0.02300	
								-1.727
-1	2	SiC4O	SiC4O	cc-pVDZ	-515.1669635393	1.0423203	-	
0	1	SiC4O	SiC4O	cc-pVDZ	-515.1286429386			

C.20. CSi₄O

Table 44. Detailed Calculation Data for CSi₄O

Q	M	Input Geometry	Output Geometry	Basis Set	Final Energy (hart)	EA (eV)	ZPE (hart)	EA (eV) w/ZPE
-1	2	cyc5_CSiSiOSi_-Si	cyc5_CSiSiOSi_-Si	cc-pVDZ	-1268.429544	-1.0949749		
-1	2	cyc3_CSiSi_-dih_SiOSi_	cyc3_CSiSi_-dih_SiOSi_	cc-pVDZ	-1268.413558			
0	1	cyc5_CSiSiOSi_-Si	cyc5_CSiSiOSi_-Si	cc-pVDZ	-1268.389287			
0	3	cyc5_CSiSiOSi_-Si	cyc5_CSiSiOSi_-Si	cc-pVDZ	-1268.376482			
0	3	cyc3_CSiSi_-dih_SiOSi_	cyc3_CSiSi_-dih_SiOSi_	cc-pVDZ	-1268.362225			
0	1	cyc3_CSiSi_-dih_SiOSi_	cyc3_CSiSi_-dih_SiOSi_	cc-pVDZ	-1268.359746			
-1	2	cyc5_CSiSiOSi_-Si	cyc5_CSiSiOSi_-Si	aug-cc-pVDZ	-1268.451064	-1.3091976		
0	1	cyc5_CSiSiOSi_-Si	cyc5_CSiSiOSi_-Si	aug-cc-pVDZ	-1268.402932			
-1	2	cyc5_CSiSiOSi_-Si	cyc5_CSiSiOSi_-Si	DFT/VDZ	-1270.987713	-1.8786073		
0	1	cyc5_CSiSiOSi_-Si	cyc5_CSiSiOSi_-Si	DFT/VDZ	-1270.918647			
-1	2	cyc5_CSiSiOSi_-Si	cyc5_CSiSiOSi_-Si	DFT/cc-pVDZ	-1271.113956	-1.8863808		
0	1	cyc5_CSiSiOSi_-Si	cyc5_CSiSiOSi_-Si	DFT/cc-pVDZ	-1271.044604			
-1	2	cyc5_CSiSiOSi_-Si	cyc5_CSiSiOSi_-Si	DFT/aug-cc-pVDZ	-1271.135341	-2.0895317	0.01152 4	-2.08458
0	1	cyc5_CSiSiOSi_-Si	cyc5_CSiSiOSi_-Si	DFT/aug-cc-pVDZ	-1271.05852		0.01134 2	
0	1	cyc5_CSiSiOSi_-Si	cyc5_CSiSiOSi_-Si	DFT/aug-cc-pVDZ	-1271.053165	-2.2351975	0.01134 2	-2.23025

C.21. C₄Si₂O

Table 45. Detailed Calculation Data for C₄Si₂O

Q	M	Input Geometry	Output Geometry	Basis Set	Final Energy (hart)	EA (eV)	ZPE (hart)	EA (eV) w/ZPE
-1	2	cyc4_CSiOSi_-C3	cyc4_CSiOSi_-C3	cc-pVDZ	-804.0839614149			
-1	2	cyc7_SiOSiC4_	cyc7_SiOSiC4_	cc-pVDZ	-804.0679139722			
0	1	cyc4_C-Si-C(C)-Si_-CO	cyc4_C-Si-C(C)-Si_-CO	cc-pVDZ	-804.0554767374			
0	1	cyc7_SiOSiC4_	cyc7_SiOSiC4_	cc-pVDZ	-804.0453901535	0.05231177 4		
0	1	cyc4_CSiOSi_-C3	cyc4_CSiOSi_-C3	cc-pVDZ	-804.0434669265			
0	1	bent_SiO-Si-C4_	cyc4_CSiOSi_-C3	cc-pVDZ	-804.0434668181			
0	3	cyc4_C-Si-C(C)-Si_-CO	cyc4_C-Si-C(C)-Si_-CO	cc-pVDZ	-804.0081617243			
0	3	cyc7_SiOSiC4_	cyc7_SiOSiC4_	cc-pVDZ	-803.9912664506			
-1	2	cyc4_C-Si-C(C)-Si_-CO		cc-pVDZ	SCF			
0	3	cyc4_CSiOSi_-C3		cc-pVDZ	SCF			
-1	2	bent_SiO-Si-C4_		cc-pVDZ	SOLVCG			
0	3	bent_SiO-Si-C4_		cc-pVDZ	SOLVCG			
0	1	bent_SiO-Si-C4_		aug-cc-pVDZ	Rotation			
0	1	cyc4_C-Si-C(C)-Si_-CO		aug-cc-pVDZ	-804.0680111933			
0	1	cyc4_CSiOSi_-C3		aug-cc-pVDZ	Rotation			
-1	2	bent_SiO-Si-C4_		aug-cc-pVDZ	Died			
-1	2	cyc4_C-Si-C(C)-Si_-CO		aug-cc-pVDZ	SCF			
-1	2	cyc4_CSiOSi_-C3		aug-cc-pVDZ	Rotation			
0	3	bent_SiO-Si-C4_		aug-cc-pVDZ	Died			
0	3	cyc4_C-Si-C(C)-Si_-CO		aug-cc-pVDZ	Died			
0	3	cyc4_CSiOSi_-C3		aug-cc-pVDZ	Died			

Table 45. Detailed Calculation Data for C₄Si₂O (continued)

Q	M	Input Geometry	Output Geometry	Basis Set	Final Energy (hart)	EA (eV)	ZPE (hart)	EA (eV) w/ZPE
-1	2	cyc4_CSiOSi_-C3	cyc4_CSiOSi_-C3	DFT/VDZ	-806.2485623054			
-1	2	bent_SiO-Si-C4	bent_SiO-Si-C4	DFT/VDZ	-806.2478060428			
0	1	cyc4_CSiOSi_-C3	cyc4_CSiOSi_-C3	DFT/VDZ	-806.1768683379			
-1	2	cyc4_C-Si-C(C)-Si_-CO	cyc4_C-Si-C(C)-Si_-CO	DFT/VDZ	-806.1720602029			
0	1	bent_SiO-Si-C4	bent_SiO-Si-C4	DFT/VDZ	-806.1471780185			
0	3	bent_SiO-Si-C4	bent_SiO-Si-C4	DFT/VDZ	-806.1176340294			
0	1	cyc4_C-Si-C(C)-Si_-CO		DFT/VDZ	SCF			
0	3	cyc4_C-Si-C(C)-Si_-CO		DFT/VDZ	SCF			
0	3	cyc4_CSiOSi_-C3		DFT/VDZ	SCF			
-1	2	cyc4_CSiOSi_-C3		DFT/cc-pVDZ	SCF	#VALUE!		
0	1	cyc4_CSiOSi_-C3	cyc4_CSiOSi_-C3	DFT/cc-pVDZ	-806.2944168697			
-1	2	bent_SiO-Si-C4	bent_SiO-Si-C4	DFT/cc-pVDZ	-806.3389632746			
0	1	bent_SiO-Si-C4	bent_SiO-Si-C4	DFT/cc-pVDZ	-806.2458565030			
-1	2	cyc4_CSiOSi_-C3	cyc4_CSiOSi_-C3	DFT/aug-cc-pVDZ	-806.3822254672	1.8541558 4		
-1	2	bent_SiO-Si-C4	bent_SiO-Si-C4	DFT/aug-cc-pVDZ	-806.3632700718			
0	1	bent_SiO-Si-C4	cyc4_CSiOSi_-C3	DFT/aug-cc-pVDZ	-806.3140579731			
0	1	cyc4_CSiOSi_-C3	cyc4_CSiOSi_-C3	DFT/aug-cc-pVDZ	-806.3140579731			
-1	2	cyc4_CSiOSi_-C3	cyc4_CSiOSi_-C3	DFT/aug-cc-pVDZ	-806.3822254672	1.8541558 4	0.02018 4	-1.89403
0	1	cyc4_CSiOSi_-C3	cyc4_CSiOSi_-C3	DFT/aug-cc-pVDZ	-806.3140579731		0.02165	
0	1	cyc4_CSiOSi_-C3	SP	DFT/aug-cc-pVDZ	-806.3005182262	-2.2224369	0.02165	-2.26231

C.22. C₂Si₄O

Table 46. Detailed Calculation Data for C₂Si₄O

Q	M	Input Geometry	Output Geometry	Basis Set	Final Energy (hart)	EA (eV)	ZPE (hart)	EA (eV) w/ZPE
-1	2	cyc4_CSiOSi_-SiCSi	cyc4_CSiOSi_-SiCSi	cc-pVDZ	-1306.248677	-0.7478997		
-1	2	cyc7_SiOSiSiSiCC_	cyc7_SiOSiSiSiCC_*	cc-pVDZ	-1306.247239			
-1	2	cyc5_Si-O-Si-C(Si)-C(Si)_	cyc5_Si-O-Si-C(Si)-C(Si)_	cc-pVDZ	-1306.240316			
-1	2	cyc6_CSiOSiCSi_-Si	cyc6_CSiOSiCSi_-Si	cc-pVDZ	-1306.236134			
-1	2	Si-(CSi)(CSi)(OSi)	Si-(CSi)(CSi)(OSi)**	cc-pVDZ	-1306.226281			
0	1	cyc6_CSiOSiCSi_-Si	cyc6_CSiOSiCSi_-Si	cc-pVDZ	-1306.22118			
0	1	cyc5_Si-O-Si-C(Si)-C(Si)_	cyc5_Si-O-Si-C(Si)-C(Si)_	cc-pVDZ	-1306.220594			
0	1	cyc7_SiOSiSiSiCC_	cyc7_SiOSiSiSiCC_	cc-pVDZ	-1306.210983			
0	1	cyc4_CSiOSi_-SiCSi	cyc4_CSiOSi_-SiCSi	cc-pVDZ	-1306.198365			
0	1	Si-(CSi)(CSi)(OSi)*	Si-(CSi)(CSi)(OSi)	cc-pVDZ	-1306.14348			
-1	2	cyc4_CSiOSi_-SiCSi	cyc4_CSiOSi_-SiCSi	aug-cc-pVDZ	-1306.278717	-1.1454960		
-1	2	cyc5_Si-O-Si-C(Si)-C(Si)_		aug-cc-pVDZ	SOLVCG			
-1	2	cyc6_CSiOSiCSi_-Si	cyc6_CSiOSiCSi_-Si	aug-cc-pVDZ	-1306.258413			
0	1	cyc6_CSiOSiCSi_-Si	cyc5_Si-O-Si-(Si)-C-(Si)-C_	aug-cc-pVDZ	-1306.236603			
0	1	cyc5_Si-O-Si-C(Si)-C(Si)_		aug-cc-pVDZ	Died			
0	1	cyc4_CSiOSi_-SiCSi	cyc4_CSiOSi_-SiCSi	aug-cc-pVDZ	-1306.221502			
-1	2	cyc5_Si-O-Si-C(Si)-C(Si)_	cyc6_CCSiSiOSi_-Si	DFT/VDZ	-1309.012239	-1.2206647		
-1	2	cyc4_CSiOSi_-SiCSi	cyc4_CSiOSi_-SiCSi	DFT/VDZ	-1308.998168			
0	1	cyc5_Si-O-Si-(Si)-C-(Si)-C_	cyc5_Si-O-Si-(Si)-C-(Si)-C_	DFT/VDZ	-1308.967362			
0	1	cyc5_Si-O-Si-C(Si)-C(Si)_	cyc5_Si-O-Si-C(Si)-C(Si)_	DFT/VDZ	-1308.961651			
0	1	cyc4_CSiOSi_-SiCSi	cyc4_CSiOSi_-SiCSi	DFT/VDZ	-1308.92725			
-1	2	cyc5_Si-O-Si-(Si)-C-(Si)-C_		DFT/VDZ	SCF			

Table 46. Detailed Calculation Data for C₂Si₄O (continued)

Q	M	Input Geometry	Output Geometry	Basis Set	Final Energy (hart)	EA (eV)	ZPE (hart)	EA (eV) w/ZPE
-1	2	cyc6_CCSiSiOSi_-Si	cyc6_CCSiSiOSi_-Si*	DFT/cc-pVDZ	-1309.156763	-1.3688935		
-1	2	cyc5_Si-O-Si-(Si)-C-(Si)-C	cyc5_Si-O-Si-(Si)-C-(Si)-C	DFT/cc-pVDZ	-1309.147782			
0	1	cyc6_CCSiSiOSi_-Si	cyc5_Si-O-Si-(Si)-C-(Si)-C	DFT/cc-pVDZ	-1309.106436			
0	1	cyc5_Si-O-Si-(Si)-C-(Si)-C	cyc5_Si-O-Si-(Si)-C-(Si)-C	DFT/cc-pVDZ	-1309.106436			
-1	2	cyc5_Si-O-Si-(Si)-C-(Si)-C	cyc5_Si-O-Si-C-(Si-Si)-C	DFT/aug-cc-pVDZ	-1309.190293	-0.3451841		
-1	2	cyc5_Si-O-Si-C-(Si-Si)-C	cyc5_Si-O-Si-C-(Si-Si)-C	DFT/aug-cc-pVDZ	-1309.190293			
-1	2	cyc6_CCSiSiOSi_-Si	cyc6_CCSiSiOSi_-Si	DFT/aug-cc-pVDZ	-1309.177602		0.34518 4	
0	1	cyc5_Si-O-Si-C-(Si-Si)-C	cyc5_Si-O-Si-C-(Si-Si)-C	DFT/aug-cc-pVDZ	-1309.122993			
0	1	cyc5_Si-O-Si-(Si)-C-(Si)-C	cyc5_Si-O-Si-(Si)-C-(Si)-C	DFT/aug-cc-pVDZ	-1309.120817		0.05920 3	
0	1	cyc6_CCSiSiOSi_-Si	cyc5_O-Si-(Si)-C-C-(Si)-Si	DFT/aug-cc-pVDZ	-1309.10973		0.36075	
-1	2	cyc5_Si-O-Si-C-(Si-Si)-C	cyc5_Si-O-Si-C-(Si-Si)-C	DFT/aug-cc-pVDZ	-1309.190293	-1.8305509	0.01593 7	-1.84834
-1	2	cyc6_CCSiSiOSi_-Si	cyc6_CCSiSiOSi_-Si	DFT/aug-cc-pVDZ	-1309.177602		0.01608 9	
0	1	cyc5_Si-O-Si-C-(Si-Si)-C	cyc5_Si-O-Si-C-(Si-Si)-C	DFT/aug-cc-pVDZ	-1309.122993		0.01659 1	
0	1	cyc5_Si-O-Si-(Si)-C-(Si)-C	cyc5_Si-O-Si-(Si)-C-(Si)-C	DFT/aug-cc-pVDZ	-1309.120817		0.01622 7	
0	1	cyc5_O-Si-(Si)-C-C-(Si)-Si	cyc5_O-Si-(Si)-C-C-(Si)-Si	DFT/aug-cc-pVDZ	-1309.109982		0.01562 5	
0	1	cyc5_Si-O-Si-C-(Si-Si)-C	SP	DFT/aug-cc-pVDZ	-1309.119119	-1.9359367	0.01659 1	-1.95373
0	1	cyc6_CCSiSiOSi_-Si	SP	DFT/aug-cc-pVDZ	-1309.098429	2.1535182 1	0.01614 8	-2.15511

Appendix D. Tools Developed for Data Analysis

Figure 52 shows the batch file used to extract data from output files. This file requires two DOS programs “grep32” and “sed”, equivalent to the UNIX programs of similar names, to be located at “I:\. The batch file should be placed in the directory with the output files and run. Output files should be named as

```
I:\grep32/q/P3.0".....MOLECULAR_ORBITALS"*.out.>.output1.txt
I:\sed "s/.....MOLECULAR_ORBITALS"//g".output1.txt.>.output2.txt
I:\sed "s/.....MOLECULAR_ORBITALS//g".output2.txt.>.output3.txt
I:\sed "s/-----//g".output3.txt.>.output4.txt
I:\sed "s/.....TOTAL ENERGY.....//g".output4.txt.>.output5.txt
I:\sed "s/.singlet./→1→/g".output5.txt.>.output6.txt
I:\sed "s/.doublet./→2→/g".output6.txt.>.output7.txt
I:\sed "s/.triplet./→3→/g".output7.txt.>.output8.txt
I:\sed "s/.out/→/g".output8.txt.>.output.txt
del .output1.txt
del .output2.txt
del .output3.txt
del .output4.txt
del .output5.txt
del .output6.txt
del .output7.txt
del .output8.txt
```

Figure 52. Batch file for extracting data from output files. (“.” represent spaces. “→” represent tabs)

“isomer.multiplicity.basis.out”. It returns a file “output.txt” with the isomer name, multiplicity, and basis on one line separated by tabs. On the next line is the optimized energy. If the energy is zero, the calculation reached the maximum number of steps before it found a minimum. If the calculation failed for some other reason, the molecule will not appear in “output.txt”.

Appendix E. Calculation Troubleshooting Guide

While calculations performed using the input template of Chapter 3 are usually successful, some calculations fail to complete correctly. The purpose of this appendix is to list several methods that can be applied to get troublesome calculations to complete. It should be pointed out that this list is not exhaustive and there are some calculations that will not converge regardless of what is done.

1. **SOGTOL:** Add `EXTRAP=.F. DAMP=.T. SOGTOL=0.00001` to the `$SCF` group. This changes the parameters for the SCF routine, making it more stable. The `SOGTOL` keyword applies only to HF and may be left out for DFT calculations. If the calculation still does not converge, the `SOGTOL` value may be lowered.
2. **MOREAD:** If a calculation on a similar molecule with the same atoms and basis set works, the vectors from the `.dat` file of the working calculation can be used as the starting vectors for the unconvergent calculation. This is described at the end of Section 3.2. If possible, vectors can be taken from a working calculation of a different multiplicity, an anion or cation of the same molecule, or for a DFT/B3LYP calculation, from a HF or BLYP calculation.
3. **RSTRCT:** Another change that can be made to the SCF routine parameters is to add `RSTRCT=.T.` to the `$SCF` group. This is especially useful for

convergence problems where the energy is fluctuating up and down by very small amounts.

4. `KDIAG`: If other methods do not work `KDIAG=3` can be added to the `$SYSTEM` group. This changes the diagonalization method to a Jacobian method. This is more accurate, but can take significantly longer computation times.

5. `QMTTOL`: For large molecules and large basis sets, the wavevectors can become linearly dependent. In these cases `QMTTOL=1.0E-5` can be added to the `$CNTRL` group. This sets the tolerance below which linearly dependent wavevectors are removed. The default is `1.0E-6`. It should be noted that removing vectors increases the energy by tens of microhartrees.

6. `DIRSCF`: For very large molecules and very large basis sets, disk space can become a problem. In these cases, `DIRSCF=.T.` can be added to the `$SCF` group. This stores integrals in memory and recalculates them when necessary rather than storing them on disk. For large molecules this can improve calculation times by requiring less frequent disk access.

Appendix F. Detailed Thermodynamics Data

Table 47. Detailed Thermodynamics Data for C_nSi_m

Molecule	E (kJ/mol)	ZPE (kJ/mol)	E (kJ/mol)	H (kJ/mol)	G (kJ/mol)	C _v (J/mol-K)	C _p (J/mol-K)	S (J/mol-K)
Si	-759655.219161	0.000000	3.718	6.197	-41.336	12.472	20.786	159.427
Si ₂	-1519614.918109	2.923346	9.731	12.210	-56.381	26.121	34.435	230.057
Si ₃	-2279621.598266	6.634518	16.812	19.291	-67.947	44.130	52.445	292.597
Si ₄	-3039679.798157	11.957245	25.832	28.311	-67.009	64.458	72.773	319.705
C	-99328.879599	0.000000	3.718	6.197	-38.188	12.472	20.786	148.870
CSi	-859380.895931	5.796564	12.103	14.582	-51.109	22.511	30.825	220.330
CSi ₂	-1619646.883578	12.443325	22.301	24.780	-57.669	37.095	45.409	276.534
CSi ₃	-2379648.102064	18.006208	30.182	32.661	-57.202	57.157	65.472	301.402
CSi ₄	-3139583.424833	22.653929	37.904	40.383	-56.809	78.157	86.471	325.986
C ₂	-199109.255492	13.222032	19.42	21.899	-37.419	20.808	29.122	198.953
C ₂ Si	-959506.747912	16.494833	27.512	29.991	-51.437	40.297	48.611	273.112
C ₂ Si ₂	-1719516.819324	24.055162	34.876	37.355	-47.142	49.518	57.833	283.405
C ₂ Si ₃	-2479540.697746	29.981325	44.841	47.320	-49.512	70.860	79.174	324.776
C ₂ Si ₄	-3239552.638776	34.796801	52.766	55.245	-47.934	93.850	102.165	346.063
C ₃	Unconverged							
C ₃ Si	-1059339.157257	29.300273	41.278	43.757	-38.913	54.826	63.140	277.277
C ₃ Si ₂	-1819519.950534	39.113965	52.104	54.583	-29.846	62.066	70.380	283.177
C ₃ Si ₃	-2579435.818809	41.789050	60.328	62.807	-46.278	87.989	96.303	365.871
C ₃ Si ₄	-3339331.694083	46.772675	67.133	69.612	-41.821	104.134	112.448	373.748
C ₄	-399136.164532	32.841562	44.938	47.416	-31.296	53.323	61.637	264.001
C ₄ Si	-1159359.217581	43.048381	56.138	58.617	-25.825	61.312	69.627	283.220
C ₄ Si ₂	-1919389.816652	48.228523	64.628	67.107	-27.900	81.295	89.609	318.656
C ₄ Si ₃	-2679307.181454	50.309233	70.893	73.372	-34.972	108.251	116.565	363.384
C ₄ Si ₄	-3439262.850558	56.576155	79.320	81.799	-34.848	118.837	127.151	391.239

Table 48. Detailed Thermodynamics Data for C_nSi_mO

Molecule	E (kJ/mol)	ZPE (kJ/mol)	E (kJ/mol)	H (kJ/mol)	G (kJ/mol)	C _v (J/mol-K)	C _p (J/mol-K)	S (J/mol-K)
O	-197035.865200	0.000000	3.718	6.197	-39.257	12.472	20.786	152.454
SiO	-957432.055169	7.110410	13.354	15.833	-47.318	21.674	29.989	211.808
Si ₂ O	-1717239.062251	10.268349	20.005	22.484	-55.685	44.004	52.319	262.183
Si ₃ O	-2477225.635551	15.281247	27.840	30.319	-62.821	60.184	68.499	312.395
Si ₄ O	-3237204.413754	18.616792	36.220	38.699	-65.876	82.676	90.991	350.744
CO	-297418.999845	13.062475	19.261	21.739	-37.167	20.810	29.125	197.573
CSiO	-1057222.489657	18.807809	27.572	30.051	-44.027	39.262	47.577	248.459
CSi ₂ O	-1817176.969130	23.970197	35.576	38.055	-49.776	54.053	62.367	294.587
CSi ₃ O	-2577255.054844	26.408180	41.726	44.205	-54.777	73.208	81.523	331.985
CSi ₄ O	-3337163.666673	29.777221	49.667	52.146	-60.448	95.424	103.739	377.644
C ₂ O	-397002.483515	23.297356	31.255	33.734	-35.822	34.578	42.893	233.293
C ₂ SiO	-1157248.467248	35.156303	46.108	48.587	-30.314	49.423	57.738	264.632
C ₂ Si ₂ O	-1917167.288417	38.616687	52.603	55.082	-40.687	65.921	74.235	321.212
C ₂ Si ₃ O	-2677144.580742	39.080766	56.040	58.519	-43.659	85.928	94.243	342.707
C ₂ Si ₄ O	-3437101.926253	43.559972	64.007	66.486	-44.996	105.863	114.177	373.913
C ₃ O	-497079.808818	40.141792	50.819	53.298	-22.484	47.467	55.781	254.173
C ₃ SiO	-1257058.306336	45.610303	59.412	61.891	-26.872	67.353	75.668	297.715
C ₃ Si ₂ O	-2017065.668388	50.025019	66.454	68.933	-31.733	81.424	89.738	337.633
C ₃ Si ₃ O	-2777133.075773	52.611621	73.052	75.531	-37.698	101.542	109.857	379.771
C ₃ Si ₄ O	0.000000							
C ₄ O	-596874.634933	50.649176	63.734	66.213	-18.627	63.952	72.266	284.555
C ₄ SiO	-1357079.059852	60.388477	77.053	79.532	-15.471	80.341	88.656	318.642
C ₄ Si ₂ O	-2116977.256085	56.842552	77.119	79.598	-30.715	100.727	109.042	369.990
C ₄ Si ₃ O	0.000000							
C ₄ Si ₄ O	0.000000							
O ₂	-394581.728322	9.832338	16.037	18.516	-42.595	20.974	29.288	204.968
CO ₂	-495000.328074	30.287118	37.181	39.660	-25.794	28.846	37.160	219.535
SiO ₂	-1154854.826919	17.3344	25.931	28.409	-42.481	37.252	45.566	237.769

Bibliography

Basis sets were obtained from the Extensible Computational Chemistry Environment Basis Set Database, Version 6/11/02, as developed and distributed by the Molecular Science Computing Facility, Environmental and Molecular Sciences Laboratory which is part of the Pacific Northwest Laboratory, P.O. Box 999, Richland, Washington 99352, USA, and funded by the U.S. Department of Energy. The Pacific Northwest Laboratory is a multi-program laboratory operated by Battelle Memorial Institute for the U.S. Department of Energy under contract DE-AC06-76RLO 1830. Contact David Feller or Karen Schuchardt for further information. Database accessed via the internet at <http://www.emsl.pnl.gov:2080/forms/basisform.html>.

Bauschlicher, Charles W. Jr. "The construction of modified virtual orbitals (MVO's) which are suited for configuration interaction calculations," *Journal of Chemical Physics*. 72: 880-885 (15 January 1980).

Becke, Axel D. "Density-functional thermochemistry. III. The role of exact exchange," *Journal of Chemical Physics*. 98: 5648-5652 (1 April 1993).

Bergeron, D. E. and A. W. Castleman, Jr. "Insights into the stability of silicon cluster ions: Reactive etching with O₂," *Journal of Chemical Physics*. 117: 3219-3223 (15 August 2002).

Bernath, Peter F. *Spectra of Atoms and Molecules*. New York: Oxford University Press, 1995.

Bode, Brett M. and Mark S. Gordon. "Fast Computation of analytical second derivatives with effective core potentials: Application to Si₈C₁₂, Ge₈C₁₂, and Sn₈C₁₂," *Journal of Chemical Physics*. 111: 8778-8784 (15 November 1999).

Brown, Theodore L., H. Eugene LeMay, Jr., and Bruce E. Bursten. *Chemistry: The Central Science, 5th Edition*. Englewood Cliffs NJ: Prentice Hall, 1991.

Burggraf, Larry W., David E. Weeks, and Xiaofeng F. Duan. "Theoretical Studies on Oxidation of Si_mC_n Molecular Clusters and Oxidation-Induced Defects near SiC Surfaces," Research Proposal. October 2002.

Chakravarthi, Srinivasan and Scott T. Dunham. "Modeling of vacancy cluster formation in ion implanted silicon," *Journal of Chemical Physics*. 89: 4758-4765 (1 May 2001).

- Davico, Gustavo E., Rebecca L. Schwarz, and W. Carl Lineberger. "Photoelectron spectroscopy of C_3Si and C_4Si_2 anions," *Journal of Chemical Physics*, 115: 1789-1794 (22 July 2001).
- Duan, Xiaofeng, Larry W. Burggraf, David E. Weeks, Gustavo E. Davico, Rebecca L. Schwarz, and W. Carl Lineberger. "Photoelectron spectroscopy of $Si_2C_3^-$ and quantum chemistry of the linear Si_2C_3 cluster and its isomers," *Journal of Chemical Physics*. 116: 3601-3611 (1 March 2002).
- Dunning, T. H. Jr. and P. J. Hay, Chapter 1 in *Methods of Electronic Structure Theory*, H. F. Shaefer III, Ed. Plenum Press, N.Y. 1977, pp 1-27.
- Dunning, Thom H. Jr. "Gaussian basis sets for use in correlated molecular calculations. I. The atoms boron through neon and hydrogen," *Journal of Chemical Physics*. 90: 1007-1023 (15 January 1989).
- Dunning, Thom. H., Jr., "Gaussian Basis Functions for Use in Molecular Calculations. III. Contraction of (10s6p) Atomic Basis Sets for the First-Row Atoms," *Journal of Chemical Physics*. 55: 716-723 (15 July 1971).
- Dupuis, Michel, and John B. Nicholas. "On the electronic structure of Si_3O_2 and its anion," *Molecular Physics*. 96: 549-553 (1999).
- Dykstra, Clifford E. *Quantum Chemistry & Molecular Spectroscopy*. Englewood Cliffs NJ: Prentice Hall, 1992.
- Eisberg, Robert, and Robert Resnick. *Quantum Physics of Atoms, Molecules, Solids, Nuclei, and Particles*. New York: John Wiley & Sons, 1985.
- Ellis, D. E., Editor. *Density Functional Theory of Molecules, Clusters, and Solids*. Dordrecht Netherlands: Kluwer Academic Publishers, 1995.
- Fournier, René, Susan B. Sinnott, and Andrew E. DePristo. "Density functional study of the bonding in small silicon clusters," *Journal of Chemical Physics*. 97: 4149-4161 (15 September 1992).
- Fox, Robert B. and Warren H. Powell. *Nomenclature of Organic Compounds* (2nd Edition). New York: Oxford University Press, 2001.
- Fuke, Kiyokazu, Keizo Tsukamoto, Fuminori Misaizu, and Masaomi Sanekata. "Near threshold photoionization of silicon clusters in the 248-146 nm region: Ionization potentials for Si_n ," *Journal of Chemical Physics*. 99:7807-7812 (15 November 1993).

- Furukawa, Kazuaki, Masaie Fujino, and Nobuo Matsumoto. "Cubic silicon cluster," *Applied Physics Letters*. 60: 2744-2745 (1 June 1992).
- Gasiorowicz, Stephen. *Quantum Physics* (2nd Edition). New York: John Wiley & Sons, 1996.
- Gaussian 98, Revision A.11.4, M. J. Frisch, G. W. Trucks, H. B. Schlegel, G. E. Scuseria, M. A. Robb, J. R. Cheeseman, V. G. Zakrzewski, J. A. Montgomery, Jr., R. E. Stratmann, J. C. Burant, S. Dapprich, J. M. Millam, A. D. Daniels, K. N. Kudin, M. C. Strain, O. Farkas, J. Tomasi, V. Barone, M. Cossi, R. Cammi, B. Mennucci, C. Pomelli, C. Adamo, S. Clifford, J. Ochterski, G. A. Petersson, P. Y. Ayala, Q. Cui, K. Morokuma, N. Rega, P. Salvador, J. J. Dannenberg, D. K. Malick, A. D. Rabuck, K. Raghavachari, J. B. Foresman, J. Cioslowski, J. V. Ortiz, A. G. Baboul, B. B. Stefanov, G. Liu, A. Liashenko, P. Piskorz, I. Komaromi, R. Gomperts, R. L. Martin, D. J. Fox, T. Keith, M. A. Al-Laham, C. Y. Peng, A. Nanayakkara, M. Challacombe, P. M. W. Gill, B. Johnson, W. Chen, M. W. Wong, J. L. Andres, C. Gonzalez, M. Head-Gordon, E. S. Replogle, and J. A. Pople, Gaussian, Inc., Pittsburgh PA, 7 May 2002.
- Glaesemann, Kurt R. and Mark S. Gordon. "Auxiliary basis sets for grid-free density functional theory," *Journal of Chemical Physics*. 112: 10738-10745 (22 June 2000).
- Glaesemann, Kurt R. and Mark S. Gordon. "Evaluation of gradient corrections in grid-free density functional theory," *Journal of Chemical Physics*. 110: 6580-6582 (1 April 1999).
- Glaesemann, Kurt R. and Mark S. Gordon. "Investigation of a grid-free density functional theory (DFT) approach," *Journal of Chemical Physics*. 108: 9959-9969 (22 June 1998).
- Gordon, Mark S., James R. Shoemaker, and Larry W. Burggraf. "Response to 'Comment on 'An *ab initio* cluster study of the structure of the Si(001) surface'" [J. Chem. Phys. 113, 9353 (2000)]," *Journal of Chemical Physics*. 113: 9355-9356 (22 November 2000).
- Granovsky, Alex A. "The PC GAMESS Homepage," <http://classic.chem.msu.su/gran/games/index.html>. (7 November 2002).
- Gross, Eberhard K. U. and Reiner M. Dreizler, Editors. *Density Functional Theory*. New York: Plenum Press, 1995.

- Hagelberg, F., S. Neeser, N. Sahoo, T. P. Das, and K. G. Weil. "Geometry and bonding in alkali-metal-atom—antimony ($A_n\text{Sb}_4$) clusters," *Physical Review A*. 50: 557-566 (July 1994).
- Hamilton, Tracy P. and Henry F. Schaefer III. "Silaketene: A product of the reaction between silylene and carbon monoxide?," *Journal of Chemical Physics*. 90: 1031-1035 (15 January 1989).
- Henry, Jean W. *Use of Quantum Mechanical Calculations to Investigate Small Silicon Carbide Clusters*. MS thesis, AFIT/GAP/ENP/01M-04. Graduate School of Engineering and Management, Air Force Institute of Technology (AU), Wright-Patterson AFB OH, March 2001 (AD-A392522).
- Hertwig, Roland H. and Wolfram Koch, "On the parameterization of the local correlation functional. What is Becke-3-LYP?," *Chemical Physics Letters*. 268: 345-351 (18 April 1997).
- Hohenberg, P. and W. Kohn. "Inhomogeneous Electron Gas," *Physical Review*. 136B: B864-B871 (9 November 1964).
- Hotop, H. and W. C. Lineberger. "Binding energies in atomic negative ions. II," *Journal of Physical Chemistry Reference Data*. 14: 731 (1985).
- Huber, K.P. and G. Herzberg. "Molecular Spectra and Molecular Structure. IV. Constants of Diatomic Molecules," *Van Nostrand Reinhold Co.* (1979).
- Ignatyev, Igor S. and Henry F. Schaeffer III. "The search for the low-lying states of the silicon carbide cluster cation Si_2C_2^+ ," *Journal of Chemical Physics*. 103: 7025-7029 (22 October 1995).
- Iwata, Yasushi, Masaaki Kishida, Makiko Muto, Shengwen Yu, Tsuguo Sawada, Akira Fukuda, Toshio Takiya, Akio Komura, and Koichiro Nakajima. "Narrow size-distributed silicon cluster beam generated using a spatiotemporal confined cluster source," *Chemical Physics Letters*. 358: 36-42 (24 May 2002).
- Jacox, M.E., D. E. Milligan, N. G. Moll, and W. E. Thompson. *Journal of Chemical Physics*. 43: 3734 (1965).
- Jones, R. O. "Energy surfaces of low-lying states of C_3 ," *Journal of Chemical Physics*. 82: 5078-5083 (1 June 1985).
- Kanemitsu, Yoshihiko, Katsunori Suzuki, Hiroshi Uto, Yasuaki masumoto, Koichi Higuchi, Soichiro Kyushin, and Hieyuki Matsumoto. "Optical Properties of Porous Silicon and Small Silicon Clusters: Search for the Origin of Visible

- Photoluminescence of Porous Silicon," *Japanese Journal of Applied Physics*. 32: 408-410 (January 1993).
- Kanemitsu, Yoshihiko, Katsunori Suzuki, Michio Kondo, and Hideyuki Matsumoto. "Luminescence from a Cubic Silicon Cluster," *Solid State Communications*. 89: 619-621 (1994).
- Kanemitsu, Yoshihiko, Katsunori Suzuki, Michio Kondo, Soichiro Kyushin, and Hideyuki Matsumoto. "Luminescence properties of a cubic silicon cluster octasilacubane," *Physical Review B*. 51: 10666-10670 (15 April 1995).
- Kéghélian, P., P. Mélinon, A. Perez, J. Lermé, C. Ray, M. Pellarin, M. Broyer, J. L. Rousset, and F. J. Cadete Santos Aires. "Properties of silicon-carbon-cluster-assembled films," *The European Physical Journal D*. 9: 639-642 (1999).
- Kendall, Rick A., Thom H. Dunning, Jr., and Robert J. Harrison. "Electron affinities of the first-row atoms revisited. Systematic basis sets and wave functions," *Journal of Chemical Physics*. 96: 6796-6806 (1 May 1992).
- Kishi, Reiko, Atsushi Nakajima, Suehiro Iwata, and Koji Kaya. "Theoretical study of silicon-sodium binary clusters. Geometrical and electronic structures of Si_nNa ($n=1-7$)," *Chemical Physics Letters*. 224: 200-206 (8 July 1994).
- Koch, Wolfram and Max C. Holthausen. *A Chemist's Guide to Density Functional Theory* (2nd Edition). Weinheim Germany: Wiley-VCH, 2001.
- Kohn, W., and L. J. Sham. "Self-Consistent Equations Including Exchange and Correlation Effects," *Physical Review*. 140A: A1133-A1138 (15 November 1965).
- Lavendy, H, JM Robbe, JP Flament, and G Pascoli. "Density functional study of silicon carbide cluster cations C_4^+ , C_3Si^+ , C_2Si_2^+ , CSi_3^+ , and Si_4^+ ," *Journal de Chimie Physique et de Physico-Chimie Biologique*. 94: 1779-1793 (1997).
- Lembke R. R., R. F. Ferrante, and W. Weltner "Carbonylsilene, diazasilene, and dicarbonylsilene molecules: electron spin resonance and optical spectra at 4 K," *Journal of the American Chemical Society*. 99: 416-423 (1977).
- Li, Guangming, Larry W. Burggraf, James R. Shoemaker, DeLyle Eastwood, and Albert E. Stiegman. "High-temperature photoluminescence in sol-gel silica containing SiC/C nanostructures," *Applied Physics Letters*. 76: 3373-3375 (5 June 2000).

- Lineberger, W. Carl. "PES Instrument," n. pag.
http://stripe.colorado.edu/~lineberg/experiments/peslab/pes_mach.htm. (7 November 2002).
- Makhtari, A., V. Raineri, L. Calcagno, F. La Via, F. Frisina, and G. Foti. "Enhanced oxidation of ion-damaged 6H-SiC," *Philosophical Magazine B*. 80: 661-667 (2000).
- McLean, A.D. and G. S. Chandler. "Contracted Gaussian basis sets for molecular calculations. I. Second row atoms, Z=11-18," *Journal of Chemical Physics*. 72: 5639-5648 (15 May 1980).
- Nakajima, Atsushi, Tetsuya Taguwa, Kojiro Nakao, Motoki Gomei, Reiko Kishi, Suehiro Iwata, and Koji Kaya. "Photoelectron spectroscopy of silicon-carbon cluster anions (Si_nC_m^-)," *Journal of Chemical Physics*. 103: 2050-2057 (8 August 1995).
- Oakes, J. M. and G. B. Ellison. "Photoelectron spectroscopy of radical anions," *Tetrahedron*, 42: 6263 (1986).
- Ohashi, N., R. Kiryu, S. Okino, and M. J. Fujitake. *Journal of Molecular Spectroscopy*, 157: 50 (1993).
- Olander, J. and K. Larsson, "Ab Initio Calculation of Adsorption to β -SiC Clusters," *Journal of Physical Chemistry B*. 103: 9604-9609 (1999).
- Orlando, R, P Azavant, M D Towler, R Doves, and C Roetti. "Cluster and supercell calculations for carbon-doped silicon," *Journal of Physics: Condensed Matter*. 8: 1123-1133 (1996).
- Oshiro, T., C. K. Lutrus, D. E. Hagen, and S. H. Suck Salk. "A Cluster Model Treatment of Oxygen Adsorption on Simulated Silicon Surfaces by Using Large Silicon Clusters," *Solid State Communications*. 100: 439-444 (1996).
- Ovcharenko, I. V., W. A. Lester, Jr, C. Xiao, and F. Hagelberg. "Quantum Monte Carlo characterization of small Cu-doped silicon clusters: CuSi_4 and CuSi_6 ," *Journal of Chemical Physics*. 114: 9028-9032 (22 May 2001).
- Pak, Michael V. and Mark S. Gordon. "Full configuration interaction and multiconfigurational spin density in boron and carbon atoms," *Journal of Chemical Physics*. 113: 4238-4241 (8 September 2000).

- Pereira, J. C. G., C. R. A. Catlow, and G. D. Price. "Ab initio Studies of Silica-Based Clusters. Part I. Energies and Conformations of Simple Clusters," *Journal of Physical Chemistry A*. 103: 3252-3267 (1999).
- Pereira, J. C. G., C. R. A. Catlow, and G. D. Price. "Ab initio Studies of Silica-Based Clusters. Part II. Structures and Energies of Complex Clusters," *Journal of Physical Chemistry A*. 103, 3268-3284 (1999).
- Petraco, Nicholas D. K., Shawn T. Brown, Yukio Yamaguchi, and Henry F. Schaefer III. "The 2-silaketenyliene (CSiO) Radical: Electronic Structure of the X $^3\Sigma^-$ and A $^3\Pi$ States," *Journal of Physical Chemistry*, 104: 10165-10172 (2000).
- Petraco, Nicholas D. K., Shawn T. Brown, Yukio Yamaguchi, and Henry F. Schaefer III. "The silaketenyliene (SiCO) molecule: Characterization of the X $^3\Sigma^-$ and A $^3\Pi$ states," *Journal of Chemical Physics*, 112: 3201-3207 (15 February 2000).
- Phillips, J. C. "Electron-correlation energies and the structure of Si₁₃," *Physical Review B*. 47: 14132-14135 (1 June 1993).
- Pitts, W.M., V. M. Donnelly, A. P. Baronavski, and J. R. McDonald. *Chemical Physics*. 61: 451 (1981).
- Pople, John A. and David L. Beveridge. *Approximate Molecular Orbital Theory*. New York: McGraw-Hill, 1970
- Raghavachari, Krishnan. "Theoretical study of small silicon clusters: Equilibrium geometries and electronic structures of Si_n (n=2-7, 10)," *Journal of Chemical Physics*. 84: 5672-5686 (15 May 1986).
- Ramond, Tanya M., Gustavo E. Davico, Rebecca L. Schwartz, and W. Carl Lineberger. "Vibronic structure of alkoxy radicals via photoelectron spectroscopy," *Journal of Chemical Physics*. 112: 1158-1169 (15 January 2000).
- Ratner, Mark A. and George C. Schatz. *Introduction to Quantum Mechanics in Chemistry*. Upper Saddle River NJ: Prentice Hall, 2001.
- Refaey, K.M.A. and J. L. Franklin. "Endoergic ion-molecule-collision processes of negative ions. III. Collisions of I⁻ on O₂, CO and CO₂," *International Journal of Mass Spectrometry and Ion Physics*. 20: 19 (1976).

- Rintelman, Jamie M. and Mark S. Gordon. "Structure and energetics of the silicon carbide clusters SiC_3 and Si_2C_2 ," *Journal of Chemical Physics*. 115: 1795-1803 (22 July 2001).
- Rittby, C. M. L. "An *ab initio* study of the structure and infrared spectrum of Si_3C ," *Journal of Chemical Physics*. 96: 6768-6772 (1 May 1992).
- Röthlisberger, Ursula, Wanda Andreoni, and Michele Parrinello. "Structure of Nanoscale Silicon Clusters," *Physical Review Letters*. 72: 665-670 (31 January 1994).
- Röthlisberger, Ursula, Wanda Andreoni, and Paolo Giannozzi. "Thirteen-atom clusters: Equilibrium geometries, structural transformations, and trends in Na, Mg, Al, and Si," *Journal of Chemical Physics*. 96: 1248-1255 (15 January 1992).
- Sari, Levant, Jason M. Gonzales, Yukio Yamaguchi, and Henry F. Schaefer III. "The $X^2\Pi$ and $A^2\Sigma^+$ electronic states of the HCSi radical: Characterization of the Renner—Teller effect in the ground state," *Journal of Chemical Physics*, 114: 4472-4478 (8 March 2001).
- Sattelmeyer, Kurt W., Henry F. Schaefer III, and John F. Stanton. "The global minimum structure of SiC_3 : The controversy continues," *Journal of Chemical Physics*. 116: 9151-9153 (1 June 2002).
- Schaftenaar G. and J. H. Noordik. "Molden: a pre- and post-processing program for molecular and electronic structures," *Journal of Computer-Aided Molecular Design*. 14: 123-134 (2000).
- Schmidt Michael W., Kim K. Baldridge, Jerry. A. Boatz, Steven T. Elbert, Mark S. Gordon, Jan H. Jensen, Shiro Koseki, Nikita Matsunaga, Kiet A. Nguyen, Shujun Su, Theresa L. Windus, Michel Dupuis, and John A. Montgomery, Jr.. "General Atomic and Molecular Electronic Structure System," *Journal of Computational Chemistry*. 14: 1347-1363 (1993).
- Shoemaker, James R., Larry W. Burggraf, and Mark S. Gordon. "SIMOMM: An Integrated Molecular Orbital/Molecular Mechanics Optimization Scheme for Surfaces," *Journal of Physical Chemistry A*. 103: 3245-3251 (1999).
- Shoemaker, James, Larry W. Burggraf, and Mark S. Gordon. "An *ab initio* cluster study of the structure of the $\text{Si}(001)$ surface," *Journal of Chemical Physics*. 112: 2994-3005 (8 February 2000).

- Stephens, P. J., F. J. Devlin, C. F. Chablowski, and M. J. Frisch. "Ab Initio Calculation of Vibrational Absorption and Circular Dichroism Spectra Using Density Functional Force Fields," *Journal of Physical Chemistry*. 98: 11623-11627 (10 November 1994).
- Szabo, Attila and Neil S. Ostlund. *Modern Quantum Chemistry: Introduction to Advanced Structure Theory*. Mineola NY: 1996.
- Van Zee, R. J., R. F. Ferrante, and W. Weltner, Jr. "ESR of the C₂¹⁷O, SiC¹⁷O, and ²⁹Si₂O molecules," *Chemical Physics Letters*. 139: 426-430 (4 Sept. 1987).
- Weeks, David. Class Handouts, CHEM 662, Quantum Chemistry. Graduate School of Engineering and Management, Air Force Institute of Technology, Wright-Patterson AFB OH, Summer Quarter 2002.
- Woon, David E. and Thom. H. Dunning, Jr. "Gaussian basis sets for use in correlated molecular calculations. III. The atoms aluminum through argon," *Journal of Chemical Physics*. 98: 1358-1371 (15 January 1993).
- Yamaguchi, Yukio, Nicholas D. K. Petraco, Shawn T. Brown, and Henry F. Schaefer III. "The 1-silaketeny radical (HSiCO): Ground and first excited electronic states," *Journal of Chemical Physics*, 112: 2168-2175 (1 February 2000).
- Yeates, Alan. Class Handouts, CHEM 662, Quantum Chemistry. Graduate School of Engineering and Management, Air Force Institute of Technology, Wright-Patterson AFB OH, Summer Quarter 2002.
- Zengin, V., B. J. Persson, K. M. Strong, and R. E. Continetti. "Study of the Low-lying Electronic States of CCO by Photoelectron Spectroscopy of CCO- and ab initio calculations," *Journal of Chemical Physics*, 105: 9740 (1996).
- Poincaré, Henri. ??????

Vita

First Lieutenant John W. Roberts Jr grew up on Roberts Green Hill Farm in rural Pennsylvania. He graduated from Central Columbia High School in Bloomsburg, Pennsylvania in 1994. He received a Bachelor of Science degree from Penn State University, in University Park, Pennsylvania in May 1999 where he majored in Physics and minored in History and Military Studies. In August 1999, he was commissioned through the Detachment 720 AFROTC at Penn State University.

His first assignment was to the F-15 System Program Office in the Aeronautical System Center at Wright-Patterson AFB, Ohio where he was the program manager for F-15 air data systems. In July 2000, he was selected to be Executive Officer to the F-15 Development System Manager. In August 2001, he entered the Graduate School of Engineering and Management, Air Force Institute of Technology. Upon graduation, he will be assigned to the Air Force Technical Application Center at Patrick AFB, Florida.

REPORT DOCUMENTATION PAGE			Form Approved OMB No. 074-0188		
<p>The public reporting burden for this collection of information is estimated to average 1 hour per response, including the time for reviewing instructions, searching existing data sources, gathering and maintaining the data needed, and completing and reviewing the collection of information. Send comments regarding this burden estimate or any other aspect of the collection of information, including suggestions for reducing this burden to Department of Defense, Washington Headquarters Services, Directorate for Information Operations and Reports (0704-0188), 1215 Jefferson Davis Highway, Suite 1204, Arlington, VA 22202-4302. Respondents should be aware that notwithstanding any other provision of law, no person shall be subject to a penalty for failing to comply with a collection of information if it does not display a currently valid OMB control number.</p> <p>PLEASE DO NOT RETURN YOUR FORM TO THE ABOVE ADDRESS.</p>					
1. REPORT DATE (DD-MM-YYYY) 25-03-2003		2. REPORT TYPE Master's Thesis		3. DATES COVERED (From - To) Jun 2002 - Mar 2003	
4. TITLE AND SUBTITLE QUANTUM MECHANICAL CALCULATIONS OF MONOXIDES OF SILICON CARBIDE MOLECULES			5a. CONTRACT NUMBER		
			5b. GRANT NUMBER		
			5c. PROGRAM ELEMENT NUMBER		
6. AUTHOR(S) Roberts, John W. Jr., First Lieutenant, USAF			5d. PROJECT NUMBER #		
			5e. TASK NUMBER		
			5f. WORK UNIT NUMBER		
7. PERFORMING ORGANIZATION NAMES(S) AND ADDRESS(S) Air Force Institute of Technology Graduate School of Engineering and Management (AFIT/EN) 2950 Hobsen Way, Building 640 WPAFB OH 45433-7765			8. PERFORMING ORGANIZATION REPORT NUMBER AFIT/GNE/ENP/03-09		
9. SPONSORING/MONITORING AGENCY NAME(S) AND ADDRESS(ES) Air Force Office of Scientific Research Attn: Mr. Michael R. Berman 4015 Wilson Boulevard, Room 713 Arlington VA 22203-1954 (703) 696-7781			10. SPONSOR/MONITOR'S ACRONYM(S)		
			11. SPONSOR/MONITOR'S REPORT NUMBER(S)		
12. DISTRIBUTION/AVAILABILITY STATEMENT APPROVED FOR PUBLIC RELEASE; DISTRIBUTION UNLIMITED.					
13. SUPPLEMENTARY NOTES					
14. ABSTRACT <p>In recent years, silicon carbide (SiC), with its wide band-gap, high thermal conductivity, and radiation resistance, has shown prospects as a semiconductor material for use in high temperature and radiation environments such as jet engines and satellites. A limiting factor in the performance of many SiC semiconductor components is the presence of lattice defects formed at oxide dielectric junctions during processing. Recent theoretical work has used small quantum mechanical systems embedded in larger molecular mechanics structures to attempt to better understand SiC surfaces, defects in SiC bulk, and SiC oxidation.</p> <p>This research uses quantum mechanical models to calculate geometries and electronic properties of small Si_mC_nO molecular clusters of silicon carbide monoxides with 0 ≤ m,n ≤ 4. Calculations are done using Hartree-Fock and Density Functional Theory (DFT) with the B3LYP functional. Post-Hartree-Fock methods are used on the CSi₂O molecule to confirm the accuracy of B3LYP. Molecular properties examined include ground state multiplicity, vibrational modes and frequencies, and geometry for both the neutral and anion, adiabatic and vertical electron affinities, and thermodynamic heats of formation. Later research will be able to use these results to study the oxidation of larger SiC structures and surfaces and their defects.</p>					
15. SUBJECT TERMS Quantum Mechanics, Silicon Carbide, Monoxide, Density Functional Theory (DFT), ab initio, Molecular Modeling, Computational Chemistry					
16. SECURITY CLASSIFICATION OF:			17. LIMITATION OF ABSTRACT	18. NUMBER OF PAGES	19a. NAME OF RESPONSIBLE PERSON
a. REPORT	b. ABSTRACT	c. THIS PAGE			Larry W. Burggraf, AFIT/ENP
U	U	U	UU	228	19b. TELEPHONE NUMBER (Include area code) (937) 255-3636, ext 45074